

GEORGIA INSTITUTE OF TECHNOLOGY
OFFICE OF RESEARCH ADMINISTRATION

RESEARCH PROJECT INITIATION
(Revised - to correct address)

Reports
File
WLB

Date: January 7, 1975

Project Title: Prediction of Cryogenic Heat Pipe Performance

Project No: E-25-649

Principal Investigator: Dr. G. T. Colwell

Sponsor: National Aeronautics and Space Administration

Agreement Period: From 1/4/75 Until 12/31/75

Type Agreement: Grant No. NSG-2054

Amount: \$16,970 AFOSR
525 GTR (E-25-329)
\$17,495 Total

Reports Required: Semi-Annual Status Report
Final Technical Report

Sponsor Contact Person (s):

Administrative Matters

Thru ORA
Mr. Ray H. Sutton
Grants Officer
National Aeronautics and
Space Administration
Ames Research Center
Moffett Field, California 94035

Technical Matters

Mr. John P. Kirkpatrick
Systems Development Branch
National Aeronautics and
Space Administration
Ames Research Center
Moffett Field, California 94035
(415) 965-6525

Assigned to: Mechanical Engineering

COPIES TO:

Principal Investigator	Library
School Director	Rich Electronic Computer Center
Dean of the College	Photographic Laboratory
Director, Research Administration	Project File
Director, Financial Affairs (2)	
Security Reports Property Office	
Patent Coordinator	Other

GEORGIA INSTITUTE OF TECHNOLOGY
OFFICE OF CONTRACT ADMINISTRATION
SPONSORED PROJECT TERMINATION

Posted
4/8
CCH

Date: April 28, 1977

Project Title: Prediction of Cryogenic Heat Pipe Performance

Project No: E-25-649

Project Director: Dr. G. T. Colwell

Sponsor: National Aeronautics and Space Administration

Effective Termination Date: 3/31/77

Clearance of Accounting Charges: 3/31/77

Grant/Contract Closeout Actions Remaining:

- ☐ Final Invoice and Closing Documents
- ☐ Final Fiscal Report
- ☐ Final Report of Inventions
- ☐ Govt. Property Inventory & Related Certificate - submitted 21 Feb 77
- ☐ Classified Material Certificate
- ☒ Other Final NASA Form 1031, w/Cumulative Cost Expenditure Report

Assigned to: ME (School/Laboratory)

COPIES TO:

Project Director
Division Chief (EES)
School/Laboratory Director
Dean/Director-EES
Accounting Office
Procurement Office
Security Coordinator (OCA) ✓
Reports Coordinator (OCA)

Library, Technical Reports Section
Office of Computing Services
Director, Physical Plant
EES Information Office
Project File (OCA)
Project Code (GTRI)
Other

E-25-649

PREDICTION OF CRYOGENIC HEAT PIPE PERFORMANCE
REPORT NUMBER I

Prepared for the
National Aeronautics and Space Administration
Under Grant NSG-2054

Prepared by

Gene T. Colwell, Associate Professor
School of Mechanical Engineering
Georgia Institute of Technology
Atlanta, Georgia 30332

July 1 , 1975

2 3567

PREDICTION OF CRYOGENIC HEAT PIPE PERFORMANCE
REPORT NUMBER I

Prepared for the
National Aeronautics and Space Administration
Under Grant NSG-2054

Prepared by

Gene T. Colwell, Associate Professor
School of Mechanical Engineering
Georgia Institute of Technology
Atlanta, Georgia 30332

July 1 , 1975

School of Mechanical Engineering
Georgia Institute of Technology
Atlanta, Georgia 30332

NASA Grant NSG-2054
REPORT NUMBER I

July 1, 1975

Approved:

Stothe P. Kezios, Director
School of Mechanical Engineering

Gene T. Colwell
Principal Investigator

William M. Sangster, Dean
College of Engineering

Thomas E. Stelson
Vice President for Research

C O N T E N T S

<u>SECTION</u>	<u>PAGE</u>
INTRODUCTION	1
RESULTS TO DATE	3
REFERENCES	21
DISTRIBUTION	22

Introduction

This report describes progress made during the period January through June of 1975 under NASA Grant NSG-2054. The work has been monitored by Jack Kirkpatrick of Ames Research Center and Stan Ollendorf of Goddard Space Flight Center.

The goals of the project as described in reference 1 are:

1. To predict steady temperature profiles in a cryogenic heat pipe in zero and one g gravity fields as a function of heat transfer up to and including capillary dry out conditions;
2. To predict transient zero g temperature and pressure in a cryogenic heat pipe resulting from sudden changes in heat fluxes; and
3. To develop equations for predicting the effects of puddling during one g operation of a cryogenic heat pipe.

Significant progress has been made towards these goals during the report period. Simplified models have been developed for use in parametric studies of steady state capillary limitations, sonic limitations, and thermal resistance. In addition considerable progress has been made in using analog computers to predict transient behavior of cryogenic heat pipes.

The present capillary limitation model is believed to yield reasonably realistic results based on limited comparisons with experimental data. The present simplified model for predicting thermal resistances yields temperature differences which are considerably smaller than published measured values. This model is now being altered to account for several real affects including contact resistances, partial evaporator dryout, and vapor Reynolds Number influence. Transient studies to date have produced approximate information on amplitude and phase relationships among heat fluxes and temperatures at various points in a heat pipe under step, ramp and sinusoidal inputs. The allowable complexity of the model is limited by the analog capacity (approximately fifty amplifiers). A new transient model is now being developed for use on a digital computer. This new model will facilitate very accurate computations. However, the analog computer will continue

Introduction

to be useful for design purposes.

Work has not yet been started on item three of the proposal which relates to puddling during one g operation. It is anticipated that this problem will be addressed in the near future.

One master of Science Thesis (References 2) has been published under the grant thus far. Several other graduate and undergraduate students are presently working on the project and it is anticipated that additional reports, papers, and theses will be produced.

RESULTS TO DATE

The effort during the period being reported on has been directed toward development of both steady state and transient computational techniques. The models developed to this point are rather simplified. However, present efforts are being directed towards improving the models to account for real effects.

Geometry

The heat pipe under consideration is 91.4 cm in length and 1.27 cm in outside diameter. The tube and capillary structures are made of 304 stainless steel and the working fluid is nitrogen. Schematics of the tube and capillary structures are shown in Figures 1 and 2. The capillary structure is formed with three different types of screen. A thin layer of fine mesh screen is used on surfaces where evaporation and condensation occur. The central slab is formed using fine mesh screen on the outside of several layers of coarse mesh screen. For steady state computations the temperatures on the outside of the tube are assumed to be known thus uncoupling the source and the radiator from the heat pipe. However, in the transient analysis a saddle and radiator have been included on the cold end of the pipe.

Steady State Operation

When designing a heat pipe for steady operation, one must consider various limitations on performance-capillary failure, entrainment, boiling, and vapor choking-and thermal resistance. During the six months being reported on, capillary and sonic limitations and thermal resistances have been studied.

Writing momentum, energy and continuity equations for steady operation of the model heat pipe at capillary limited heat transfer and making the standard simplifying assumptions the following equation is obtained.

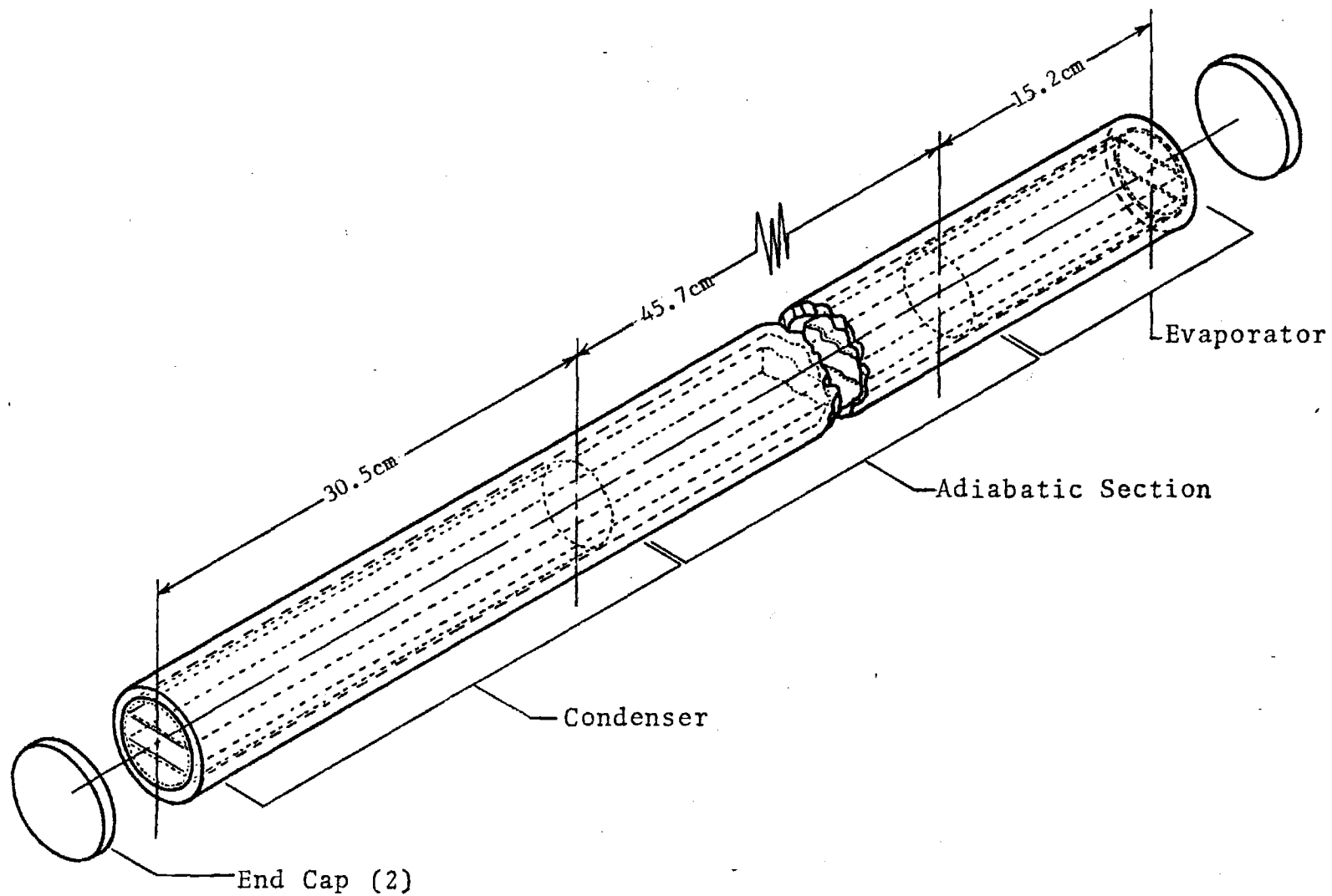


Figure 1. General Layout of Heat Pipe

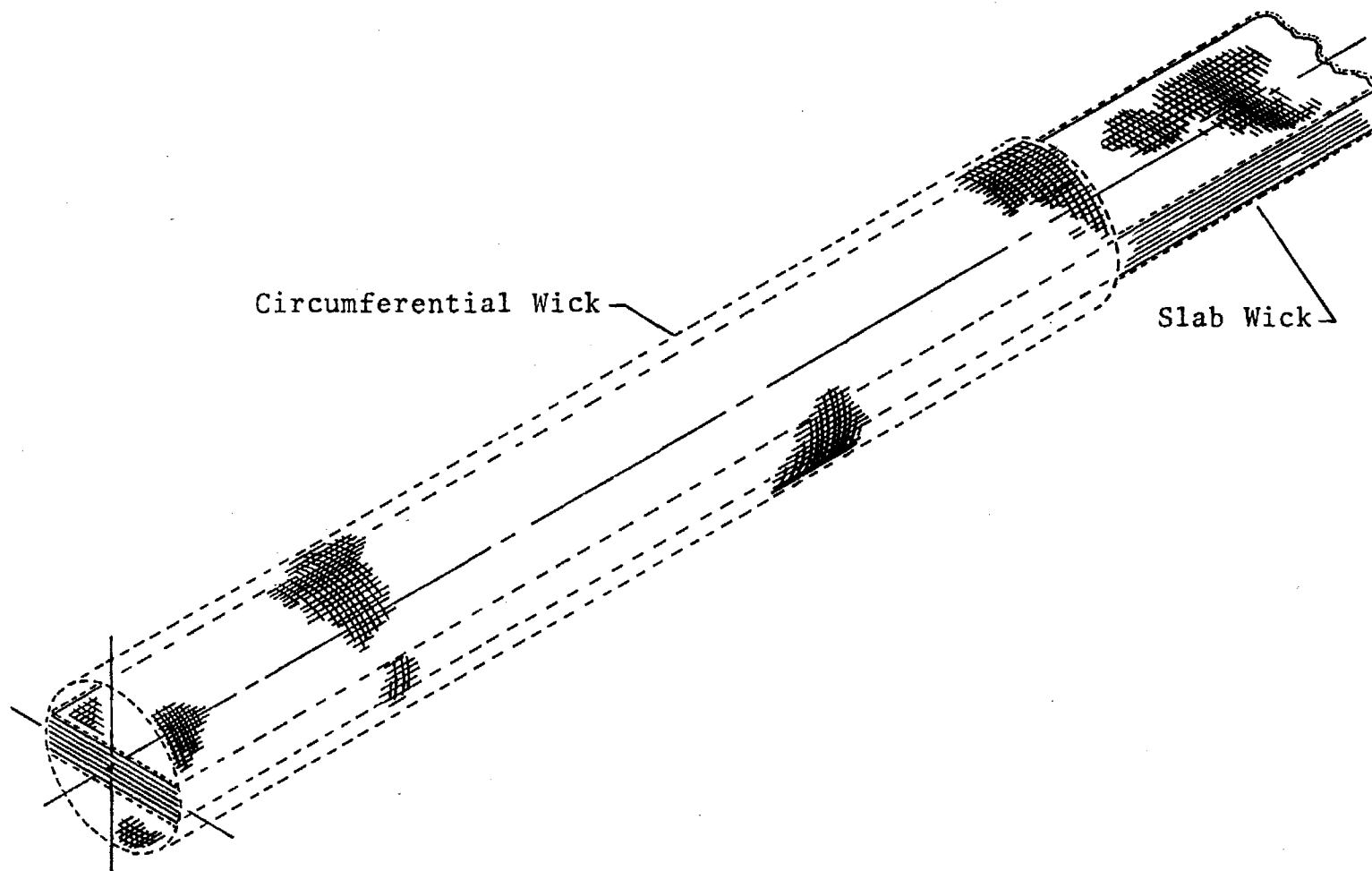


Figure 2. Close-Up of Composite Slab and Circumferential Wick at Heat Transfer Section

Results to Date

$$\dot{Q}_{CL} = \frac{2N/r_p}{\frac{\bar{K}\ell_{eff}}{b\delta_T} + \frac{K_C L}{4n_C \delta_C} \left(\frac{1}{\ell_e} + \frac{1}{\ell_c}\right) + \frac{8\mu_V \rho_L \ell_{eff}}{\pi \mu_L \rho_V r_v^4}}$$

where

\dot{Q}_{CL} = Capillary limited heat transfer rate

$$N = \frac{\sigma h_{fg} \rho_L}{\mu_L} = \text{"Heat Pipe Number"}$$

σ = surface tension of liquid

h_{fg} = heat of vaporization

ρ_L = liquid density

μ_L = liquid dynamic viscosity

r_p = pore radius at evaporator surface

$$\bar{K} = \frac{\delta_T}{\frac{n_A \delta_A}{K_A} + \frac{n_B \delta_B}{K_B}} = \text{effective inverse permeability for slab based on approach velocity.}$$

δ_T = total thickness of slab

n_A = number of layers of fine mesh in slab

n_B = number of layers of coarse mesh in slab

δ_A = thickness of a single layer of material A

δ_B = thickness of a single layer of material B

K_A = inverse permeability for material A based on approach velocity

K_B = inverse permeability for material B based on approach velocity

ℓ_{eff} = effective length of liquid path in slab

b = width of slab

K_C = inverse permeability for material at evaporator and condenser surfaces based on approach velocity

L = average distance traveled by liquid in circumferential capillary structure at evaporator or condenser (approximately 45° arc)

n_c = number of layers of capillary material on circumference

δ_c = thickness of a single layer of material C

ℓ_e = axial length of evaporator section

ℓ_c = axial length condenser section

μ_v = dynamic viscosity of vapor

ρ_v = density of vapor

r_v = hydraulic radius of vapor space

The thermal resistance of the pipe may be used to compute the heat rate in terms of overall temperature difference.

$$\dot{Q} = \frac{T_e - T_c}{R_T}$$

where

T_e = temperature of outside wall of pipe at evaporator

T_c = temperature of outside wall of pipe at condenser

R_T = overall thermal resistance

The overall thermal resistance includes resistances in the pipe wall at evaporator and condenser, in the combination of wick and working fluid at both ends of the pipe, at liquid-vapor interfaces at both ends, and in the vapor.

$$R_T = \frac{\ln(r_A/r_B)}{2\pi k_{p_e} \ell_e} + \frac{\ln(r_B/r_C)}{2\pi k_{w_2} \ell_e} +$$

$$+ \frac{(2\pi)^{1/2} R^{3/2} T_2^{5/2}}{4\pi r_C \ell_e P_{V_2} h_{fg}^2 g_c^{1/2}} + \frac{8\mu_v^{\ell} \text{eff } T_3 \left(\frac{1}{\rho_v} - \frac{1}{\rho_L}\right)}{\pi \rho_v h_{fg_3}^2 r_v^4} +$$

$$+ \frac{(2\pi)^{1/2} R^{3/2} T_5^{5/2}}{4\pi r_C \ell_c P_{V_5} h_{fg_5}^2 g_c^{1/2}} + \frac{\ln(r_B/r_C)}{2\pi k_{w_5} \ell_c} + \frac{\ln(r_A/r_B)}{2\pi k_{p_c} \ell_c}$$

where

k_{w_2}, k_{w_5} = effective thermal conductivity of wick and working fluid combination at temperatures T_2 and T_5

$$\frac{k_w}{L} = \frac{1}{A [2D+C]} + \frac{2.0}{ADB} + \frac{1}{B^2}$$

k_L = thermal conductivity of liquid working fluid.

$$A = \frac{r_p}{r_{ws}} + 1.0$$

$$B = \frac{r_{ws}}{r_p} + 1.0$$

$$C = \frac{r_p}{r_{ws}} - 1.0$$

$$D = \frac{k_L}{k_p}$$

k_p = thermal conductivity of pipe material

r_A = outside radius of pipe

r_B = inside radius of pipe

r_C = inside radius of circumferential wick

R = specific gas constant

T_2 = temperature of liquid - vapor interface at evaporator end

T_3 = temperature of vapor at evaporator end

T_5 = temperature of liquid - vapor interface at condenser end

P_{V_2} = saturation pressure corresponding to T_2

P_{V_5} = saturation pressure corresponding to T_5

g_c = conversion constant

Figures 3 and 4 show block flow diagrams of computer programs used to solve for capillary limitations and for thermal resistances. These programs have been

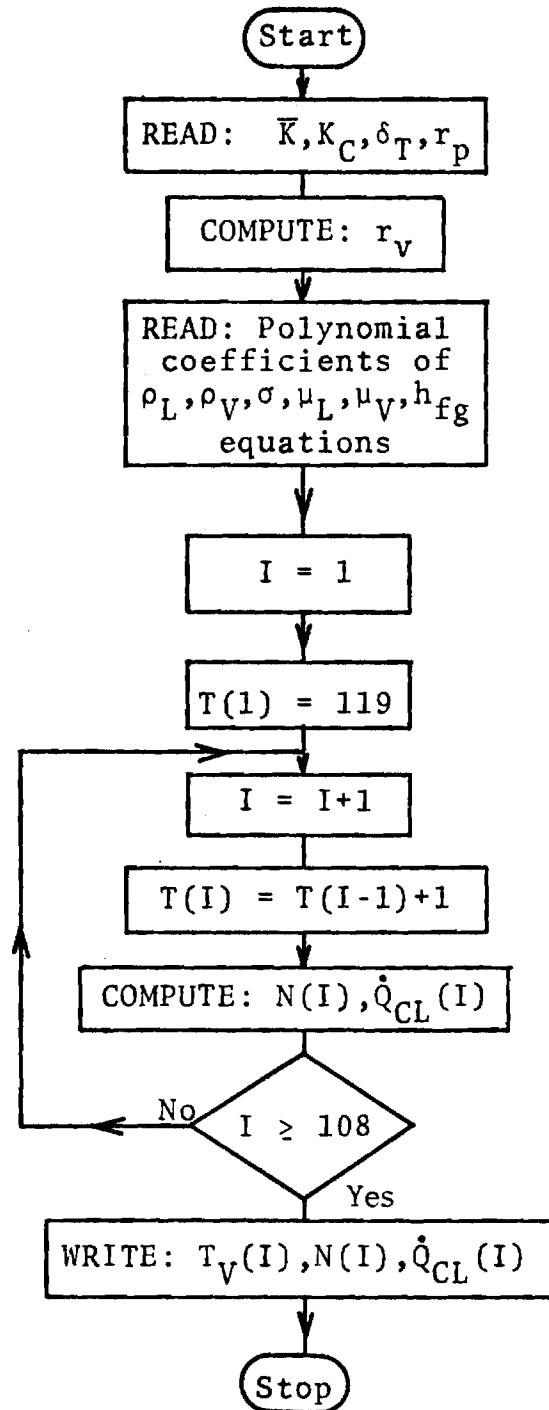


Figure 3. Flow Diagram of Computer Program Used for Calculating the Heat Pipe Number and the Capillary Limited Heat Transfer Rate

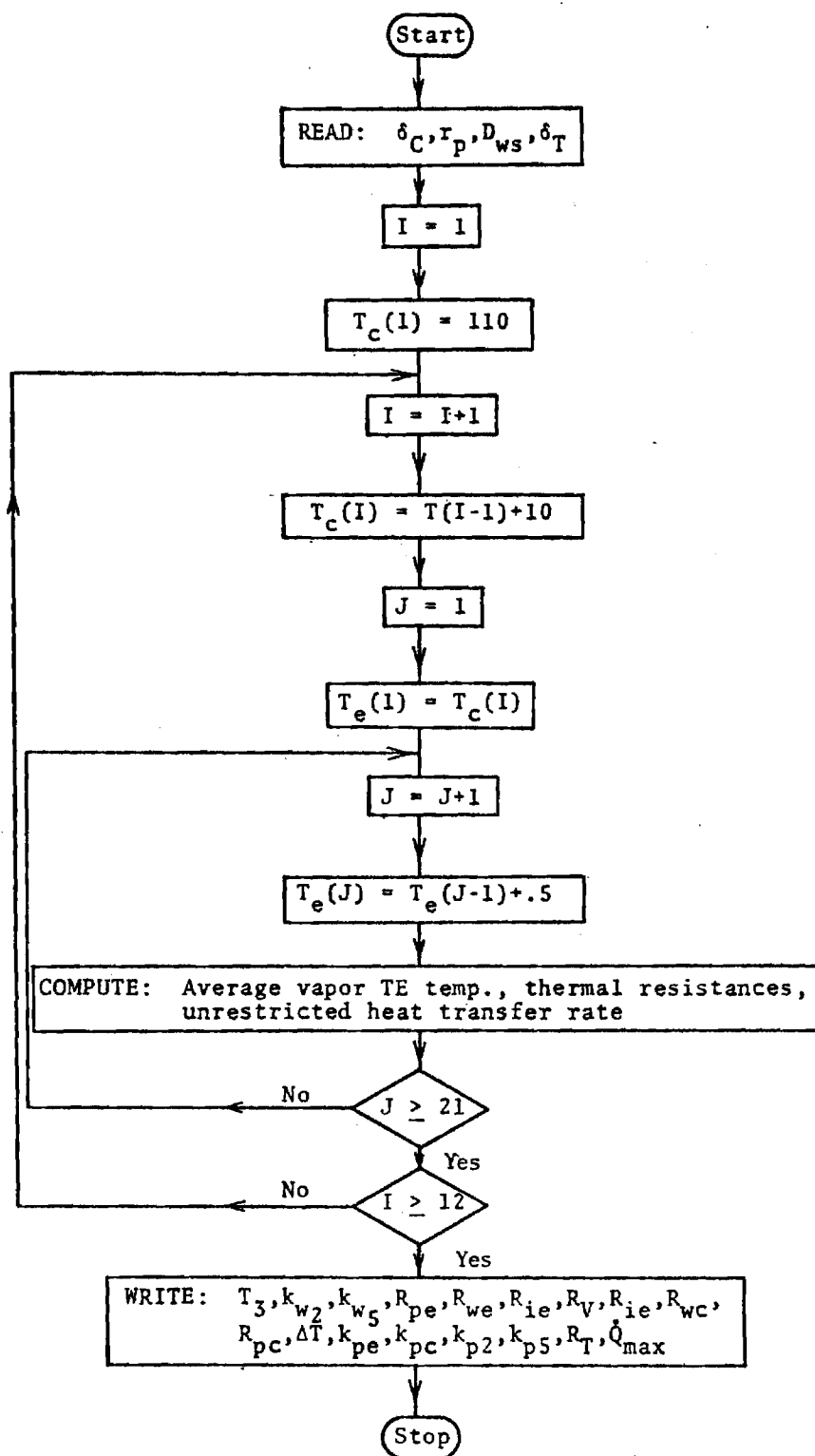


Figure 4. Flow Diagram of Computer Program Used for Calculating the Thermal Resistance

Results to Date

used to study approximately one hundred different capillary arrangements. Results of computations made for one of these arrangements are shown in Figure 5. In this case the total slab thickness was 0.341cm and was formed using four layers of 400 mesh screen and five layers of 30 mesh screen. The capillary structure on the evaporator and condenser surfaces consisted of two layers of 400 mesh screen. A study of Figure 5 shows that this pipe is capable of transporting a very respectable heat rate. The temperature drops shown on this figure are ideal numbers based on the equation listed previously in this report. Real temperature differences for this type of heat pipe are considerably larger than the values shown. Contact resistances where source and sink are connected to the heat pipe cause large temperature drops. In addition several other factors associated with the heat pipe itself affect overall temperature drop. It is well known that the capillary structure at the evaporator partially dries out even at fairly low heat fluxes and the majority of the surface is often dry as the capillary limit is approached. This partial dryout causes a smaller zone of evaporation and hence larger thermal gradients are required to give a certain heat rate. Small clearances between layers of capillary structure and between the structure and the pipe walls cause rather large temperature drops. Vapor velocity profiles affect condensation and hence resistance. These real affects are now being incorporated into the thermal resistance model and it is expected that results of computations using the more realistic model will be reported on in the next status report.

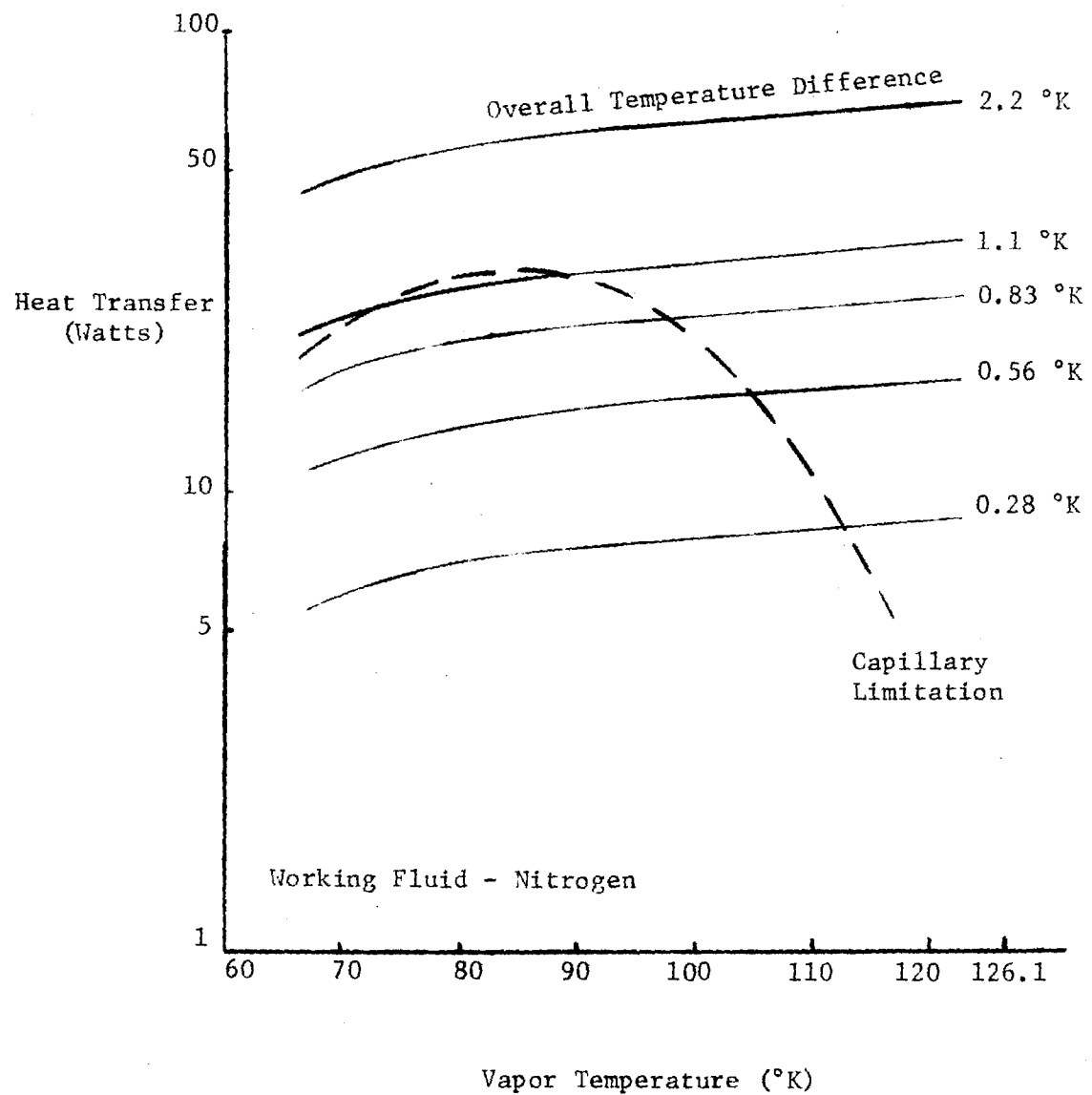


Figure 5. Predicted Performance

Transient Operation

A rather simplified transient model of a cryogenic slab type heat pipe with radiator connected is shown in Figure 6. Due to limited analog computer capacity relatively few nodes were used. The equations written for this model are:

$$Q_e = \frac{2\pi \ell_e k_p}{\ln(r_A/r_B)} (T_e - T_1) + \frac{\rho_p c_{pe} V_p}{2} \frac{dT_e}{d\theta}$$

$$\begin{aligned} \frac{dT_1}{d\theta} = & \frac{4\pi \ell_e k_p}{[\rho_p c_{pe} V_p + \rho_w c_{we} V_w] \ln(r_A/r_B)} (T_e - T_1) \\ & + \frac{4\pi \ell_e k_w}{[\rho_p c_{pe} V_p + \rho_w c_{we} V_w] \ln(r_B/r_C)} (T_{vap} - T_1) \end{aligned}$$

$$\begin{aligned} \frac{dT_{vap}}{d\theta} = & \frac{4\pi k_w \ell_e}{[\rho_w c_{we} V_w + \rho_w c_{wc} V_w + 2m_a c_a] \ln(r_B/r_C)} (T_1 - T_{vap}) \\ & + \frac{4\pi k_w \ell_c}{[\rho_w c_{we} V_w + \rho_w c_{wc} V_w + 2m_a c_a] \ln(r_B/r_C)} (T_2 - T_{vap}) \end{aligned}$$

$$\begin{aligned} \frac{dT_2}{d\theta} = & \frac{4\pi k_w \ell_c}{[\rho_p c_{pe} V_p + \rho_w c_{wc} V_w] \ln(r_B/r_C)} (T_{vap} - T_2) \\ & + \frac{4\pi k_p \ell_c}{[\rho_p c_{pe} V_p + \rho_w c_{wc} V_w] \ln(r_A/r_B)} (T_c - T_2) \end{aligned}$$

$$\frac{dT_c}{d\theta} = \frac{4\pi k_p \ell_c}{\rho_p c_{pe} V_p \ln(r_A/r_B)} (T_2 - T_c) + \frac{4\pi r_a \ell_c}{\rho_p c_{pe} V_p R_c} (T_r - T_c)$$

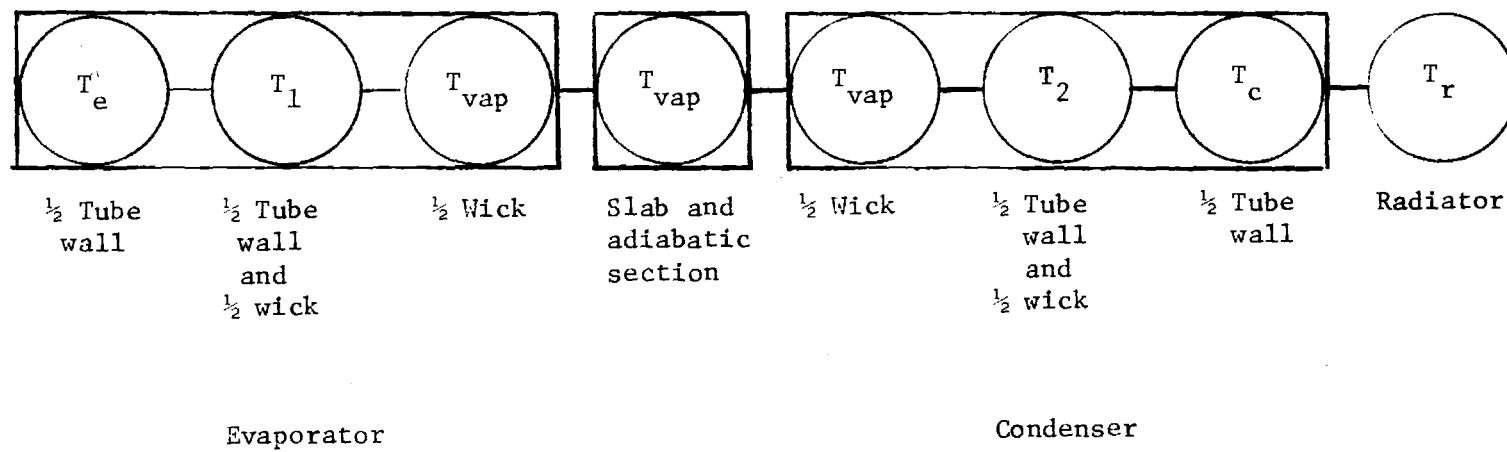


Figure 6. Analog Model

$$\frac{dT_r}{d\theta} = \frac{2\pi r_a \ell_c}{m_r c_r} (T_c - T_r) - \frac{\epsilon A_r \sigma}{m_r c_r} T_r^4 + \frac{Q_{space}}{m_r c_r}$$

Limiter

$$(T_1 - T_{vap}) \leq \frac{Q_{CL} \ln(r_B/r_C)}{2\pi k_w \ell_e}$$

where

A_r = area of radiator

c_a = effective specific heat of adiabatic section and slab

c_p = specific heat of pipe material

c_r = specific heat of radiator

m_a = mass of adiabatic section and slab

m_r = mass of radiator

Q_e = heat flux into evaporator

Q_{space} = heat flux into radiator

Q_r = net heat flux from radiator

R_c = contact resistance between node c and node r

T_e = temperature node e

T_1 = temperature node 1

T_{vap} = temperature node vap

T_2 = temperature node 2

T_c = temperature node c

T_r = temperature node r

V_{ep} = volume of pipe material in evaporator

V_{cp} = volume of pipe material in condensor

V_{ew} = volume of wick material in evaporator

V_{cw} = volume of wick material in condensor

ϵ = emmissivity of radiator

ρ_p = density of pipe material

ρ_w = effective density of wick and working fluid

σ = Stefan-Boltzman constant

θ = time

The limiter equation allows one to include the capillary limitation in computations.

Figure 7 shows a schematic of the analog computer circuit. Note that inclusion of the radiator introduces non-linear terms in the equations. However, these non-linear terms have thus far caused no difficulties in the computations.

Figures 8, 9, and 10 show sample results of the computations. Figure 8 shows performance for a step change of 5°K in the evaporator temperature. Notice that heat transfer at the hot end (Q_e) is limited for some time due to capillary limitations. The system has essentially stabilized after 60 seconds. Figure 9 shows how all paramameters vary for a relatively fast sine wave. Notice that the capillary limitation considerably affects heat transfer through the evaporator. As expected, the computations indicate progressively smaller oscillations in temperature as one moves away from the evaporator and finally the radiator increases with time but oscillates very little. There is a considerable phase shift between oscillations in different temperatures. Figure 10 shows the system changes for a relatively slow variation in evaporator temperature. Evaporator heat transfer is again limited by capillary restrictions. The amplitude of temperature oscillations tends to be more uniform throughout the pipe than in the case where fast oscillations were considered. There are large phase shifts.

Work is currently under way towards a goal of developing a much more accurate transient model for use on a digital computer. It is anticipated that both digital and analog computers will be of use in the future in predicting transient behavior.

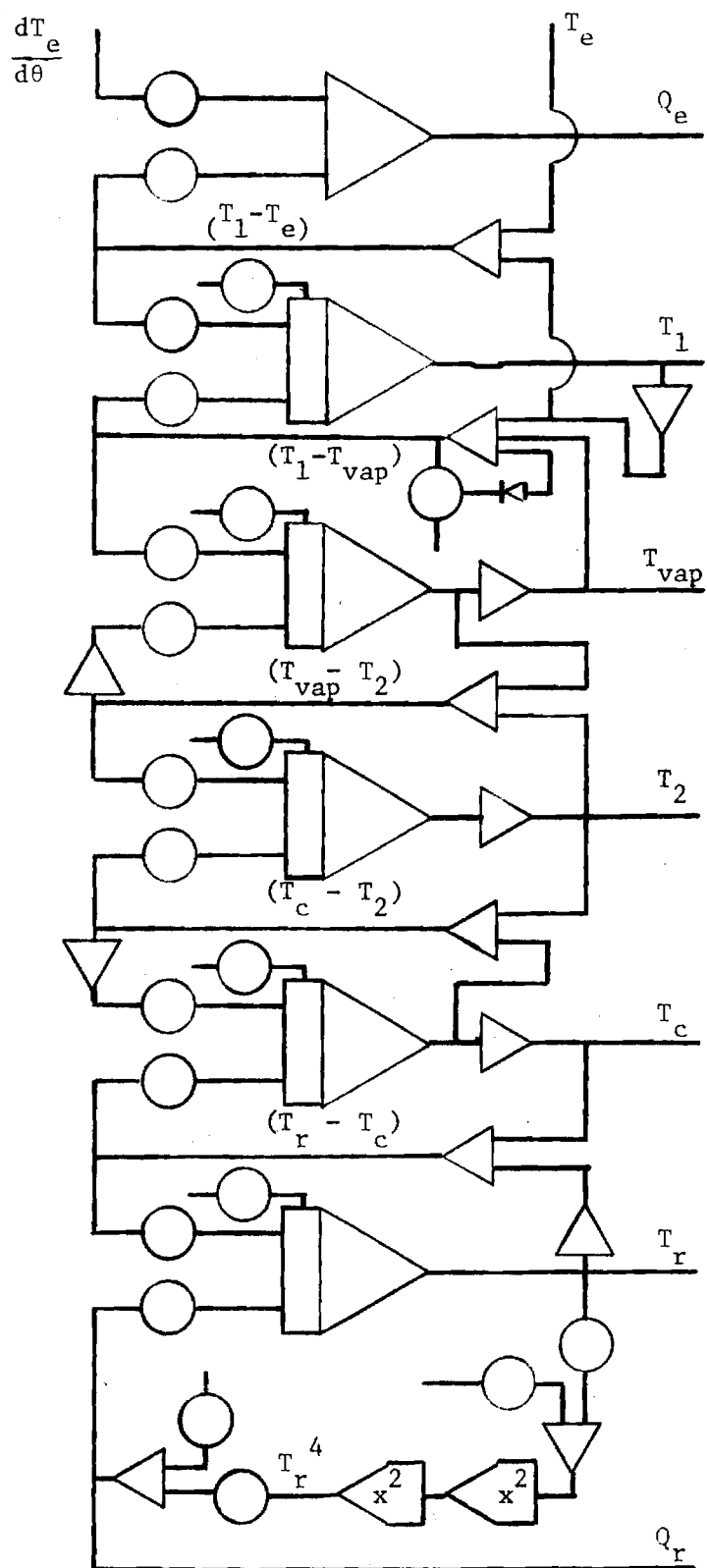


Figure 7. Analog Circuit

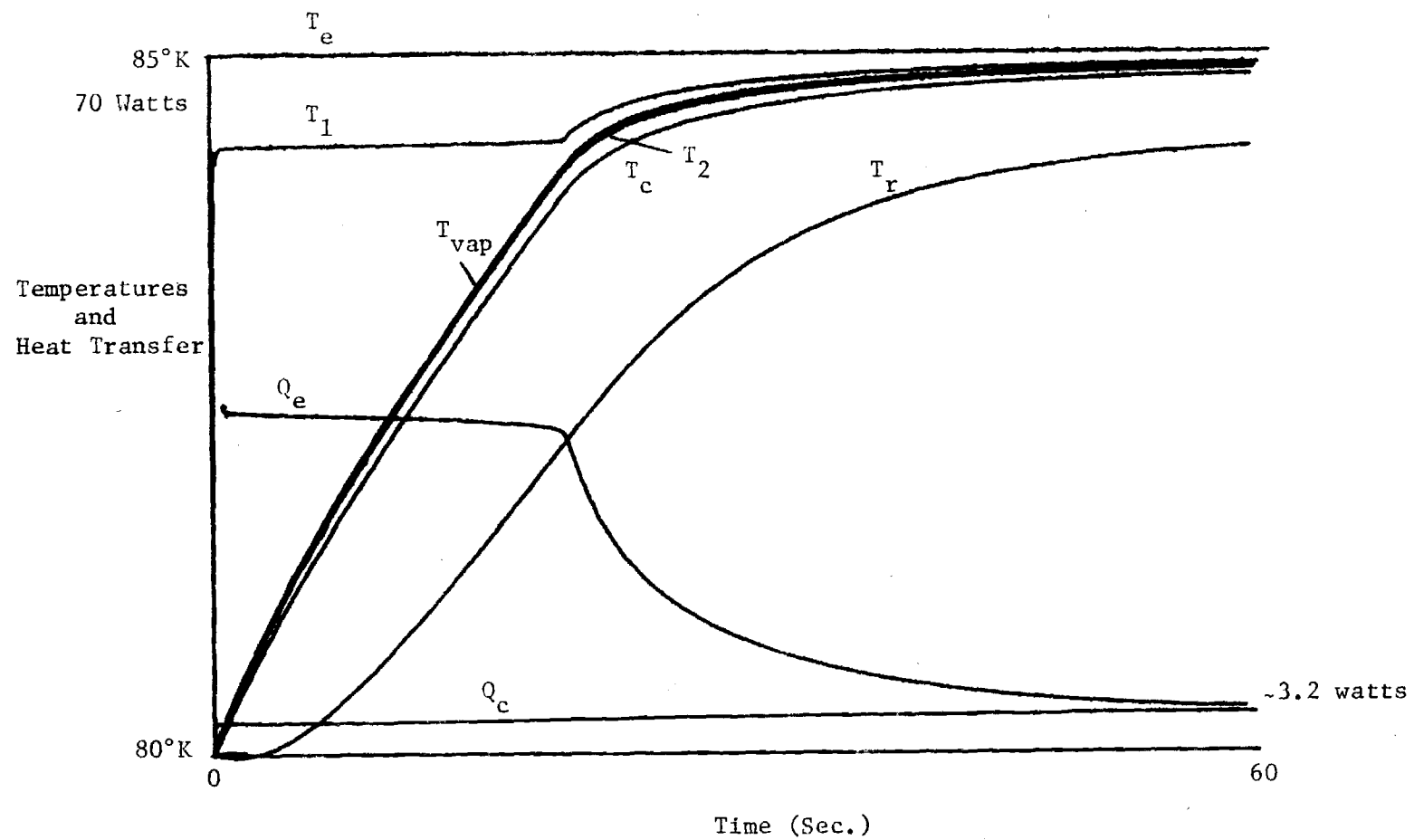


Figure 8. Step Temperature Change

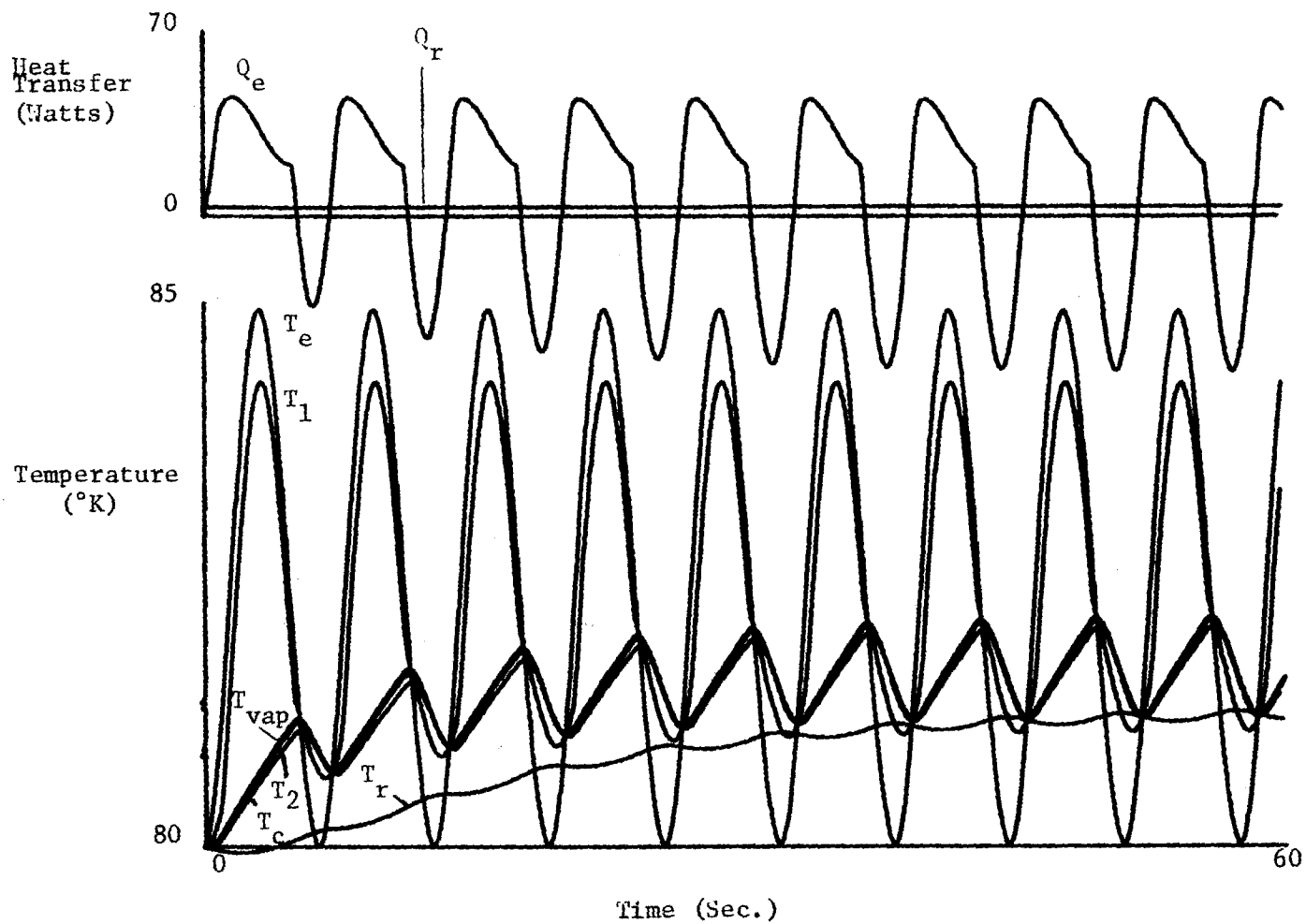


Figure 9. Fast Sine Wave

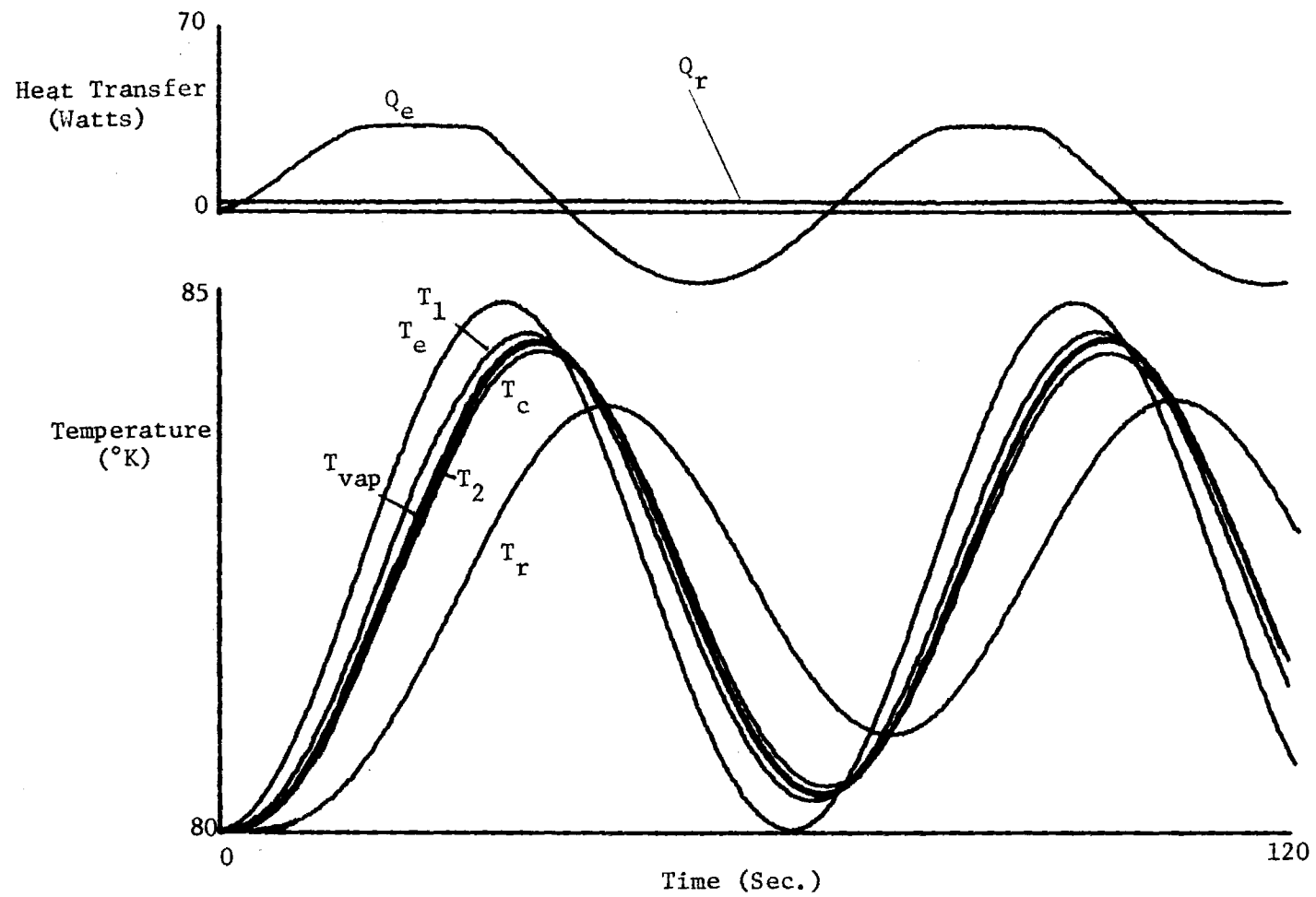


Figure 10. Slow Sine Wave

References

1. Colwell, G. T., "Prediction of Cryogenic Heat Pipe Performance", Georgia Institute of Technology Proposal, JGB/G 4003.43, October 31, 1974.
2. Hare, J. D., "Performance of a Nitrogen Heat Pipe with Various Capillary Structures", M.S. Thesis, Georgia Institute of Technology, June 1975.

Distribution

1. NASA Scientific and Technical Information Facility Post Office Box 33
College Park, Maryland 20740 (2 copies).
2. NASA Ames Research Center Moffett Field, California 94035

John P. Kirkpatrick (5 copies)
Robert J. Debs
Manfred Groll
Craig McCreight
Masahide Murakami
Ray H. Sutton
3. NASA Goddard Space Flight Center Code 732
Greenbelt, Maryland 20771

Stanford Ollendorf (5 copies)
Yashuhiro Kamotani
Allan Sherman
4. Georgia Institute of Technology
Office of Research Administration (5)
Vice President for Research (1)
Dean College of Engineering (1)
Director, School of Mechanical Engineering (3)
Gene T. Colwell (10)

E-25-649

GEORGIA INSTITUTE OF TECHNOLOGY
School of Mechanical Engineering
Atlanta, Georgia



PREDICTION OF CRYOGENIC HEAT PIPE PERFORMANCE
ANNUAL REPORT FOR 1975
REPORT NUMBER II

Prepared for the
National Aeronautics and Space Administration
Under
Grant NSG-2054

Prepared by
Gene T. Colwell, Associate Professor
School of Mechanical Engineering
Georgia Institute of Technology
Atlanta, Georgia 30332

February 1, 1976

PREDICTION OF CRYOGENIC HEAT PIPE PERFORMANCE
ANNUAL REPORT FOR 1975
REPORT NUMBER II

Prepared for the
National Aeronautics and Space Administration
Under
Grant NSG-2054

Prepared by

Gene T. Colwell, Associate Professor
School of Mechanical Engineering
Georgia Institute of Technology
Atlanta, Georgia 30332


February 1, 1976

GEORGIA INSTITUTE OF TECHNOLOGY
School of Mechanical Engineering
Atlanta, Georgia 30332

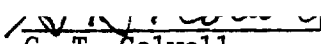
NASA Grant NSG-2054
Annual Report for 1975
Report Number II

February 1, 1976

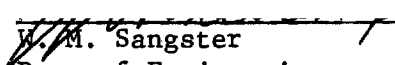
Approved:



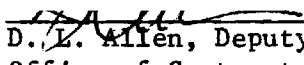
S. P. Kezios, Director
School of Mechanical Engineering



G. T. Colwell
Principal Investigator



W. M. Sangster
Dean of Engineering



D. L. Allen, Deputy Director
Office of Contract Administration

CONTENTS

<u>SECTION</u>	<u>PAGE</u>
ACKNOWLEDGEMENTS	iii
LIST OF FIGURES	iv
LIST OF TABLES.	vi
INTRODUCTION	1
RESULTS TO DATE	6
CONCLUSIONS	58
REFERENCES	59
DISTRIBUTION	60
APPENDIX - THERMAL RESISTANCE PROGRAM	61

ACKNOWLEDGEMENTS

The writer wishes to acknowledge the essential contributions to this program made by people associated with NASA and Georgia Tech. At Georgia Tech James Hare, Don Priester, and David Ruis handled programing and operation of the digital and analog computers used to generate the data presented herein. Jack Kirkpatrick, Bob Debs, Manfred Groll, Craig McCreight, and Masahide Murakami of the NASA Ames Research Center reviewed the work at various stages and made valuable suggestions. Stan Ollendorf of the NASA Goddard Space Flight Center was primarily responsible for initiation of the project and he has continually provided encouragement, supervision and direction. Allan Sherman, of GSFC, has worked closely with the GIT team for about two years. He has suggested sizes, shapes, temperature ranges, and heat fluxes of current practical interest. In addition he has offered constructive criticism of the theoretical approaches used. The writer also wishes to acknowledge the contributions of Yashu Kamotani and Roy McIntosh of GSFC, who reviewed the theoretical approaches.

LIST OF FIGURES

<u>FIGURE</u>	<u>PAGE</u>
1. General Layout of Heat Pipe	2
2. Close-up of Composite Slab and Circumferential Wick at Heat Transfer Section	3
3. Capillary Structure	9
4. Dryout Angles	12
5. ΔT VS. T_V at Constant Q - Case 1	20
6. R_{TOT} , R_{WE} , R_{WC} VS. T_V for $Q = 22$ Watts - Case 1	21
7. R_{PE} , R_{PC} VS. T_V for $Q = 22$ Watts - Case 1	22
8. R_{IE} , R_{IC} VS. T_V for $Q = 22$ Watts - Case 1	23
9. R_V VS. T_V for $Q = 22$ Watts - Case 1	24
10. ΔT VS. T_V at Constant Q - Case 6	25
11. R_{TOT} , R_{WE} , R_{WC} VS. T_V for $Q = 22$ Watts - Case 6	26
12. R_{PE} , R_{PC} VS. T_V for $Q = 22$ Watts - Case 6	27
13. R_{IE} , R_{IC} VS. T_V for $Q = 22$ Watts - Case 6	28
14. R_V VS. T_V for $Q = 22$ Watts - Case 6	29
15. ΔT VS. T_V at Constant Q - Case 2	30
16. ΔT VS. T_V at Constant Q - Case 3	31
17. ΔT VS. T_V at Constant Q - Case 4	32
18. ΔT VS. T_V at Constant Q - Case 5	33
19. ΔT VS. T_V at Constant Q - Case 7	34
20. ΔT VS. T_V at Constant Q - Case 8	35
21. ΔT VS. T_V at Constant Q - Case 9	36
22. Capillary Limitations	41
23. Analog Model	42
24. Analog Circuit	46
25. Step Temperature Change	47

LIST OF FIGURES CON'T

	<u>PAGE</u>
26. Fast Sine Wave	48
27. Slow Sine Wave	49
28. Heat Pipe Model	51
29. Polar to Rectangular Transformation	55
30. Computation Grid	56

LIST OF TABLES

<u>TABLE</u>	<u>PAGE</u>
I. Values of Parameters for Cases Considered in This Study	19
II. Description of Composite Wick Systems Considered in This Study	40

INTRODUCTION

In January of 1975 work was started at Georgia Tech on a project aimed at gaining a better understanding of the various design parameters which affect steady state and transient operation of cryogenic heat pipes. This report briefly describes the progress made on the project during the period January through December of 1975. Financial support has come from NASA under grant NSG-2054 and the work has been monitored by Jack Kirkpatrick of Ames Research Center and Stan Ollendorf of Goddard Space Flight Center. One M.S. thesis (reference 1) which is directly related to the project was published in June of 1975 and a second thesis in the area is currently being prepared and should be published about July 1976. It is anticipated that several papers will be published in recognized technical journals over the next few years as a result of the work.

Heat Pipe Under Study

A 304 stainless steel heat pipe with slab type capillary structure and nitrogen as the working fluid was studied in the temperature range of 60°K to 120°K. The pipe is 1.27 cm in outside diameter and 9.14 cm in total length. Figures 1 and 2 show geometry of the pipe and the configuration of the capillary structure. In the transient studies, described in detail in this report, saddles are included at evaporator and condenser ends and a radiator is included at the condenser end.

Summary of Results to Date

The work performed under the grant is divided into two main areas. The first area includes development of accurate steady state equations for predicting capillary limitations and development of equations for

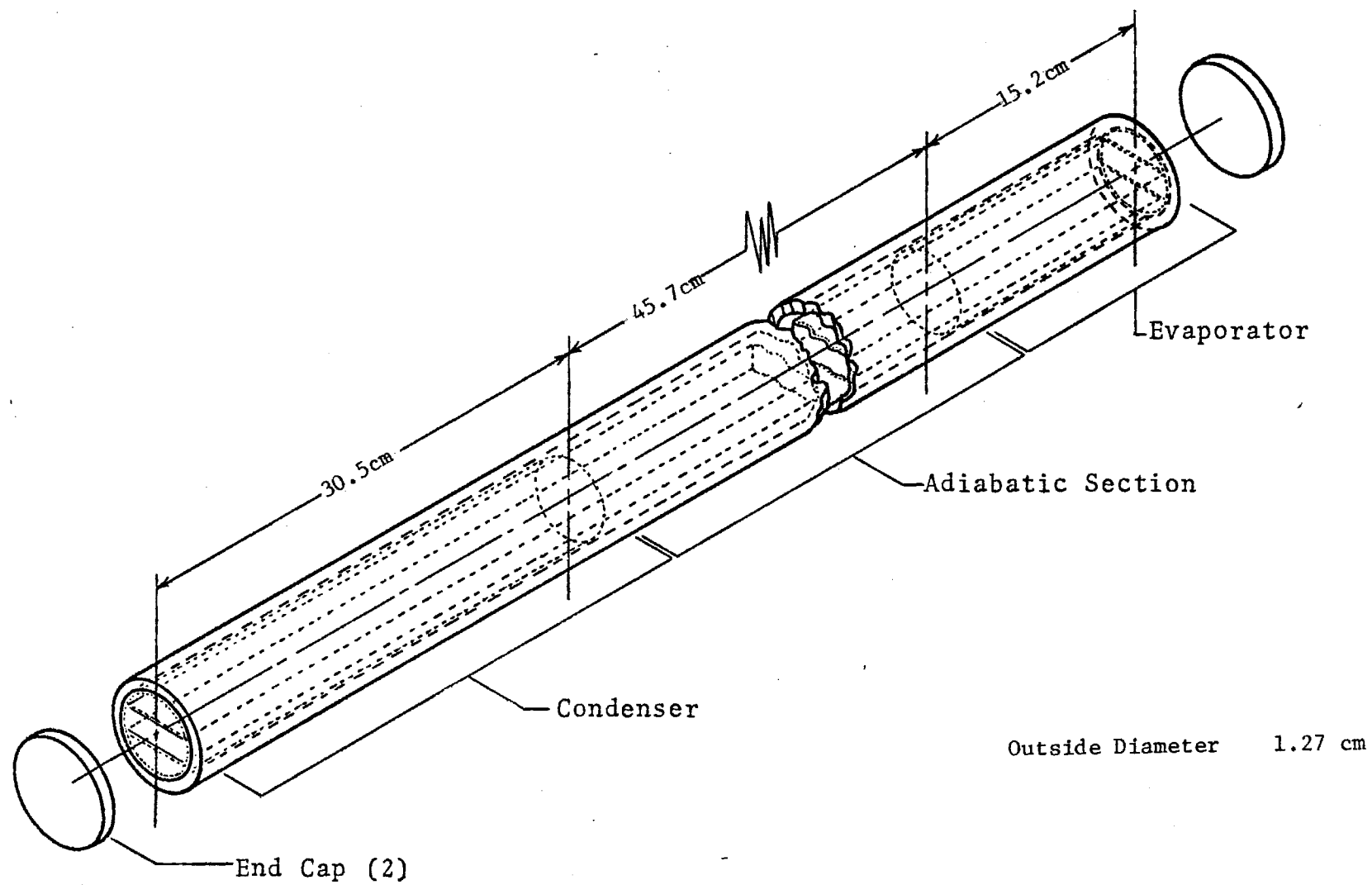


Figure 1. General Layout of Heat Pipe

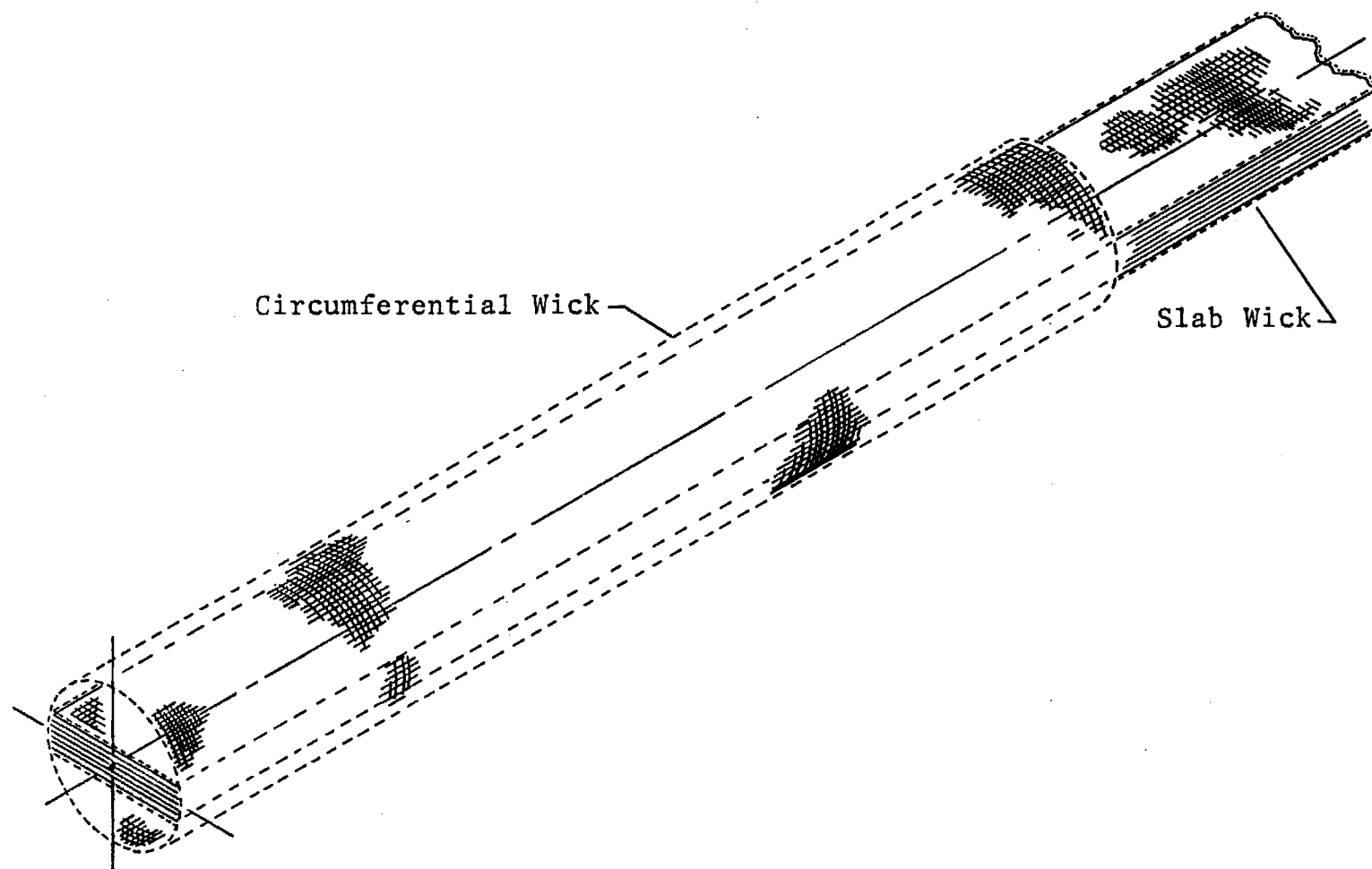


Figure 2. Close-Up of Composite Slab and Circumferential Wick at Heat Transfer Section

predicting thermal resistances. Extensive computer surveys were run using the equations developed and it was found that a heat pipe of the type described above could transfer as much as 30 to 40 watts with an overall temperature drop of a few degrees Kelvin. The second area of study was the transient operation of cryogenic heat pipes. The problem was first studied with the aid of an analog computer and currently a digital computer approach is being pursued. Results of the analog work, which is limited to small transients and does not account for fluid dynamics, show the effects of small step temperature changes and the effects of fast and slow sine wave variations of small amplitude on heat pipe operating parameters. The digital program now under development will be much more powerful in that large transients, even including the case of start-up from the supercritical state, can be studied. At present a simplified model, which does not include fluid dynamic effects, is being successfully examined on a digital computer. The next step is to incorporate fluid dynamic effects.

Future Plans

The main theoretical effort is now being directed towards making the transient model, which is being examined on a digital computer, more realistic and more flexible. It is expected that this work will require another six months assuming that current levels of effort are maintained.

Some effort is now being directed to planning some low temperature heat pipe experiments which could be used to generate data for verifying and modifying both steady state and transient models. In the near term the experiments would be carried out in a laboratory on earth. Also some initial thought has been given to the idea of a space experiment. The National Aeronautics and Space Administration currently is designing

a "Long Duration Exposure Facility" and a "Sky Lab" either of which would be ideal for this type of space experiment.

RESULTS TO DATE

During Calendar 1975 significant progress has been made both in the steady state and transient parts of the work. Computer programs are now on hand for predicting capillary limitations, and steady state thermal resistances for slab type cryogenic heat pipes. An analog scheme has been developed which handles small transients and work is progressing on a much more powerful digital solution scheme which will be able to handle large transients including startup from the supercritical region. Each of these steady state and transient approaches will be discussed in detail.

Steady State Thermal Resistances

In the typical design of a heat pipe, little attention is given to predicting thermal resistances. This is the case because accurate predictions are extremely difficult in most systems. It is not uncommon to underestimate overall heat pipe temperature drops by an order of magnitude.

In the present analysis resistances are considered in the pipe wall at the condenser and evaporator, in the layers of capillary material around the circumference of the evaporator and condenser surfaces, in the fluid gaps between layers of capillary material, at liquid vapor interfaces, and in the vapor region. In addition it has been assumed that the circumferential portion of the capillary structure partially dries as heat transfer is increased towards the capillary limitation. This problem is discussed in detail in references 2 through 5. Results of several studies, see reference 2, suggest that in long heat pipes part of the condenser surface may not be active at relatively low heat

transfer rates. This effect has been considered in developing a thermal resistance model at the condenser end.

The following nomenclature is used in computing thermal resistances.

d_f	distance between centers of screen filaments
g_c	conversion factor
h_{fg}	enthalpy of vaporization of N_2
k_f	conductivity of stainless steel screen filaments or of the stainless steel pipe
k_ℓ	conductivity of liquid nitrogen
k_p	conductivity of stainless steel pipe
k_w	conductivity of the liquid filled screen portion of the wick
ℓ_{ax}	axial length
ℓ_{ca}	active condenser length
ℓ_{cd}	length of condenser at design conditions
ℓ_E	length of evaporator section
ℓ_{eff}	effective length of vapor path
N	number of screen layers
p_v	vapor pressure
Q	heat transfer rate
Q_{MAX}	capillary limitation
R	ideal gas constant
r_A	outer radius of pipe wall
r_B	inner radius of pipe wall
r_C	inner radius of wick
r_{CHD}	hydraulic radius of complete wick structure
r_f	distance between centers of screen filaments
R_{IC}	resistance of interface at condenser

R_{IE}	resistance of liquid vapor interface at evaporator
R_{PC}	resistance of pipe wall at condenser
R_{PE}	resistance of pipe wall at evaporator
R_{TOT}	total resistance
R_V	resistance of vapor
R_{WC}	resistance of wick at condenser
R_{WE}	resistance of wick at evaporator
T_C	temperature of outer surface of pipe at condenser
T_E	temperature of outer surface of pipe at evaporator
T_{LI}	temperature of liquid at the liquid vapor interface
T_{PCI}	temperature of inner surface of pipe at condenser
T_{PEI}	temperature of inner surface of pipe at evaporator
T_V	vapor temperature
W_T	wall thickness of pipe
β	thickness of liquid layers between screen layers
ΔT	$T_E - T_C$
μ_V	viscosity of vapor
ρ_l	density of liquid
ρ_v	density of vapor
θ	angle within each quadrant over which liquid is present in the wick at the evaporator
δ_T	thickness of central slab

The equations developed for computing resistances are given in the following list.

The resistance of circumferential layers of capillary structure and working fluid gaps is (see Figure 3)

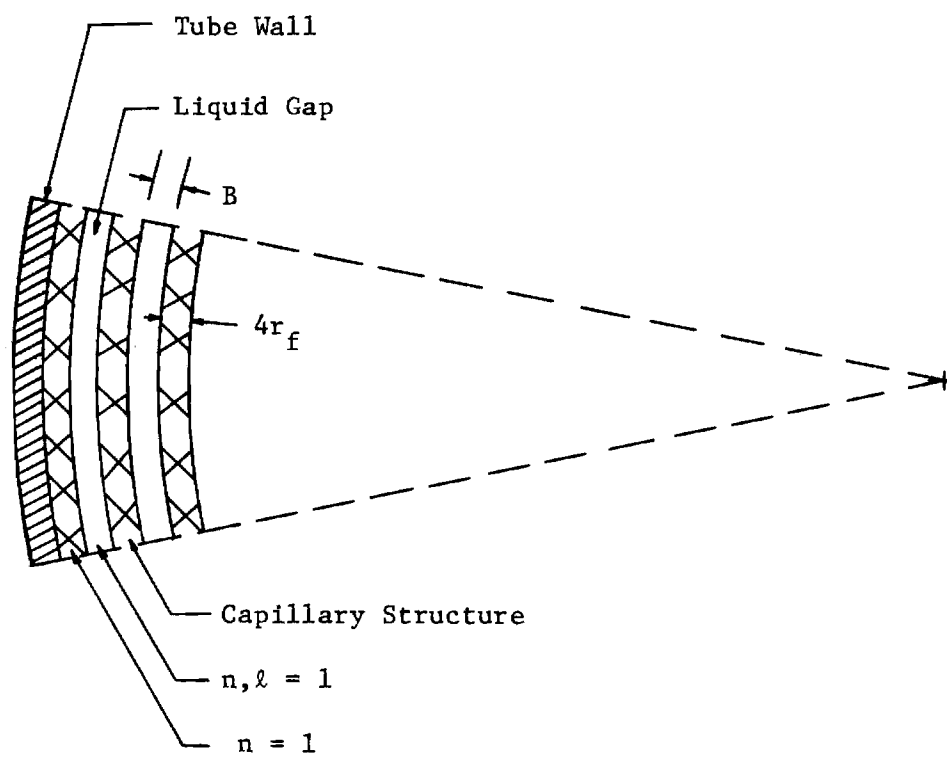


Figure 3. Capillary Structure

$$R_w = \sum_{n=1}^N R_n + \sum_{n=1}^{N-1} R_{n,\ell} \quad (1)$$

$$R_n = \frac{\ell_n \frac{r_B - (n-1)4r_f - (n-1)\beta}{r_B - n4r_f - (n-1)\beta}}{2\pi k_w \ell_{ax}} \quad (2)$$

$$R_{n,\ell} = \frac{\ell_n \frac{r_B - n4r_f - (n-1)\beta}{r_B - n4r_f - n\beta}}{2\pi k_\ell \ell_{ax}} \quad (3)$$

Dry out of the evaporator surface is accounted for by (see Figure 4)

$$\theta = \frac{\frac{\pi}{2}}{1 + \frac{Q}{Q_{MAX}}} \quad (4)$$

Assume that the active condenser length is $\ell_{ca} = \ell_{cd} \frac{Q}{Q_{MAX}}$.

The wick resistance at the condenser then becomes

$$R_{WC} = \sum_{n=1}^N R_n + \sum_{n=1}^{N-1} R_{n,\ell} \quad (5)$$

$$R_n = \frac{\frac{Q_{MAX}}{Q} \ell_n \frac{r_B - (n-1)4r_f - (n-1)\beta}{r_B - n4r_f - (n-1)\beta}}{2\pi k_w \ell_{cd}} \quad (6)$$

$$R_{n,\ell} = \frac{\frac{Q_{MAX}}{Q} \ell_n \frac{r_B - n4r_f - (n-1)\beta}{r_B - n4r_f - n\beta}}{2\pi k_\ell \ell_{cd}} \quad (7)$$

The wick resistance at the evaporator is

$$R_{WE} = \left[1 + \frac{Q}{Q_{MAX}} \right] \left[\sum_{n=1}^N R_n + \sum_{n=1}^{N-1} R_{n,\ell} \right] \quad (8)$$

$$R_n = \frac{\ln \frac{r_B - (n-1) 4r_f - (n-1)\beta}{r_B - 4n r_f - (n-1)\beta}}{2\pi k_w \ell_E} \quad (9)$$

$$R_{n,\ell} = \frac{\ln \frac{r_B - 4nr_f - (n-1)\beta}{r_B - 4nr_f - n\beta}}{2\pi k_\ell \ell_E} \quad (10)$$

The effective thermal conductivity of the fluid-metal combination in a typical single layer is (reference 2)

$$k_w = k_\ell \left\{ \frac{1}{\frac{d_f}{2r_f} \left[2 \frac{k_\ell}{k_f} + \frac{d_f}{2r_f} - 2 \right]} + \frac{2}{\frac{d_f}{2r_f} \left(\frac{k_\ell}{k_f} \right) \left[\frac{2r_f}{d_f - 2r_f} + 1 \right]} + \frac{1}{\left[\frac{2r_f}{d_f - 2r_f} + 1 \right]^2} \right\} \quad (11)$$

The resistance of the pipe wall in the condenser and evaporator sections is

$$R_{PC} = \frac{Q_{MAX}}{Q} \frac{\ln \frac{r_A}{r_B}}{2\pi k_f \ell_{cd}} \quad (12)$$

$$R_{PE} = \left[1 + \frac{Q}{Q_{MAX}} \right] \frac{\ln \frac{r_A}{r_B}}{2\pi k_f \ell_E} \quad (13)$$

The interfacial resistances at condenser and evaporator ends is approximated as

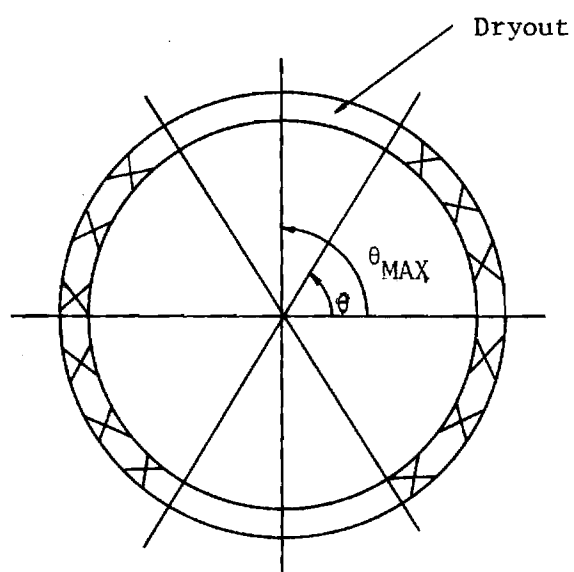


Figure 4. Dryout Angles

$$R_{IC} = \frac{Q_{MAX}}{Q} \frac{(2\pi)^{1/2} R^{3/2} T_{LI}^{5/2}}{4\pi r_c \ell_{cd} p_v h_{fg}^2 g_c^{1/2}} \quad (14)$$

$$R_{IE} = \left[1 + \frac{Q}{Q_{MAX}} \right] \frac{(2\pi)^{1/2} R^{3/2} T_{LI}^{5/2}}{4\pi r_c \ell_E p_v h_{fg}^2 g_c^{1/2}} \quad (15)$$

The resistance of the vapor is computed by assuming fully developed laminar flow and accounting for the obstruction presented by the slab with a hydraulic diameter.

$$R_V = \frac{8 \mu_v \ell_{eff} T_V \left(\frac{1}{\rho_v} - \frac{1}{\rho_\ell} \right)}{\pi \rho_v h_{fg}^2 r_{CHD}} \quad (16)$$

$$r_{CHD} = \frac{\pi r_C^2 - 2 r_C \delta_T}{2\pi r_C - 2 \delta_T + 4 r_C} \quad (17)$$

Hare (reference 1) has developed equations, based on National Bureau of Standards data, which give nitrogen properties and stainless steel properties in the temperature range of 60°K to 125°K.

Vapor Pressure [lb_f/ft²]

$$p_v = 1.71041 \times 10^{-6} (T)^5 - 1.20901 \times 10^{-3} (T)^4 + 3.71275 \times 10^{-1} (T)^3 - 5.70868 \times 10 (T)^2 + 4.28513 \times 10^3 (T) - 1.25125 \times 10^5 \quad (18)$$

Density of Liquid and Vapor [lb_m/ft³]

$$\rho_\ell = - 5.8917 \times 10^{-13} (T)^7 + 4.50297 \times 10^{-10} (T)^6 - 1.15298 \times 10^{-7} (T)^5 + 4.95327 \times 10^{-6} (T)^4 + 2.9749 \times 10^{-3} (T)^3 - 5.98552 \times 10^{-1} (T)^2 + 4.54425 \times 10 (T) - 1.21455 \times 10^3 \quad (19)$$

$$\begin{aligned}\rho_v = & 1.39324 \times 10^{-13} (T)^7 - 1.042325 \times 10^{-10} (T)^6 + 2.638736 \times 10^{-8} (T)^5 \\ & - 1.14015 \times 10^{-6} (T)^4 - 6.78395 \times 10^{-4} (T)^3 + 1.385389 \times 10^{-1} (T)^2 \\ & - 1.07628 \times 10 (T) + 3.10045 \times 10^2\end{aligned}\quad (20)$$

Viscosity of Vapor and Liquid $[(lb_f - sec)/ft^2]$

$$\begin{aligned}\mu_v = & 8.55910 \times 10^{-21} (T)^7 - 6.55918 \times 10^{-18} (T)^6 + 1.70105 \times 10^{-15} (T)^5 \\ & - 8.08553 \times 10^{-14} (T)^4 - 4.27309 \times 10^{-11} (T)^3 + 8.90377 \times 10^{-9} (T)^2 \\ & - 6.94007 \times 10^{-7} (T) + 1.99577 \times 10^{-5}\end{aligned}\quad (21)$$

$$\begin{aligned}\mu_l = & 4.48282 \times 10^{-14} (T)^4 + 2.34251 \times 10^{-11} (T)^3 \\ & - 3.55312 \times 10^{-9} (T)^2 + 3.14221 \times 10^{-8} (T) + 2.16226 \times 10^{-5}\end{aligned}\quad (22)$$

Thermal Conductivity of Liquid Nitrogen $[\frac{Btu}{hr ft ^\circ R}]$

$$\begin{aligned}k_l = & 1.0970566 \times 10^{-11} (T)^5 - 9.2427627 \times 10^{-9} (T)^4 + 3.090593 \times 10^{-6} (T)^3 \\ & - 5.1457532 \times 10^{-4} (T)^2 + 4.2210737 \times 10^{-2} (T) - 1.26105\end{aligned}\quad (23)$$

Heat of Vaporization $[Btu/lb_m]$

$$\begin{aligned}h_{fg} = & - 4.11334 \times 10^{-11} (T)^6 + 2.0908 \times 10^{-8} (T)^5 - 1.43119 \times 10^{-6} (T)^4 \\ & - 1.03235 \times 10^{-3} (T)^3 + 2.61594 \times 10^{-1} (T)^2 - 2.40246 \times 10 (T) \\ & + 8.89614 \times 10^2\end{aligned}\quad (24)$$

Surface Tension $[lb_f/ft]$

$$\begin{aligned}\sigma = & 6.70239 \times 10^{-12} (T)^4 - 4.60497 \times 10^{-9} (T)^3 + 1.19096 \times 10^{-6} (T)^2 \\ & - 1.44813 \times 10^{-4} (T) + 7.58324 \times 10^{-3}\end{aligned}\quad (25)$$

Ratio of Specific Heats of Nitrogen

$$k = 1.572403 \times 10^{-6} (T)^2 - 8.6844907 \times 10^{-4} (T) + 1.52913275\quad (26)$$

Thermal Conductivity of Stainless Steel $[Btu/ft hr ^\circ R]$

$$k_f = - 4.02016 \times 10^{-5} (T)^2 + 3.20878 \times 10^{-2} (T) + 1.30266\quad (27)$$

where T = temperature in degrees Rankine.

For any heat pipe of specific structure there are four primary variables directly related to the thermal properties of the heat pipe. These are T_E , T_C , T_V , and Q . Among these four variables any two are independent while the other two are dependent.

The present numerical procedure involves first specifying Q and T_C and then making use of the fundamental relationship of temperature, resistance, and heat transfer rate to calculate temperatures at several locations along the path of heat flow and to calculate the thermal resistance of the various sections of the heat pipe. The temperatures calculated are only approximate since the simple resistance equation

$$Q = \frac{\Delta T}{R}$$

is based on the assumption of constant conductivity across the heat flow path between the two locations at which the temperatures are known. This approximation should not lead to appreciable errors since the length of each heat flow path considered is small and consequently the value of ΔT is small.

The equations which results from applying this method cannot be solved analytically because of the presence of high order terms, so an iterative solution is necessary. The iteration process used in this analysis converges rapidly on the solution, partly as a result of knowing the range in which the solution lies, so that the computer time required for this portion of the numerical analysis is not large. The iterative procedure converged on the solution to an accuracy of 4 decimal places in an average of only 2 iterations.

An outline of the numerical procedure is now given

I. Specify Q and T_C

(Q will vary from 10 Watts to 30 Watts)

(T_C will range from 60°K to 125°K)

Approximation: $T_{LI} \cong T_V$

This is an excellent approximation since the resistance of the liquid-vapor interface is extremely small. (R_I is typically about 0.0001 °K/Watt)

The properties of each section will be evaluated at a temperature which is the mean of the temperature of the boundaries of the section.

Algebraic manipulation of the equation $Q = (T_{PCI} - T_C)/R_{PC}$ yields

$$\begin{aligned} \frac{\alpha_1}{4} T_{PCI}^3 + \left(\frac{\alpha_1 T_C}{2} + \frac{\alpha_2}{2} - \frac{\alpha_1 T_C}{4} \right) T_{PCI}^2 + \left(\frac{\alpha_1 T_C^2}{4} + \frac{\alpha_2 T_C}{2} + \alpha_3 - \frac{\alpha_1 T_C^2}{2} - \frac{T_C \alpha_2}{2} \right) T_{PCI} \\ + \left(-\frac{\alpha_1}{4} T_C^3 - \frac{\alpha_2}{2} T_C^2 - \alpha_3 T_C - \frac{Q_{MX}}{2\pi\ell_{cd}} \ln \frac{r_A}{r_B} \right) = 0 \end{aligned} \quad (28)$$

$$\text{where } \alpha_1 = -4.02016 \times 10^{-5} \quad \alpha_2 = 3.20878 \times 10^{-2} \quad \alpha_3 = 1.30266$$

II. Solve equation 28 for T_{PCI} .

III. Assume a value for T_V and compute $T' = (T_V + T_{PCI})/2$.

IV. Compute k_ℓ from equation 23 for $T = T'$.

V. Compute k_f from equation 27 for $T = T'$.

VI. Compute k_w from equation 11.

VII. Compute $\sum_{n=1}^N R_n$ from equation 6.

VIII. Compute $\sum_{n=1}^{N-1} R_{n,\ell}$ from equation 7.

IX. Solve Equation 29 for T_V using linear interpolation method, repeating steps IV, V, AND VI.

$$\frac{T_V - T_{PCI}}{Q \sum_{n=1}^N R_n + Q \sum_{n=1}^{N-1} R_{n,\ell}} - 1 = 0 \quad (29)$$

- X. Compute R_{WC} from equation 5.
- XI. Take $T' = [T_{PEI} + T_V] / 2$.
- XII. Compute k_ℓ from equation 23 at T' .
- XIII. Compute k_f from equation 27 at T' .
- XIV. Compute k_w from equation 11 at T' .
- XV. Assume values of T_{PEI} and determine T_{PEI} using iteration, repeating steps XI through XIV and using equation 30.

$$\frac{T_{PEI} - T_V}{Q \left[1 + \frac{Q}{Q_{MAX}} \right] \left\{ \sum_{n=1}^N R_n + \sum_{n=1}^{N-1} R_{n,\ell} \right\}} - 1 = 0 \quad (30)$$

- XVI. Compute R_{WE} from equation 8.
- XVII. Solve equation 31 for T_E .

Substituting metal conductivity equation into $Q = (T_E - T_{PEI})/R_{PE}$ gives

$$\begin{aligned} & \frac{\alpha_1}{4} T_E^3 + \left(-\frac{\alpha_1}{4} T_{PEI} + \frac{\alpha_1}{2} T_{PEI} + \frac{\alpha_2}{2} \right) T_E^2 \\ & + \left(-\frac{\alpha_1}{2} T_{PEI}^2 - \frac{\alpha_2}{2} T_{PEI} + \frac{\alpha_1}{4} T_{PEI}^2 + \frac{\alpha_2}{2} T_{PEI} + \alpha_3 \right) T_E \\ & + \left(-\frac{\alpha_1}{4} T_{PEI}^3 - \frac{\alpha_2}{2} T_{PEI}^2 - \alpha_3 T_{PEI} - \frac{Q \ln \frac{r_A}{r_B}}{4\theta \ell_E} \right) = 0 \end{aligned} \quad (31)$$

- XVIII. Compute k_{pE} from equation 27.

- XIX. Compute R_{PE} from equation 13.
- XX. Compute h_{fg} from equation 24 at $T = T_V$
- XXI. Compute p_v from equation 18 at $T = T_V$
- XXII. Compute R_{IC} from equation 14 at $T = T_V$
- XXIII. Compute R_{IE} from equation 15.
- XXIV. Let $\ell_{eff} = 3.0 \text{ ft} - \ell_E/2 - (\ell_{cd}/2)Q/Q_{MAX}$.
- XXV. Compute μ_v from equation 21.
- XXVI. Compute ρ_v from equation 18.
- XXVII. Compute ρ_ℓ from equation 19.
- XXVIII. Compute R_V from equation 16.
- XXIX. Compute $R_{TOT} = R_{PE} + R_{WE} + R_{IE} + R_V + R_{IC} + R_{WC} + R_{PC}$ and alternate equation $R_{TOT} = (T_E - T_C)/Q$.

The complete computer program is given in Appendix A.

The effects on thermal resistance of changing the size of liquid gaps, wall thickness, mesh size, and number of circumferential layers of capillary structure has been examined on the computer for a nitrogen heat pipe. Table I shows some of the geometries studied. Figures 5 through 21 show how temperature difference and resistance change with changes in operating temperature and heat flux for the cases described in Table I.

Several figures related to Cases 1 and 6 are included to show order of magnitudes for resistances for these two extreme cases. Only one plot is given for each of the other cases. It is interesting to note that overall temperature difference may increase or decrease with increasing vapor temperature at constant heat flux. For example in Case 1 the heat pipe temperature difference increases as the vapor temperature increases while just the opposite is true in Case 6.

Case #	Wall Thickness(mm)	Mesh Size	Filament Radius(mm)	Distance Between Filament Centers	Number of Screen Layers	Thickness of Fluid Layers(mm)
1	1.0150	400	0.0155	0.06919	2	0.03048
2	0.3968	400	0.0155	0.06919	2	0.03048
3	2.0300	400	0.0155	0.06919	2	0.03048
4	1.0150	250	0.0241	0.1198	2	0.03048
5	1.0150	100	0.0815	0.2937	2	0.03048
6	1.0150	400	0.0155	0.06919	1	---
7	1.0150	400	0.0155	0.06919	3	0.03048
8	1.0150	400	0.0155	0.06919	2	0.01524
9	1.0150	400	0.0155	0.06919	2	0.06096

Table I. Values of Parameters for Cases Considered in This Study

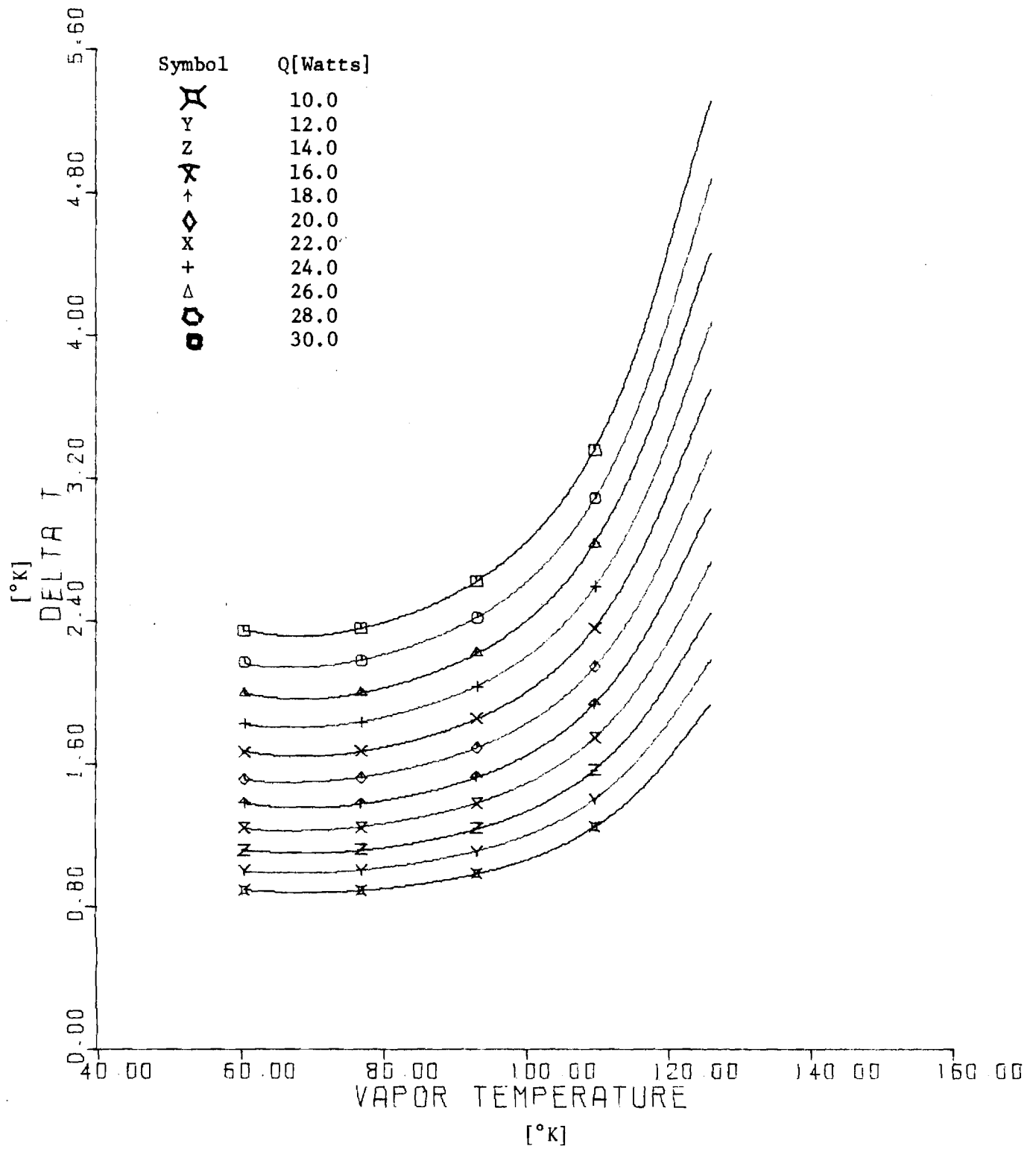


Figure 5. ΔT vs. T_v at constant Q - Case 1

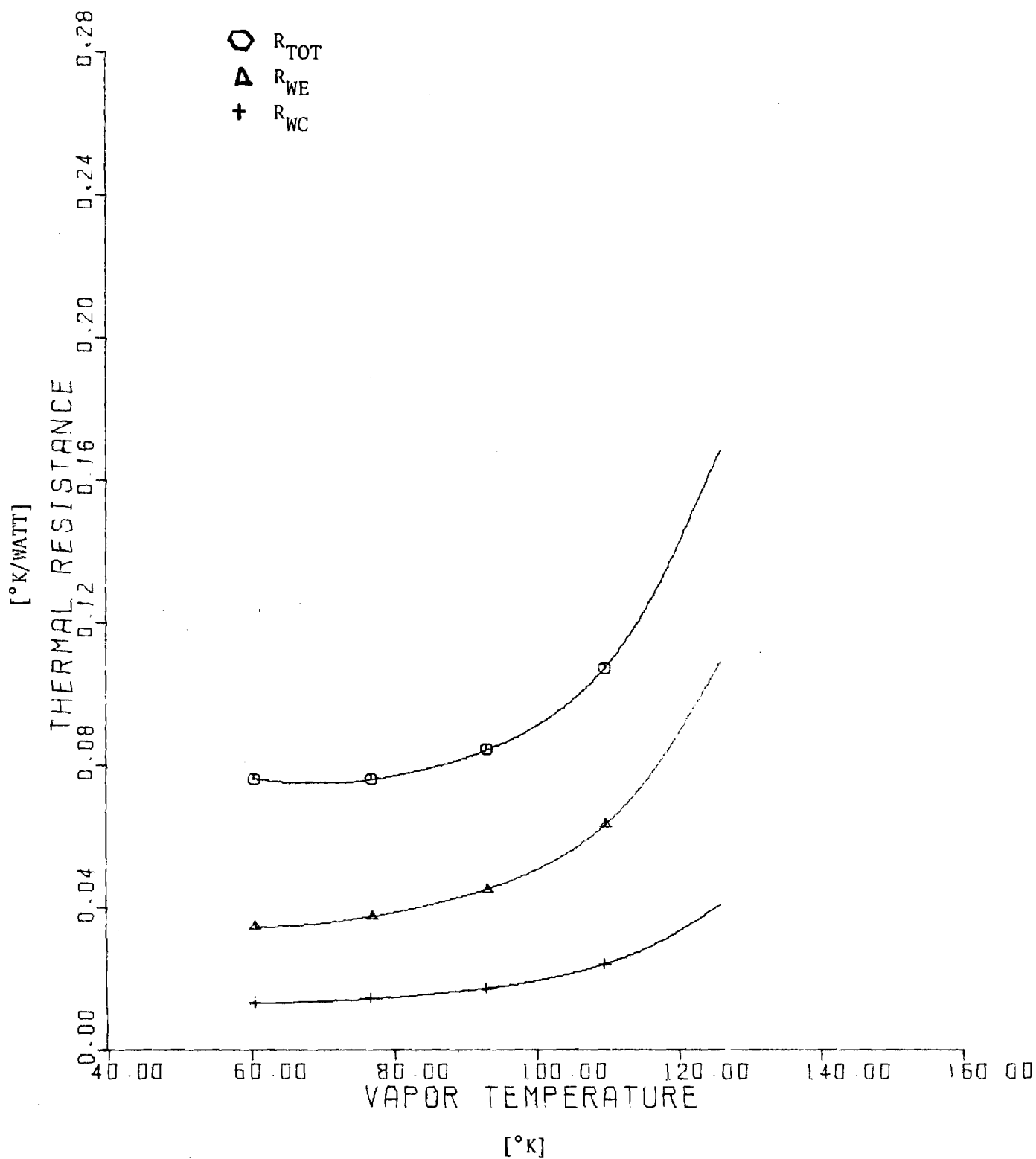


Figure 6. R_{TOT} , R_{WE} , R_{WC} vs. T_V for $Q = 22$ Watts - Case 1

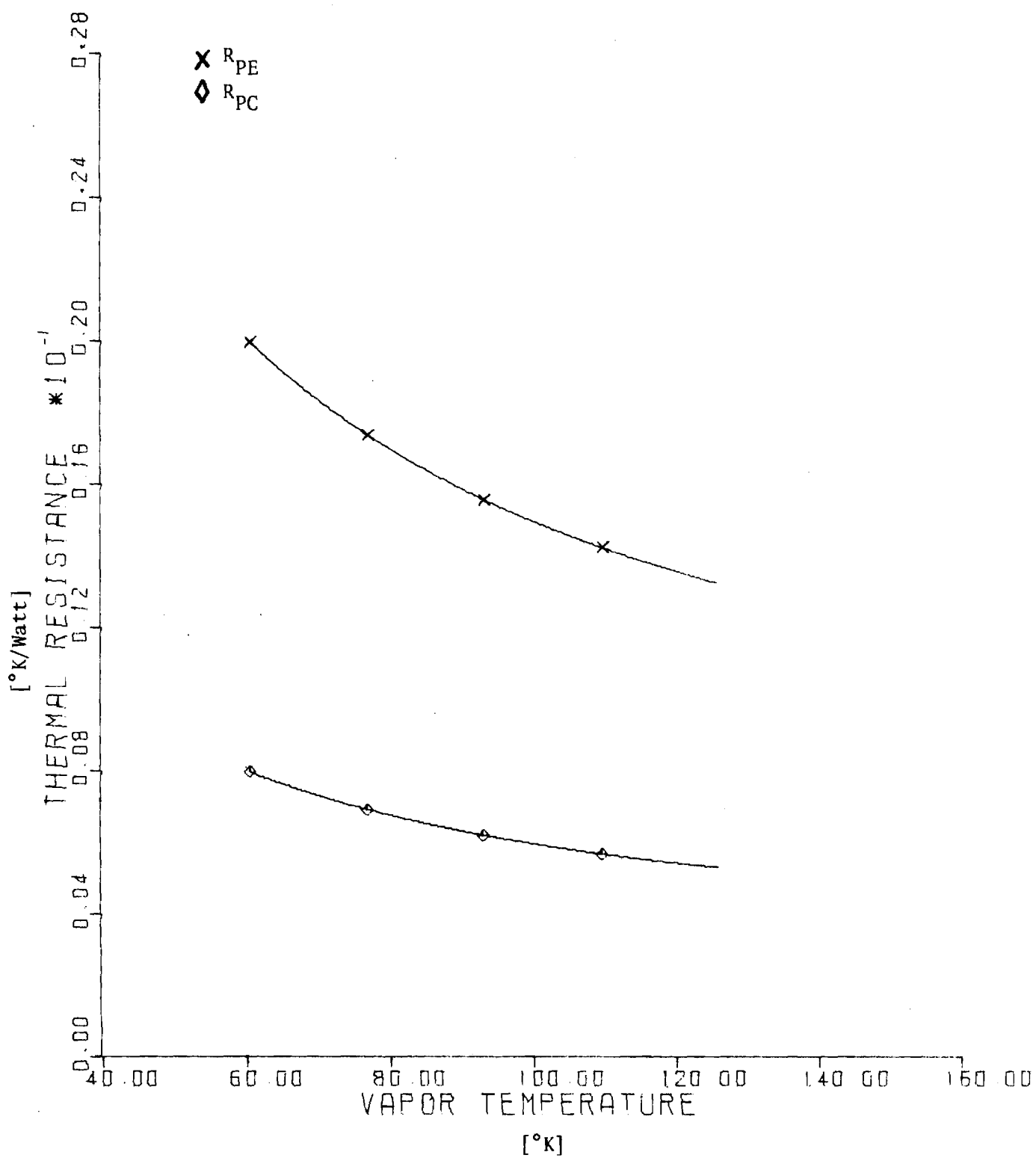


Figure 7. R_{PE} , R_{PC} VS. T_V for $Q = 22$ Watts - Case 1

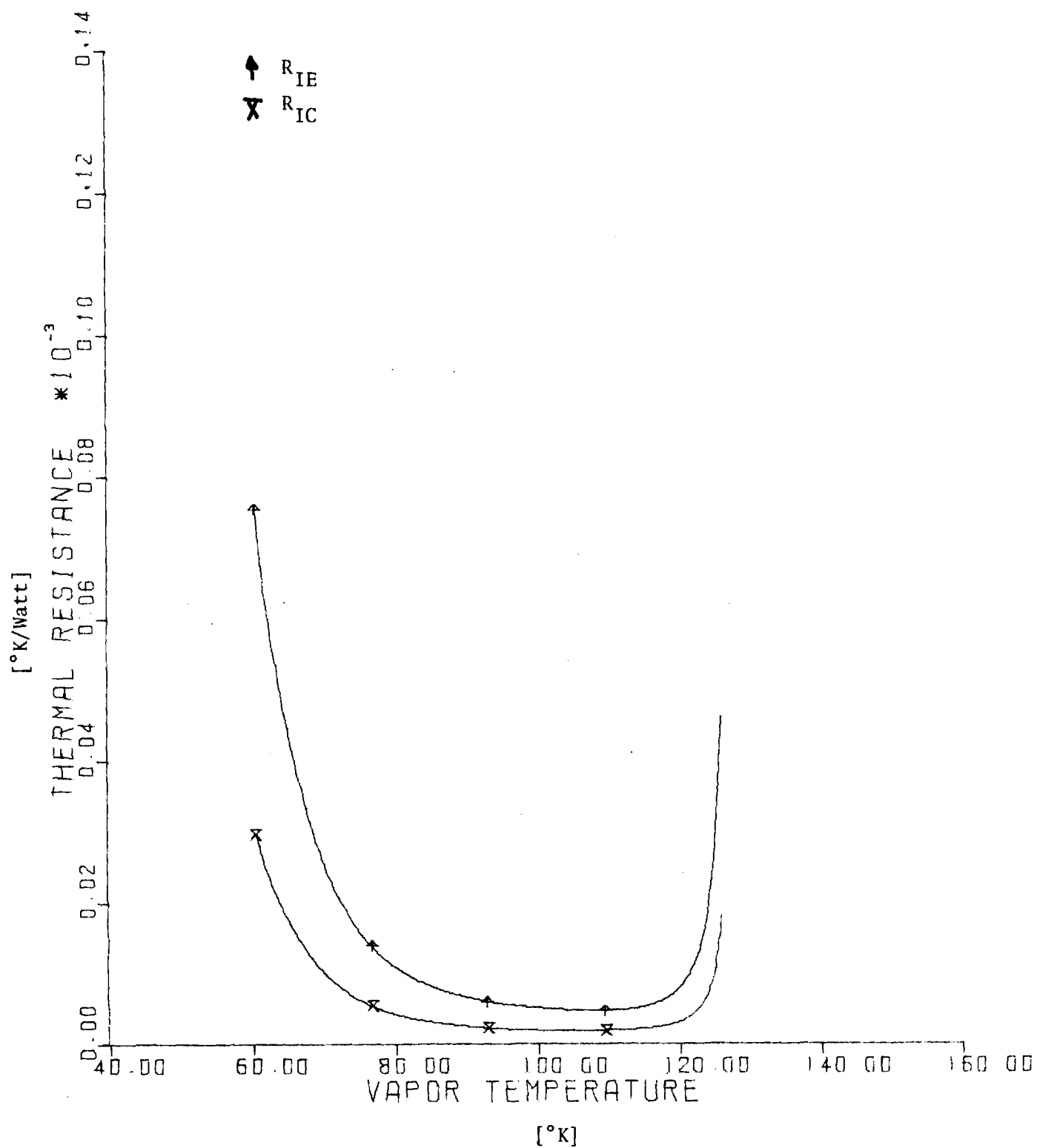


Figure 8. R_{IE} , R_{IC} VS. T_V for $Q = 22$ Watts - Case 1

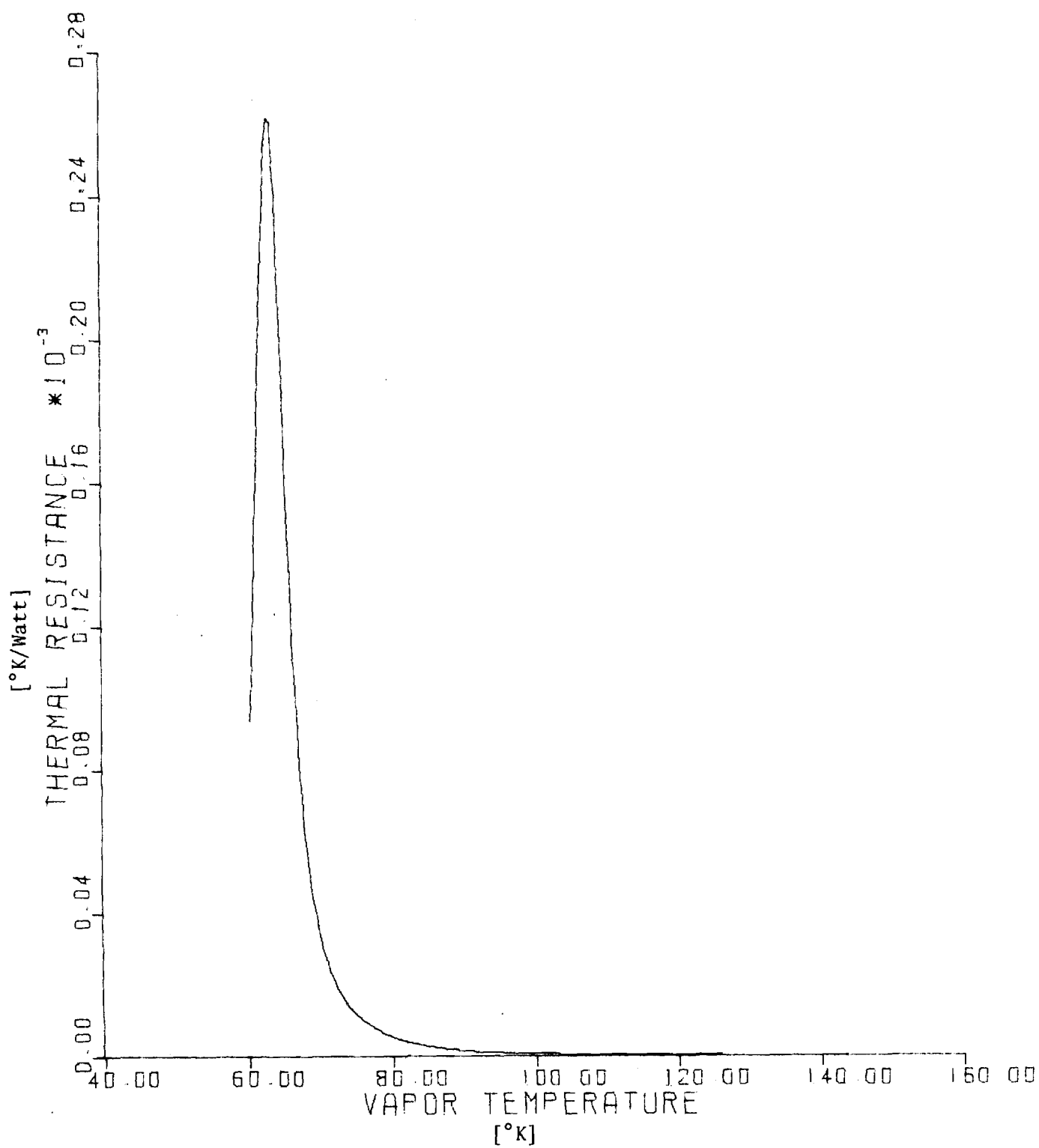


Figure 9. R_V VS. T_V for $Q = 22$ Watts - Case 1

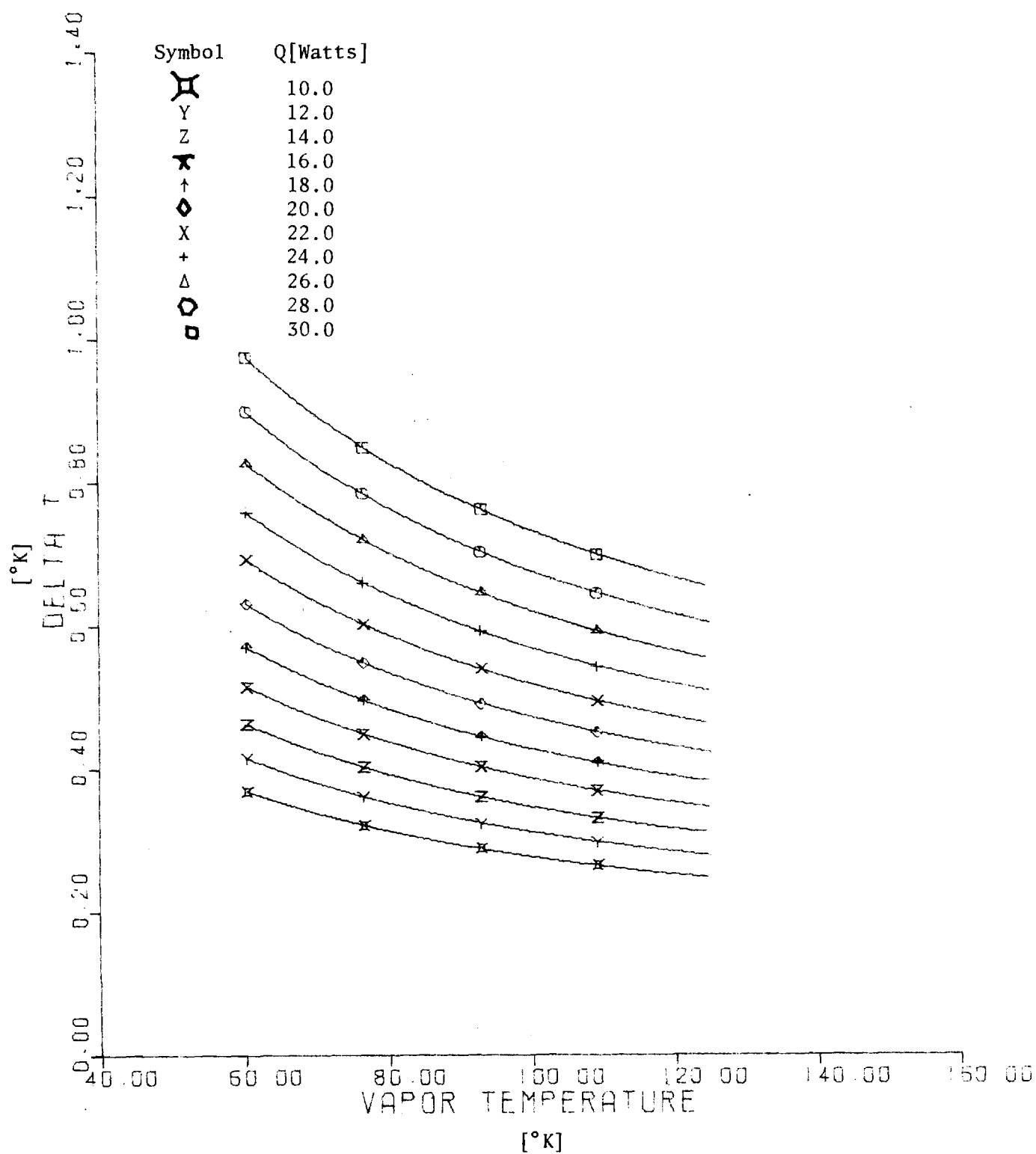


Figure 10. ΔT VS. T_v at Constant Q - Case 6

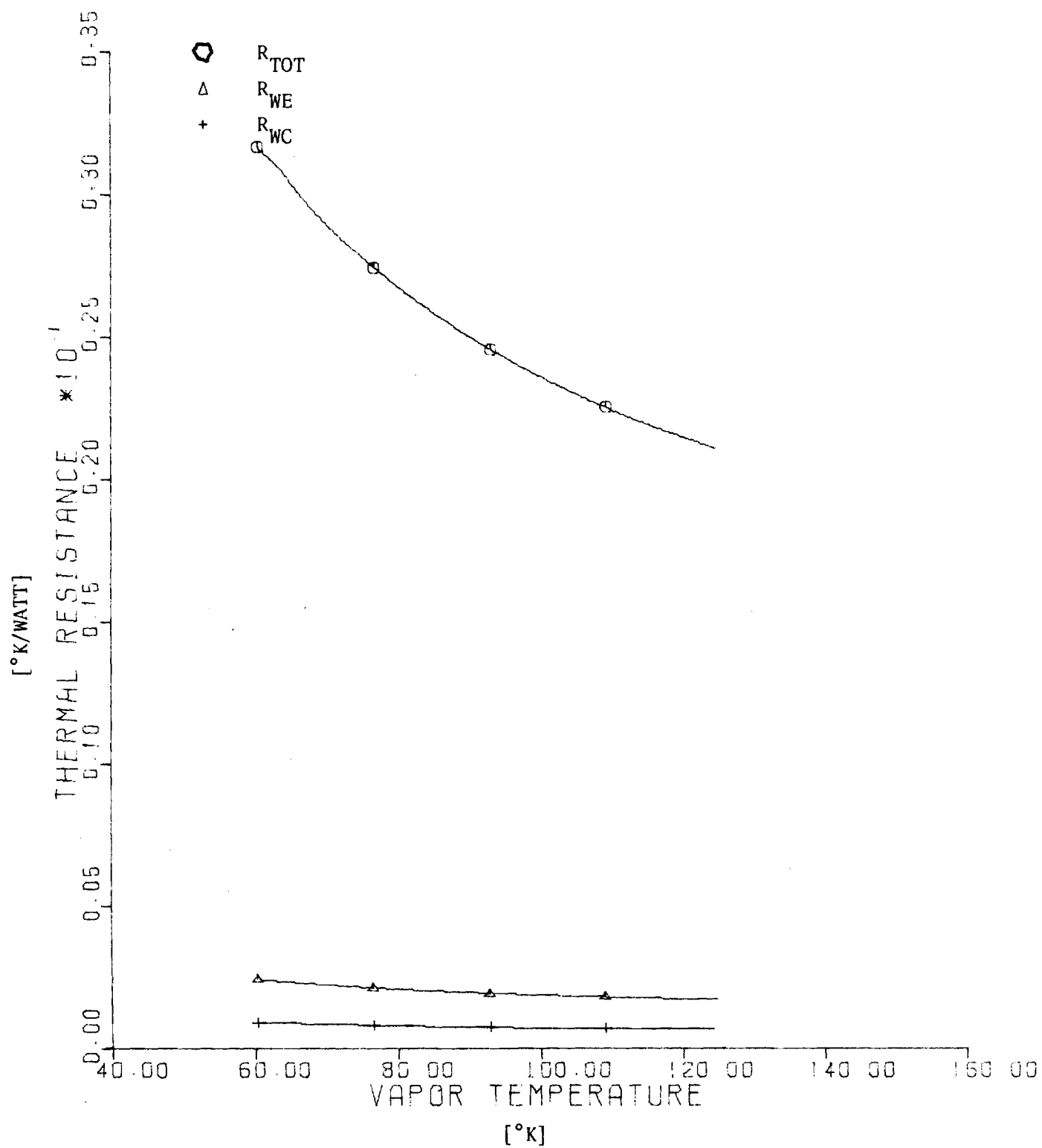


Figure 11. R_{TOT} , R_{WE} , R_{WC} VS. T_V for $Q = 22$ Watts - Case 6

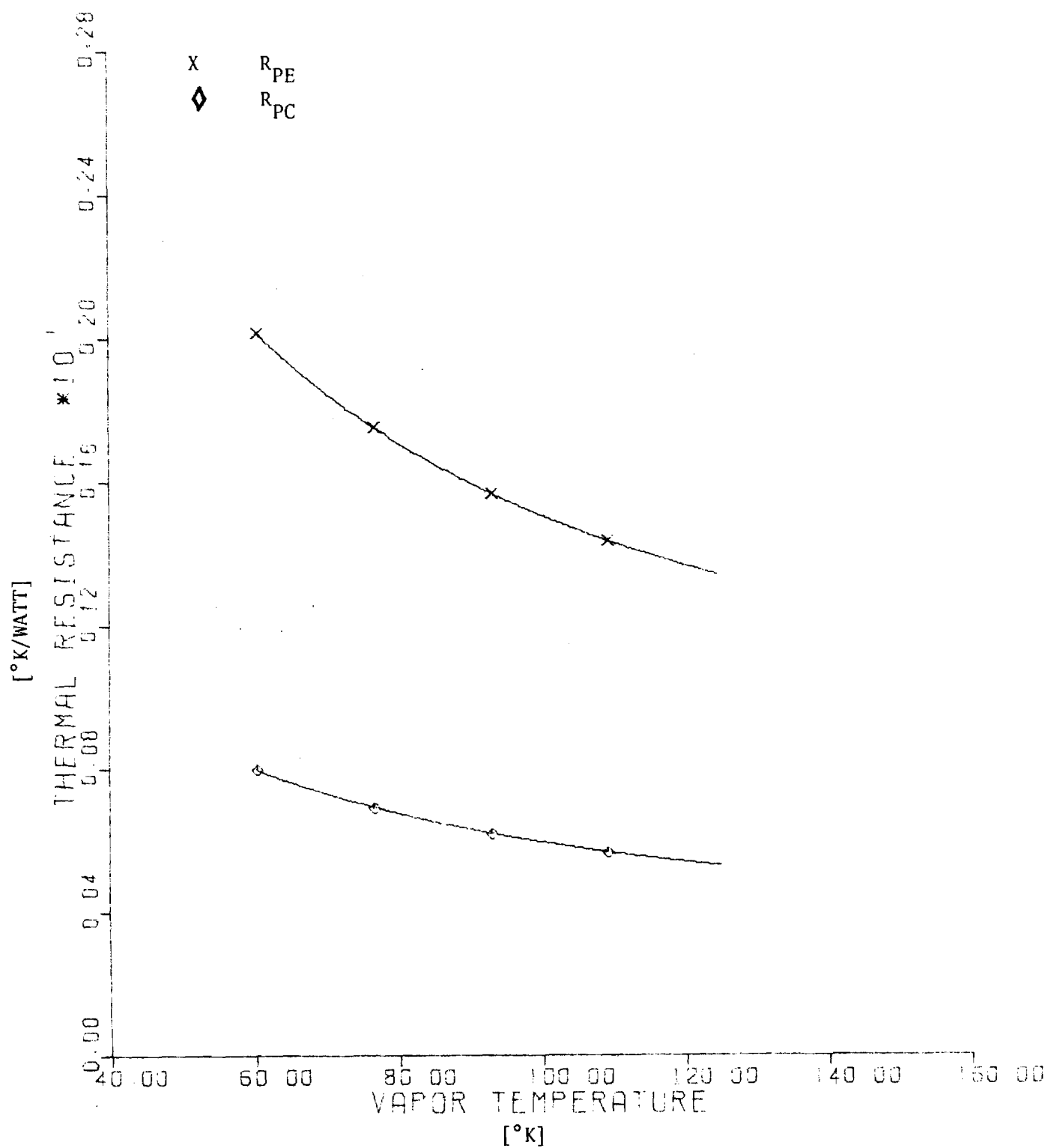


Figure 12. R_{PE} , R_{PC} VS. T_v for $Q = 22$ Watts - Case 6

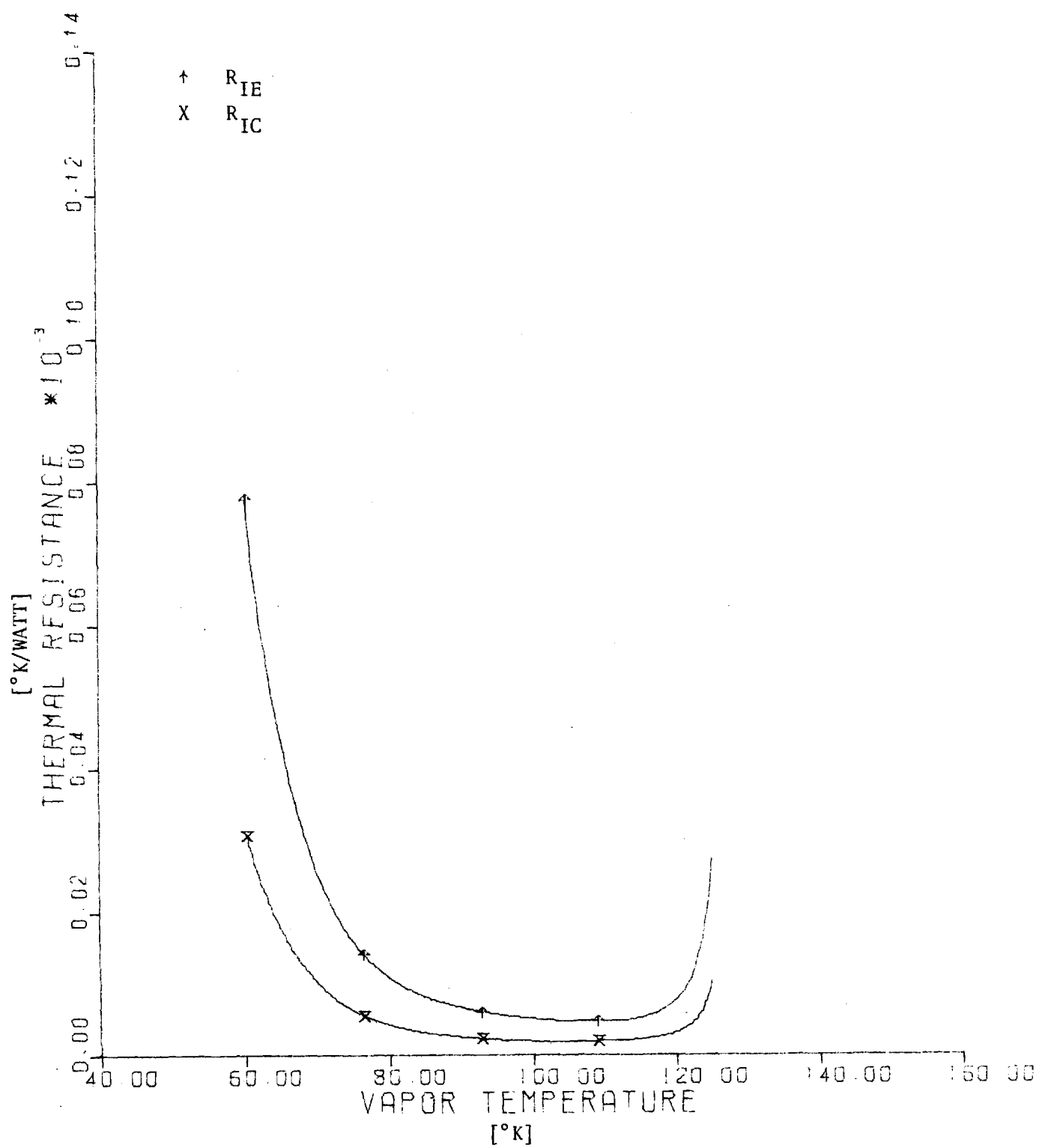


Figure 13. R_{IE} , R_{IC} VS. T_V for $Q = 22$ Watts - Case 6

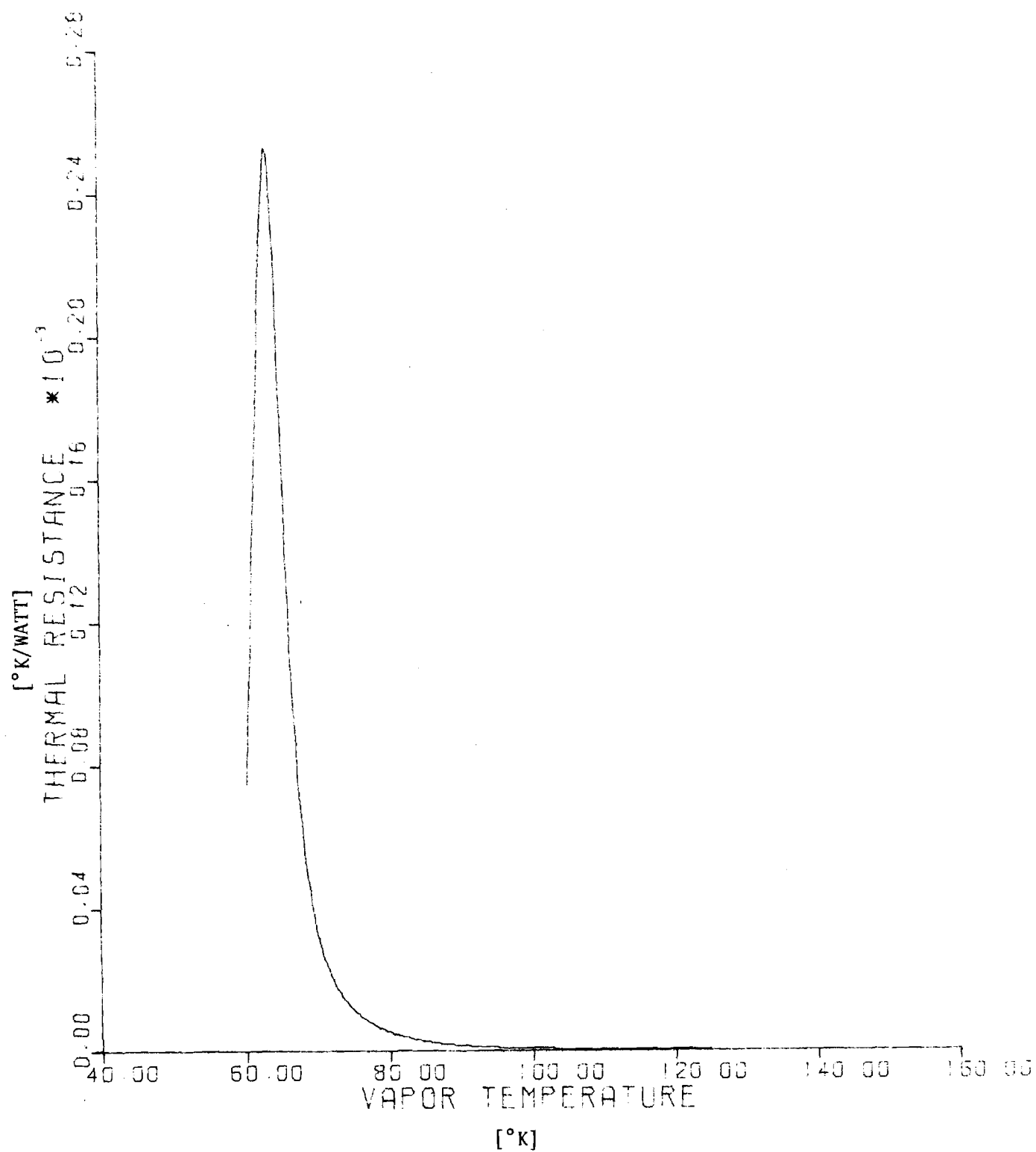


Figure 14. R_V VS. T_V for $Q = 22$ Watts - Case 6

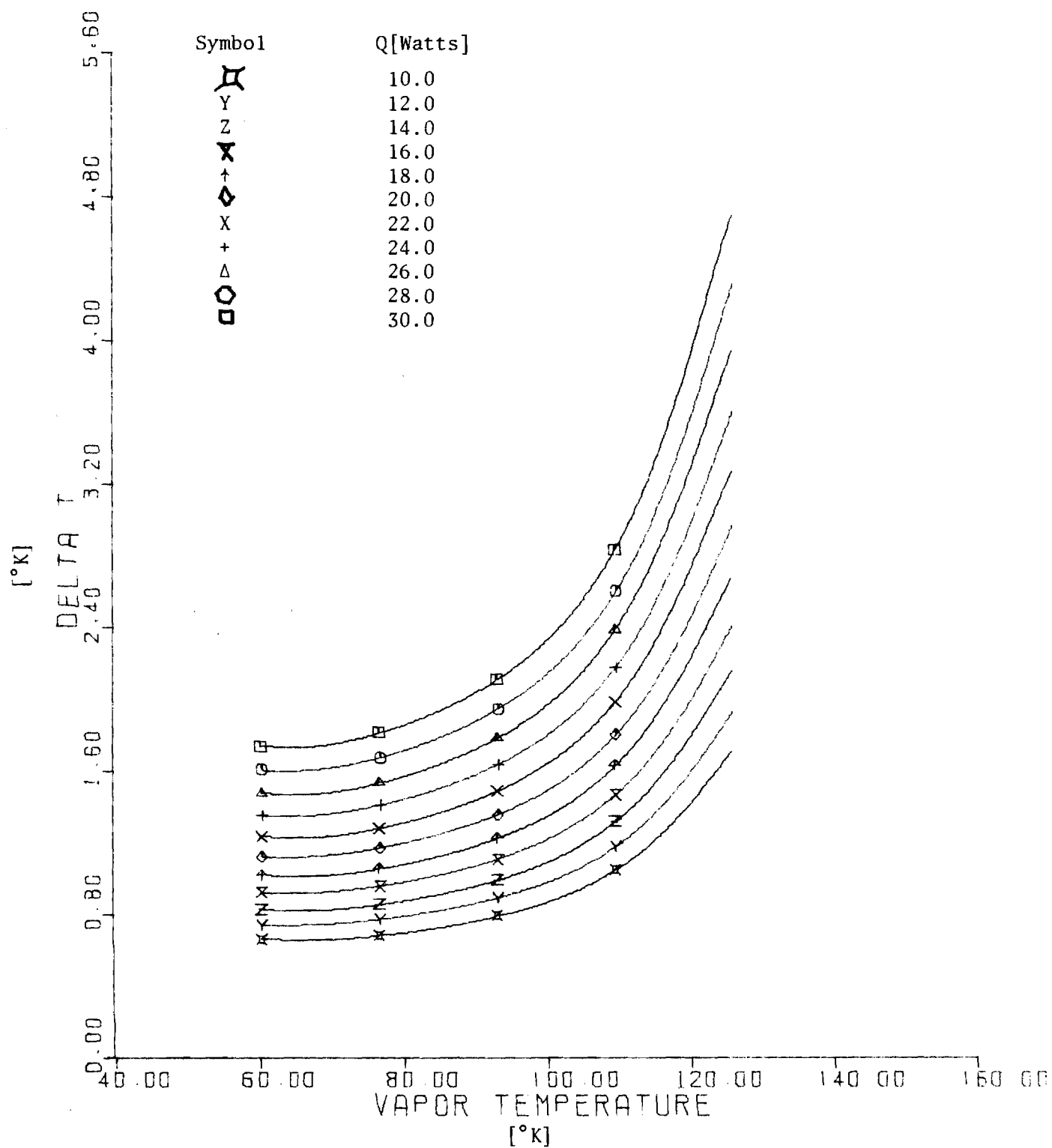


Figure 15. ΔT VS. T_v at Constant Q - Case 2

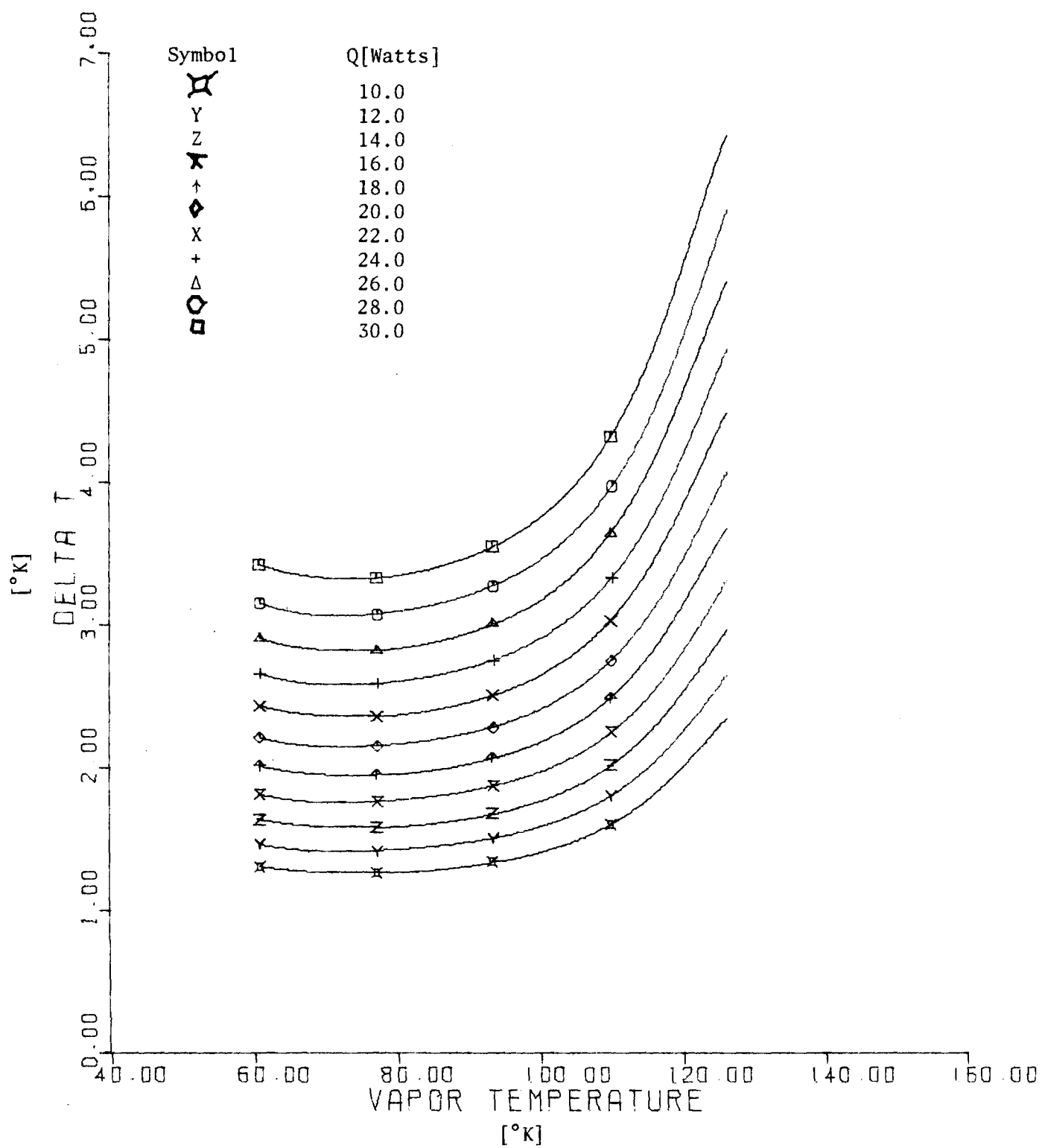


Figure 16. ΔT VS. T_V at Constant Q - Case 3

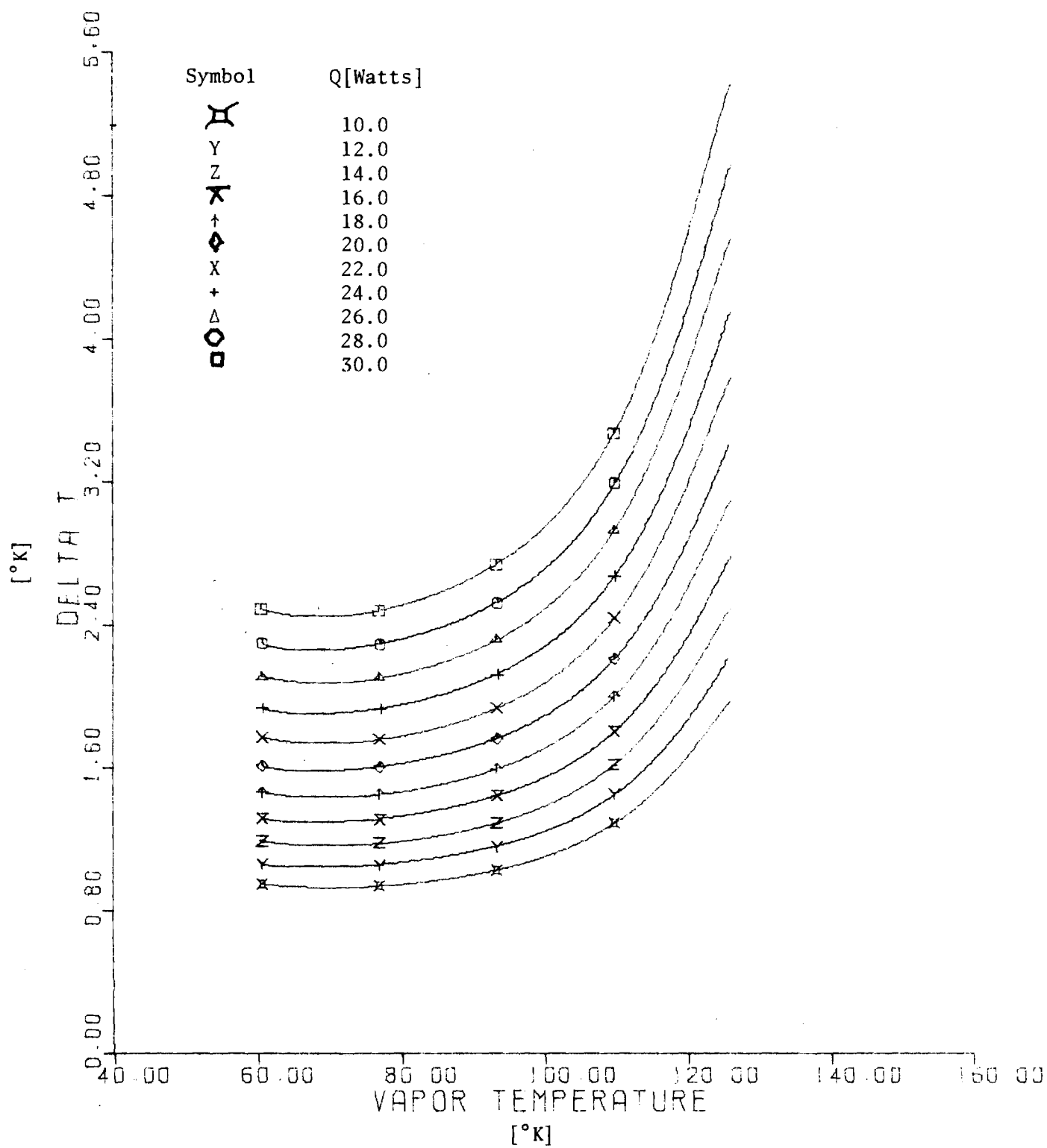


Figure 17. ΔT VS. T_V at Constant Q - Case 4

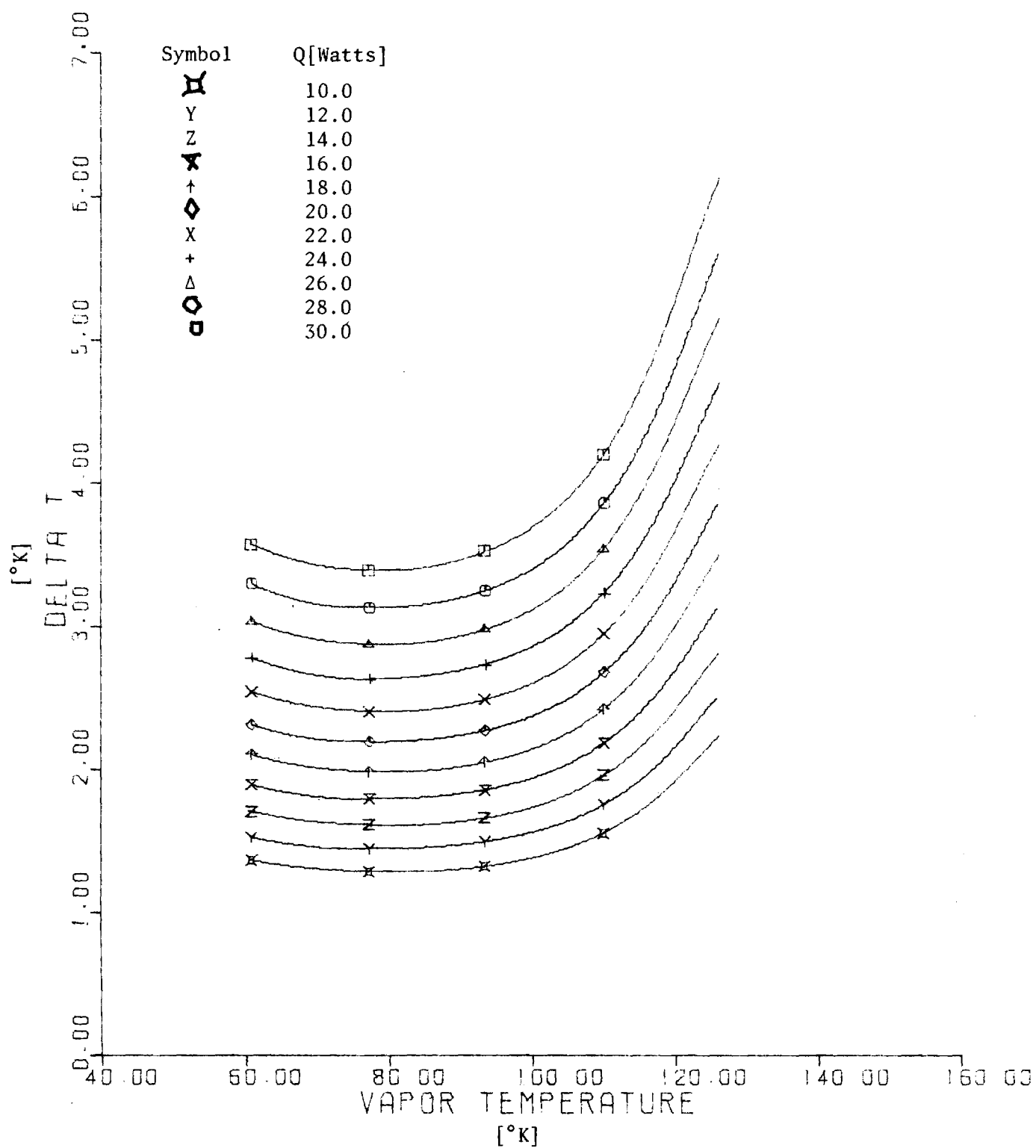


Figure 18. ΔT VS. T_V at Constant Q - Case 5

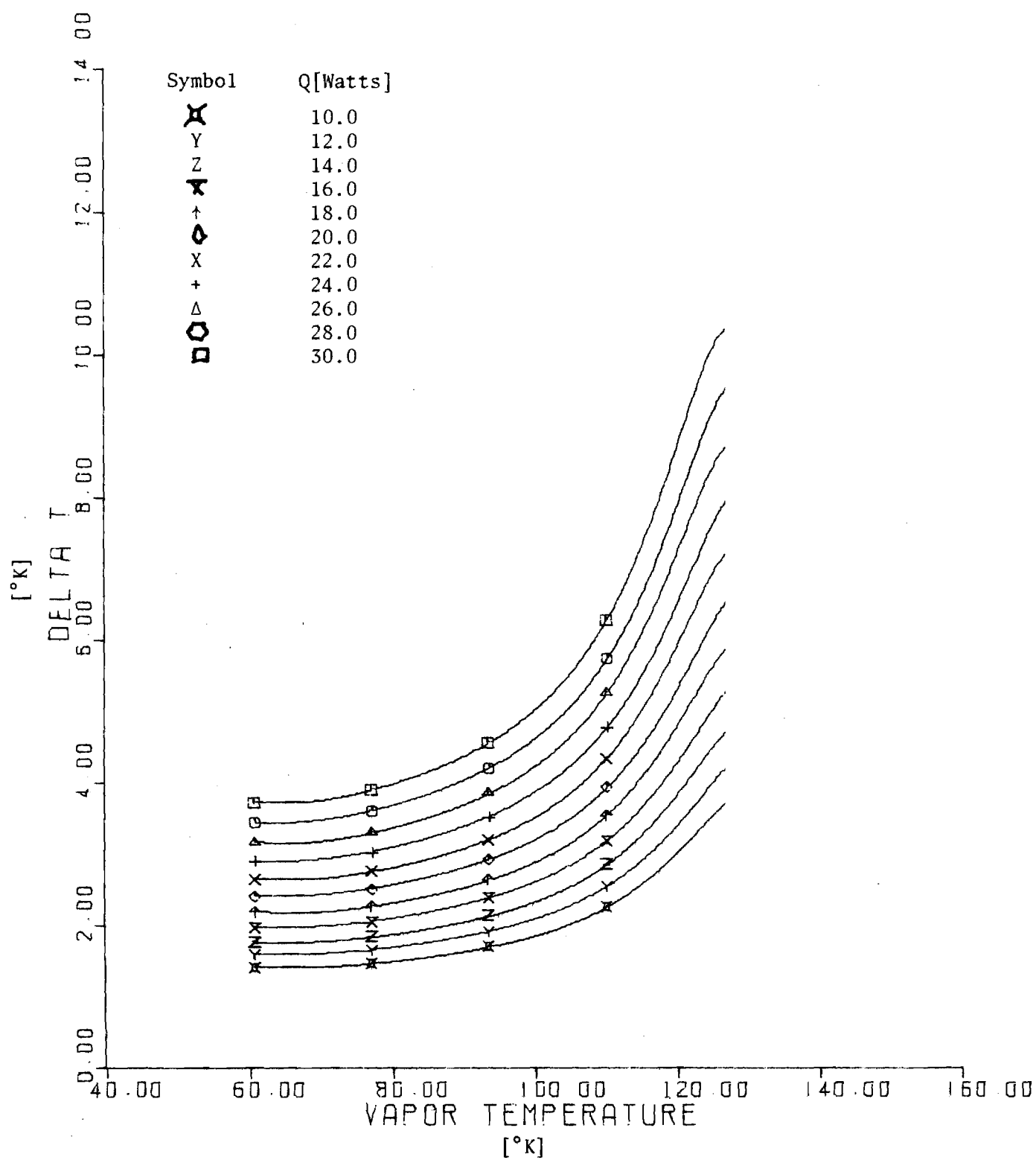


Figure 19. ΔT VS. T_v at Constant Q - Case 7

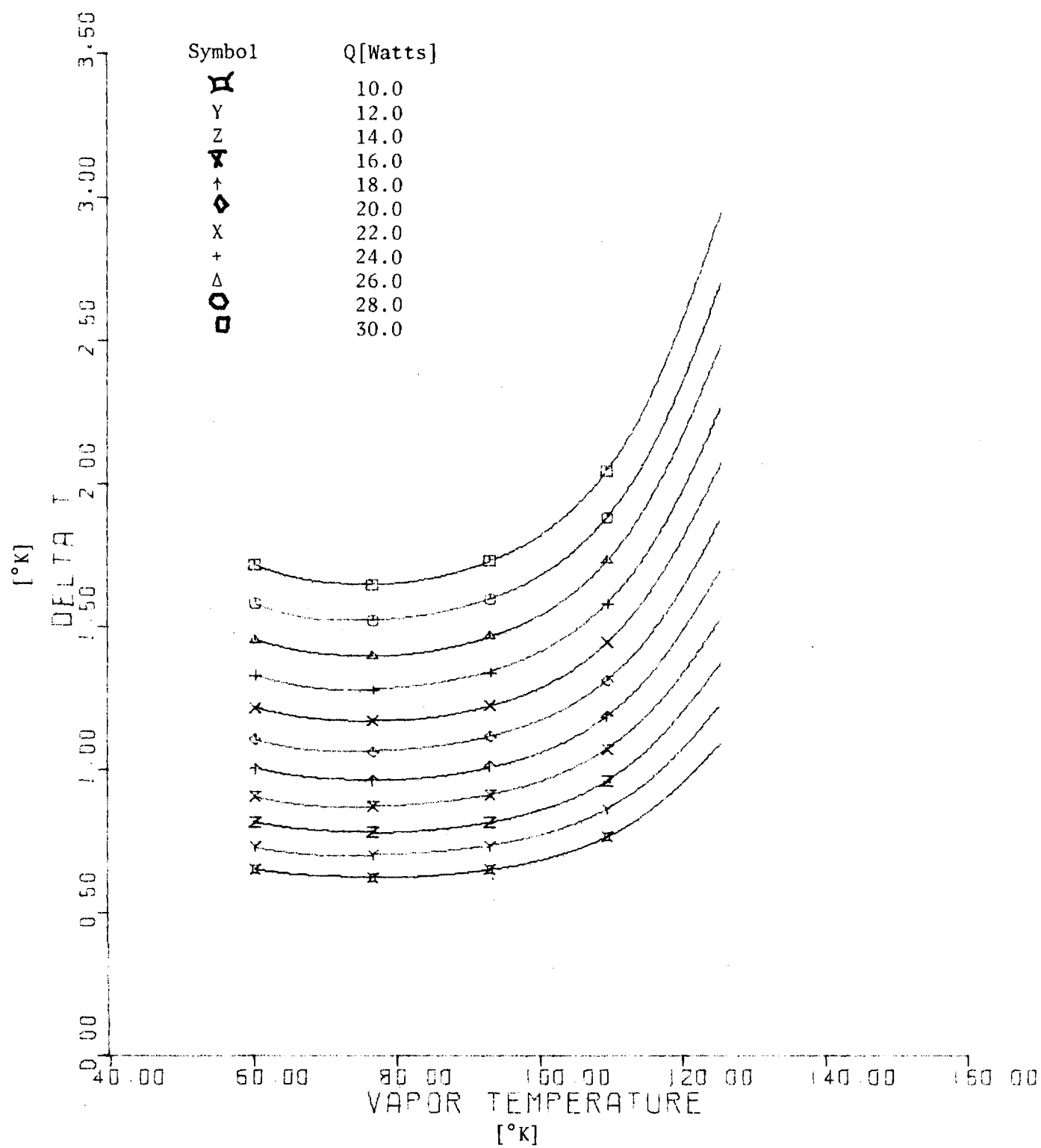


Figure 20. ΔT VS. T_v at Constant Q - Case 8

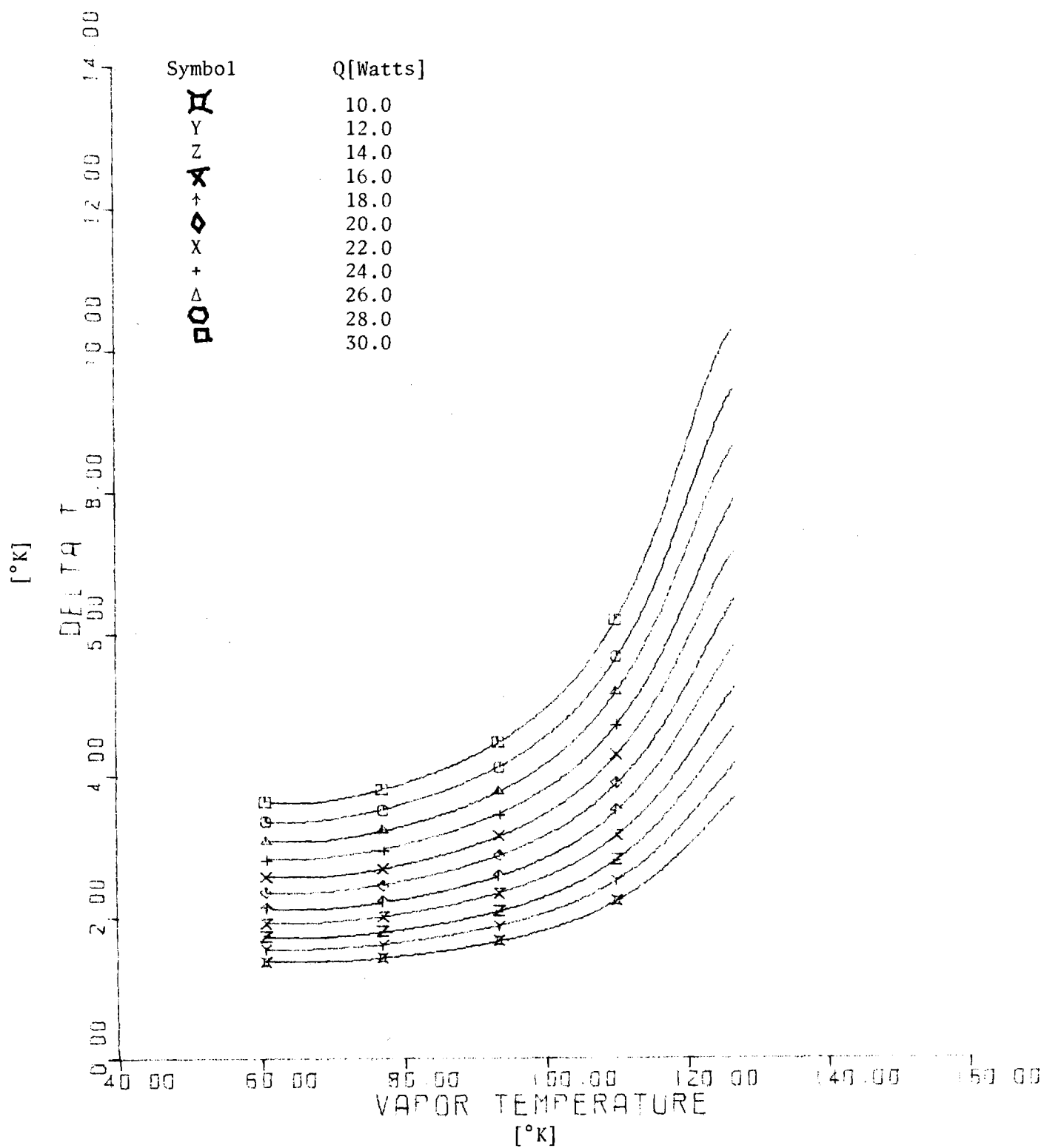


Figure 21. ΔT VS. T_V at Constant Q - Case 9

The reason for these different trends is that the thermal conductivity of liquid nitrogen decreases with increasing temperature while the conductivity of stainless steel increases with increase in temperature. In Case 1 the conductivity of the metal controls the effective conductivity of the fluid metal combination whereas in Case 6, the liquid nitrogen controls the effective conductivity of the combination.

Capillary Limitations

Writing momentum, energy and continuity equations for steady operation of the model heat pipe at capillary limited heat transfer and making the standard simplifying assumptions the following equation is obtained.

$$\dot{Q}_{CL} = \frac{2N/r_p}{\frac{\bar{K} \ell_{eff}}{b \delta_T} + \frac{K_C L}{4n_C \delta_C} \left(\frac{1}{\ell_e} + \frac{1}{\ell_c} \right) + \frac{8\mu_V \rho_L \ell_{eff}}{\pi \mu_L \rho_V r_V^4}} \quad (32)$$

where

\dot{Q}_{CL} = Capillary limited heat transfer rate

$$N = \frac{\sigma h_{fg} \rho_L}{\mu_L} = \text{"Heat Pipe Number"}$$

σ = surface tension of liquid

h_{fg} = heat of vaporization

ρ_L = liquid density

μ_L = liquid dynamic viscosity

r_p = pore radius at evaporator surface

$$\bar{K} = \frac{\delta_T}{\frac{n_A \delta_A}{K_A} + \frac{n_B \delta_B}{K_B}} = \text{effective inverse permeability for slab based on approach velocity.}$$

δ_T = total thickness of slab

n_A = number of layers of fine mesh in slab

n_B = number of layers of coarse mesh in slab

δ_A = thickness of a single layer of material A

δ_B = thickness of a single layer of material B

K_A = inverse permeability for material A based on approach velocity

K_B = inverse permeability for material B based on approach velocity

ℓ_{eff} = effective length of liquid path in slab

b = width of slab

K_c = inverse permeability for material at evaporator and condenser surfaces based on approach velocity

L = average distance traveled by liquid in circumferential capillary structure at evaporator or condenser (approximately 45° arc)

n_c = number of layers of capillary material on circumference

δ_c = thickness of a single layer of material C

ℓ_e = axial length of evaporator section

ℓ_c = axial length condenser section

μ_v = dynamic viscosity of vapor

ρ_v = density of vapor

r_v = hydraulic radius of vapor space

Approximately one hundred different capillary arrangements were studied in order to determine capillary limitations. Table II shows geometric parameters for six of the combinations examined. Capillary limitations as a function of vapor temperature are shown in Figure 22 for each of the combinations listed in Table II.

Transient Analog Computer Studies

A rather simplified transient model of a cryogenic slab type heat pipe with radiator connected is shown in Figure 23. Due to limited analog computer capacity relatively few nodes were used. The equations written for this model are:

$$Q_e = \frac{2\pi \ell_e k_p}{\ln(r_A/r_B)} (T_e - T_1) + \frac{\rho_c c_{pe} V_p}{2} \frac{dT_e}{d\theta} \quad (33)$$

Table II. Description of Composite Wick Systems Considered in this Study

Wick Composition Number	Screen Mesh Size			Number of Layers			Screen Thickness - m			Total Thickness of Slab - m
	A	B	C	n_A	n_B	n_C	$\delta_A \times 10^4$	$\delta_B \times 10$	$\delta_C \times 10^4$	$\delta_T = n_A \delta_A + n_B \delta_B$
1	250	100	250	2	8	1	0.867	0.314	0.866	2.68
2	400	50	400	2	5	1	0.744	0.448	0.744	2.39
3	400	30	400	2	4	1	0.744	0.622	0.744	2.64
4	400	30	400	4	5	2	0.744	0.622	0.744	3.41

Wick Composition Number	Wire Diameter "C" Layer	Pore Radius "C" Layer	Inverse Permeability-1/m ²			Effective Permeability - 1/m ²
	m x 10 ⁴	m x 10 ⁴	$K_A \times 10^{-9}$	$K_B \times 10^{-7}$	$K_C \times 10^{-9}$	$\bar{K} = \delta_T / (\frac{n_A \delta_A}{K_A} + \frac{n_B \delta_B}{K_B}) \times 10^{-7}$
1	0.482	0.359	58.4	2,610	58.4	2,716
2	0.311	0.191	163	195	163	207
3	0.311	0.191	163	63.5	163	67.3
4	0.311	0.191	163	63.5	163	69.6

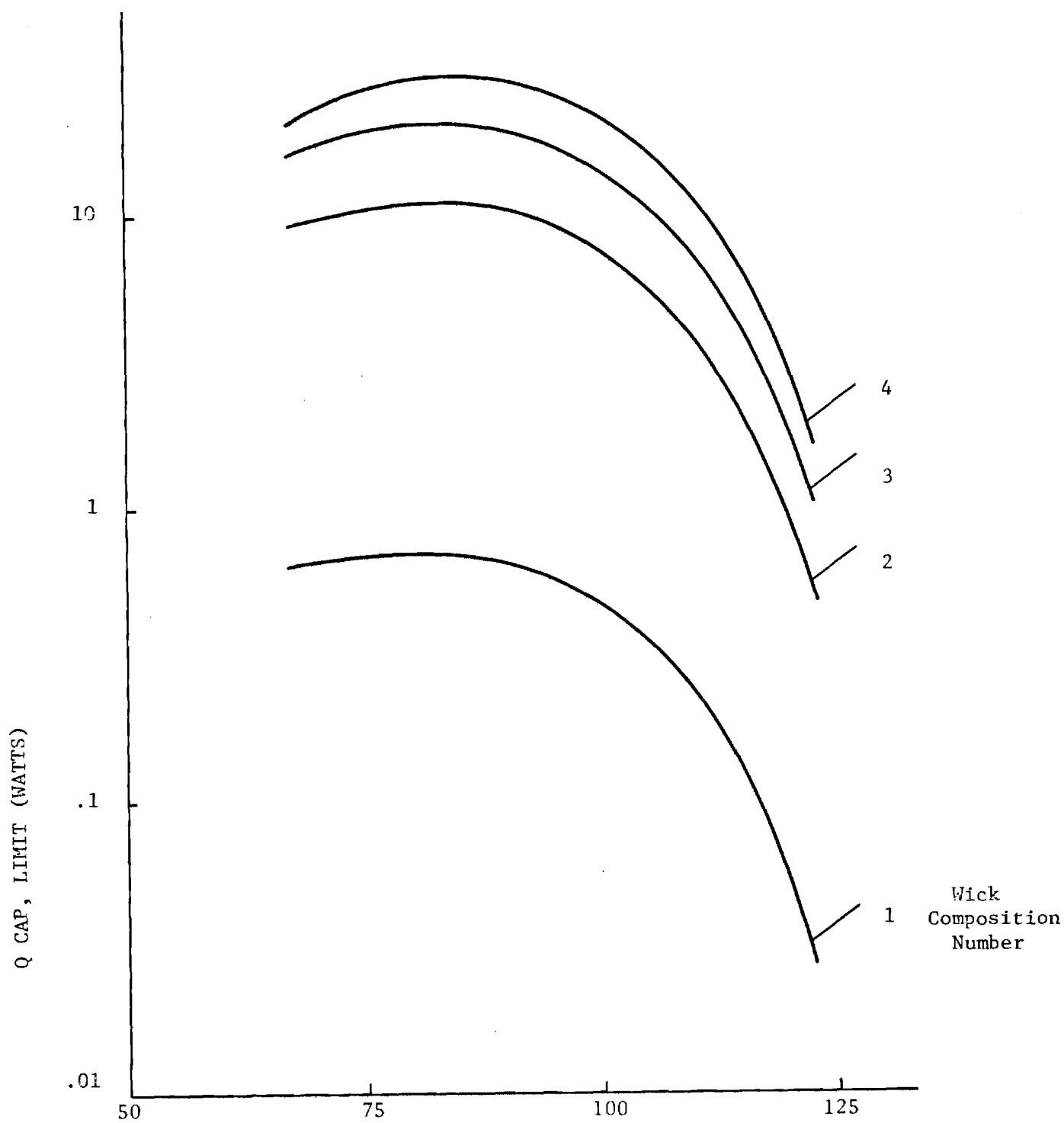


Figure 22. VAPOR TEMPERATURE (°K)

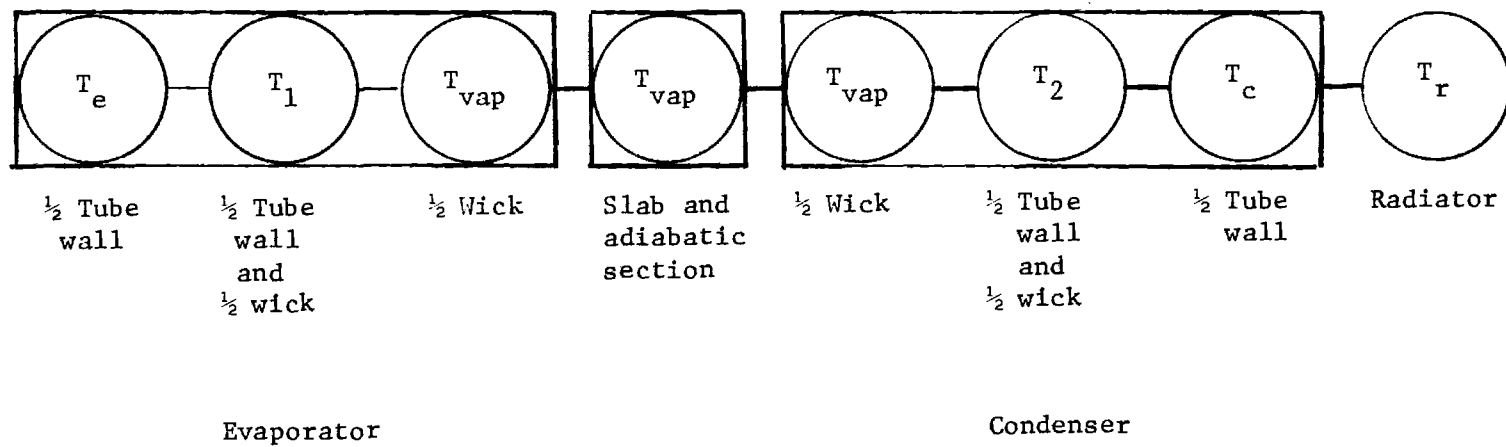


Figure 23 Analog Model

$$\begin{aligned} \frac{dT_1}{d\theta} = & \frac{4\pi \ell_e k_p}{[\rho_p c_{pe} V_p + \rho_w c_{we} V_p] \ln(r_A/r_B)} (T_e - T_1) \\ & + \frac{4\pi \ell_e k_w}{[\rho_p c_{pe} V_p + \rho_w c_{we} V_w] \ln(r_B/r_C)} (T_{vap} - T_1) \end{aligned} \quad (34)$$

$$\begin{aligned} \frac{dT_{vap}}{d\theta} = & \frac{4\pi k_w \ell_e}{[\rho_w c_{we} V_w + \rho_w c_{wc} V_w + 2m_a c_a] \ln(r_B/r_C)} (T_1 - T_{vap}) \\ & + \frac{4\pi k_w \ell_c}{[\rho_w c_{we} V_w + \rho_w c_{wc} V_w + 2m_a c_a] \ln(r_B/r_C)} (T_2 - T_{vap}) \end{aligned} \quad (35)$$

$$\begin{aligned} \frac{dT_2}{d\theta} = & \frac{4\pi k_w \ell_c}{[\rho_p c_{pc} V_p + \rho_w c_{wc} V_w] \ln(r_B/r_C)} (T_{vap} - T_2) \\ & + \frac{4\pi k_p \ell_c}{[\rho_p c_{pc} V_p + \rho_w c_{wc} V_w] \ln(r_A/r_B)} (T_c - T_2) \end{aligned} \quad (36)$$

$$\frac{dT_c}{d\theta} = \frac{4\pi k_p \ell_c}{\rho_p c_{pc} V_p \ln(r_A/r_B)} (T_2 - T_c) + \frac{4\pi r_a \ell_c}{\rho_p c_{pc} V_p R_c} (T_r - T_c) \quad (37)$$

$$\frac{dT_r}{d\theta} = \frac{2\pi r_a \ell_c}{m_r c_r} (T_c - T_r) - \frac{\epsilon A_r \sigma}{m_r c_r} T_r^4 + \frac{Q_{space}}{m_r c_r} \quad (38)$$

Limiters

$$(T_1 - T_{vap}) \leq \frac{Q_{CL} \ln(r_B/r_C)}{2\pi k_w \ell_e}$$

where

A_r = area of radiator

c_a = effective specific heat of adiabatic section and slab

c_p = specific heat of pipe material

c_r = specific heat of radiator

m_a = mass of adiabatic section and slab

m_r = mass of radiator

Q_e = heat flux into evaporator

Q_{space} = heat flux into radiator

Q_r = net heat flux from radiator

R_c = contact resistance between node c and node r

T_e = temperature node e

T_1 = temperature node 1

T_{vap} = temperature node vap

T_2 = temperature node 2

T_c = temperature node c

T_r = temperature node r

V_{ep} = volume of pipe material in evaporator

V_{cp} = volume of pipe material in condensor

V_{ew} = volume of wick material in evaporator

V_{cw} = volume of wick material in condensor

ϵ = emmissivity of radiator

ρ_p = density of pipe material

ρ_w = effective density of wick and working fluid

σ = Stefan-Boltzman constant

θ = time

The limiter equation allows one to include the capillary limitation in computations.

Figure 24 shows a schematic of the analog computer circuit. Note that inclusion of the radiator introduces non-linear terms in the equation. However, these non-linear terms have thus far caused no difficulties in the computations.

Figures 25, 26, and 27 show sample results of some computations performed for a nitrogen heat pipe of configuration. Figure 25 shows performance for a step change of 5°K in the evaporator temperature. Notice that heat transfer at the hot end (Q_e) is limited for some time due to capillary limitations. The system has essentially stabilized after 60 seconds. Figure 26 shows how all parameters vary for a relatively fast sine wave. Notice that the capillary limitation considerably affects heat transfer through the evaporator. As expected, the computations indicate progressively smaller oscillations in temperature as one moves away from the evaporator and finally the radiator increases with time but oscillates very little. There is a considerable phase shift between oscillations in different temperatures. Figure 27 shows the system changes for a relatively slow variation in evaporator temperature. Evaporator heat transfer is again limited by capillary restrictions. The amplitude of temperature oscillations tends to be more uniform throughout the pipe than in the case where fast oscillations were considered. There are large phase shifts.

Transient Digital Computer Studies

The analog computer program described above is limited to small transients and thus is of limited use. For this reason a digital computer program is now being developed to handle transient computations. The

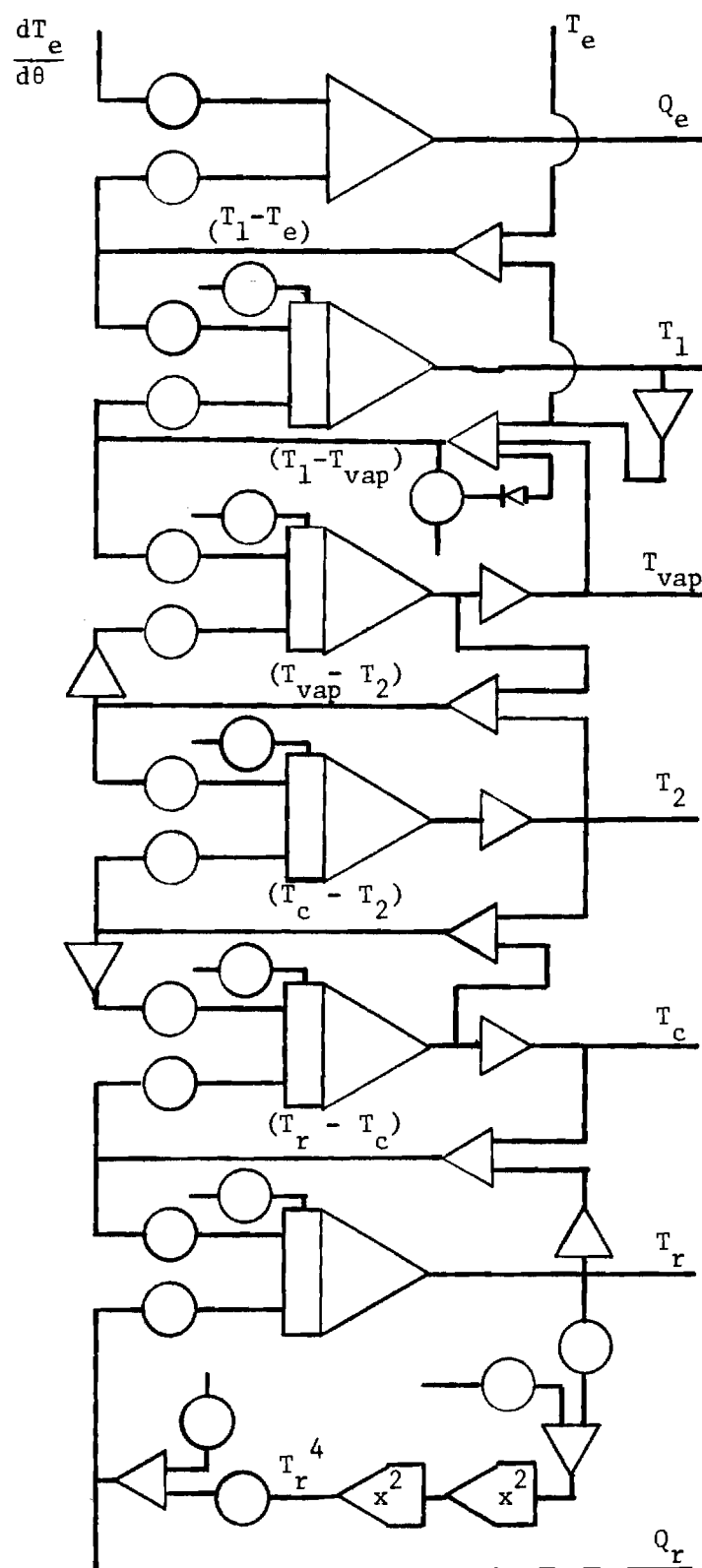


Figure 24. Analog Circuit

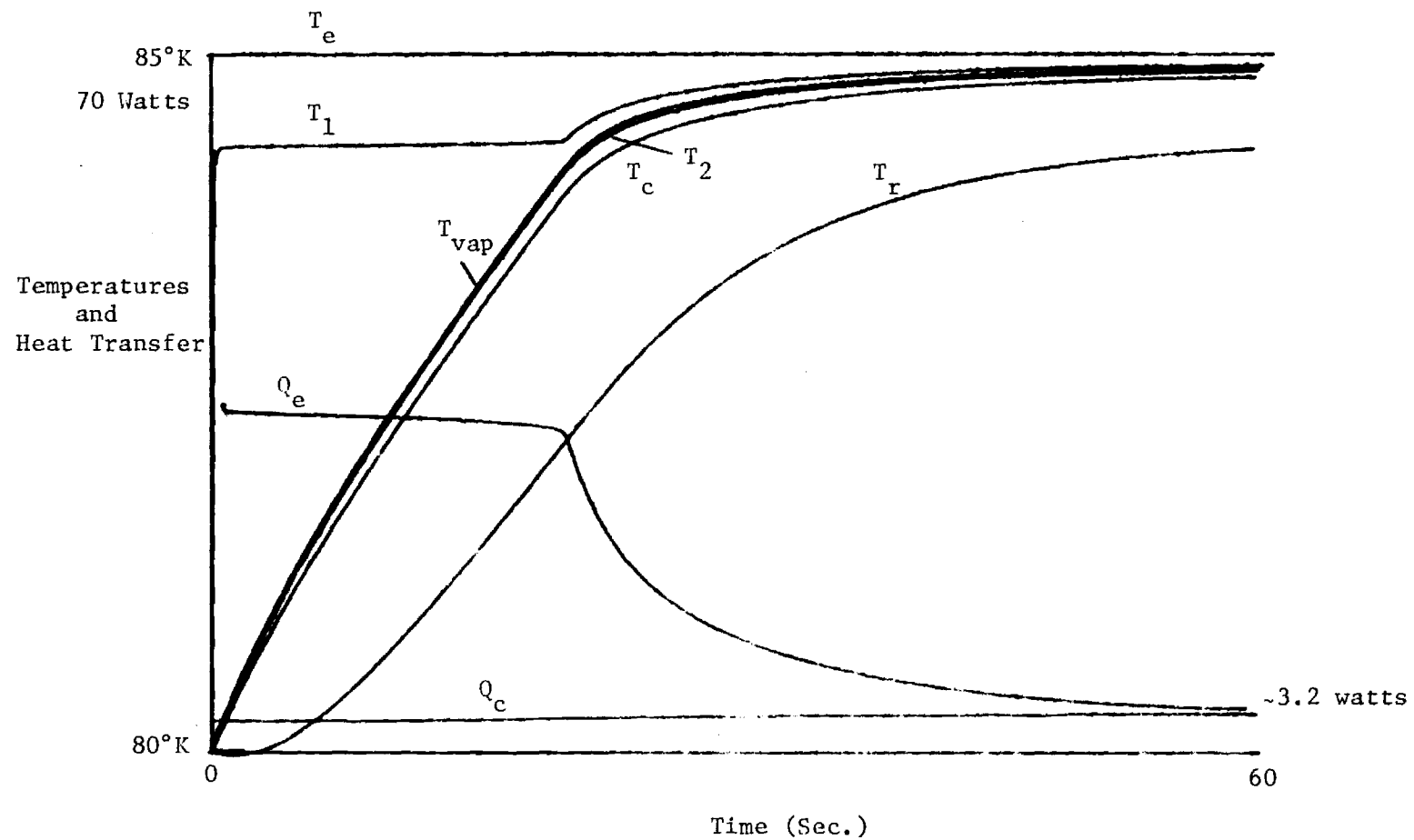


Figure 25. Step Temperature Change

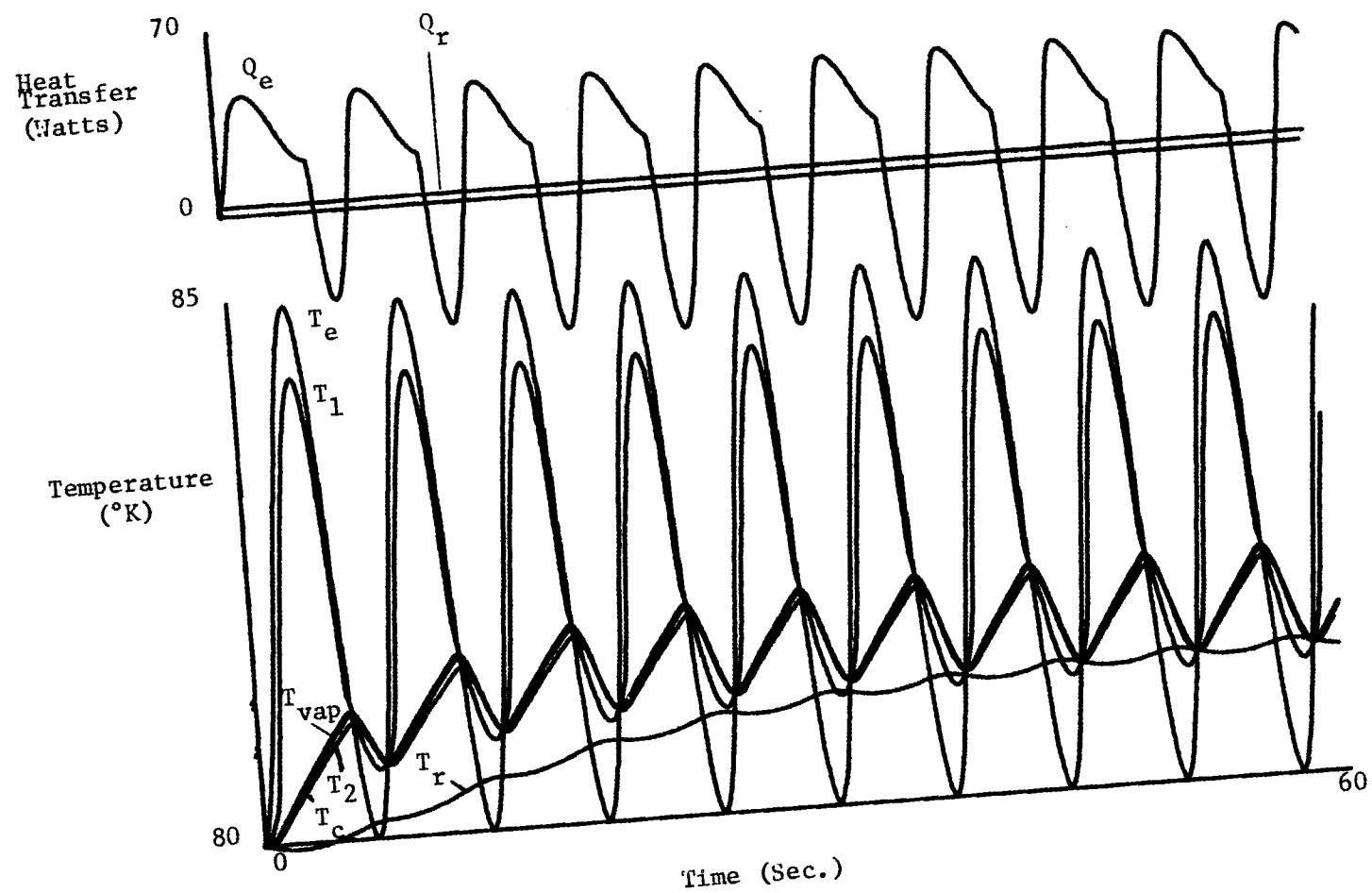


Figure 26. Fast Sine Wave

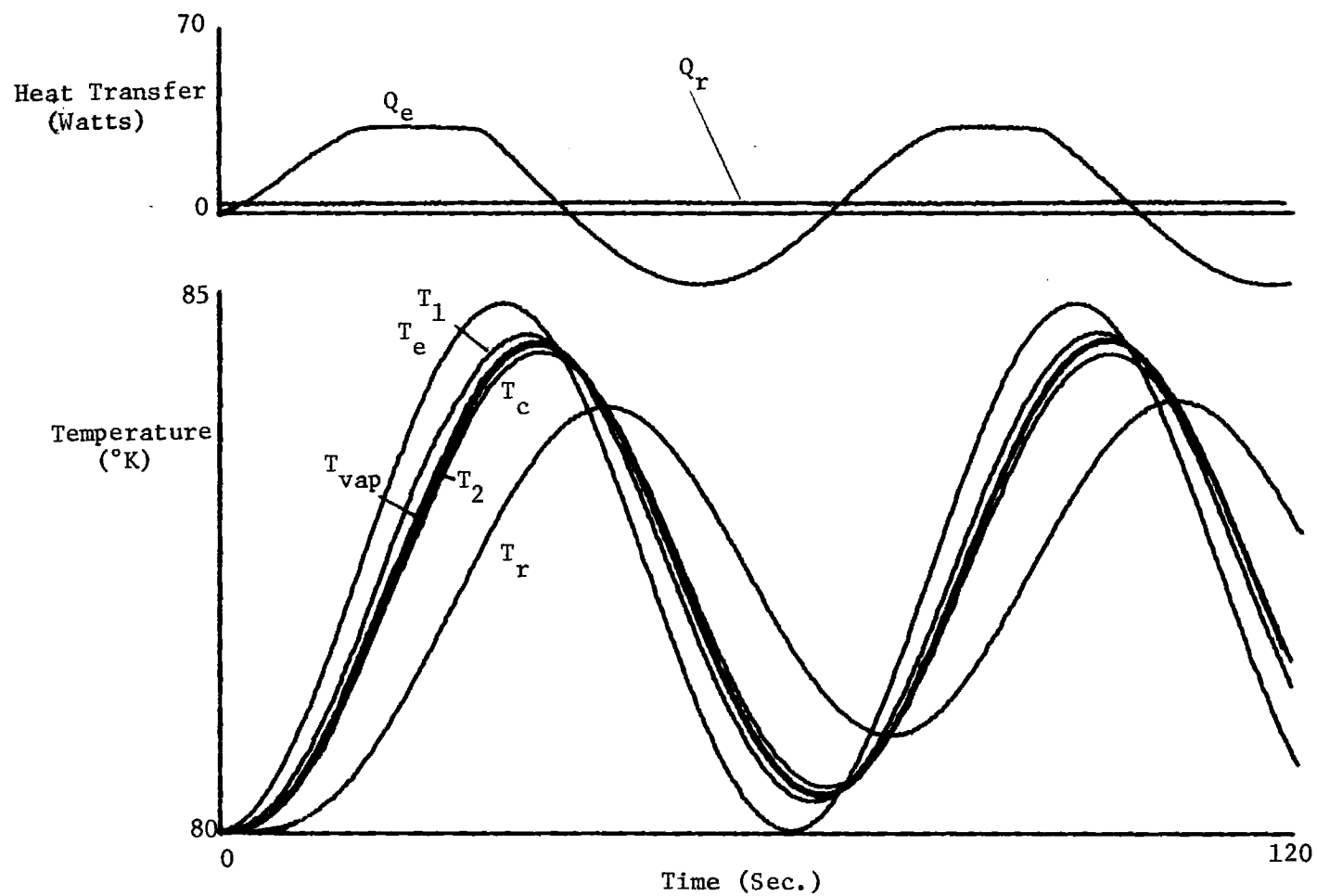


Figure 27. Slow Sine Wave

new approach will allow predictions to be made for various start-up situations including start-up from the supercritical state.

The digital work is now in the early stages of development. Fluid dynamic affects have not yet been incorporated. However, it is anticipated that these important affects can be readily included at the appropriate stage.

In the preliminary model now being studied several assumptions are made. (See Figure 28)

Evaporator saddle:	lumped mass, contact resistance to pipe wall, known heat input or fixed temperature.
Wall:	nodes in r and θ directions, contact resistance to wick.
Wick:	dryout circumferentially as $f(Q)$ innermost layer of nodes at same temperature as vapor.
Vapor:	lumped system, includes mass of slab, linear temperature drop along tube.
Adiabatic section	
and condenser:	nodes in r, z directions, nodes become active as $f(Q)$, innermost node of wick at same temperature as vapor.
Wick:	contact resistance to pipe wall.
Wall:	contact resistance to radiator.
Radiator:	lumped mass with known heat input or fixed temperature.
Axial conduction:	evaporator temperatures averaged for boundary condition in adiabatic section, weighted fraction of total heat transfer in axial direction subtracted from each evaporator node.

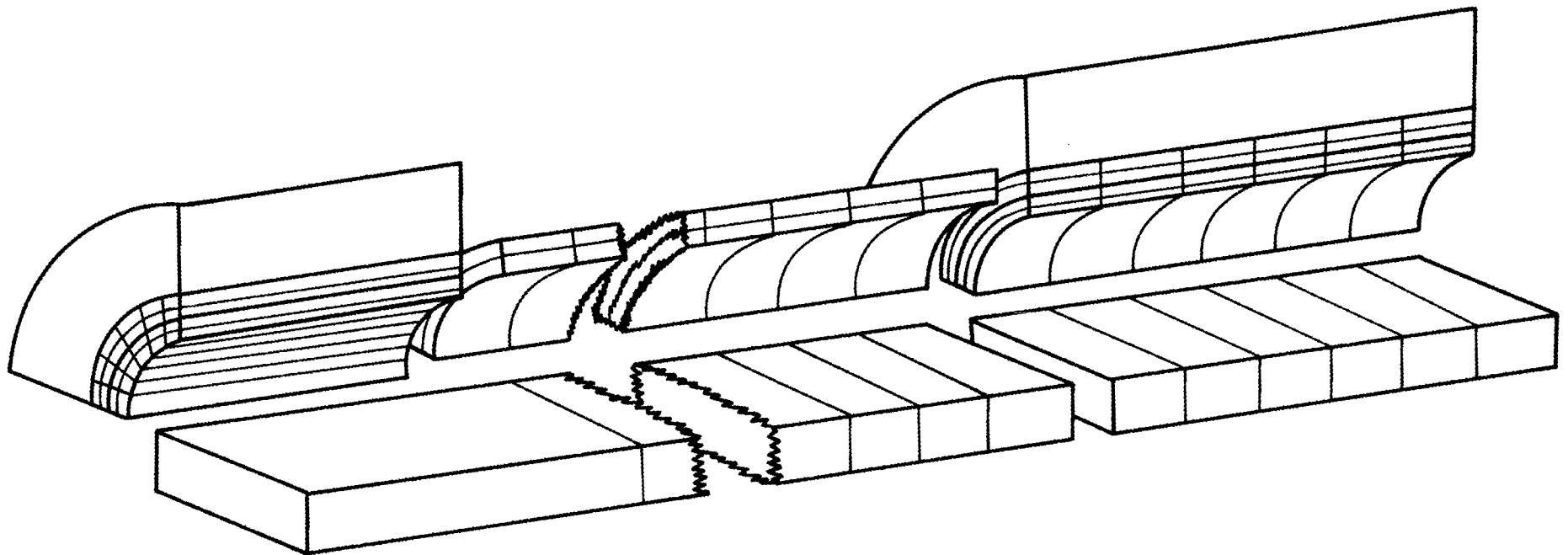


Figure 28. Heat Pipe Model

Thermal properties: constant at the temperature of the last time step.

The nomenclature used in the digital approach is:

A_R	area of radiator
c_R	specific heat of radiator
c_S	specific heat of saddle
c_V	specific heat of vapor and slab
k_W	thermal conductivity of wick
l_C	length of adiabatic and condenser section
l_E	length of evaporator
m_R	mass of radiator
m_S	mass of saddle
m_V	mass of vapor and slab
NIE	number radial nodes in evaporator
NJE	number circumferential nodes in evaporator
NIC	number radial nodes in condenser
NJC	number axial nodes in condenser
Q_{IR}	heat input to radiator from space
Q_{IS}	heat input to saddle
R_C	contact resistance pipe to saddle or radiator
r_I	inside radius of pipe
r_i	radius at node i
r_O	outside radius of pipe
$T_{C,i,j}^n$	temperature of condenser node i,j at time step n
$T_{E,i,j}^n$	evaporator node temperature at i,j
T_R	radiator temperature
T_S	saddle temperature

T_v	vapor temperature
α	thermal diffusivity of pipe wall
Δx	$1/NI \ln(r_o/r_I)$ (see coordinate transformation)
Δy	$2\pi/NJE$ (circumferential node width)
Δz	ℓ_c/NJC (axial node width)
$\Delta \theta$	time increment
ϵ	emissivity of radiator
σ	Stefan-Boltzman constant

It is convenient to transform from cylindrical to rectangular coordinates.

In cylindrical coordinates $\nabla^2 T$ is

$$\frac{\partial^2 T}{\partial r^2} + \frac{1}{r} \frac{\partial T}{\partial r} + \frac{1}{r} \frac{\partial^2 T}{\partial \phi^2} + \frac{\partial^2 T}{\partial z^2}$$

Make the following substitutions (See Figure 29).

$$x = \ln r/r_c$$

$$y = \phi$$

$$z = z$$

thus

$$\frac{\partial T}{\partial r} = \frac{\partial T}{\partial x} \frac{dx}{dr} + \frac{\partial T}{\partial \phi} \frac{dy}{dr} = \frac{1}{r} \frac{\partial T}{\partial x}$$

$$\frac{\partial^2 T}{\partial r^2} = \frac{\partial}{\partial r} \left(\frac{1}{r} \frac{\partial T}{\partial x} \right) = \frac{\partial^2 T}{\partial x^2} \frac{1}{r^2} - \frac{1}{r^2} \frac{\partial T}{\partial x}$$

$$\frac{\partial^2 T}{\partial \phi^2} = \frac{\partial^2 T}{\partial y^2}$$

$$\frac{\partial^2 T}{\partial z^2} = \frac{\partial^2 T}{\partial z^2}$$

Substitution into $\bar{\nabla}^2 T$

$$\frac{1}{r^2} \frac{\partial^2 T}{\partial x^2} - \frac{1}{r^2} \frac{\partial T}{\partial x} + \frac{1}{r^2} \frac{\partial T}{\partial x} + \frac{1}{r^2} \frac{\partial T}{\partial y^2} + \frac{\partial^2 z}{\partial z^2}$$

or

$$\frac{1}{r^2} \frac{\partial^2 T}{\partial x^2} + \frac{1}{r^2} \frac{\partial^2 T}{\partial y^2} + \frac{\partial^2 T}{\partial z^2}$$

Figure 30 shows the transformed computer grid for each of the various regions. The computational procedure for each time step

$\Delta\theta(n \rightarrow n+1)$ is: 1) Explicit Balance on T_s

$$T_s^{n+1} = \frac{Q_{IE} \Delta\theta}{m_s c_s} + \frac{2\Delta\theta \pi r_o \ell_e}{(NJE)(m_s)(c_s)(R_c)} \sum_{j=1}^{NJE} (T_{E_{i,j}}^n - T_s^n) + T_s^n,$$

2) Explicit Balance on Vapor

$$T_v^{n+1} = \frac{2\Delta\theta k_w \ell_e \pi}{\Delta x m_v c_v NJE} \sum_{j=1}^{NJE} (T_{E_{NJE-1,j}}^n - T_v^n) \\ + \frac{2\Delta\theta k_w \ell_c \pi}{\Delta x m_v c_v NJC} \sum_{j=1}^{NJC} (T_{c_{NJC-1,j}}^n - T_v^n) + T_v^n;$$

3) Explicit Balance on Radiator

$$T_R^{n+1} = \frac{2\Delta\theta \ell_c \pi r_o}{m_R c_R R_c NJC} \sum_{j=1}^{NJC} (T_{c_{i,j}}^n - T_R^n) \\ - \frac{A_R \sigma \epsilon \Delta\theta}{m_R c_R} (T_R^n)^4 + \frac{Q_{IR} \Delta\theta}{m_R c_R} + T_R^n;$$

4) Alternating direction implicit evaluation of evaporator grid.

(developed next page); and

5) Alternating direction implicit evaluation of condenser grid.

(similar to 4)

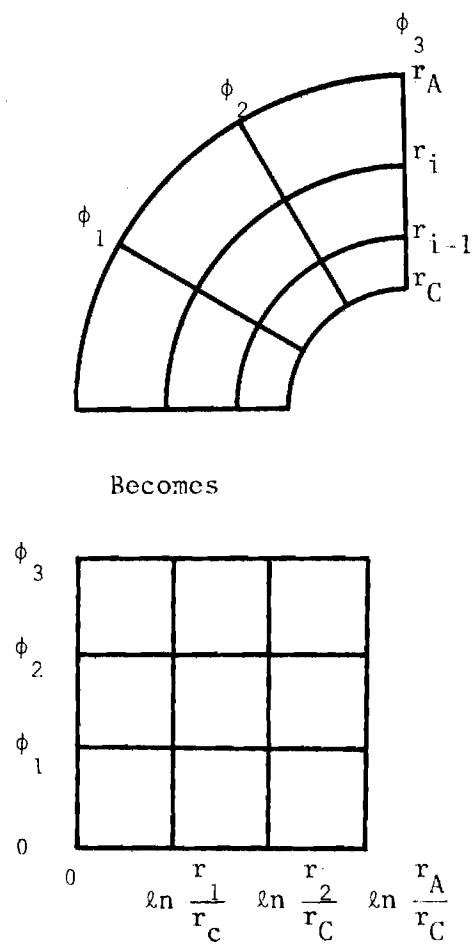


Figure 29. Polar to Rectangular Transformation

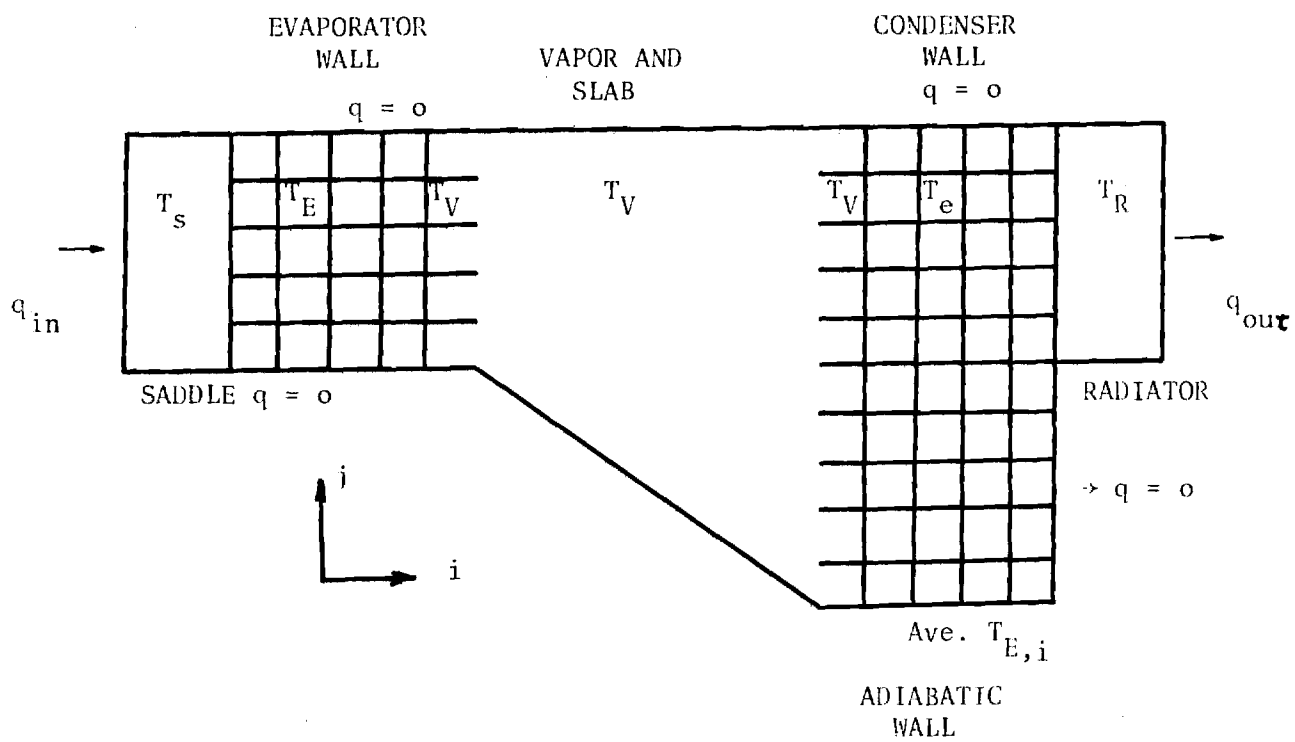


Figure 30. Computation Grid

As an example of the implicit equations used, consider an interior evaporator node for an i sweep.

$$\begin{aligned} \frac{r_i^2}{\alpha} \frac{T_{E,i,j}^{n+1/2} - T_{E,i,j}^n}{\Delta\theta/2} = & \frac{1}{(\Delta x)^2} \left(T_{E,i-1,j}^{n+1/2} + T_{E,i+1,j}^{n+1/2} - 2T_{E,i,j}^{n+1/2} \right) \\ & + \frac{1}{(\Delta y)^2} \left(T_{E,i,j-1}^n + T_{E,i,j+1}^n - 2T_{E,i,j}^n \right) \\ & - \left(\frac{T_{E,i,j}^n}{\sum_{j=1}^{NJE} T_{E,i,j}^n} \right) \left(T_{c,i,1}^n - \frac{1}{NJE} \sum_{j=1}^{NJE} T_{E,i,j}^n \right) \left(\frac{r_i}{\Delta z} \right)^2 \end{aligned}$$

The equation can be rewritten as

$$\begin{aligned} - \left(\frac{\Delta\theta}{2(\Delta x)^2} \right) \left(T_{E,i-1,j}^{n+1/2} \right) + \left(\frac{r_i^2}{\alpha} + \frac{\Delta\theta}{(\Delta x)^2} \right) \left(T_{E,i,j}^{n+1/2} \right) - \left(\frac{\Delta\theta}{2(\Delta x)^2} \right) \left(T_{E,i,j+1}^{n+1/2} \right) = \\ \frac{\Delta\theta}{2(\Delta y)^2} \left(T_{E,i,j+1}^n + T_{E,i,j-1}^n \right) + \left(\frac{r_i^2}{\alpha} - \frac{\Delta\theta}{(\Delta y)^2} \right) T_{E,i,j}^n \\ - \left(\frac{r_i^2 \Delta\theta}{2(\Delta z)^2} \right) \left(\frac{T_{E,i,j}^n}{\sum_{j=1}^{NJE} T_{E,i,j}^n} \right) \left(T_{c,i,1}^n - \frac{1}{NJE} \sum_{j=1}^{NJE} T_{E,i,j}^n \right). \end{aligned}$$

References 6 through 9 have been utilized extensively in developing the approach described above.

CONCLUSIONS

The primary general goal of this project was to develop techniques for predicting transient operation of cryogenic heat pipes. In particular the work was aimed towards development of schemes for predicting start up from various initial conditions such as those encountered in the supercritical regime. In accomplishing these goals it was necessary to first study steady state operation. The steady state work included prediction of performance limitations and thermal resistances. The transient part of the project has been divided into two areas: subcritical operation and supercritical operation.

During calendar 1975 the steady state part of the program was essentially completed and some results of computations are included in this report. The development of schemes for predicting transient operation is progressing well at this time and some preliminary results are included herein.

It is significant to note that several graduate and undergraduate students have received valuable training while performing tasks under this grant. One M.S. thesis, directly related to the project, was published during 1975 and it is expected that another one will be completed about July 1976.

REFERENCES

1. Hare, J. D., "Performance of a Nitrogen Heat Pipe with Various Capillary Structures", M.S. Thesis, Georgia Institute of Technology June 1975.
2. Williams, C. L., and G. T. Colwell, "Heat Pipe Model Accounting for Variable Evaporator and Condenser Lengths", AIAA Journal, Volume 12, Number 9, September 1974.
3. Abhat, A. and R. A. Seban, "Boiling and Evaporation From Heat Pipe Wicks with Water and Acetone", ASME Journal of Heat Transfer, Aug. 1974.
4. Levitan, M. M. and T. L. Perelman, "Fundamentals of Heat Pipe Theory and Design", Sov. Phys. Tech. Phys., Vol. 19, No. 8, February 1975.
5. Chun, K. R., "Some Experiments on Screen Wick Dry-Out Limits", ASME Paper 71-WA/HT-6.
6. Roache, Patrick J., Computational Fluid Dynamics, Hermosa Publishers, Albuquerque, N.M., 1972.
7. Clausing, A. M., "Numerical Methods in Heat Transfer", Advanced Heat Transfer, Ed. by B. T. Chao, University of Illinois Press, Chicago, 1969.
8. Larkin, B. K., "Some Stable Explicit Approximations to the Diffusion Equation", Mathematics of Computation, 18, 196-202 (1964).
9. Carnahan, B., H. A. Luther, and J. O. Wilkes, Applied Numerical Methods, Wiley, New York, 1957.

DISTRIBUTION

1. (2 copies) NASA Scientific and Technical Information Facility,
Post Office Box 33, College Park, Maryland 20740.
2. NASA Ames Research Center, Moffett Field, California 94035
(5 copies) John P. Kirkpatrick
Robert J. Debs
Manfred Groll
Craig McCreight
Masahide Murakami
Ray H. Sutton
3. NASA Goddard Space Flight Center, Code 732, Greenbelt, Maryland 20771
(5 copies) Stanford Ollendorf
Yashuhiro Kamotani
Roy McIntosh
Allan Sherman
4. John D. DiBattista, Mail Stop 158B, LDEF Project Office, NASA Langley
Research Center, Hampton, Virginia 23665
5. Georgia Institute of Technology
(5 copies) Office of Research Administration
Vice President for Research
Dean, College of Engineering
(3 copies) Director, School of Mechanical Engineering
(20 copies) Gene T. Colwell

APPENDIX

THERMAL RESISTANCE PROGRAM


```
7230 FORMAT(T30,F12.8,T45,F12.8,T60,F12.8,T75,F5.1,T82,F12.8)
      WRITE(6,7777)
      SLABTH=8.0E-3
      LE=0.5
      LCD=1.0
      RA=0.04167
      Q=102.39
      QMAX=102.39
      DQ=-6.826
      PI=3.14159
      A1=-4.02016E-5
      A2=3.20878E-2
      A3=1.30266
      TCINC=0.5879396985
      RR=RA-WT
      RC=RR-4.0*RF*N=BETA*(N-1.0)
      RCHD=(PI*RC*RC-2.0*RC*SLABTH)/(2.0*PI*RC-2.0*SLABTH+4.0*RC)
      DO 300 K=1,2
      TC=108.0
      DO 190 J=1,200
1      THETA=(PI/2.0)/(1.0+(Q/QMAX))
      VI=INT(N)
C
C      COMPUTING TPCI AND RPC
C
      COUNT=0
      EPS1=0.001
      TPCI=TC
      LASTI=TC
4      F=FUNCA(TPCI)
      IF(F)5,20,7
5      F1=F
      TP1=TPCI
6      TPCI=TPCI+0.5
      F=FUNCA(TPCI)
      IF(F)6,20,10
7      F2=F
      TP2=TPCI
8      TPCI=TPCI+0.5
      F=FUNCA(TPCI)
      IF(F)9,20,8
9      F1=F
      TP1=TPCI
      GO TO 13
10     F2=F
      TP2=TPCI
      GO TO 13
13     TP3=(TP1+F2-TP2+F1)/(F2-F1)
      F3=FUNCA(TP3)
      ZA=ABS(LASTI-TP3)
      LASTI=TP3
      IF(ZA-EPS1)21,21,14
14     TP1=TP2
      TP2=TP3
      F1=F2
      F2=F3
      COUNT=COUNT+1
```

```

      GO TO 13
20    WRITE(6,1030)TPCI
1030  FORMAT(T30,"TPCI =",I38,F7.2,T50,"DOUBTFUL")
      GO TO 30
21    TPCI=TP3
      IF(GATE.NE.0.0)GO TO 30
      WRITE(6,1040)TPCI,COUNT,F3
1040  FORMAT(T30,"TPCI =",I38,F7.2,T50,"COUNT =",T59,I5,T65,"F =",T69,
      CF6.3)
      WRITE(6,2222)
30    TAV=(TPCI+TC)/2.0
      RPC=ALOG(RA/RB)/(2.0*PI*(A1*TAV*TAV+A2*TAV+A3)*LCD*(Q/QMAX))
C
C      COMPUTING TV AND RWC
C
      PSUM=0.0
      DO 40I=1,N1
      FI=FLOAT(I)
      TERM=ALOG((RB-(FI-1.0)*4.0*RF-(FI-1.0)*BETA)/(RB-4.0*FI*RF-(FI-1)
      (*BETA))
      PSUM=TERM+PSUM
40    CONTINUE
      SUMA=PSUM
      PSUM=0.0
      NM1=N1-1
      DO 42I=1,NM1
      FI=FLOAT(I)
      TERM=ALOG((RB-4.0*FI*RF-(FI-1.0)*BETA)/(RB-4.0*FI*RF-FI*BETA))
      PSUM=TERM+PSUM
42    CONTINUE
      SUMR=PSUM
      IF(NM1.EQ.0)SUMR=0.0
C
C      ITERATIVE SOLUTION BY LINEAR INTERPOLATION METHOD
C
50    TV=TPCI
      EPS2=0.001
51    TAV=(TV+TPCI)/2.0
52    F=FUNCR(TV,TAV)
      IF(F)60,90,70
60    F1=F
      TVX1=TV
61    TV=TV+5.0
      TAV=(TV+TPCI)/2.0
      F=FUNCR(TV,TAV)
      IF(F)61,90,63
63    F2=F
      TV2=TV
      GO TO 79
68    F2=F
      TV2=TV
70    TV=TV+5.0
      TAV=(TV+TPCI)/2.0
      F=FUNCR(TV,TAV)
      IF(F)71,90,70
71    F1=F
      TVX1=TV

```

```

79  COUNT=0
80  TV3=(TVX1*F2-TV2*F1)/(F2-F1)
    TAV=(TV3+IPC1)/2.0
    COUNT=COUNT+1
    ZB=ABS(TV3-TV2)
    IF(ZB.LE.EPS2)GO TO 91
    F3=FUNCC(TV3,TAV)
    F1=F2
    TVX1=TV2
    F2=F3
    TV2=TV3
    GO TO 80
90  WRITE(6,2010)TV,COUNT
2010 FORMAT(150,"TV =",155,F8.2,165,"COUNT =",173,15,185,"DOUBTFUL")
91  TV=TV3
    IF(GATE.NE.0.0)GO TO 95
    WRITE(6,2000)TV,COUNT,F3
2000 FORMAT(130,"TV =",135,F8.2,150,"COUNT =",158,15,165,"F =",169,
    CF6.3)
    WRITE(6,2222)
95  CONTINUE
    RWC=(1.0/(2.0*PI*KW(TAV)*LCD*Q/QMAX))*SUMA+(1.0/(2.0*PI*KL(TAV)*LC
    CD*Q/QMAX))*SUMH
C
C  AT EVAPORATOR --- COMPUTATION OF IPEI AND RWE
C
    IPEI=TV
    TAV=(IPEI+TV)/2.0
    F=FUNCC(IPEI,TAV)
    IF(F)100,125,115
100  IP1=IPEI
    F1=F
102  IPEI=IPEI+5.0
    TAV=(IPEI+TV)/2.0
    F=FUNCC(IPEI,TAV)
    IF(F)102,125,105
105  IP2=IPEI
    F2=F
    GO TO 120
115  IP2=IPEI
    F2=F
116  IPEI=IPEI+5.0
    TAV=(IPEI+TV)/2.0
    F=FUNCC(IPEI,TAV)
    IF(F)116,125,119
119  IP1=IPEI
    F1=F
120  COUNT=0
    EPS3=0.001
121  IP3=(IP1*F2-IP2*F1)/(F2-F1)
    COUNT=COUNT+1
    TAV=(IP3+TV)/2.0
    ZC=ABS(IP3-IP2)
    IF(ZC.LE.EPS3)GO TO 124
    F3=FUNCC(IP3,TAV)
    F1=F2
    IP1=IP2

```

```

      F2=F3
      TP2=TP3
      GO TO 121
125  WRITE(6,2080)TPET,COUNT
2080  FORMAT(T50,"TPEI =",T57,F8.2,T67,"COUNT =",T75,I5,T85,"DOURTFUL")
124  IF(GATE.NE.0.0)GO TO 130
126  WRITE(6,2090)TP3,COUNT,F3
2090  FORMAT(T30,"TPEI =",T37,F8.2,T50,"COUNT =",T58,I5,T64,"F =",T68,
      CF6.3)
      WRITE(6,2222)
130  TPET=TP3
      RWE=(PI/(2.0*THETA))*((1.0/(2.0*PI*LE))*(SUMA/KW(TAV)+SUMB/KL(TAV
      C)))
C
C      COMPUTATION OF TE AND RPE
C
      TE=TPET
      F=FUNCD(TE)
      IF(F)150,180,165
150  TE1=TE
      F1=F
151  TE=TE+1.0
      F=FUNCD(TE)
      IF(F)151,181,153
153  TE2=TE
      F2=F
      GO TO 170
165  TE2=TE
      F2=F
166  TE=TE+1.0
      F=FUNCD(TE)
      IF(F)168,181,166
168  TE1=TE
      F1=F
170  CT=0
      EPS4=0.001
171  TE3=(TE1+F2-TE2+F1)/(F2-F1)
      CT=CT+1
      ZD=ABS(TE3-TE2)
      IF(ZC,IF,EPS4)GO TO 180
      F3=FUNCD(TE3)
      F1=F2
      TE1=TE2
      F2=F3
      TE2=TE3
      GO TO 171
180  TE=TE3
      F=F3
      IF(GATE.NE.0.0)GO TO 183
181  WRITE(6,3030)TE,F,CT
3030  FORMAT(T30,"TE =",F8.2,T45,"F =",T46,F10.3,T60,"CT =",T65,I5)
183  TAV=(TE+TPET)/2.0
      RPE=(PI/(2.0*THETA))*ALOG(RA/RB)/(2.0*PI*LE*KF(TAV))
C
C      COMPUTATION OF INTERFACIAL RESISTANCE
C
      HEG=778.16*(-4.11334E-11*TV**6.0+2.0908E-8*TV**5.0-1.43119E-6*

```

CIV**4.0-1.03235E-3*TV**3.0+2.61594E-1*TV*TV-2.40246E+1*TV+8.89614
CE+2)

PV=1.71041E-6*TV**5.0-1.20901E-3*TV**4.0+3.71275E-1*TV**3.0
C-5.70868E+1*TV*TV+4.28513E+3*TV-1.25125E+5
LCA=LCD*Q/QMAX

C
C
C

UNITS OF RIC AS COMPUTED HERE ARE (SEC R / LRF FT)

RTC=14.408*TV**2.5/(RC*LCA*PV*HFG*HFG)
RIE=(PI/(2.0*THETA))*RIC*LCA/LE

C
C
C
C
C

COMPUTATION OF VAPOR RESISTANCE
UNITS ARE (SEC R / LRF FT)

LEFF=3.0-LE/2.0-LCD*Q/(2.0*QMAX)
MOV=8.5591E-21*TV**7.0-6.55918E-18*TV**6.0+1.70105E-15*TV**5.0-8.
C08533E-14*TV**4.0-4.27309E-11*TV**3.0+8.90377E-9*TV*TV-6.94007E-7
C*TV+1.99577E-5
ROV=1.39324E-13*TV**7.0-1.042325E-10*TV**6.0+2.638736E-8*TV**5.0
C-1.14015E-6*TV**4.0-6.78395E-4*TV**3.0+1.385389E-1*TV*TV-1.07628
CE+1*TV+3.10045E+2
ROL=-5.8917E-13*TV**7.0+4.50297E-10*TV**6.0-1.15298E-7*TV**5.0+4.9
C5327E-6*TV**4.0+2.9749E-3*TV**3.0-5.98552E-1*TV*TV+4.54425E+1*TV-1
C.21455E+3
RV=8.0*MOV*LEFF*TV*(1.0/ROV-1.0/ROL)/(PI*ROV*HFG*HFG*RCHD**4.0)

C
C
C

UNIT CONVERSION

S1=0.4097
RVSI=S1*RV
RIESI=S1*RIE
RICSI=S1*RIC
S2=1.8957
RPCSI=S2*RPC
RPESI=S2*RPE
RWCSI=S2*RWI
RWESI=S2*RWE
S3=0.5556
ICSI=S3*IC
IPCTSI=S3*IPCI
IVSI=S3*IV
IPETSI=S3*IPET
TESI=S3*IE
QSI=Q*0.2930
RIOT=RPESI+RWESI+RIESI+RVSI+RICSI+RWCSI+RPCSI
S4=304.8
XRIOT=(TESI-ICSI)/QSI
DESI=S4*DF
RESI=S4*RF
BETASI=S4*BFIA
RAST=S4*RA
WIST=S4*WT
DELTAT=TESI-ICSI

C
C
C

WRITING AND SETTING UP ARRAYS

IF(K.NE.1)GO TO 185

```

      TV1(J)=TVSI
      RT1(J)=RTOT
      RWE1(J)=RWESI
      RWC1(J)=RWCSI
      GO TO 188
185   IF(K,NE.11)GO TO 187
      TV11(J)=TVSI
      RT11(J)=RTOT
      RWE11(J)=RWESI
      RWC11(J)=RWCSI
      GO TO 188
187   IF(K,NE.5)GO TO 188
      TV5(J)=TVSI
      RT5(J)=RTOT
      RPE5(J)=RPESI
      RWF5(J)=RWESI
      RIE5(J)=RIESI
      RV5(J)=RVSI
      RIC5(J)=RICS1
      RWC5(J)=RWCSI
      RPC5(J)=RPCSI
188   CONTINUE
      AYTV(J)=TVSI
      AYDT(J)=DELTAT
      AYQ(J)=QSI
      AYRTOT(J)=RTOT
      AYRPE(J)=RPESI
      AYRWF(J)=RWESI
      AYRIE(J)=RIESI
      AYRV(J)=RVSI
      AYRIC(J)=RICS1
      AYRWC(J)=RWCSI
      AYRPC(J)=RPCSI
      AYIC(J)=ICS1
      GATE=1.0
      IC=IC+ICINC
190   CONTINUE
      WRITE(6,3333)
3333  FORMAT(1H1)
      WRITE(6,6063)
6063  FORMAT(T20,"UNITS ---",T35,"TEMPERATURE -- K",T55,"RESISTANCE -- K
C/WALL",T79,"HEAT TRANSFER RATE -- WATTS")
      WRITE(6,7777)
      WRITE(6,7777)
      WRITE(6,7777)
      WRITE(6,7777)
7777  FORMAT(1H0)
      WRITE(6,5005)
5005  FORMAT(T5,"Q",T22,"TV",T29,"DELTAT",T38,"RTOT",T49,"RPE",T60,
C"RWF",T71,"RIE",T82,"RV",T93,"RIC",T104,"RWC",T115,"RPC",T126,"IC"
C)
      WRITE(6,2222)
      DO 200 J=1,200,6
      WRITE(6,5000)AYQ(J),AYTV(J),AYDT(J),AYRTOT(J),AYRPE(J),AYRWF(J),AY
CRTE(J),AYRV(J),AYRIC(J),AYRWC(J),AYRPC(J),AYIC(J)
5000  FORMAT(T2,F6.2,T20,F6.2,T28,F6.2,T35,E10.4,T46,E10.4,T57,E10.4,
CT68,E10.4,T79,E10.4,T90,E10.4,T101,E10.4,T112,E10.4,T123,F8.2)

```



```
200  CONTINUE
      Q=Q+DQ
C
C      PLOTTING DT .VS. TV AT CONSTANT Q
C
      IF(K.NE.1)GO TO 510
      CALL SCALE(AYTV,6.0,200,+1)
      FVTV=AYTV(201)
      DVTV=AYTV(202)
      AYDT(201)=0.0
      CALL SCALE(AYDT,7.0,201,+1)
      FVDT=AYDT(202)
      DVDT=AYDT(203)
      CALL AXIS(0.0,0.0,17HVAPOR TEMPERATURE,-17,6.0,0.0,FVTV,DVTV)
      CALL AXIS(0.0,0.0,7HDELTA T,+7,7.0,90.0,FVDT,DVDT)
510  CONTINUE
      AYIV(201)=FVTV
      AYIV(202)=DVTV
      AYDT(201)=FVDT
      AYDT(202)=DVDT
      CALL LINE(AYIV,AYDT,200,1,+50,SYM)
      SYM=SYM+1
300  CONTINUE
      CALL PLOT(XP,0.0,-3)
C      ARRAY #5
C      PLOTTING RTOT,RWF,RWC, VS. TV
C
      CALL SCALE(TV5,6.0,200,+1)
      FVTV=TV5(201)
      DVTV=TV5(202)
      RT5(201)=0.0
      CALL SCALE(RT5,7.0,201,1)
      FVR=RT5(202)
      DVR=RT5(203)
      RT5(201)=FVR
      RT5(202)=DVR
      CALL AXIS(0.0,0.0,17HVAPOR TEMPERATURE,-17,6.0,0.0,FVTV,DVTV)
      CALL AXIS(0.0,0.0,18THERMAL RESISTANCE,+18,7.0,90.0,FVR,DVR)
      SYM=1
      CALL LINE(TV5,RT5,200,1,+50,SYM)
      SYM=SYM+1
      RWE5(201)=FVR
      RWE5(202)=DVR
      RWC5(201)=FVR
      RWC5(202)=DVR
      CALL LINE(TV5,RWE5,200,1,+50,SYM)
      SYM=SYM+1
      CALL LINE(TV5,RWC5,200,1,+50,SYM)
C
C      PLOTTING RPF,RPC, VS. TV
C
      SYM=SYM+1
      CALL PLOT(XP,0.0,-3)
      IF(RPE5(1).GT.RPC5(1))610,615
610  RPF5(201)=0.0
      CALL SCALE(RPF5,7.0,201,1)
      FVR=RPF5(202)
```

```

        DVR=RPE5(203)
        GO TO 618
615    RPC5(201)=0.0
        CALL SCALE(RPC5,7.0,201,1)
        FVR=RPC5(202)
        DVR=RPC5(203)
618    CONTINUE
        RPE5(201)=FVR
        RPE5(202)=DVR
        RPC5(201)=FVR
        RPC5(202)=DVR
        CALL AXIS(0.0,0.0,17,HVAPOR TEMPERATURE,-17,6.0,0.0,FVTV,DVTV)
        CALL AXIS(0.0,0.0,18,THERMAL RESISTANCE,+18,7.0,90.0,FVR,DVR)
        CALL LINE(TVS,RPE5,200,+1,+50,SYM)
        SYM=SYM+1
        CALL LINE(TVS,RPC5,200,+1,+50,SYM)
C
C      PLOTTING RTE,RTC VS. TV
C
        SYM=SYM+1
        CALL PLOT(XP,0.0,-3)
        IF(RTE5(1).GT. RTC5(1))650,655
650    RTE5(201)=0.0
        CALL SCALE(RTE5,7.0,201,1)
        FVR=RTE5(202)
        DVR=RTE5(203)
        GO TO 659
655    RTC5(201)=0.0
        CALL SCALE(RTC5,7.0,201,1)
        FVR=RTC5(202)
        DVR=RTC5(203)
659    CONTINUE
        RTE5(201)=FVR
        RTE5(202)=DVR
        RTC5(201)=FVR
        RTC5(202)=DVR
        CALL AXIS(0.0,0.0,17,HVAPOR TEMPERATURE,-17,6.0,0.0,FVTV,DVTV)
        CALL AXIS(0.0,0.0,18,THERMAL RESISTANCE,+18,7.0,90.0,FVR,DVR)
        CALL LINE(TVS,RTE5,200,1,+50,SYM)
        SYM=SYM+1
        CALL LINE(TVS,RTC5,200,1,+50,SYM)
C
C      PLOTTING RV VS. TV
C
        SYM=SYM+1
        CALL PLOT(XP,0.0,-3)
        CALL SCALE(RV5,7.0,200,+1)
        FVR=RV5(201)
        DVR=RV5(202)
        CALL AXIS(0.0,0.0,17,HVAPOR TEMPERATURE,-17,6.0,0.0,FVTV,DVTV)
        CALL AXIS(0.0,0.0,18,THERMAL RESISTANCE,+18,7.0,90.0,FVR,DVR)
        CALL LINE(TVS,RV5,200,1,0,0)
C      ARRAYS = 1
C
C      RTOT,RWF,PWC
C
        SYM=SYM+1

```

```

      CALL PLOT(XP,0.0,-3)
      CALL SCALE(TV1,6.0,200,+1)
      FVTV=TV1(201)
      DVTV=TV1(202)
      RT1(201)=0.0
      CALL SCALE(RT1,7.0,201,1)
      FVR=RT1(202)
      DVR=RT1(203)
      RT1(201)=FVR
      RT1(202)=DVR
      RWF1(201)=FVR
      RWF1(202)=DVR
      RWC1(201)=FVR
      RWC1(202)=DVR
      CALL AXIS(0.0,0.0,17HVAPOR TEMPERATURE,-17,6.0,0.0,FVTV,DVTV)
      CALL AXIS(0.0,0.0,18THERMAL RESISTANCE,+18,7.0,90.0,FVR,DVR)
      CALL LINE(TV1,RT1,200,1,+50,SYM)
      SYM=SYM+1
      CALL LINE(TV1,RWF1,200,1,+50,SYM)
      SYM=SYM+1
      CALL LINE(TV1,RWC1,200,1,+50,SYM)

C
C      ARRAYS # 11
C
C      RTOT,RWF,RWC
C
      SYM=SYM+1
      CALL PLOT(XP,0.0,-3)
      CALL SCALE(TV11,6.0,200,+1)
      FVTV=TV11(201)
      DVTV=TV11(202)
      RT11(201)=0.0
      CALL SCALE(RT11,7.0,201,1)
      FVR=RT11(202)
      DVR=RT11(203)
      RT11(201)=FVR
      RT11(202)=DVR
      RWF11(201)=FVR
      RWF11(202)=DVR
      RWC11(201)=FVR
      RWC11(202)=DVR
      CALL AXIS(0.0,0.0,18THERMAL RESISTANCE,+18,7.0,90.0,FVR,DVR)
      CALL AXIS(0.0,0.0,17HVAPOR TEMPERATURE,-17,6.0,0.0,FVTV,DVTV)
      CALL LINE(TV11,RT11,200,1,+50,SYM)
      SYM=SYM+1
      CALL LINE(TV11,RWF11,200,1,+50,SYM)
      SYM=SYM+1
      CALL LINE(TV11,RWC11,200,1,+50,SYM)
      CALL PLOT(XP,0.0,-3)
400  CONTINUE
      CALL PLOT(1.0,1.0,999)
2222 FORMAT(1H )
99  STOP
      END

```

GEORGIA INSTITUTE OF TECHNOLOGY
ATLANTA, GEORGIA 30332

**OFFICE OF
THE DIRECTOR OF
FINANCIAL AFFAIRS**

July 27, 1977

NASA
Ames Research Center
Moffett Field, Ca. 94035

Attn: Financial Management Div. 203-18


Gentlemen:

Enclosed are the Final-Cumulative Cost Expenditure Report and the Final Grantee Quarterly Cash Requirement Report for Grant Number NSG-2054 for the period ending 3/31/77.

Also enclosed is Georgia Institute of Technology check number 049278 in the amount of \$ 861.96 representing cash received in excess of expenditures.

If you have questions or desire additional information, please let us know.

Sincerely yours,

 Evan Crosby
Associate Director of
Financial Affairs

EC/bs
Encl:

cc: Dr. G. T. Colwell
Mr. E. E. Renfro
Mr. A. H. Becker ✓
File E-25-649

GRANTS

Final-Cumulative Cost Expenditure Report

1. Cumulative Award	\$ 21,270.00
2. Cumulative Costs	20,408.04
(a) Balance	861.96
3. Cost Sharing	744.90

Certification: To the best of our knowledge all costs due from the U. S. Government in the performance of NASA Grant Number NSG-2054, are included in this cumulative cost statement. No additional costs will be billed for the services provided thereunder.

Georgia Institute of Technology
Institution Name

2277
Evan Crosby
Authorized Approving Official

Associate Director of Fin. Affairs
Title

July 27, 1977
Date

Enclosure

GRANTEE QUARTERLY CASH REQUIREMENT REPORT

NASA - Ames Research Center

Moffett Field, Ca. 94035

Attn: Financial Management Div. 203-18

FROM: 3/31/77

Georgia Institute of Technology, Atlanta,

GRANT NO. (1)	AMOUNT OF AWARD (2)	EXPENDED THIS QUARTER (3)	EXPENDED TO DATE (4)	ANTICIPATED EXPENDITURES NEXT QUARTER (5)	CASH RECEIVED TO DATE (6)	CASH REQUIRED NEXT QUARTER (7)	
8-2054	21,270.00	67.99	20,408.04	-0-	21,270.00	(861.96)	
9. LAST PAYMENT VOUCHER DRAWN		10. CASH REQUIRED NEXT QUARTER - COL. (7) (Enter breakdown for each month in quarter)			11. EST. CASH RE- QUIRED FOR FIRST MONTH OF NEXT SUC- CEEDING QUARTER		I CERTIFY THAT NO INTEREST WAS E
DATED		1ST MO. IN QTR. (Amt.)	2D MO. IN QTR. (Amt.)	3D MO. IN QTR. (Amt.)	TITLE Associate Director of Financial SIGNATURE		

GEORGIA INSTITUTE OF TECHNOLOGY
ATLANTA, GEORGIA 30332

DATE

07/26/77

49278

049278

CHECK AMOUNT	ITEM DESCRIPTION	ACCOUNT	REQ NO	OBJ CODE	AMOUNT
861.96	REFUND OF UNEXPENDED FUNDS AT END OF PROJECT GRANT NSG 2054 RETURN TO T A FOWLER	RF-41343			861.96

BATCH NO 015-0-9-12 TOTAL

861.96

DETACH BEFORE DEPOSITING AND RETAIN FOR YOUR FILES

STATE OF GEORGIA		STATE OF GEORGIA		STATE OF GEORGIA	
Georgia Institute of Technology ATLANTA, GEORGIA 30332					
PAY TO THE ORDER OF					
NASA AMES RESEARCH CENTER MOFFETT FIELD CA 94035					
DATE		CHECK NUMBER		049278	
07/26/77		49278			
PAY EXACTLY		NET AMOUNT			
*****861.96		*****861.96			
CHECK VOID IF NOT CASHED WITHIN 120 DAYS					
OPERATING ACCOUNT					
TO: THE NATIONAL BANK OF GEORGIA ATLANTA, GEORGIA					
64-25 610					
VICE PRESIDENT FOR BUSINESS AND FINANCE					
THIS CHECK IS IN PAYMENT OF A STATE OBLIGATION AND MUST BE PAID AT PAR					



E-25-649

Georgia Institute of Technology
School of Mechanical Engineering
Atlanta, Georgia



PREDICTION OF CRYOGENIC HEAT PIPE PERFORMANCE

Final Report

Prepared for the
National Aeronautics and Space Administration
under
Grant NSG-2054

Prepared by
Gene T. Colwell, Professor

March 31, 1977

Georgia Institute of Technology
School of Mechanical Engineering
Atlanta, Georgia

PREDICTION OF CRYOGENIC HEAT PIPE PERFORMANCE

Final Report

Prepared for the
National Aeronautics and Space Administration
under
Grant NSG-2054

Prepared by
Gene T. Colwell, Professor

March 31, 1977

Georgia Institute of Technology
School of Mechanical Engineering
Atlanta, Georgia
30332

NASA Grant NSG-2054
Final Report
March 31, 1977

Approved:

S. P. Kezios, Director
School of Mechanical Engineering

Gene T. Colwell
Principal Investigator

ACKNOWLEDGEMENTS

The author wishes to express his gratitude to Stan Ollendorf of the Goddard Space Flight Center for continued encouragement and advice over the past two years. In addition Al Sherman of the Goddard Space Flight Center and Craig McCreight of the Ames Research Center contributed greatly to the project.

SUMMARY

This report describes work performed in the School of Mechanical Engineering at the Georgia Institute of Technology under NASA grant NSG-2054. The project was started in January of 1975 and completed in March of 1977. Two M.S. theses [8,28], which are directly related to the project, have been published and it is expected that at least one paper will be published in a technical journal as a result of work performed under the grant.

The main goal of the work has been to study theoretically the transient behavior of very low temperature heat pipes. A powerful technique has been developed for predicting transient three dimensional temperature distributions and heat fluxes for heat pipes operating under a wide variety of conditions. Radiating, conducting, and convecting external environments can be handled. In addition, startup from the supercritical state can be accommodated.

TABLE OF CONTENTS

	Page
ACKNOWLEDGEMENTS.	i
SUMMARY	ii
LIST OF TABLES.	v
LIST OF ILLUSTRATIONS	vi
NOMENCLATURE.	viii
I. INTRODUCTION.	1
A. Statement of Problem	
B. Background	
C. Literature Survey	
II. THEORETICAL DEVELOPMENT	8
A. Description of Digital Model	
B. Solution Methods	
C. Fluid Dynamic Effects	
D. Logic Solution	
E. Description of Analog Model	
III. RESULTS AND COMPARISONS	37
IV. CONCLUSIONS AND RECOMMENDATIONS	58
APPENDICES	
A. TRANSFORMATION OF COORDINATE SYSTEMS.	61
B. THERMODYNAMIC PROPERTY.	64
C. WICK-WALL INTERFACE NODES	66
D. COMPUTER CODE	69
E. DISCUSSION OF STABILITY AND ACCURACY OF NUMERICAL TECHNIQUES.	86

	Page
F. CALCULATION OF THERMAL CONDUCTIVITY.	88
G. ANALOG SCALING	90
H. DERIVATION OF EXPONENTIAL MODEL.	92
REFERENCES	93
DISTRIBUTION	96

LIST OF TABLES

Table	Page
1. Dimensions and Materials of Heat Pipe Considered in this Study.	9
2. Parameters for Case Studies	41

LIST OF ILLUSTRATIONS

Figure		Page
1.	General Layout of Heat Pipe.	10
2.	Closeup of Composite Slab and Circumferential Wick at Heat Transfer Section.	11
3.	Capillary Structure.	12
4.	Heat Pipe Model.	13
5.	Computation Grid and Boundary Conditions	21
6.	Cooling Jacket Used in Model	24
7.	Model of Fluid Flow in Slab.	25
8.	Flow Diagram of Computer Program	29
9.	Schematic Diagram of Analog Model.	34
10.	Analog Circuit	35
11.	Comparison of Model with Experimental Data from the Literature.	38
12.	Comparison of Exponential, Analog and Digital Models for Heat Pipe with Cooling Jacket	40
13.	Comparison of Analog and Digital Model for Case 1	42
14.	Effect of Changing Wall Thickness.	44
15.	Effect of Changing Number of Wick Layers	45
16.	Effect of Changing Thickness of Fluid Gap.	46
17.	Effect of Changing Slab Compositions	47
18.	Comparison of Startup at Different Power Levels.	48
19.	Comparison of Startup at Different Temperatures.	50

Figure	Page
20. Development of Overall Temperature Gradients. . .	51
21. Comparison of Heat Pipe Response with Cooling Jacket or Radiating Surface Heat Sink	52
22. Response of Radiating Heat Sink	53
23. Startup from Supercritical.	54
24. Comparison of Predicted Fluid Velocity with Data from Literature.	55
25. Velocity with Position in Composite Slab.	57
26. Polar to Rectangular Transformation	63
27. Wick-Wall Interface Nodes	67

NOMENCLATURE

A_C	cross-sectional area of slab
A_i	constant coefficient for node i
A_R	surface area of radiator
B_i	constant coefficient for node i
c_{CJ}	composite specific heat for cooling jacket
c_f	specific heat of coolant
C_i	constant coefficient for node i
c_p	specific heat of pipe wall
c_R	specific heat of radiator
c_T	composite specific heat for total system
c_V	composite specific heat for vapor region
c_w	composite specific heat for screen and fluid gaps
d_f	distance between filament centers in screen
D_i	constant coefficient for node i
h_C	surface coefficient
h_{fg}	heat of vaporization of working fluid
\bar{K}	effective inverse permeability of slab
K_P	thermal conductivity of pipe wall
K_w	thermal conductivity of wick
L	distance from fluid source to fluid front in slab
ℓ_C	condenser length
ℓ_E	evaporator length
\dot{m}	mass flow rate of working fluid in slab

m_{CJ}	mass of cooling jacket and fluid
\dot{m}_f	mass flow rate of coolant
m_R	mass of radiating heat sink
m_T	total mass of heat pipe and cooling jacket
m_V	total mass of vapor region
NIC	number of radial nodes in condenser grid
NIE	number of radial nodes in evaporator grid
NJE	number of circumferential nodes in evaporator grid
NKC	number of axial nodes in condenser grid
NKA	number of axial condenser nodes in adiabatic section
NL	number of layers of screen in wick
Q_{cap}	capillary limited heat transfer rate
Q_E	Heat flux at evaporator surface
Q_{max}	maximum heat transfer rate for scaling analog
Q_{space}	heat flux into radiator from space
r	radial coordinate
r_B	inner radius of pipe wall
r_f	filament radius in screen
r_I	inner radius of wick
r_i	radius at node i
r_O	outer radius of pipe wall
r_p	pore radius of screen
SF	scaling factor for wick nodes
$T_{1,2,\dots,6}$	temperature of node 1, 2, ..., 6 in analog model
t	time
t_{max}	representative time used for scaling analog

T_{CJ}	temperature of cooling jacket
T_C	temperature of condenser
$TC_{i,k}^n$	temperature of condenser node i,k at time n
T_E	temperature of evaporator
$TE_{i,j}^n$	temperature of evaporator node i,j at time n
T_I	incoming temperature of coolant
T_{min}	minimum temperature for scaling analog
T_{max}	maximum temperature for scaling analog
T_R	temperature of radiator
T_V	temperature of vapor region
V	velocity of fluid in slab
v_{pC}	volume of pipe wall in condenser
v_{pE}	volume of pipe wall in evaporator
v_{wC}	volume of wick in condenser
v_{wE}	volume of wick in evaporator
x	transformed radial coordinate
y	transformed circumferential coordinate
z	axial coordinate
α	thermal diffusivity
β	width of fluid gap
Δ	finite difference operator
ϵ	emmisivity of radiator
μ_ℓ	viscosity of liquid nitrogen
ρ_ℓ	density of liquid nitrogen
ρ_p	density of pipe wall
ρ_w	density of wick

σ	Stefan-Boltzman constant
σ_{ℓ}	surface tension of liquid nitrogen
ϕ	circumferential coordinate in evaporator

I. INTRODUCTION

A. Statement of Problem

Investigations into the performance of cryogenic heat pipes have been in progress at the Georgia Institute of Technology for several years. In continuation of these investigations the goal of this study has been to gain a better understanding of the transient response of cryogenic heat pipes and heat pipe systems. A method for predicting behavior of heat pipes during startup or changes in thermal transport has been developed. Included in the model are provisions for simulating startup from temperatures above the critical point of the working fluid.

B. Background

A heat pipe is a device that transfers large quantities of heat with a relatively small temperature gradient. The containing envelope has an internal wick structure and a liquid in near equilibrium with its vapor phase. The phenomena of conduction and phase change are combined to make high thermal conductance possible. The basic theory, design, and operation of heat pipes are well discussed by Cotter [1], Chisolm [2], and others.

As heat is added to the evaporator of a heat pipe

some of the fluid in the wick evaporates thus increasing the vapor pressure. The increased pressure drives some of the warm vapor to the condenser. The condensing vapor gives up energy which is conducted through the wall and transferred from the heat pipe. Due to evaporation the liquid-vapor interface recedes into the capillary structure and thus decreases the radius of curvature of the meniscus in the heated end. Condensation on the capillary structure at the cool end increases the meniscus radius in the condenser. This difference in radii of curvature creates the driving force to pump the liquid back to the evaporator [1].

The heat pipe startup mode described above assumes the vapor density at the ambient temperature is high enough for a continuum flow to exist and that the capillary structure is filled with working fluid. Such startup is referred to as uniform startup by Cotter [3]. A second mode of startup occurs if the vapor pressure is low and molecular flow exists at ambient temperatures. Heating produces a continuum in the evaporator and transition zone between the evaporator and condenser. Often the working fluid is in a frozen state and must melt before startup can occur. This mode takes about two and one half times longer than uniform startup assuming the working fluid is not frozen prior to startup. Non-condensable gases, when present in the vapor space, creates a third mode of startup. During heating the non-condensables are swept into the cold end of the condenser.

This method of startup can be accomplished very quickly or very slowly depending on the quantity of non-condensables present.

At steady state, for some types of capillary structures, that part of the evaporator capillary furthest from the condenser may be dried out. The wick geometry and meniscus radius determine how much of the evaporator is actively working. Colwell and Williams [4] suggested that the axial vapor Reynolds number may determine the length along which condensation actually occurs in the condenser. Assuming a saturated wick before startup the development of these phenomena do affect startup times.

If the heat pipe is at a temperature above the critical point of the working fluid before startup, all of the fluid will be in a single phase supercritical state. Before the evaporation-condensation cycle can begin the fluid must first be cooled below the critical temperature at the cool end. Capillary action will then pump the liquid along the wick back to the evaporator. The velocity of the fluid in the wick is on the order of centimeters per minute [5]. The entire heat pipe must be reflexed before any significant heat transfer can take place.

In the design of a heat pipe system it is important to understand the startup of the system and the response to a change in power level. The parameters affecting transient response of a heat pipe must be determined. The goal of

this project was to develop a technique for predicting the startup and response times for various heat pipes.

C. Literature Survey

The performance of heat pipes in an outer space environment was evaluated by Kirkpatrick and Brennan [6] using the Applications Technology Satellite (ATS-F). They concluded that for space applications heat pipes can be useful temperature control devices. Sherman and Brennan [7] performed a study of low temperature heat pipes for spacecraft uses. Nitrogen and oxygen were determined to be best fluids for operation in the cryogenic temperature range. The composite slab wick was said to be a reliable porous media for present day and projected NASA applications.

Recent work at the Georgia Institute of Technology has been directed to understanding the steady state performance of a heat pipe similar to the one in this study. Hare [8] performed a theoretical study of a performance of a cryogenic heat pipe using nitrogen as the working fluid. Polynomial expressions were developed for predicting the thermal properties as a function of temperature. Mass- and heat-transport equations were combined to give capillary and sonic limitations on the performance of the pipe and the thermal resistances of each heat pipe component. A study was made on the effects of changing the composite slab and wick structure.

Colwell [9] used a similar approach to study the effects

of fluid gaps in the circumferential wick. Partial dryout and vapor Reynolds number effect were added through a simplified approach. The effect of changing wall thickness, number of wick layers and mesh size was also modeled.

A coupled heat transfer diffusion model was used by Saaski [26] to model a gas controlled heat pipe. The device was 45.48 cm long with an inside radius of 1.288 cm and used methanol as the working fluid. Experimental response curves were compared with curves predicted with the model. Agreement is very good, both curves reaching 95 percent of steady state values in about 130 seconds.

In a study of the dynamic behavior of heat pipes Groll, et al. [10] determined that small power variations around the operating point of a heat pipe present no special problems. The discussion is primarily concerned with heat pipes in the 200 K to 500 K temperature range. A one-dimensional model was developed for prediction of heat pipe response and examples of normal startup and startup failure were presented. Groll concluded that the dynamic response of heat pipes can be adequately treated with a simple mathematical model.

Another startup model was developed by Cotter [3]. Linear relationships were found for predicting uniform startup and startup with non-condensable gases present. Various modes of heat pipe startup are described and mechanisms which might affect successful startup are discussed. From this model the response time for most high performance heat pipes

is between 10 and 100 seconds.

Chato and Streckert [5] ran a series of tests with a water heat pipe. The device was 81.9 cm long with an inside diameter of 7.62 cm. Experimental values of maximum heat flux were in the middle of the range predicted by horizontal wicking tests. During normal operation, temperatures in the vapor region did not vary by more than $1/2^{\circ}\text{C}$. Attempts to measure transients failed since the heat pipe responded faster than the heating and cooling system. They estimated the response time of the heat pipe at less than twenty seconds.

Smirnov, et al. [11] developed a model for predicting startup of gas controlled heat pipes. Their calculations were in good agreement with experimental results. The dynamic response of buffered and unbuffered heat pipes was modeled by Rice and Azad [12]. Their model agreed with experimental data for a sodium heat pipe and for a water heat pipe.

To operate, a heat pipe must have a source and sink. Any measured response must take the source and sink into account. Should the heat sink radiate the incoming energy a phenomenon referred to by Anand, et al. [13] as temperature choking takes place. The radiating surface must adjust its temperature up or down to be in equilibrium with the incoming energy. This movement in turn forces the heat pipe to adjust its operating temperature. The response of such a system would be different from a system with a condenser bath for cooling.

Calimbas and Hulett [14] ran tests on an avionic heat pipe. The device used water as a working fluid. The inside diameter was 6.35 cm and it was 60.96 cm long. Condenser cooling was accomplished by a forced air heat exchanger. The system took fifteen minutes to adjust to a change in the heater level.

A water heat pipe with a glass bead capillary structure was built and tested by Cosgrove, et al. [15]. Cooling was accomplished by evaporation of methanol. A steady state model was developed consisting of basic mass, energy and momentum balances. Predicted values were in close agreement with experimental results. After a change in power approximately thirty-five minutes were required for the system to reach a steady state.

All of the literature indicates that heat pipes have very small response times. Since the mass of heating and cooling systems is greater than that of a heat pipe they respond more slowly. Transient data from experiments reflect the response time of the heaters and cooling jackets used in the experiments. Any attempt to model such a system must include an accurate model of the heating and cooling apparatus.

II. THEORETICAL DEVELOPMENT

This study is concerned with a cryogenic heat pipe with a composite slab wick. Geometry and physical characteristics were suggested by the sponsoring agency. Dimensions and materials are given in Table 1 and Figure 1. The configuration of the composite slab and wick is shown in Figures 2 and 3.

The response of this heat pipe has been studied on analog and digital computers. A system of nodes is used to develop a set of time dependent equations accounting for the heat capacity of the system. Due to a limited capacity, the nodal system used for the analog model is fairly simple and limited to small transient. The model assumes constant properties and does not include any effects of fluid dynamics. The digital model includes a much finer nodal system and fluid dynamics. Property equations in the program permit the variation of properties with temperature. Both models predict response and temperature profiles for the heat pipe.

A. Description of the Digital Model

For the digital model the heat pipe is broken into its three main parts: evaporator, vapor region, and condenser which includes the adiabatic section. Figure 4 shows the

Table 1. Dimensions and Materials for the Heat Pipe
Considered in this Study

Total length	.9144 meters
Length of evaporator	.1524 meters
Length of condenser	.3048 meters
Length of adiabatic section	.4572 meters
Outside diameter of pipe	.635 centimeters
Wall thickness	.1015 centimeters
Working fluid	Nitrogen
Material of pipe and capillary structure	304 stainless steel
Wick configuration	circumferential wick with composite central slab
Slab	4 layers 400 mesh around 5 layers 30 mesh screen
Circumferential wick	2 layers 400 mesh screen
Fluid gap	.003048 centimeters

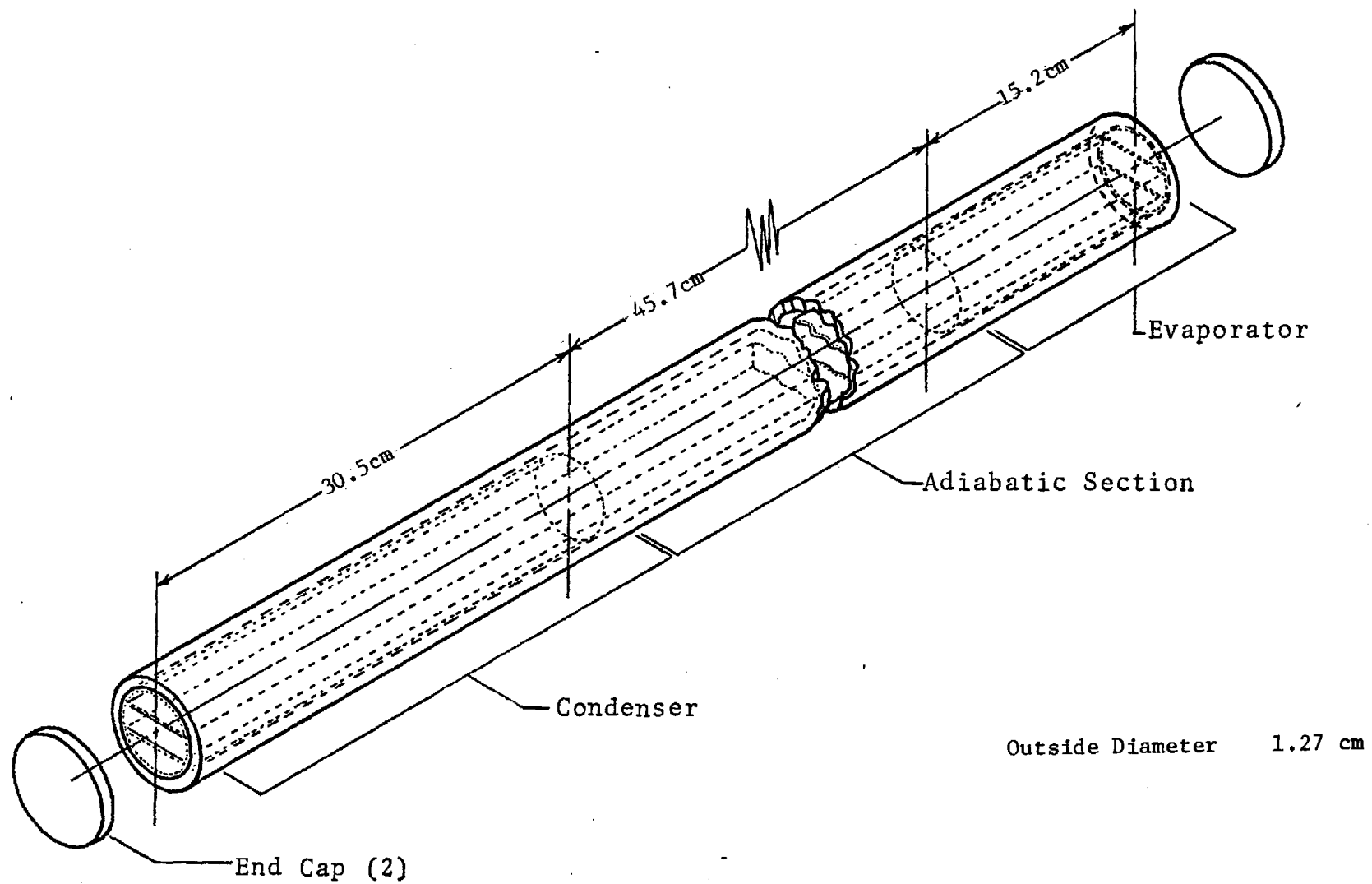


Figure 1. General Layout of Heat Pipe

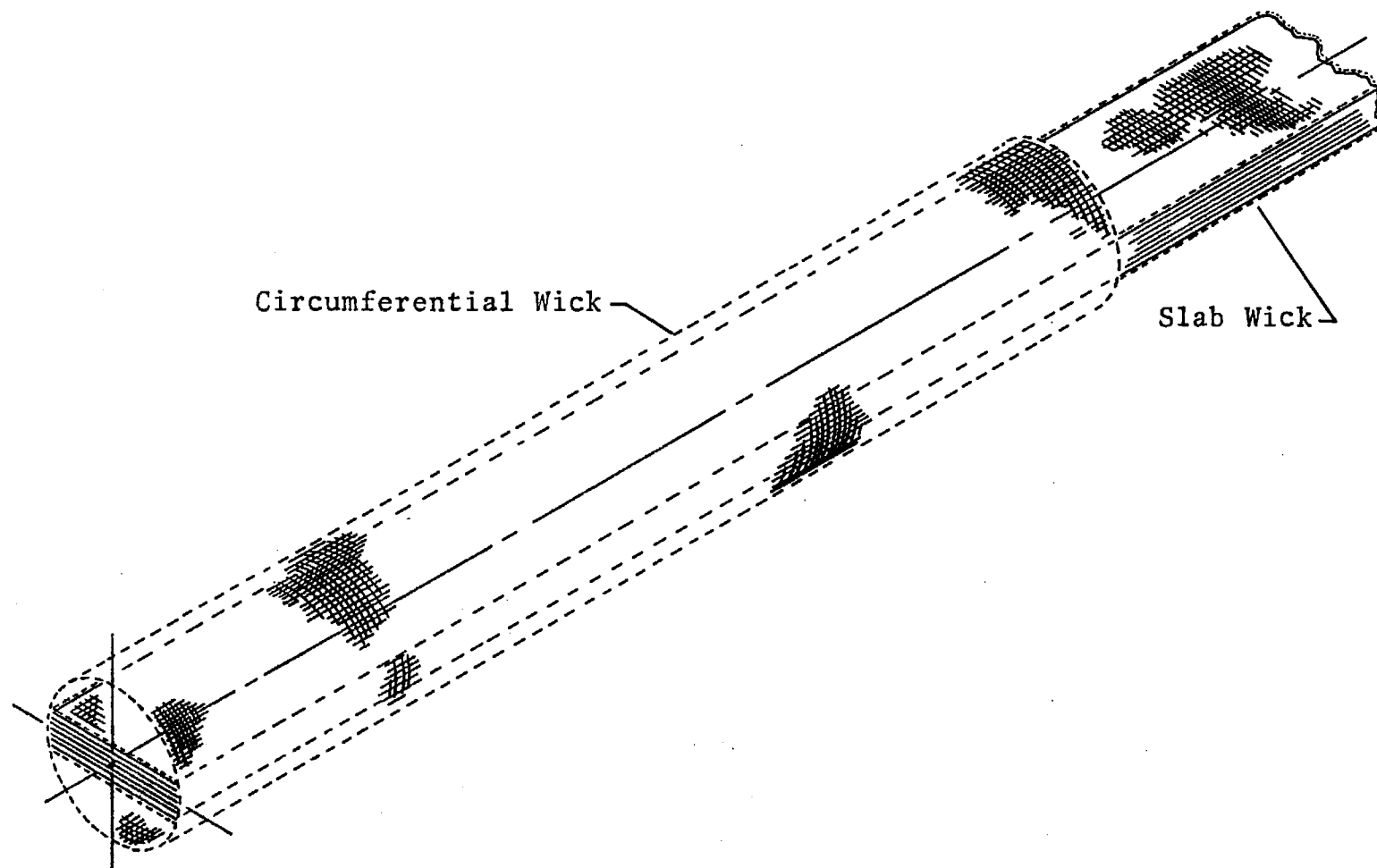


Figure 2. Close-Up of Composite Slab and Circumferential Wick
at Heat Transfer Section

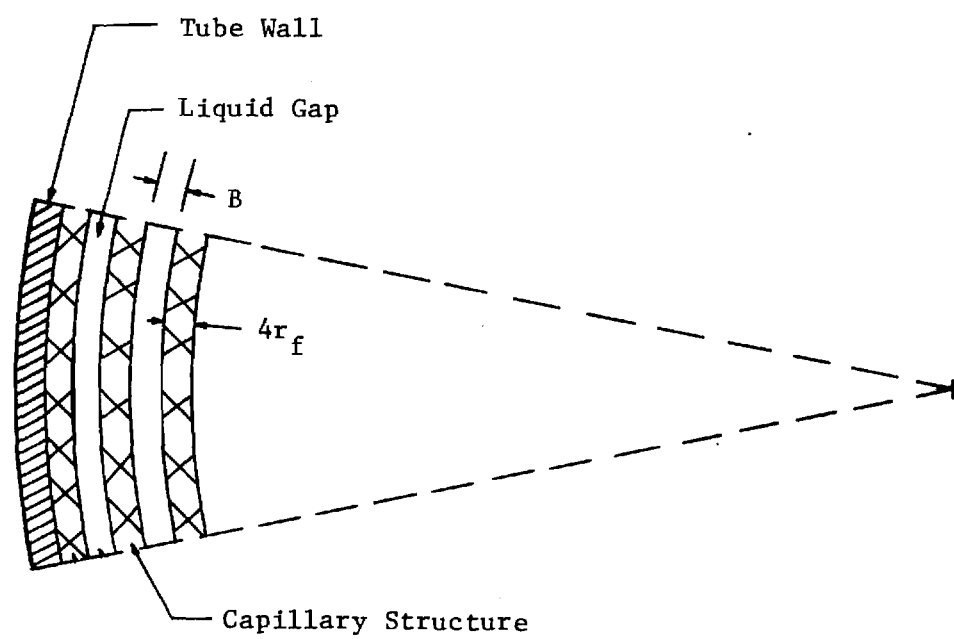


Figure 3. Capillary Structure

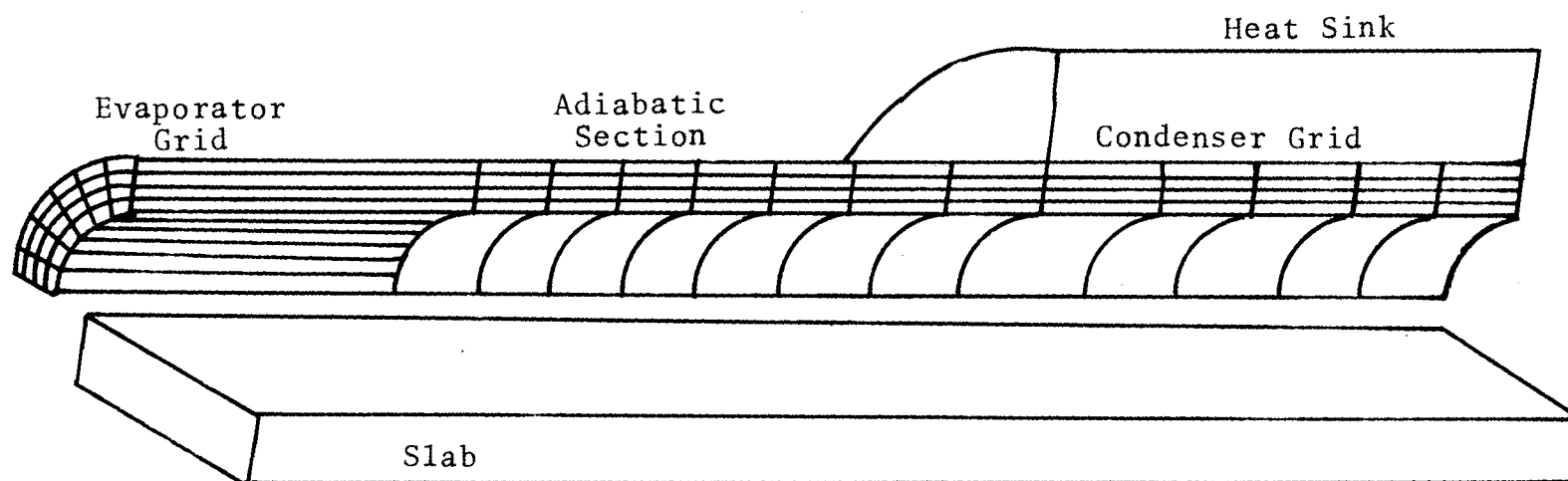


Figure 4. Heat Pipe Model

parts of the heat pipe and the nodal system used for solutions. Basic heat transfer equations are written for each part and the equations are coupled at the boundaries.

A two-dimensional model of the evaporator has been developed that permits temperature variation in the radial and circumferential directions. Symmetry is assumed such that only a 90° section is modeled. In this way the effects of partial burn-out in the circumferential wick can be studied.

The vapor region is modeled as a lumped mass system. The system includes the vapor, the slab, and the innermost part of the wick along the entire length of the heat pipe. The vapor temperature is assumed to vary only with time having the same value in both the evaporator and condenser.

Condenser and adiabatic sections are modeled as two dimensional in the radial and axial directions. This arrangement permits study of Reynolds number effects and axial conduction.

Conditions at the surface of the evaporator and condenser can be modeled in several ways. The surface temperature can be fixed, a known heat flux can be made to exist at the surface, or an evaporator or condenser saddle can be added. The condenser saddle can be cooled with a cooling jacket or a radiating surface.

B. Solution Methods

Basic heat transfer equations can be written for each

section of the heat pipe. The result is a system of three coupled differential equations:

Evaporator:

$$\frac{1}{\alpha} \frac{\partial T_E}{\partial t} = \frac{\partial^2 T_E}{\partial r^2} + \frac{1}{r} \frac{\partial T_E}{\partial r} + \frac{1}{r} \frac{\partial^2 T_E}{\partial \phi^2} + \frac{\partial^2 T_E}{\partial z^2} \quad (2.1)$$

Vapor:

$$m_V c_V \frac{dT_V}{dt} = 2\pi r_I \ell_E K_W \left. \frac{\partial T_E}{\partial r} \right|_{r=r_I} + 2\pi r_I \ell_C K_W \left. \frac{\partial T_C}{\partial r} \right|_{r=r_I} \quad (2.2)$$

Condenser:

$$\frac{1}{\alpha} \frac{\partial T_C}{\partial t} = \frac{\partial^2 T_C}{\partial r^2} + \frac{1}{r} \frac{\partial T_C}{\partial r} + \frac{\partial^2 T_C}{\partial z^2} \quad (2.3)$$

These equations are transient conduction equations and do not account for fluid dynamics directly. As will be shown in the next section, in uniform startup with a fully wetted wick the time for fluid velocity response is very small. In the case of startup from the supercritical, these effects can be handled by manipulation of boundary conditions in the nodal system.

The equation for the vapor region is first order in time only. Finite difference techniques permit solving for the vapor temperature explicitly at each time step. The

equation can be written in finite difference form as:

$$m_V c_V \frac{T_V^{n+1} - T_V^n}{t^{n+1} - t^n} = \frac{2\pi r_I \ell_E K_W}{NJE \Delta x r_I} \sum_{j=1}^{NJE} (T_{NIE-1,j}^n - T_V^n) + \frac{2\pi c_I \ell_C K_W}{NKC \Delta x c_I} \sum_{k=1}^{NKC} (T_{NIC-1,k}^n - T_V^n) \quad (2.4)$$

Which can be solved explicitly

$$T_V^{n+1} = \frac{2\pi \ell_E K_W \Delta t}{NJE \Delta x m_V c_V} \sum_{j=1}^{NJE} (T_{NIE-1,j}^n - T_V^n) + \frac{2\pi \ell_C K_W \Delta t}{NKC \Delta x m_V c_V} \sum_{k=1}^{NKC} (T_{NIC-1,k}^n - T_V^n) + T_V^n \quad (2.5)$$

Note that the heat transfer into the vapor region is equated to the heat transfer across the inner nodes of the evaporator and condenser sections.

The partial differential equations that describe heat transfer in the evaporator and condenser sections can be solved with a grid system of nodes. The curvilinear system is made rectangular with a change of variables. Details of this variable change are given in Appendix A. A heat balance is written for each node equating net heat gain with the change in temperature of that node. The resulting systems of equations are solved with an alternating direction implicit method.

Two finite difference approximations of equation (2.1) are used alternately to sweep through the evaporator grid for each time step. These two equations are given by: For the first half time step

$$\begin{aligned}
 \rho_p c_p r_i^2 \frac{TE_{i,j}^{n+1/2} - TE_{i,j}^n}{t^{n+1/2} - t^n} = & \frac{K_p}{\Delta x^2} (TE_{i+1,j}^{n+1/2} + TE_{i-1,j}^{n+1/2} - 2TE_{i,j}^{n+1/2}) \\
 & + \frac{K_p}{\Delta y^2} (TE_{i,j+1}^n + TE_{i,j-1}^n - 2TE_{i,j}^n) \\
 & - \frac{K_p TE_{i,j}^n}{\sum_{j=1}^{NJE} TE_{i,j}^n} \left(\sum_{j=1}^{NJE} TE_{i,j}^n - TC_{i,1}^n \right) \left(\frac{r_i^2}{\Delta z^2} \right) \quad (2.6)
 \end{aligned}$$

And for the second half time step

$$\begin{aligned}
 \rho_p c_p r_i^2 \frac{TE_{i,j}^{n+1} - TE_{i,j}^{n+1/2}}{t^{n+1} - t^{n+1/2}} = & \frac{K_p}{\Delta x^2} (TE_{i+1,j}^{n+1/2} + TE_{i-1,j}^{n+1/2} - 2TE_{i,j}^{n+1/2}) \\
 & + \frac{K_p}{\Delta y^2} (TE_{i,j+1}^{n+1} + TE_{i,j-1}^{n+1} - 2TE_{i,j}^{n+1}) \\
 & - \frac{K_p TE_{i,j}^n}{\sum_{j=1}^{NJE} TE_{i,j}^n} \left(\sum_{j=1}^{NJE} TE_{i,j}^n - TC_{i,1}^n \right) \left(\frac{r_i^2}{\Delta z^2} \right) \quad (2.7)
 \end{aligned}$$

Note that the equations are implicit in only one direction and this direction changes with each half time step.

The last term in each equation accounts for heat conducted axially along the tube. An artificial node is created at the evaporator end of the adiabatic section. At each radial location the artificial node has a temperature equal to the average temperature of the evaporator nodes at that same radial location. This node provides a constant temperature boundary condition for the condenser and adiabatic grid. A weighted fraction of the total heat conducted axially is subtracted from each evaporator node.

Casting equation (2.6) in a different form gives

$$\begin{aligned}
 & - \left(\frac{\Delta t K_p}{2(\Delta x)^2 \rho_p c_p r_i} \right) TE_{i+1,j}^{n+1/2} + \left(1 + \frac{\Delta t K_p}{(\Delta x)^2 \rho_p c_p r_i} \right) TE_{i,j}^{n+1/2} \\
 & - \left(\frac{\Delta t K_p}{2(\Delta x)^2 \rho_p c_p r_i} \right) TE_{i-1,j}^{n+1/2} = \left(\frac{\Delta t K_p}{2(\Delta y)^2 \rho_p c_p r_i} \right) (TE_{i,j+1}^n + TE_{i,j-1}^n) \\
 & \quad \left(1 - \frac{\Delta t K_p}{(\Delta y)^2 \rho_p c_p r_i} \right) TE_{i,j}^n \\
 & - \left(\frac{\Delta t K_p}{2\rho_p c_p (\Delta z)^2} \right) \left(\frac{TE_{i,j}^n}{\sum_{j=1}^{NJE} TE_{i,j}^n} \right) \left(\frac{1}{NJE} \sum_{j=1}^{NJE} TE_{i,j}^n - TC_{i,1} \right) \quad (2.8)
 \end{aligned}$$

This equation can be used to construct a matrix of NIE equations for each value of j . Each equation is of the form:

$$A_i TE_{i-1,j}^{n+1/2} + B_i TE_{i,j}^{n+1/2} + C_i TE_{i+1,j}^{n+1/2} = D_i \quad (2.9)$$

and the resulting matrix is shown below:

$$\begin{vmatrix} B_1 & C_1 & 0 & \dots & \dots & 0 & 0 \\ A_2 & B_2 & C_2 & 0 & \dots & 0 & 0 \\ 0 & A_3 & B_3 & C_3 & \dots & 0 & 0 \\ \vdots & \vdots & \vdots & \vdots & \vdots & \vdots & \vdots \\ 0 & 0 & 0 & \dots & A_{NIE-1} & B_{NIE-1} & C_{NIE-1} \\ 0 & 0 & 0 & \dots & 0 & A_{NIE} & B_{NIE} \end{vmatrix} = \begin{vmatrix} D_1 \\ D_2 \\ \vdots \\ \vdots \\ D_{NIE} \end{vmatrix}$$

This matrix is tridiagonal and can be solved with a modified Gaussian elimination technique [16]. This particular subroutine permits any combination of boundary conditions at either end of the array. A matrix is constructed and solved for each value of j giving values at each location for the first half time step. The second equation (2.7) is then used to construct and solve a matrix of NJE equations for each value of i . This solution technique is known as the alternating direction implicit. It has the advantage of being very stable with respect to time and yet being fairly simple to solve numerically.

A similar derivation in the condenser and adiabatic section gives:

$$\begin{aligned}
& - \left(\frac{\Delta t K_p}{2(\Delta x)^2 \rho_p c_p r_i} \right) TC_{i+1,k}^{n+1/2} + \left(1 + \frac{\Delta t K_p}{(\Delta x)^2 \rho_p c_p r_i} \right) TC_{i,k}^{n+1/2} \\
& - \left(\frac{\Delta t K_p}{2(\Delta x)^2 \rho_p c_p r_i} \right) TC_{i-1,k}^{n+1/2} = \left(\frac{\Delta t K_p}{2(\Delta z)^2 \rho_p c_p} \right) (TC_{i,k+1}^n + TC_{i,k-1}^n) \\
& + \left(1 - \frac{\Delta t K_p}{(\Delta z)^2 \rho_p c_p} \right) TC_{i,k}^n
\end{aligned} \tag{2.10}$$

In the formulation of the equations the thermal properties are assumed constant. Expressions were developed by Hare [8] which permitted evaluation of properties as a function of temperature. These expressions have been modified to work with International units and additional expressions have been developed for specific heats. Appendix B lists the polynomials used. These expressions are used to calculate new properties whenever the vapor temperature has changed by more than a specified amount.

Special coefficients are required for the interface of the pipe wall and the wick. These expressions are developed in Appendix C.

The three equations were coupled at the boundaries. Figure 5 is a schematic diagram of the computational grid and boundary conditions. The temperature of the innermost node of both evaporator and condenser is calculated as a part of the vapor region and held as a constant temperature

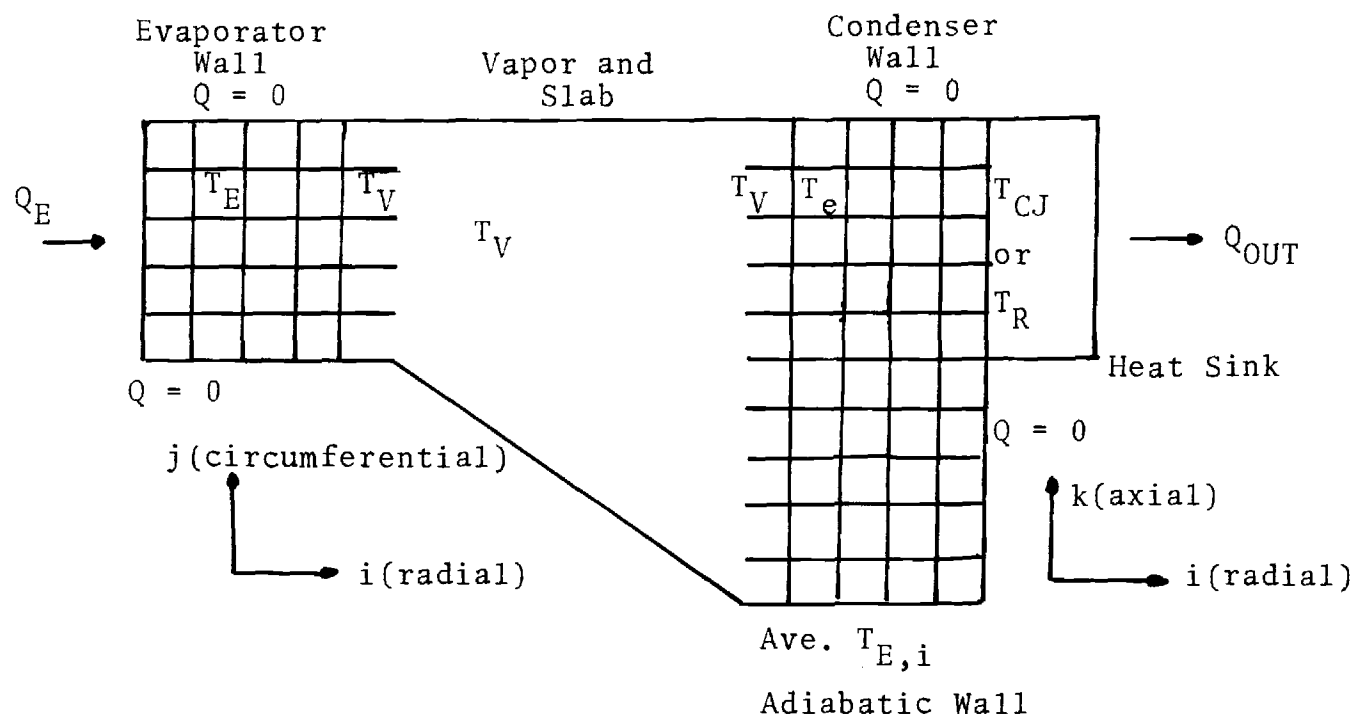


Figure 5. Computation Grid

boundary for both regions. Due to symmetry both ends of the evaporator grid can be assumed adiabatic. Also the outer surface of the adiabatic section and the lower end of the condenser are insulated. The vapor equation is in time only and therefore requires only an initial condition. Boundary conditions at the outer surface of the evaporator and condenser can be modified to better model the total system of which the heat pipe is a part.

Cooling of the condenser saddle can be accomplished either of two ways. For a radiating condenser a heat balance gives

$$m_R c_R \frac{dT_R}{dt} = 2\pi r_O \ell_C h_C (T_C - T_R) - A_R \sigma \epsilon T_R^4 + Q_{space}$$

which can be solved explicitly as:

$$T_R^{n+1} = \frac{2\Delta t \rho r_O \Delta z h_C}{m_R c_R} \sum_{k=NKA+1}^{NKC} (T_{C,NIC,k}^n - T_R^n) - \frac{A_R \sigma \epsilon \Delta t}{m_R c_R} T_R^{n4} + \frac{Q_{space}^n \Delta t}{m_R c_R} + T_R^n$$

If a cooling jacket is to be used the following equation has to be solved:

$$m_{CJ} c_{CJ} \frac{dT_{CJ}}{dt} = 2\pi r_O \ell_C h_C (T_C - T_{CJ}) + \dot{m}_f c_f (T_I - T_{CJ})$$

or

$$T_{CJ}^{n+1} = \frac{2\Delta t \pi r_O \Delta z h_C}{m_{CJ} c_{CJ}} \sum_{k=NKA+1}^{NKC} (T_{NIC,k}^n - T_{CJ}^n) + \frac{\dot{m}_f c_f \Delta t}{m_{CJ} c_{CJ}} (T_I^n - T_{CJ}^n) + T_{CJ}^n$$

This equation assumes a cooling jacket as shown in Figure 6. Both of these heat sink models are coupled to the condenser with a surface coefficient.

C. Fluid Dynamic Effects

If the startup of a heat pipe is to proceed smoothly fluid must be able to reach the evaporator capillary structure at the same rate that evaporation occurs. Fluid flow in the slab can be modeled as shown in Figure 7. A one dimensional momentum balance can be written for the case where evaporator burnout has occurred:

$$\frac{2\sigma_\ell}{r_p} A_c - \bar{K} \frac{\mu_\ell \dot{m} L}{\rho_\ell A_c} A_c = \frac{d}{dt} (A_c L V_{\rho\ell}) \quad (3.1)$$

If the length is assumed equal to the distance from the midpoint of the condenser to the midpoint of the evaporator the equation can be solved for the velocity as a function of time. The result is:

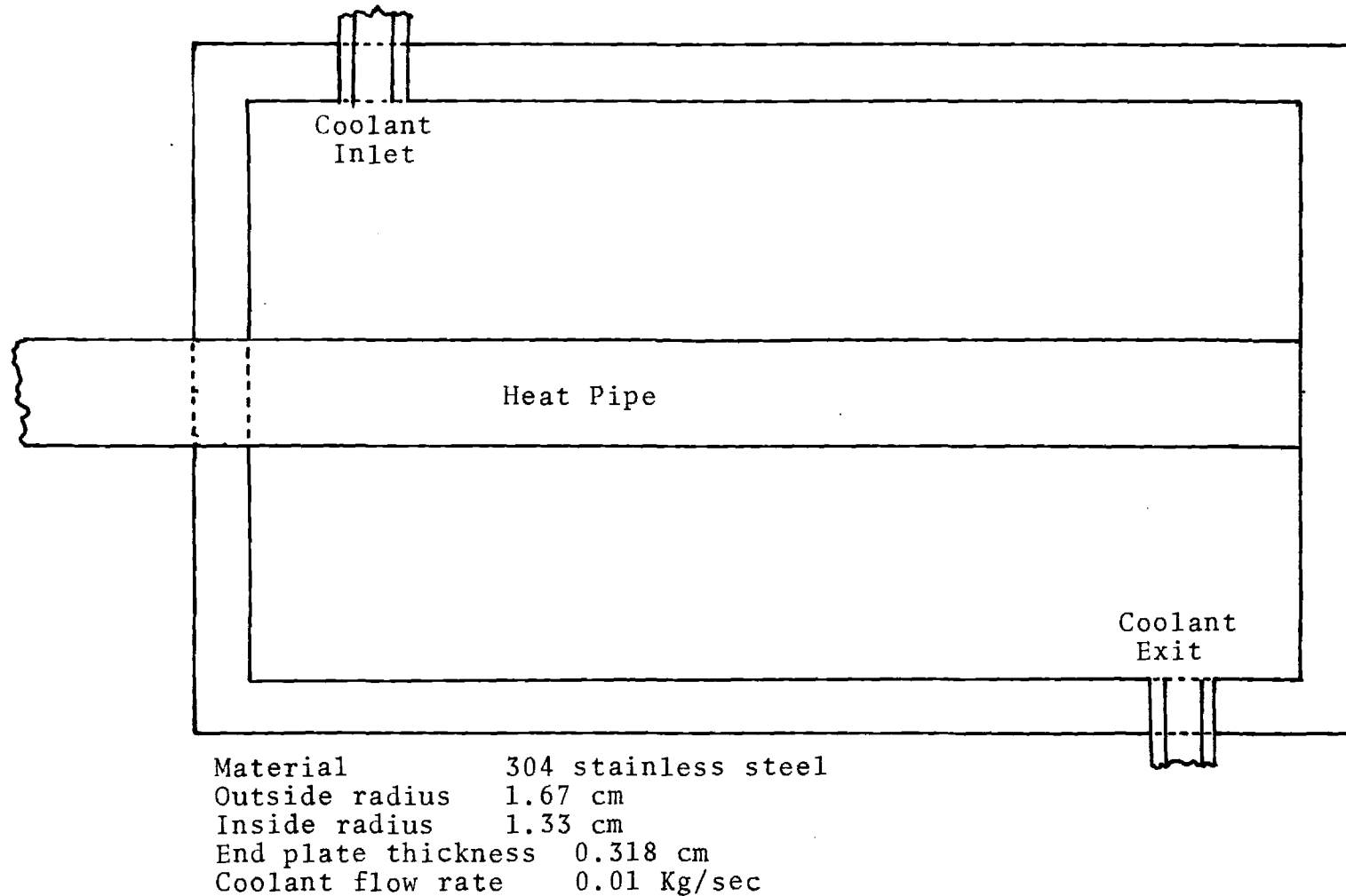


Figure 6. Cooling Jacket Used in Model

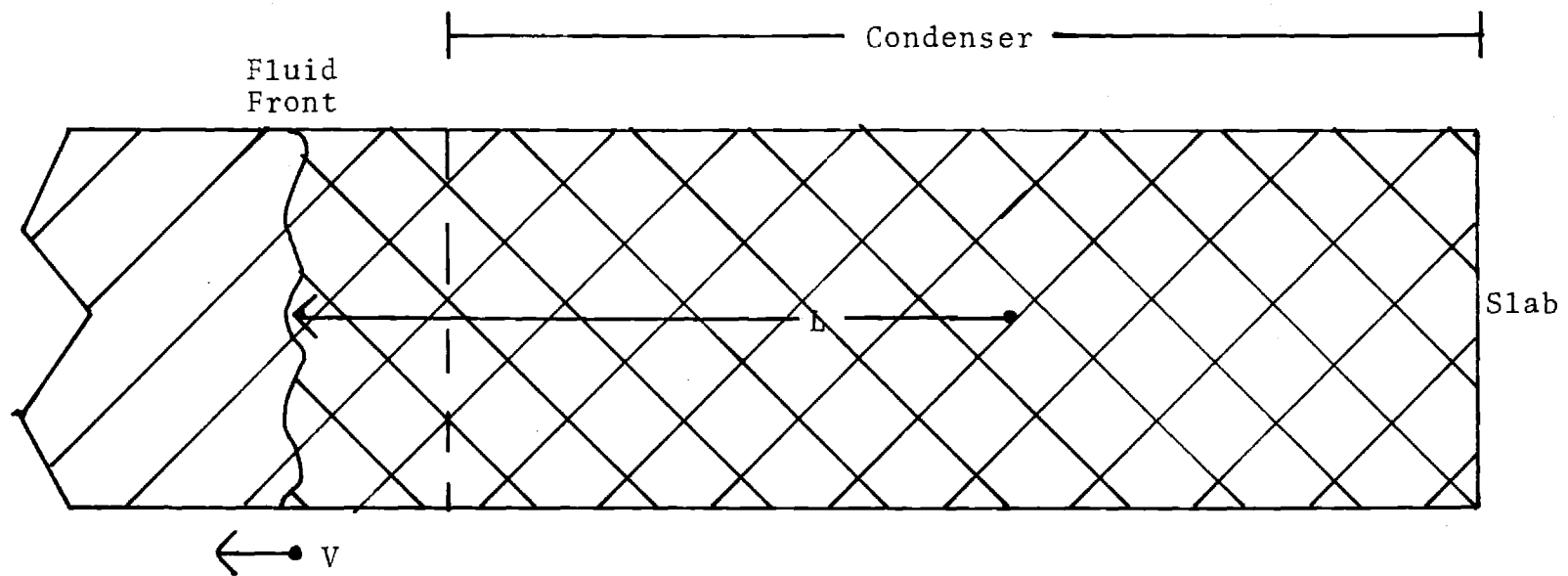


Figure 7. Model of Fluid Flow in Slab

$$V(t) = \frac{2\sigma_\ell}{\bar{K}\mu_\ell r_p L} \left(1 - e^{-\left(\bar{K} \frac{\mu_\ell}{\rho_\ell}\right)t}\right) \quad (3.2)$$

From this expression it can be seen that the time required for the fluid to reach a steady state velocity in an initially wetted capillary structure is a function of viscosity, inverse permeability, and density. For the particular heat pipe under study the fluid velocity reaches better than ninety percent of its steady state value in less than 0.05 seconds. Although this model is no doubt over simplified it does show that fluid velocities do develop very rapidly and would present no problem to startup in this heat pipe.

Velocity in the slab can be used to predict the capillary limited heat transfer rate with

$$Q_{cap} = \rho_\ell V A_c h_{fg} \quad (3.3)$$

Heat transfer from the evaporator can be limited to this value by restricting the number of nodes interacting with the vapor region.

In simulating startup from the supercritical an expression must be developed to predict the location of the fluid as it is pumped back towards the evaporator. Assume uniform and rapid condensation over the entire condenser surface when the temperature drops below the critical value.

Equation (3.1) can be solved explicitly in finite difference form:

$$V^{n+1} = \frac{\Delta t}{L^n} \left(\frac{2\sigma_\ell}{r_p \rho_\ell} - \bar{K} \frac{\mu_L^n V^n}{\rho_\ell} - V^{n^2} \right) + V^n \quad (3.4)$$

The length in equation (3.4) is allowed to vary with time as the fluid moves along the slab. The location of the fluid can be calculated from:

$$L = \int_0^t V dt \quad (3.5)$$

or in finite differences:

$$L^{n+1} = L^n + V^{n+1} \Delta t \quad (3.6)$$

An initial condition is needed for each equation. The initial velocity is assumed to be zero and the initial length is assumed to be one half the length of the condenser, measured from the midpoint of the condenser.

This length L , the distance from the center of the condenser to the fluid front, is used to calculate the node through which the fluid is currently moving. All nodes containing fluid are coupled with the vapor region. Those nodes still without fluid are insulated from the vapor. This manipulation of boundary conditions, made possible through

the use of the tridiagonal subroutine, permits any combination of nodes in the evaporator or condenser to actively working with or insulated from the vapor region.

D. Logic of Solution

The preceding equations were solved simultaneously on a Control Data Corporation Cyber-74 computer. A flow chart outlining the solution procedure is shown in Figure 8. The computer program is listed in Appendix D.

After reading dimensions and initial conditions a subroutine is called that calculates the properties and coefficients for each equation. The time steps are then started, each step requiring one pass through the program. Each of the equations is solved in a subroutine.

For each time step the new values of the vapor region and the heat sink temperatures are calculated first. These solutions are explicit and use evaporator and condenser values from the last time step. The new temperatures of the vapor and heat sink are then used as boundary conditions in the implicit solution of the evaporator and condenser system of equations.

The same subroutine that solves for a new vapor temperature also calculates the position of the fluid in the slab and determines which nodes in the evaporator and condenser are currently active. Because the vapor solution is explicit and has little mass it tends to become unstable.

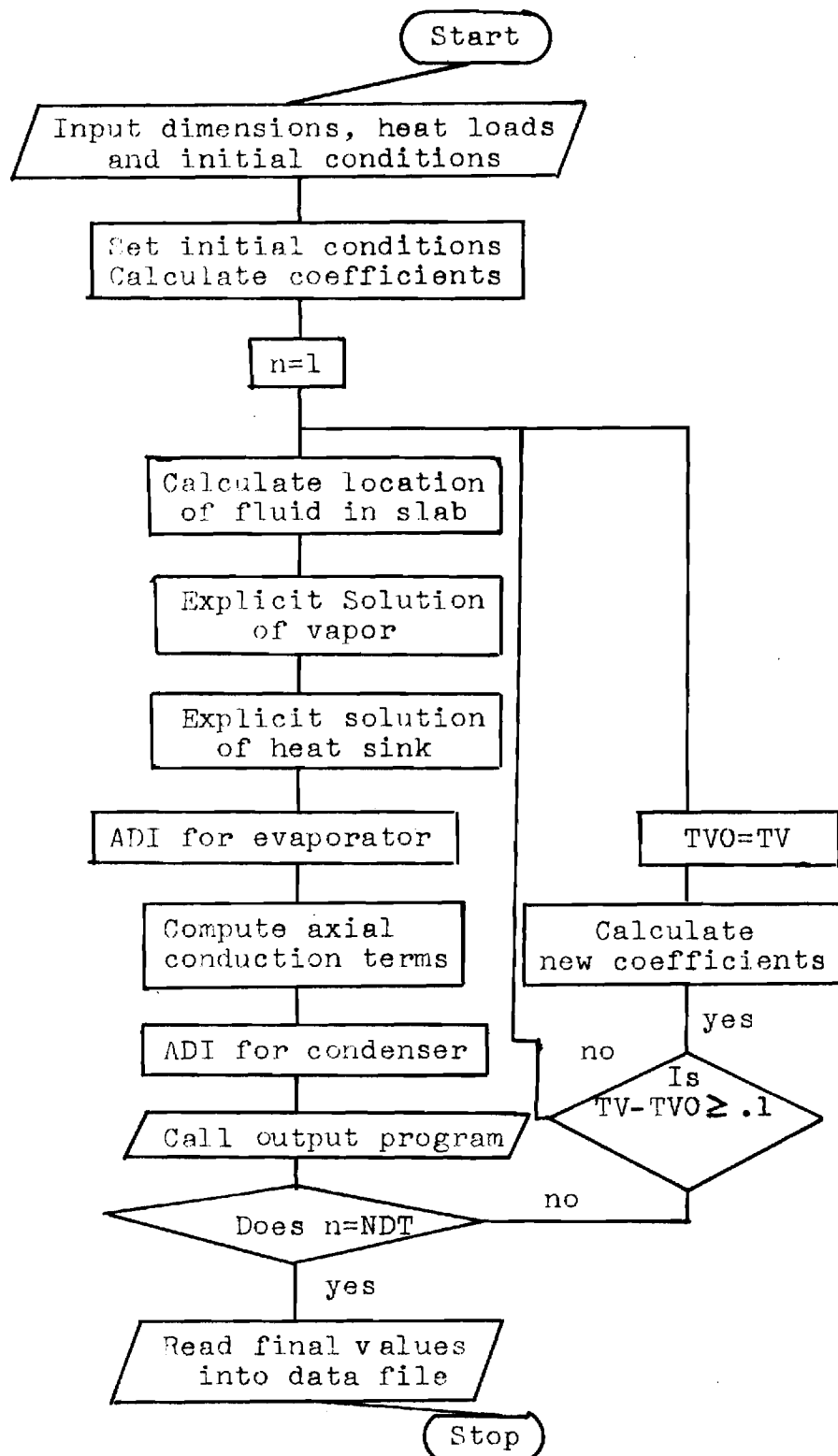


Figure 8. Flow Diagram of Computer Program

A discussion of stability is presented in Appendix E. This unstable tendency is overcome by allowing the program to calculate a smaller time step for the vapor region and iterate a sufficient number of times to complete the total time step.

The equation for the heat sink is solved in a separate subroutine. This routine can handle either a radiating heat sink or a cooling jacket. The solution is explicit but the mass is sufficiently large that stability is no problem.

Both the evaporator and condenser matrices are solved separately in the same subroutine. Inputs to the subroutine are temperatures at each node, coefficients, and boundary conditions. The subroutine calls the tridiagonal subroutine for solution of each row of the matrix. This technique is described in detail in references [16, 17, 18].

After each time step several checks are made. The current vapor temperature is compared to temperature used for calculation of property values. If the new value is different from the old by more than 0.1 K new coefficients are calculated using properties calculated at the new temperature.

Another check is performed to determine if the system is changing rapidly. If the system is changing temperature at a rate less than that specified the time step is doubled and new coefficients are calculated. Thus several different time steps may be used during a single run. The response time of the vapor region is less than the time steps normally

used. This presents no problem since inherent in the solution technique is the assumption that the system response is linear across a single time step. Thus the vapor temperature merely tracks the temperature changes in the evaporator and condenser sections. However when the time step is changed the vapor response is solved explicitly with evaporator and condenser temperatures calculated for the old value of the time step. The vapor temperature will then lag the rest of the solution by one half of a time step slowing down the response of the entire system. To correct for this problem the change in the vapor temperature is always multiplied by the ratio of the new time step to the old time step. In essence this procedure amounts to predicting the temperatures of the evaporator and condenser nodes that interact with the vapor for the new time step. Since this change of time step only occurs when the system is changing at a very slow rate any error that occurs would be small.

In startup from the supercritical the average specific heat of the slab changes as the fluid moves through it. Whenever the fluid reaches a new node the values are calculated again taking into account the additional fluid in the slab.

Values used for thermal conductivity of the wick are a weighted average of the thermal conductivities of the fluid and the screen. Effective thermal conductivity of the screen-fluid combination is evaluated using the method of Williams

[24]. Details of this development are in Appendix F.

Specific heats of the wick and slab are also weighted averages of the specific heats of the components.

E. Description of the Analog Model

A simplified model of the heat pipe was used for transient studies with an analog computer. This model assumed one dimensional conduction in the radial direction. Overall temperature drops and response times can be predicted with this technique for small perturbations.

The approach used for the analog computer was to break the heat pipe into nodes. A heat balance was written for each node equating the net heat gain with temperature increase. The result is a system of first order differential equations in time with temperature the dependent variable.

Since the computer capacity was limited only five nodes are used. Node 1 is composed of the outer half of the evaporator wall and is located at the evaporator surface. The inner half of the evaporator wall and the outer half of the wick make up node 2 which is located at the interface of the wick and wall. The vapor region, slab and adiabatic wall and wick are the components of node 3 located at the interface of wick and vapor region. Like node 2, node 5 is composed of one half of the wick and the inner half of the condenser wall and is located at the interface of condenser wick and wall. Node 6 is the outer half of the condenser

wall and like node 1 is located at the surface. Figure 9 is a schematic diagram of the nodes and their locations.

Equations for the six nodes are listed below. See Appendix G for a discussion of scaling the equations for use on the analog computer.

Condenser cooling is accomplished by means of a jacket with a circulating fluid. An additional node, number 6 permits the modeling of this jacket.

The analog computer circuit for these equations is shown in Figure 10.

$$\frac{dT_1}{dt} = \frac{4\pi \ell_E K_p}{\rho_p c_p v_{pE} \ln(r_o/r_B)} (T_2 - T_1) + \frac{2Q_E}{\rho_p c_p v_p} \quad (4.1)$$

$$\begin{aligned} \frac{dT_2}{dt} = & \frac{4\pi \ell_E K_p}{[\rho_p c_p v_{pE} + \rho_w c_w v_{wE}] \ln(r_o/r_B)} (T_1 - T_2) \\ & + \frac{4\pi \ell_E K_w}{[\rho_p c_p v_{pE} + \rho_w c_w v_{wE}] \ln(r_B/r_I)} (T_3 - T_2) \end{aligned} \quad (4.2)$$

$$\begin{aligned} \frac{dT_3}{dt} = & \frac{4\pi \ell_E K_w}{[\rho_p c_p v_{pE} + \rho_w c_w v_{wE} + m_a c_a] \ln(r_B/r_I)} (T_2 - T_3) \\ & + \frac{4\pi \ell_C K_w}{[\rho_p c_p v_{pC} + \rho_w c_w v_{wC} + m_a c_a] \ln(r_B/r_I)} (T_4 - T_3) \end{aligned} \quad (4.3)$$

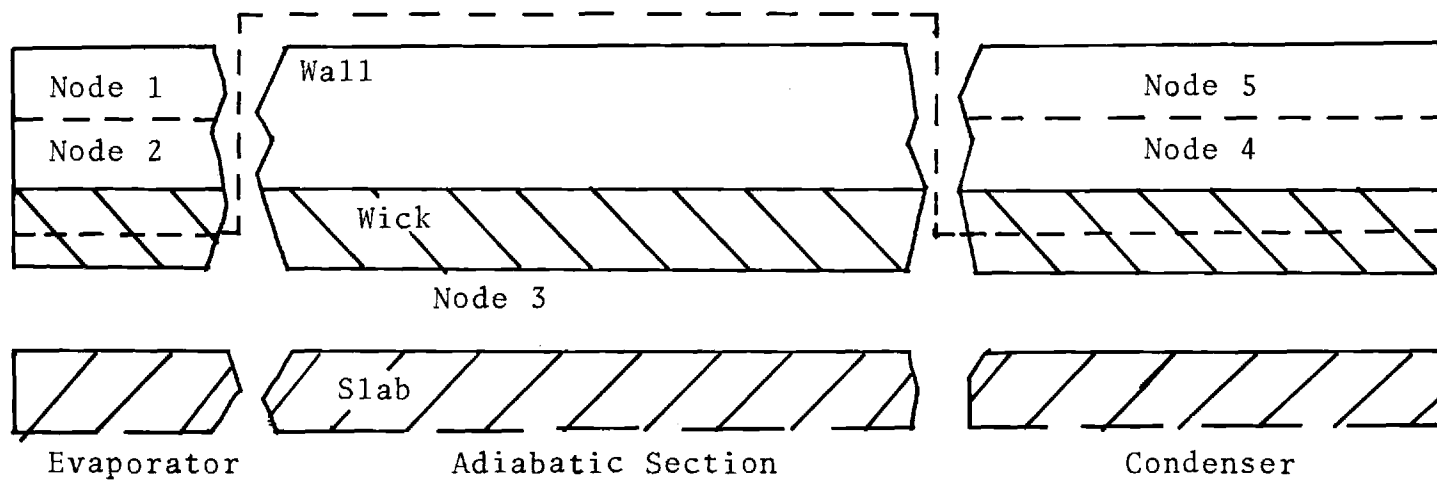


Figure 9. Schematic Diagram of Analog Model

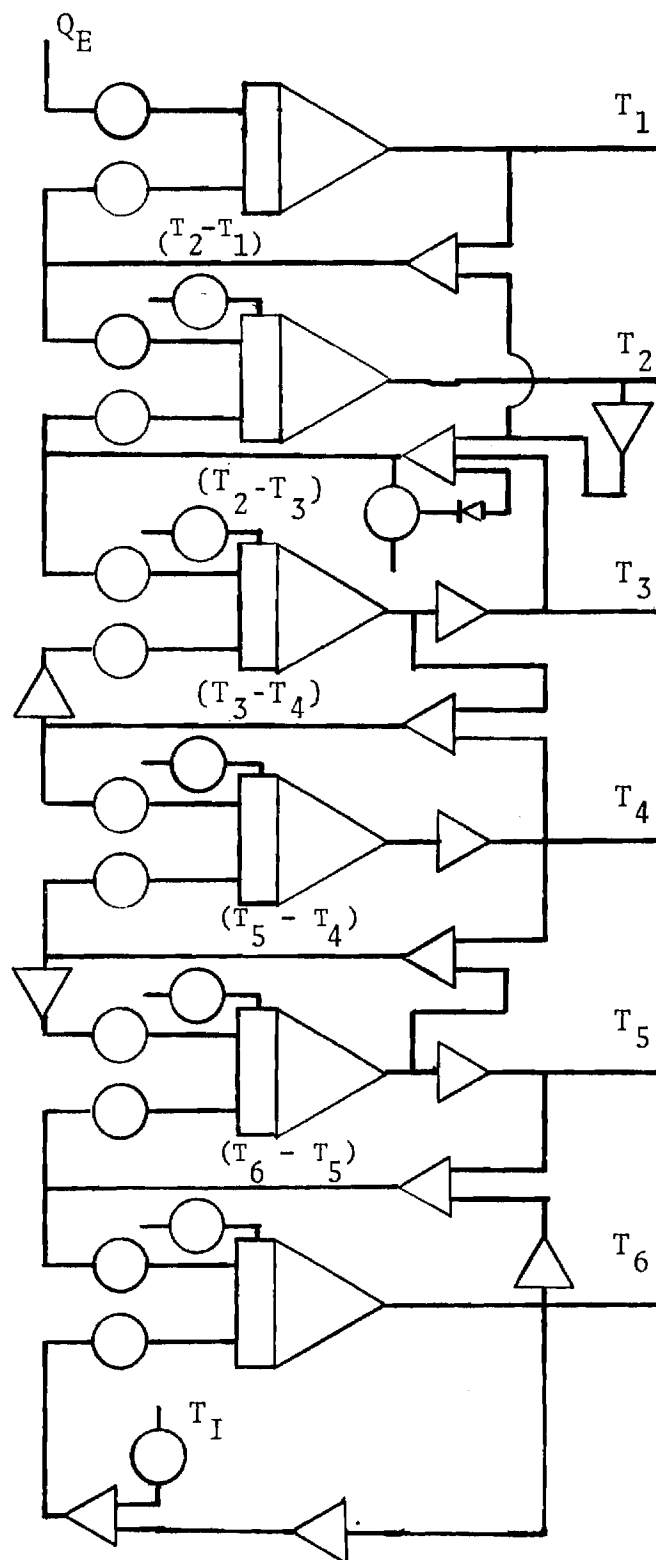


Figure 10. Analog Circuit

$$\begin{aligned} \frac{dT_4}{dt} = & \frac{4\pi \ell_C K_w}{[\rho_p c_{p,pC} + \rho_w c_{w,wC}] \ln(r_B/r_I)} (T_3 - T_4) \\ & + \frac{4\pi \ell_C K_p}{[\rho_p c_{p,pC} + \rho_w c_{w,wC}] \ln(r_O/r_B)} (T_5 - T_4) \end{aligned} \quad (4.4)$$

$$\begin{aligned} \frac{dT_5}{dt} = & \frac{4\pi \ell_C K_p}{\rho_p c_{p,pC} \ln(r_O/r_B)} (T_4 - T_5) \\ & + \frac{4\pi r_O \ell_C h_C}{\rho_p c_{p,pC}} (T_6 - T_5) \end{aligned} \quad (4.5)$$

$$\frac{dT_6}{dt} = \frac{2\pi r_O \ell_C h_C}{m_{CJ} c_{CJ}} (T_5 - T_6) + \frac{\dot{m}_f c_f}{m_{CJ} c_{CJ}} (T_I - T_6) \quad (4.6)$$

III. RESULTS AND COMPARISONS

The digital model has been used to model the heat pipe studied by Saaski [26]. The heat pipe modeled had an evaporator and condenser each 15.24 cm long and a 15.0 cm adiabatic section. Methanol was used for the working fluid. The inside radius was 1.288 cm and the wall thickness was 0.080 cm. One layer of 200 mesh screen was used as a circumferential wick. An air gap of 0.022 cm was maintained between the condenser surface and the heat sink for a per-unit-length gap conductance of approximately 0.0443 W/cm-K. The temperature of the vapor region is non-dimensionalized by defining

$$\frac{\Delta T_V}{\Delta T_{Vm}} = \frac{T_V(t) - T_{Vo}}{T_{Vm} - T_{Vo}}$$

where T_{Vo} is the initial vapor temperature and T_{Vm} is the steady state vapor temperature. Saaski's data reaches 95 percent of steady state values in approximately 130 seconds. The predicted curve using the technique of this study responds more slowly reaching 95 percent of steady state in 160 seconds. Both curves are shown in Figure 11.

The digital model of the heat pipe has been used to study three different cryogenic heat pipe systems. Systems

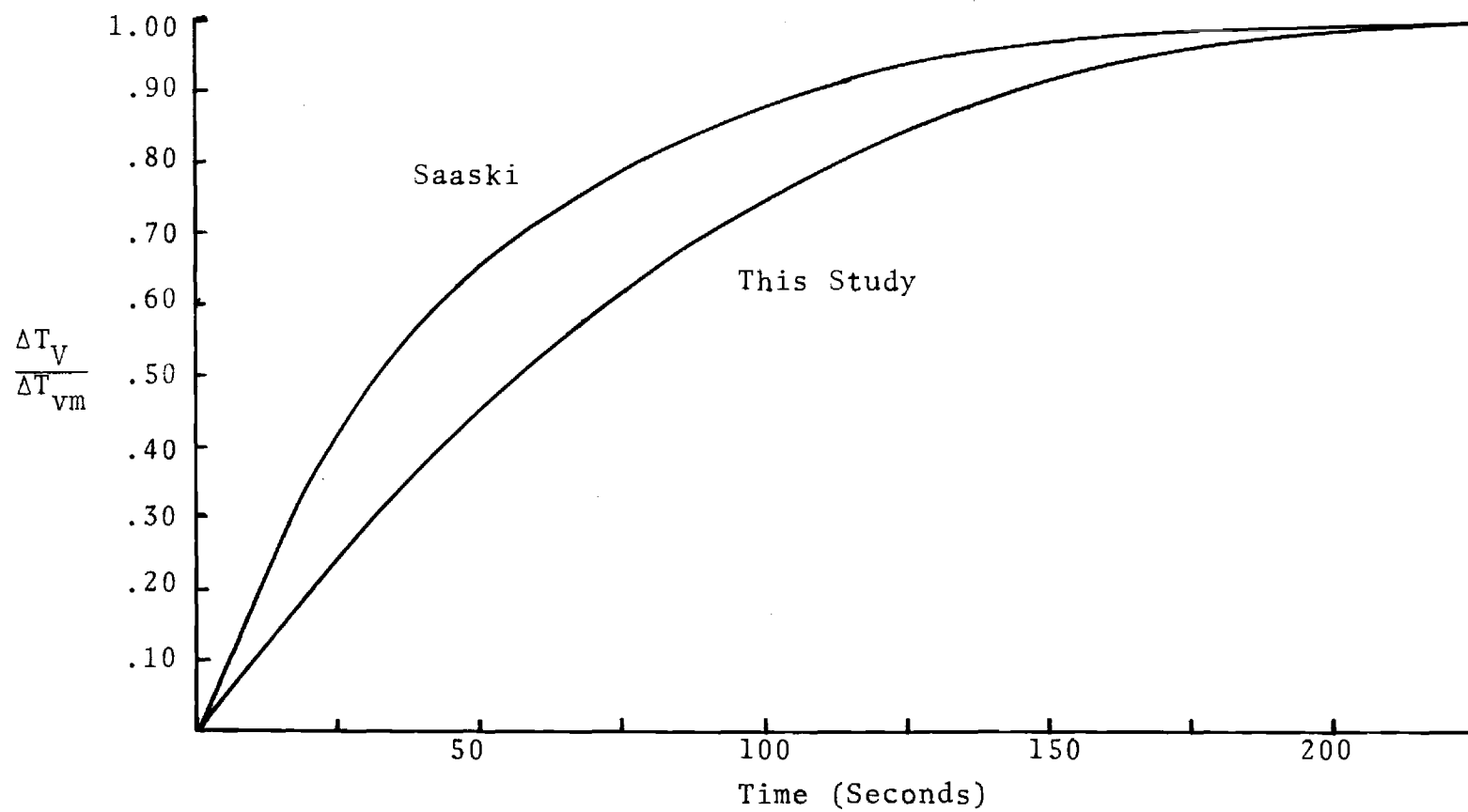


Figure 11. Comparison of Model with Experimental Data from the Literature

are varied by changing boundary conditions on the condenser surface. The effect of varying heat pipe design parameters was studied using a model with the condenser surface temperature fixed. Other systems modeled used a cooling jacket and a radiating surface as heat sinks.

Similar studies have been performed on the constant condenser temperature heat pipe and the cooling jacket using the analog model.

An even simpler model can be developed if the system is assumed to be a lumped mass. Details of this development for a heat pipe with a cooling jacket are given in Appendix H. The result is a simple exponential equation. This model should have a faster response than the more complex models, since no temperature gradient must develop. A comparison of digital, analog, and exponential models for startup from isothermal at 100 K to a heat load of 15 watts is shown in Figure 12. In each case the condenser heat sink is a cooling jacket with liquid nitrogen at 100 K as the coolant. All three models predict similar responses.

The digital model of a system with a constant condenser surface temperature was used to study effects of varying design parameters. In each case the heat pipe is initially isothermal at 100 K. A heat flux of 15 watts is imposed on the evaporator surface and the heat pipe adjusts to steady state. Table 2 lists the various cases studied.

Figure 13 compares analog and digital response curves

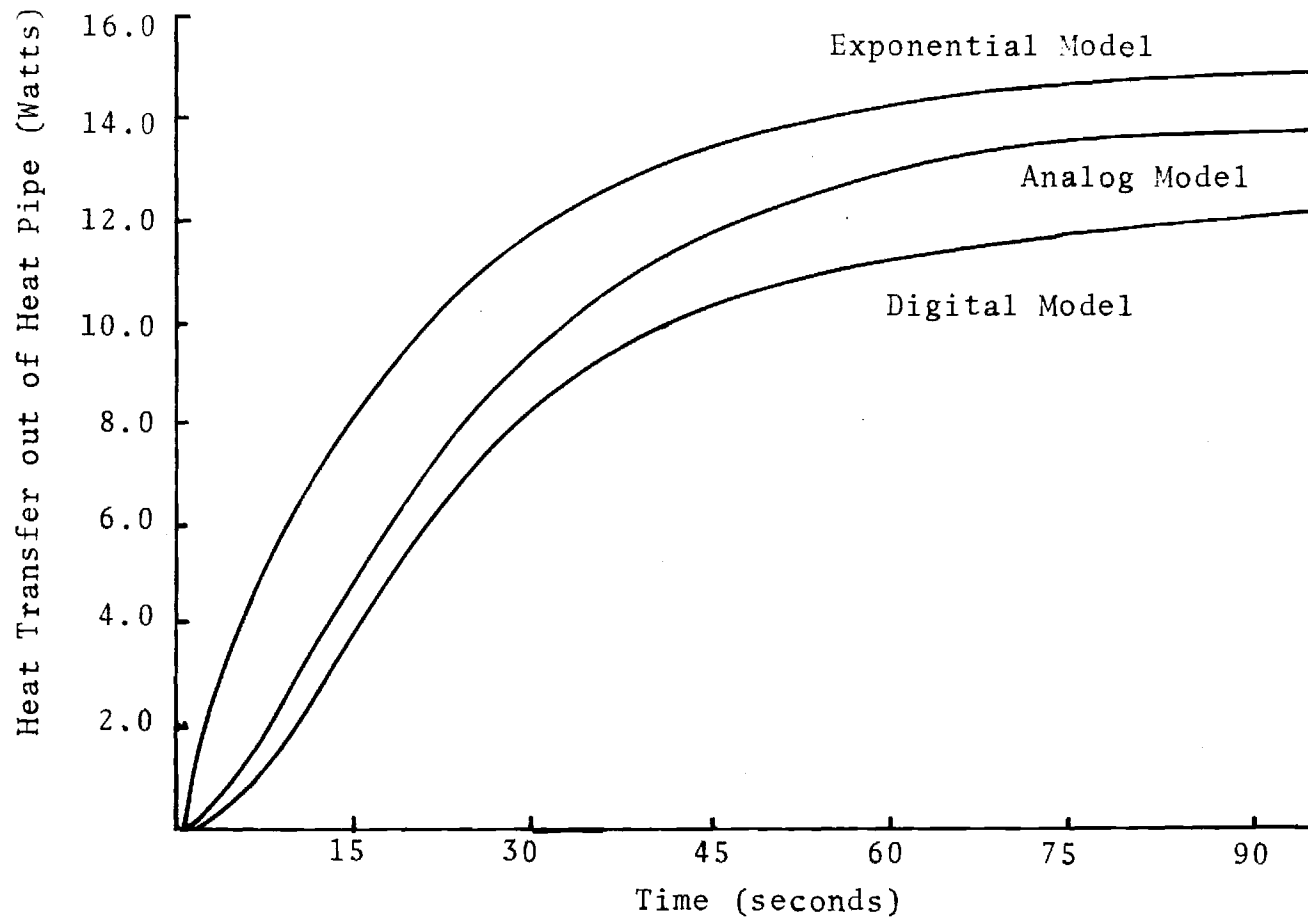


Figure 12. Comparison of Exponential, Analog, and Digital Models for Heat Pipe with Cooling Jacket

Table 2. Parameters for Cases Studied

Case No.	Modification
1	Standard Heat Pipe as described Table 1
2	Wall thickness .2030 cm
3	Wall thickness .4060 cm
4	Circumferential wick of 4 layers 400 mesh
5	Circumferential wick of 8 layers 400 mesh
6	Fluid gap .006096 cm
7	Fluid gap .012192 cm
8	Slab 2 layers 400 mesh 2 layers 30 mesh
9	Slab 8 layers 400 mesh 10 layers 30 mesh

In each case the heat pipe is initially isothermal at 100 K. A heat flux of 15 watts is imposed on the evaporator surface. The only modification from the heat pipe of Table 1 is that listed.

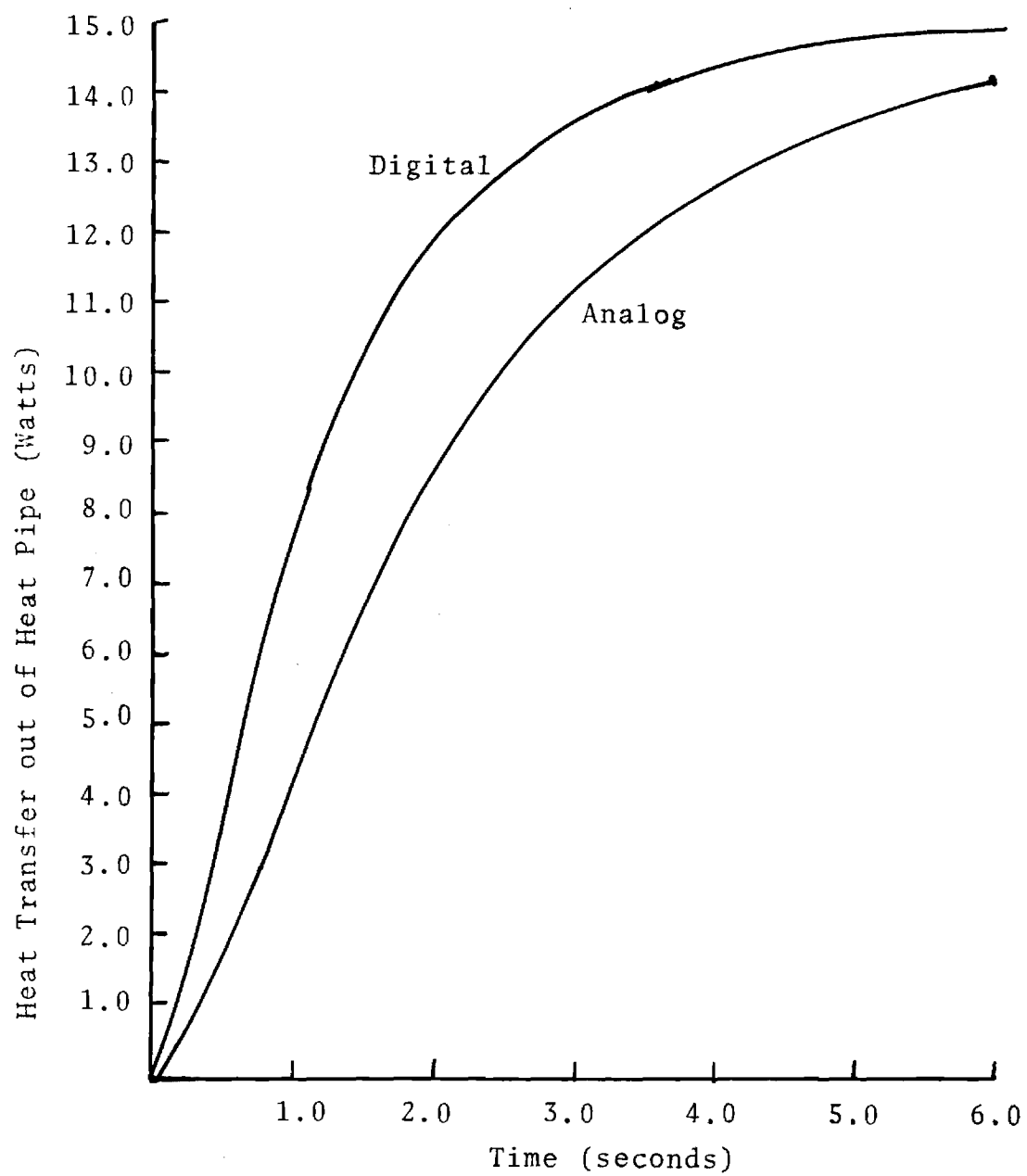


Figure 13. Comparison of Analog and Digital Model for Case 1

for case 1. The slower response of the analog curve is due to the different nature of the nodal systems employed.

The effect of changing the wall thickness is shown in Figure 14. Since the pipe wall is the major portion of the heat pipe mass, any change would have a great effect on heat pipe response. The pipe wall is also the largest thermal resistance in the heat pipe. Thus increasing the wall thickness requires a larger overall temperature difference. The time required for this temperature profile to develop slows response.

Increasing the number of layers of circumferential wick also increases the steady state temperature drop from evaporator to condenser. This effect as well as the added mass slow response as shown in Figure 15.

Figures 16 and 17 show the effect of changing the size of the fluid gap and the configuration of the composite slab. As the curves show the change in response time is very small.

Due to the nature of the model the response takes the same time for any heat input. Figure 18 shows the response for a heat input of 5 watts and 15 watts. Also shown is the response of a heat pipe to a power change from 5 to 15 watts. Each curve is for a heat pipe with a constant temperature condenser. In all three cases 95 percent of total change is achieved at the same time.

The thermal properties used in the model vary with temperature. The effect of this phenomena on response is

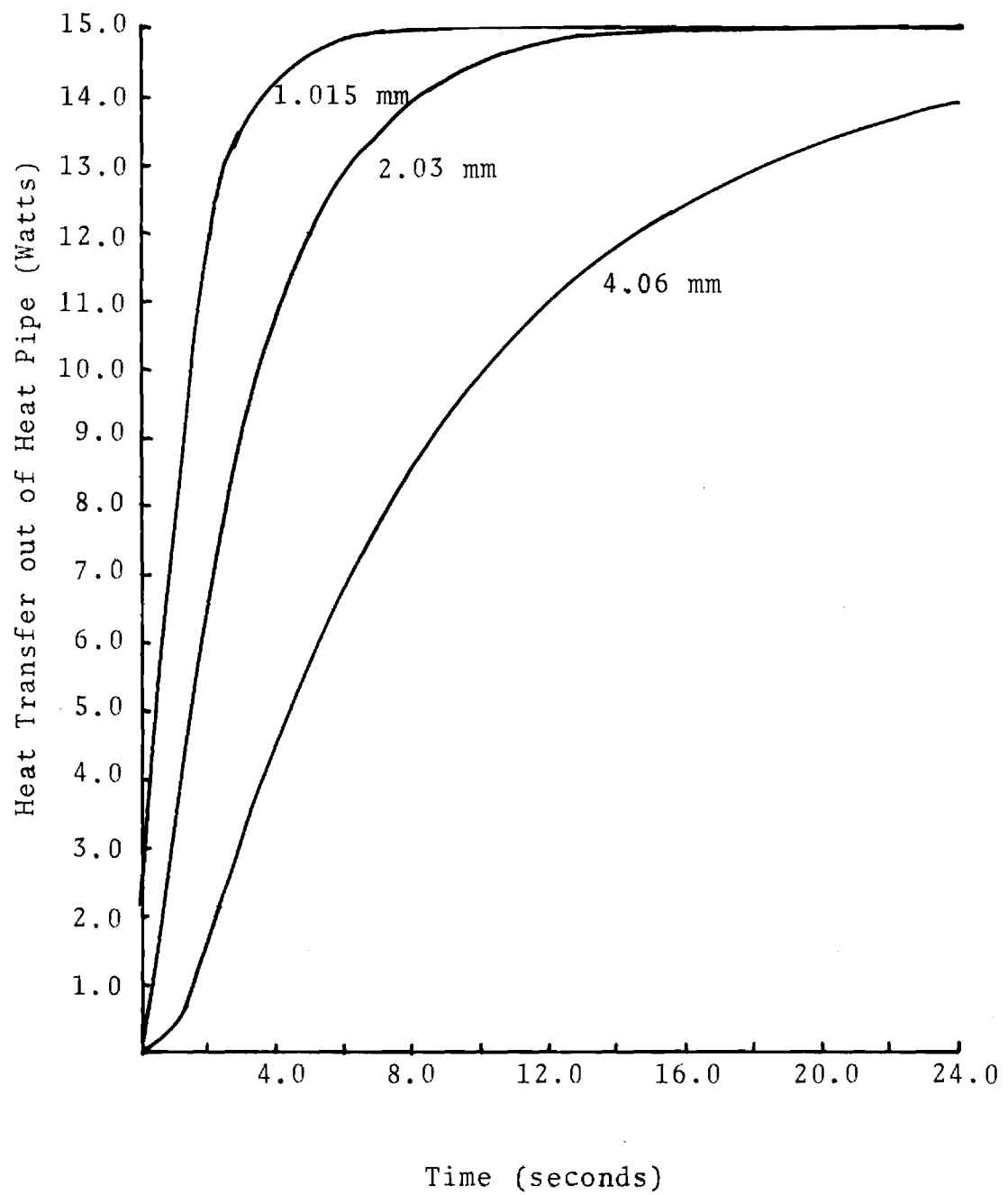


Figure 14. Effect of Changing Wall Thickness

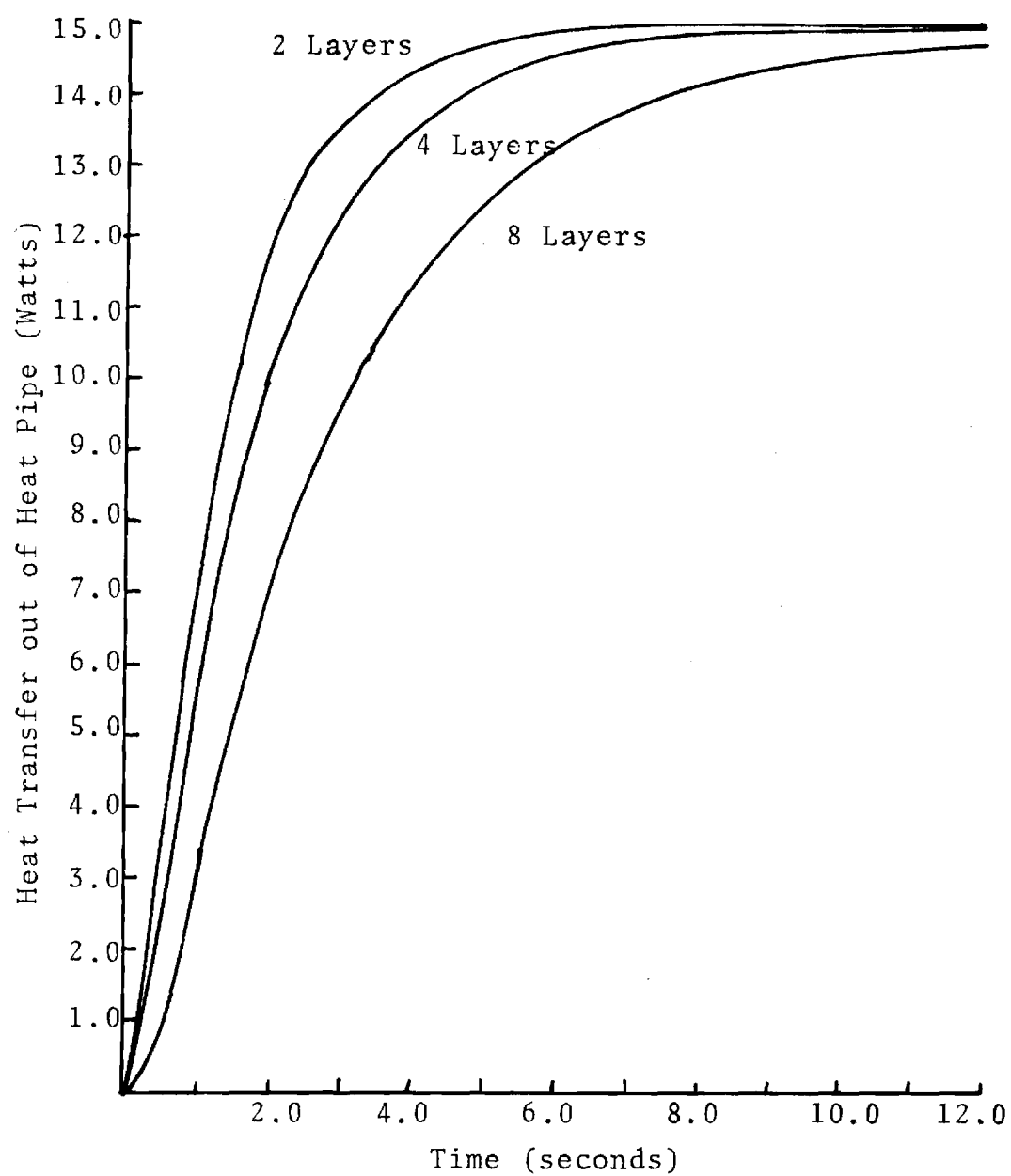


Figure 15. Effect of Changing Number of Wick Layers

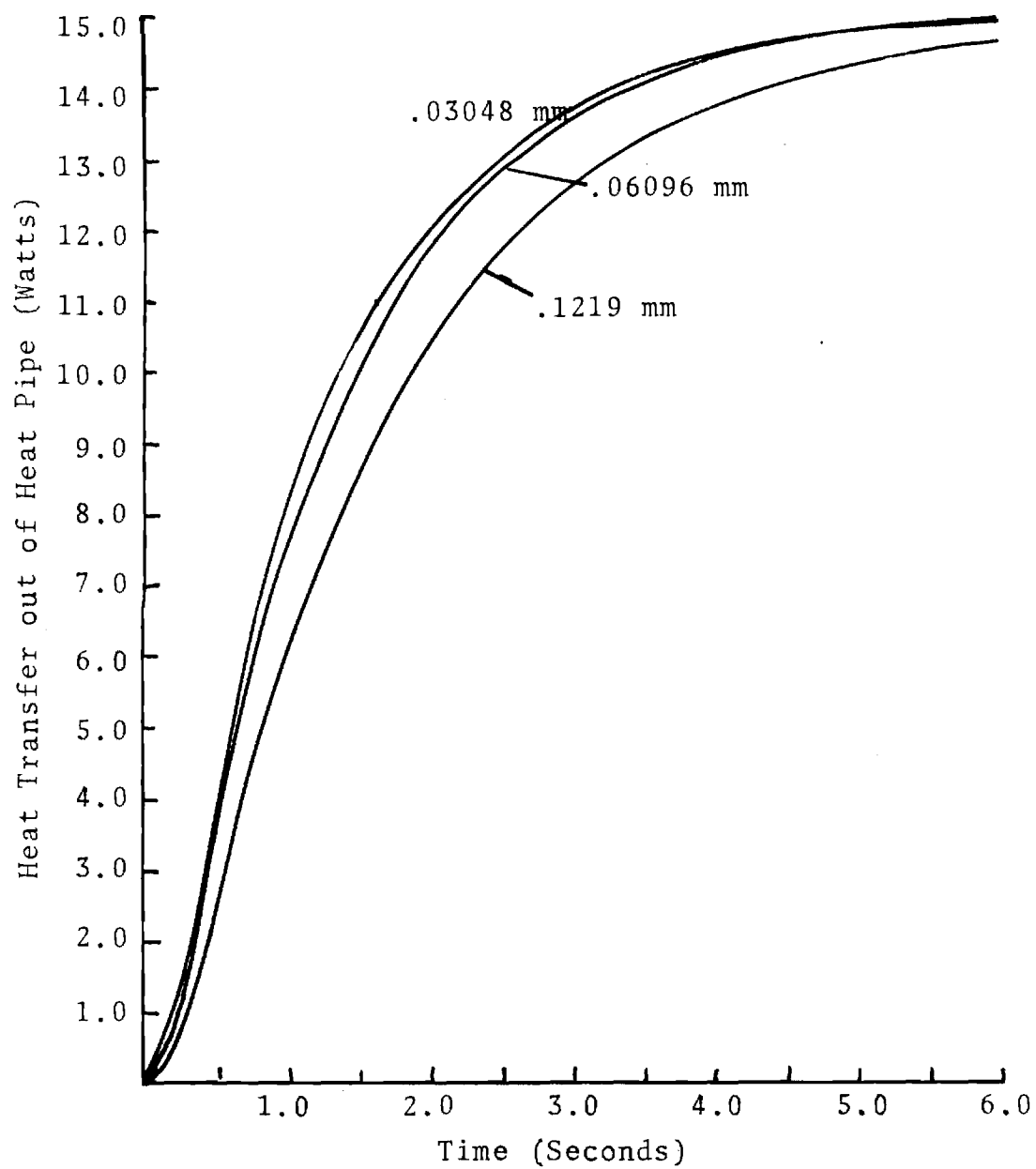


Figure 16. Effect of Changing Thickness of Fluid Gap

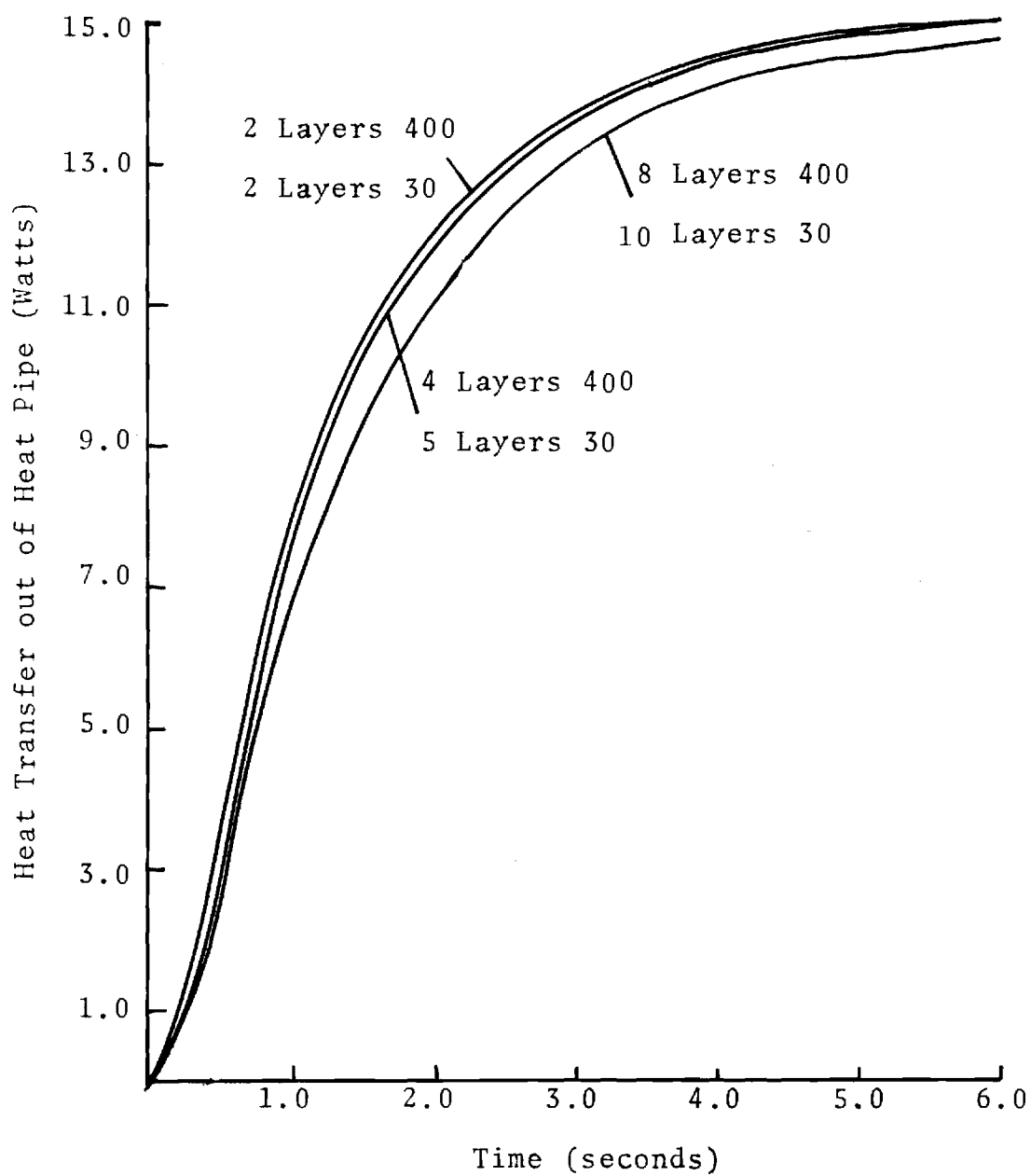


Figure 17. Effect of Changing Slab Composition

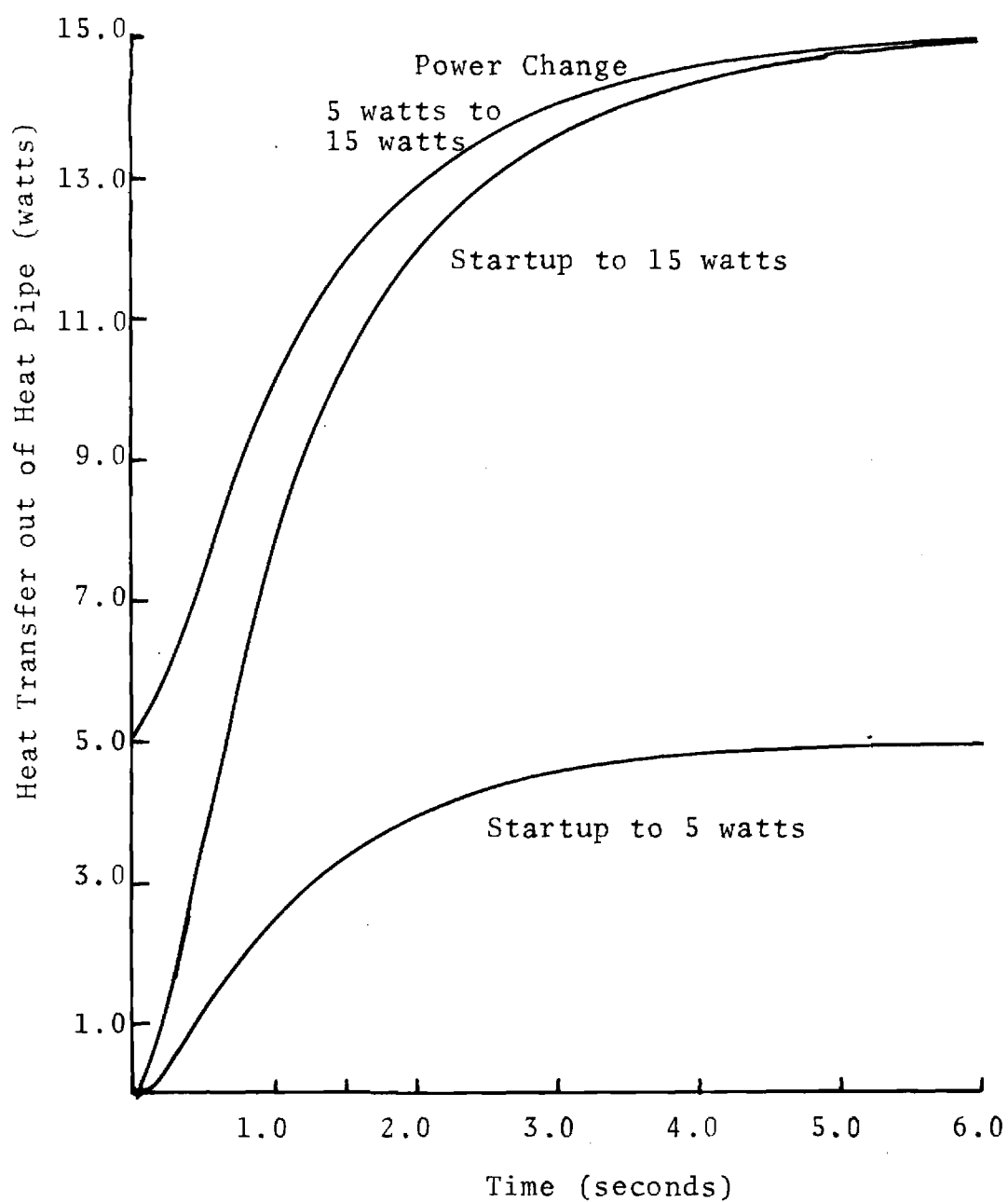


Figure 18. Comparison of Startup at Different Power Levels

shown in Figure 19. All three cases show an initially isothermal heat pipe with a constant condenser surface temperature. A heat flux of 15 watts is imposed on the evaporator. Curves are shown for startup from 80, 100, and 120 K. At the lower temperature the specific heats are smaller and the response is faster. At 120 K the capillary limitation is less than 15 watts. The effect of capillary limitation is also shown in Figure 19. The development of the overall temperature difference is shown in Figure 20. Note that at 120 K capillary burnout causes evaporator temperature to increase rapidly.

A heat pipe system with a cooling jacket and one with a radiating surface are compared in Figures 21 and 22. Since the heat leaving the radiating surface is dependent on the temperature alone the response time is much greater. This demonstrates the phenomena of temperature choking referred to by Anand, et al. [13].

Startup from the supercritical is shown in Figure 23. A heat flux of 5 watts is imposed on a heat pipe initially isothermal at 130 K. Cooling is imposed at the same time with a jacket with a coolant at 100 K and a surface coefficient of $1000 \text{ W/m}^2\text{-K}$. The evaporator surface temperature climbs sharply until fluid reaches it. The temperature falls rapidly and the heat pipe begins working.

Figure 24 compares wicking velocity calculated using equations 3.4 and 3.6 with velocities from the work of Symons

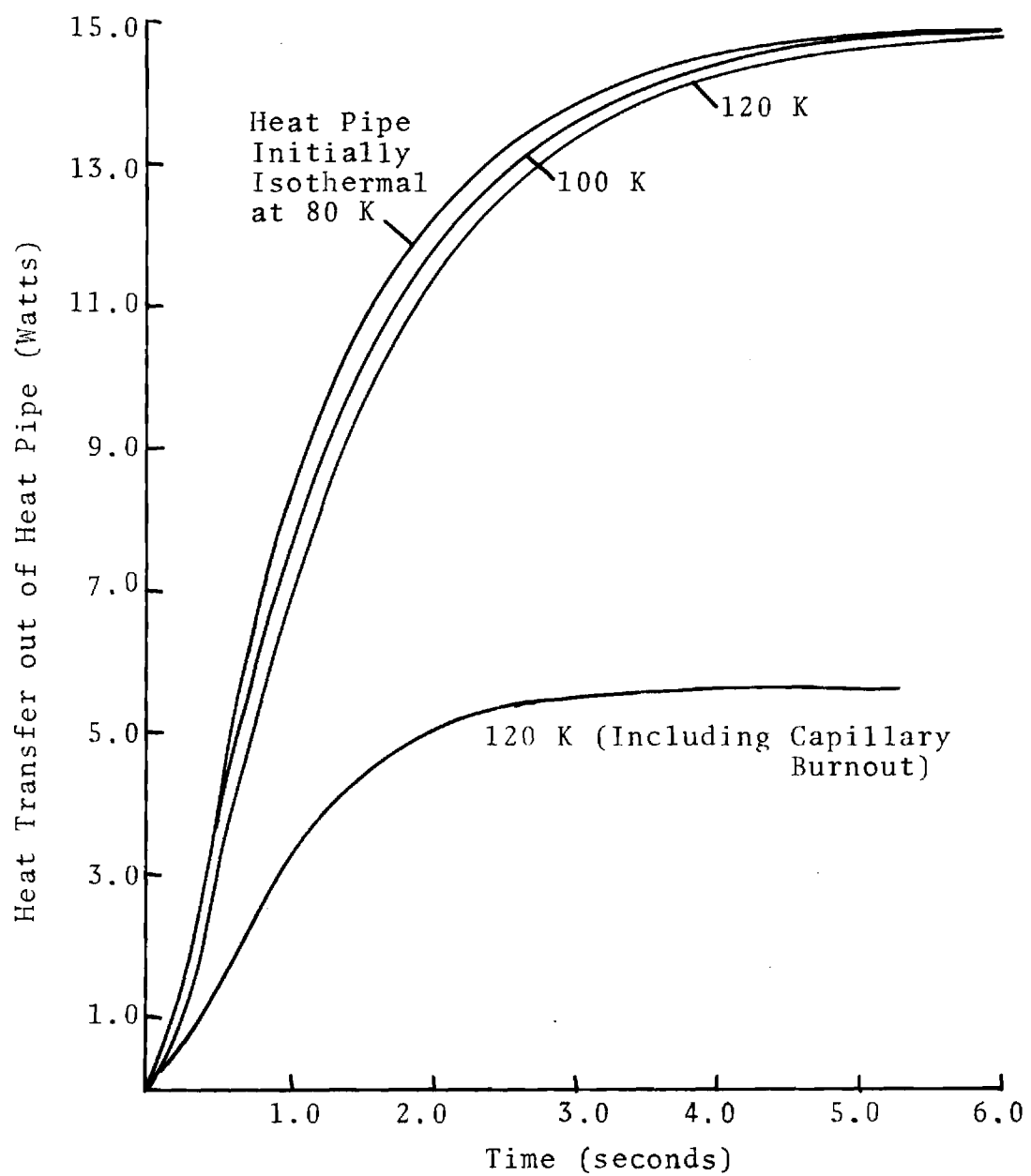


Figure 19. Comparison of Startup at Different Temperatures

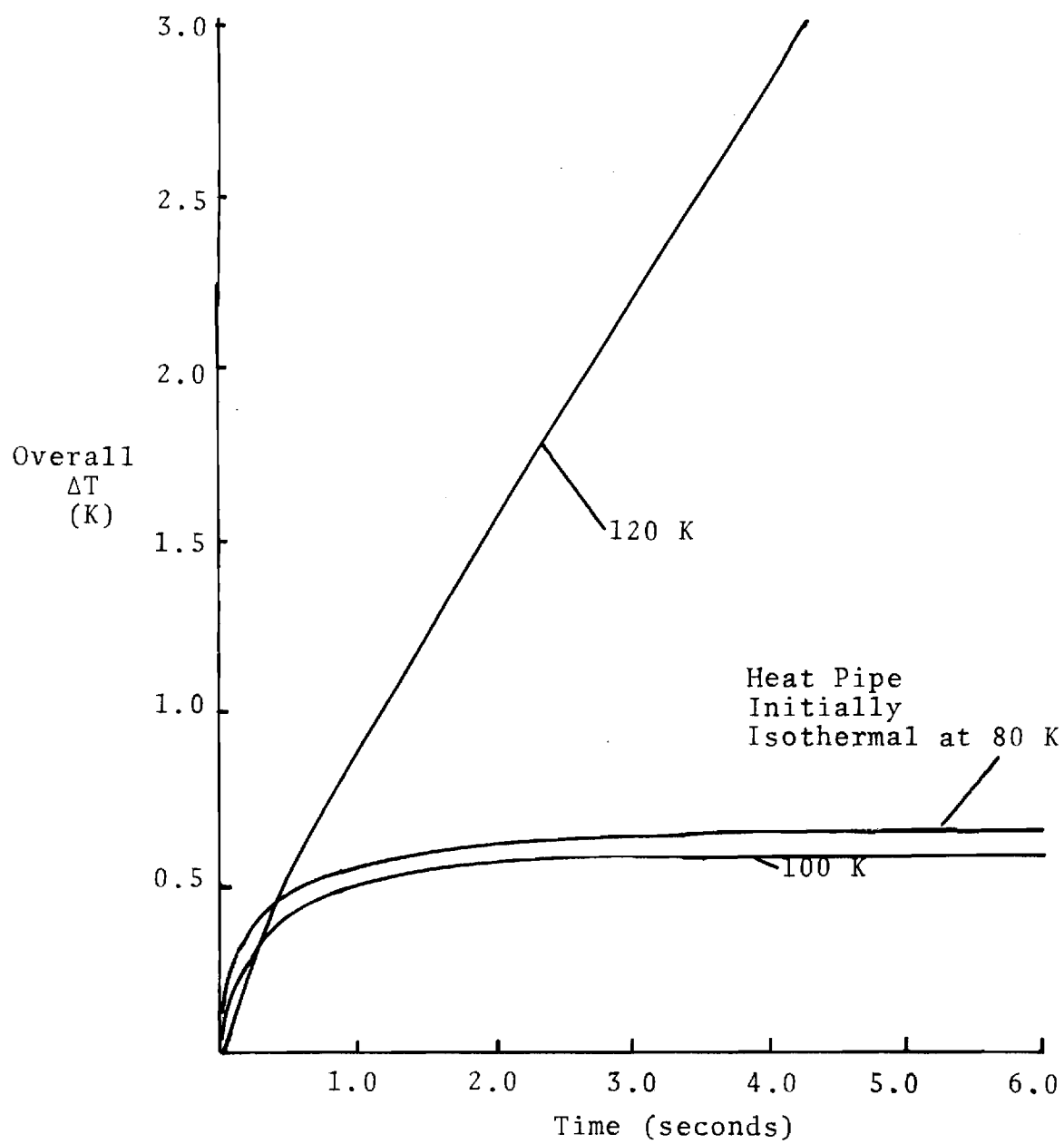


Figure 20. Development of Overall Temperature Gradients

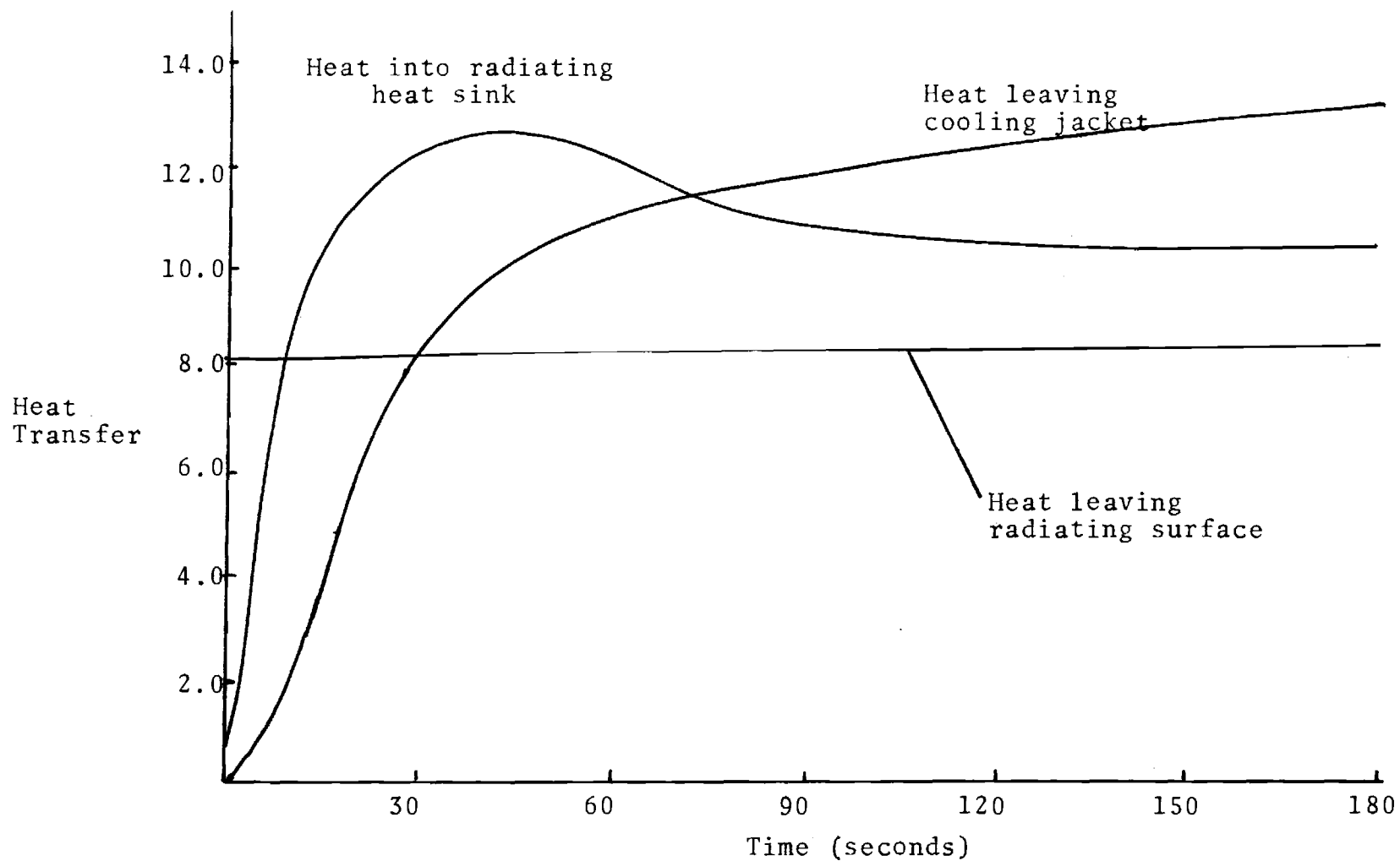


Figure 21. Comparison of Heat Pipe Response with Cooling Jacket or Radiating Surface Heat Sink

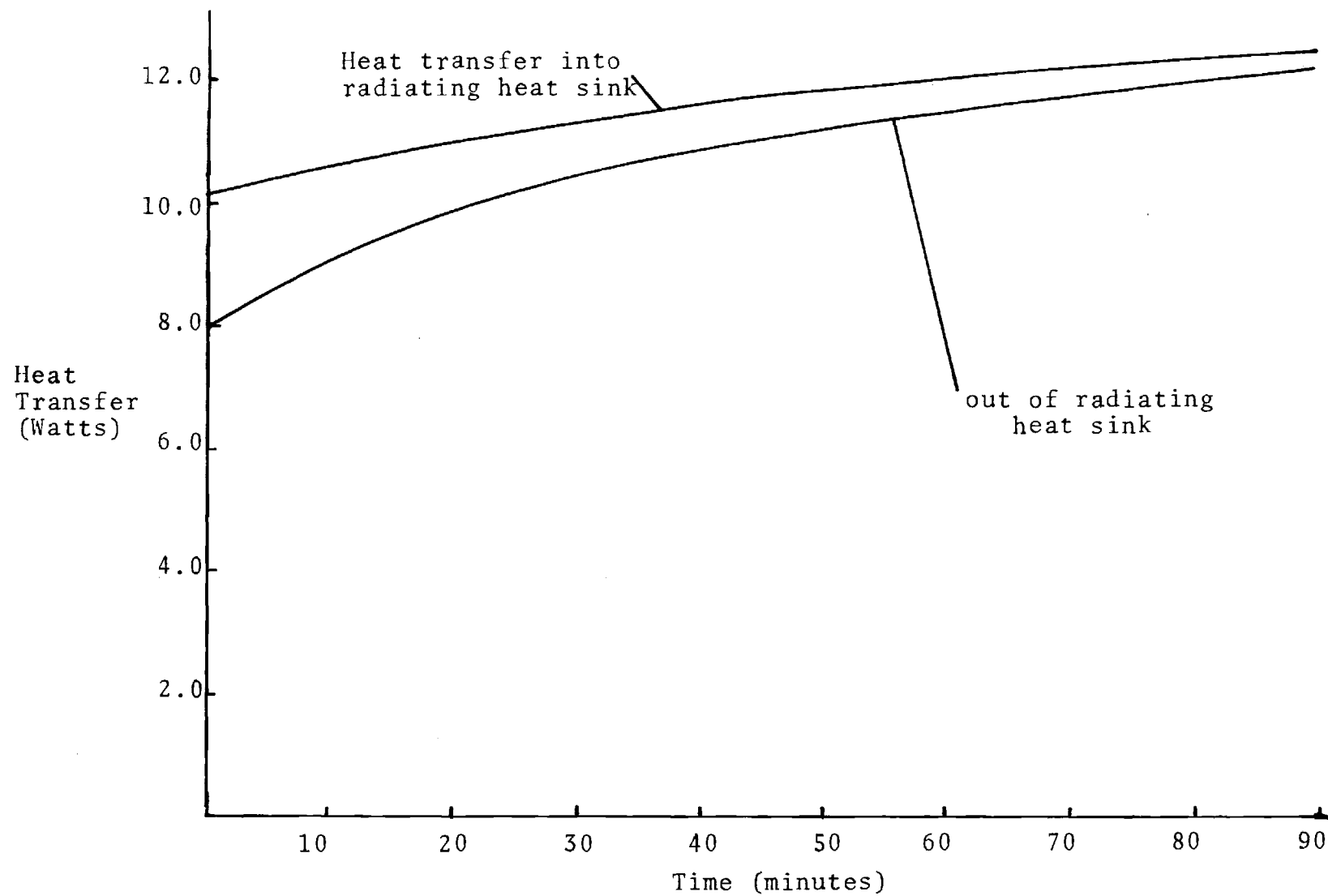


Figure 22. Response of Radiating Heat Sink

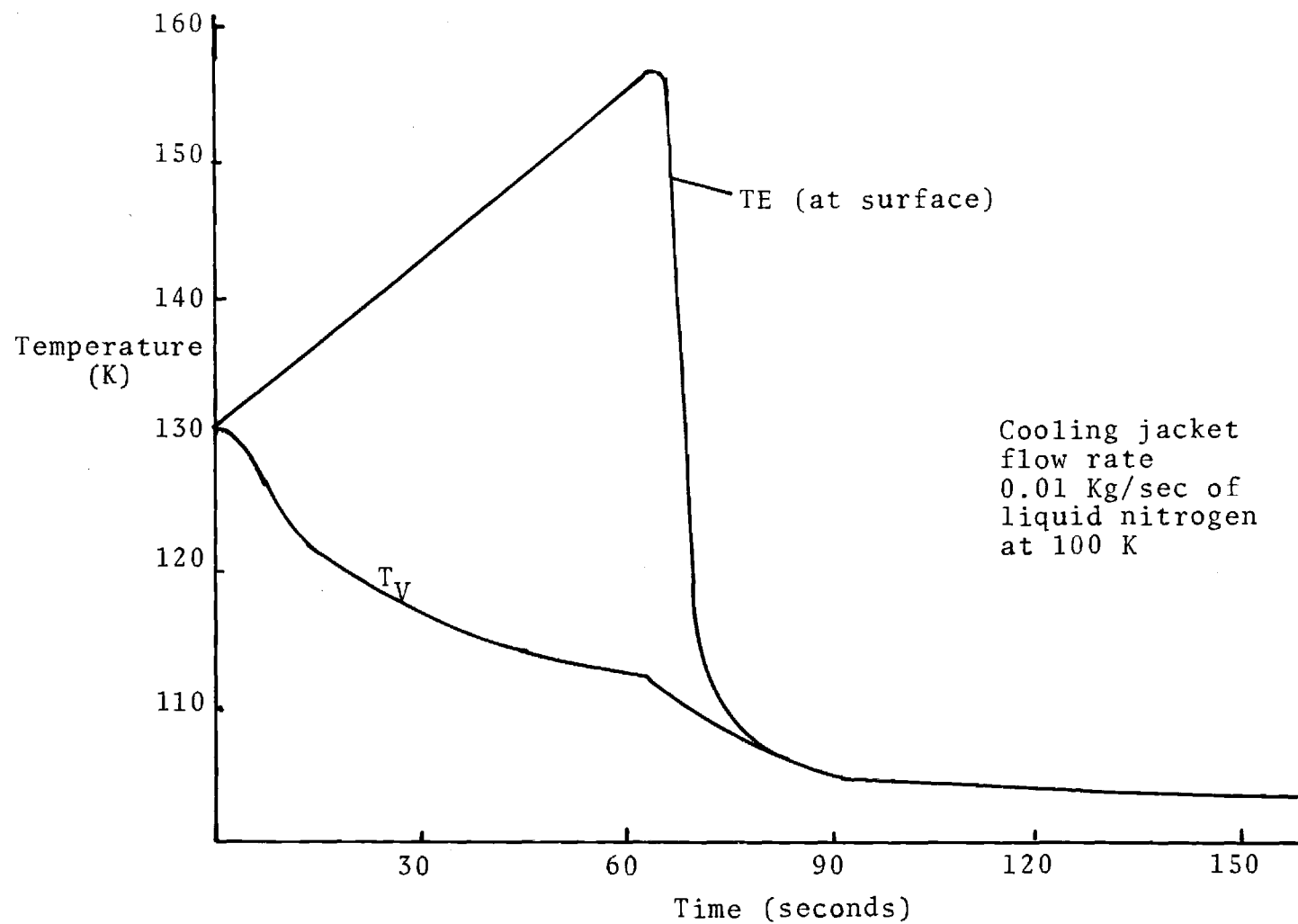


Figure 23. Startup from Supercritical

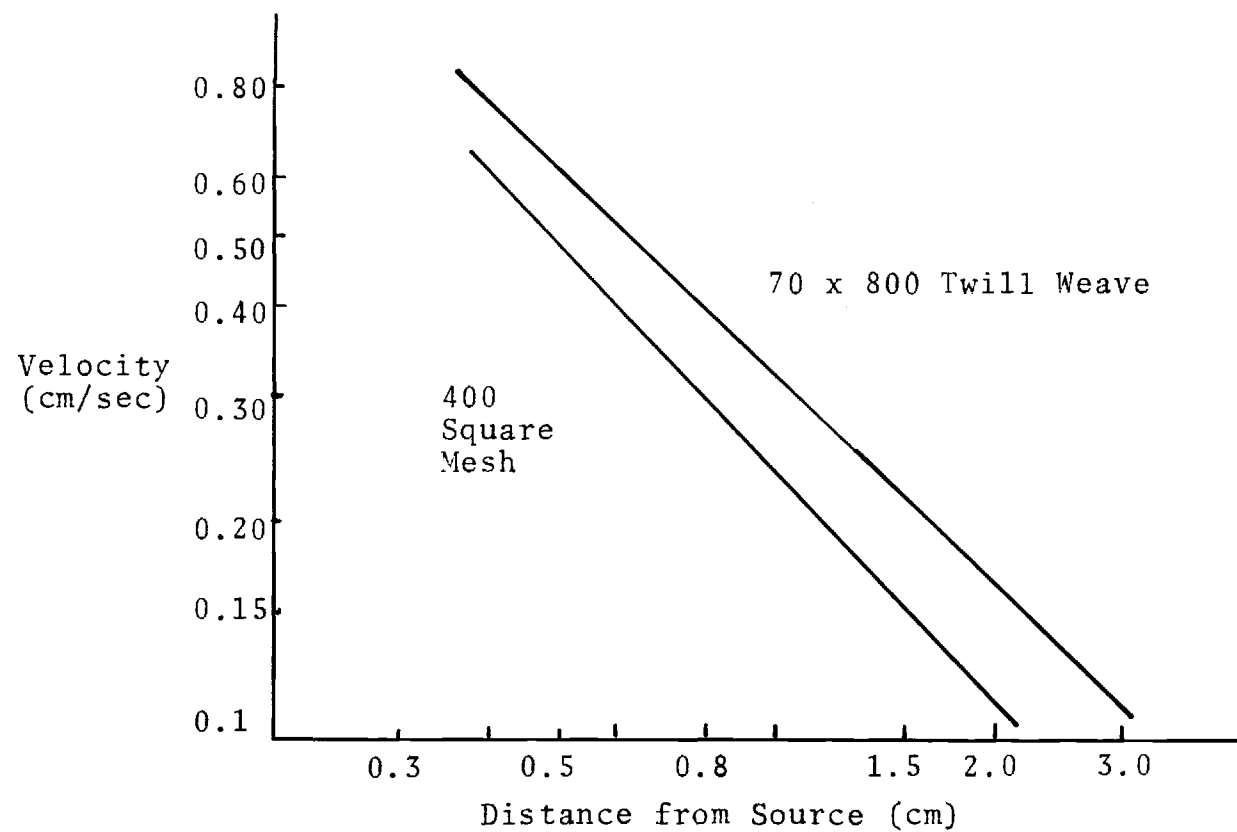


Figure 24. Comparison of Predicted Fluid Velocity with Data from Literature

[27]. For both curves the working fluid is methanol. Since the capillary structures are not the same the velocities do not agree exactly. However they are of the same order of magnitude.

Wicking velocity in the composite slab is shown in Figure 25. The velocities are much larger than those of Figure 24 because of the nature of the composite slab. The effective inverse permeability is relatively small due to the presence of the 30 mesh screen yet the pumping pressure is relatively high due to the outer layers of 400 mesh screen.

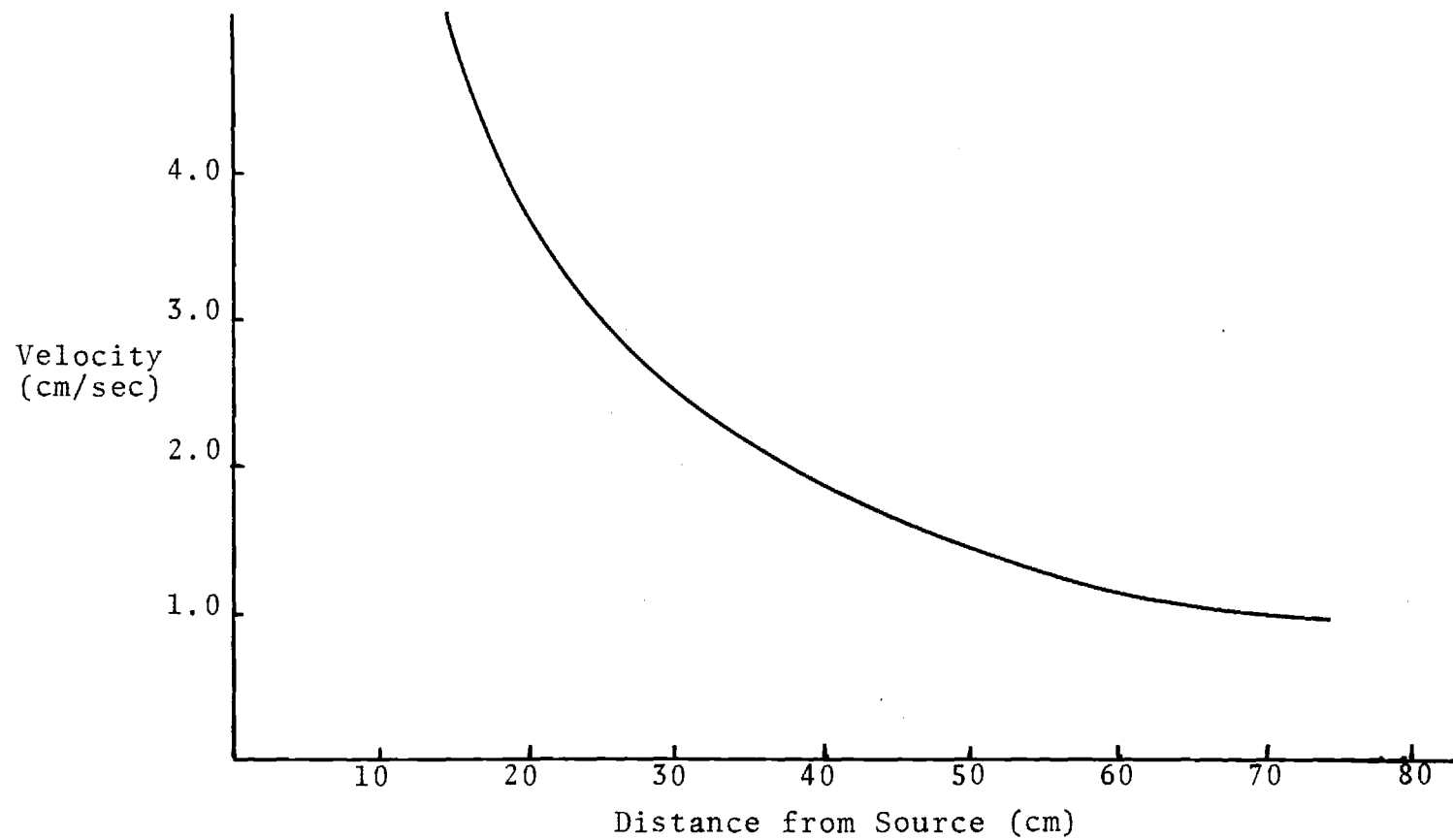


Figure 25. Velocity with Position in Composite Slab

IV. CONCLUSIONS AND RECOMMENDATIONS

This study has developed a technique for predicting transient response of heat pipes. Predicted response curves were compared with experimental data from the literature and agreement was good. Results from the digital studies have been compared with those from more simple analog and exponential models and trends are found to be similar.

The analog model provides a good method for estimating response for small transients. Because of the large node spacing and assumption of constant property values the results are not as accurate as the digital model and the effects of fluid dynamics and startup from the supercritical could not be included. An attempt to improve the analog model would have required more analog computing capability than was available.

A much better technique for modeling transients is provided by the digital model. Thermal properties are allowed to vary with temperature and the effects of fluid dynamics are included. It was found that in accurately modeling experimental data it was difficult to account for response times of heating and cooling systems and the added masses of instrumentation and insulation. A simple approach was developed for including

startup from the supercritical.

The stability of the alternating direction implicit solution procedure was found to be very good. (See Appendix E for a discussion of stability.) The program remained stable for time steps as large as thirty seconds. Had an explicit solution of the same node system been attempted, time steps on the order of 10^{-3} seconds would have been necessary to maintain stability. With the ADI method some oscillations would occur near the boundaries when the time steps were large and the system was changing temperature rapidly.

In any continuation of this work many improvements could be made in the computer code to decrease running time. In addition the equations which are used to predict wick re-priming after dryout could be improved.

APPENDICES

APPENDIX A

TRANSFORMATION OF COORDINATE SYSTEMS

It is convenient to transform the cylindrical coordinate system that describes the heat pipe to one that is rectangular. In cylindrical coordinates $\nabla^2 T$ is

$$\frac{\partial^2 T}{\partial r^2} + \frac{1}{r} \frac{\partial T}{\partial r} + \frac{1}{r} \frac{\partial^2 T}{\partial \phi^2} + \frac{\partial^2 T}{\partial z^2}$$

Make the following substitutions

$$x = \ln(r_0/r_I)$$

$$y = \phi$$

$$z = z$$

Thus

$$\frac{\partial^2 T}{\partial r^2} = \frac{\partial}{\partial r} \left(\frac{1}{r} \frac{\partial T}{\partial x} \right) = \frac{\partial^2 T}{\partial x^2} \frac{1}{r^2} - \frac{1}{r^2} \frac{\partial T}{\partial x}$$

$$\frac{\partial^2 T}{\partial \phi^2} = \frac{\partial^2 T}{\partial y^2}$$

$$\frac{\partial^2 T}{\partial z^2} = \frac{\partial^2 T}{\partial z^2}$$

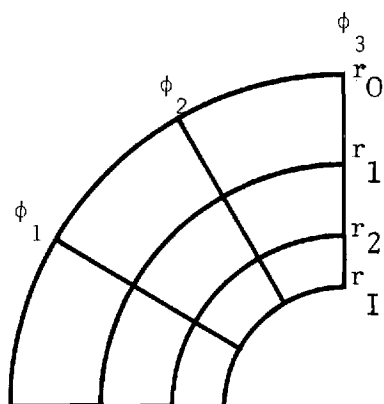
Substitution back into $\bar{v}^2 T$

$$\frac{1}{r^2} \frac{\partial^2 T}{\partial x^2} - \frac{1}{r^2} \frac{\partial T}{\partial x} + \frac{1}{r^2} \frac{\partial T}{\partial x} + \frac{1}{r^2} \frac{\partial^2 T}{\partial y^2} + \frac{\partial^2 T}{\partial z^2}$$

or

$$\frac{1}{r^2} \frac{\partial^2 T}{\partial x^2} + \frac{1}{r^2} \frac{\partial^2 T}{\partial y^2} + \frac{\partial^2 T}{\partial z^2}$$

This transformation simplifies calculation and makes finite difference approximation of the equations easier. Figure 26 shows the result of this transformation.



Becomes

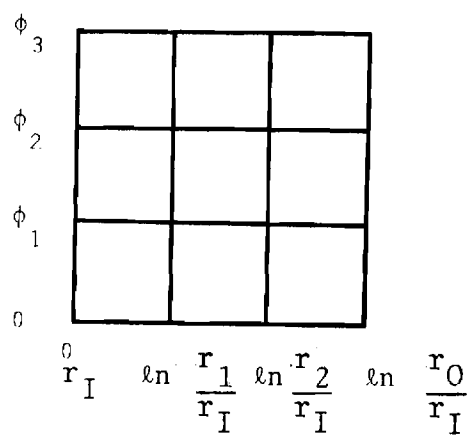


Figure 26. Polar to Rectangular Transformation

APPENDIX B

THERMODYNAMIC PROPERTY EQUATIONS

In his thesis Hare [8] developed polynomial expressions for the thermal properties of nitrogen and stainless steel as a function of temperature. A least squares regression analysis program on a Wang 720 calculator was used. These equations have been converted to International units and are presented here. Expressions for the specific heats of nitrogen, stainless steel and aluminum were developed using the same technique and data from references [23,25].

T = temperature in degrees Kelvin

Properties of liquid nitrogen

Density (Kg/m^3)

$$\begin{aligned} \rho_l = & -5.7784 \times 10^{-10} T^7 + 2.45356 \times 10^{-7} T^6 - 3.49017 \times 10^{-5} T^5 \\ & + 8.3300 \times 10^{-4} T^4 + 2.7794 \times 10^{-1} T^3 - 3.10677 \times 10 T^2 \\ & + 1.31038 \times 10^3 T - 1.94571 \times 10^4 \end{aligned}$$

Viscosity (N-sec/m^2)

$$\begin{aligned} \mu_l = & -2.25319 \times 10^{-11} T^4 + 6.541176 \times 10^{-9} T^3 - 5.51203 \times 10^{-7} T^2 \\ & + 2.708099 \times 10^{-6} T + 1.0352966 \times 10^{-3} \end{aligned}$$

Surface tension (N/m)

$$\begin{aligned} \sigma_l = & 1.026812 \times 10^{-9} T^4 - 3.919365 \times 10^{-7} T^3 + 5.631364 \times 10^{-5} T^2 \\ & - 3.804096 \times 10^{-3} T + 1.1066907 \times 10^{-1} \end{aligned}$$

Heat of vaporization (J/Kg)

$$h_{fg} = - 3.25198085 \times 10^{-6} T^6 + 9.1831855 \times 10^{-4} T^5 \\ - 3.4922526 \times 10^{-2} T^4 - 1.3994675 \times 10^1 T^3 + \\ 1.9701130 \times 10^3 T^2 - 1.005187 \times 10^5 T + 2.0678544 \times 10^6$$

Thermal conductivity (W/m-K)

$$K_{\ell} = 3.586226 \times 10^{-10} T^5 - 1.6795344 \times 10^{-7} T^4 + \\ 3.120013 \times 10^{-5} T^3 - 2.8859648 \times 10^{-3} T^2 + \\ 1.3152021 \times 10^{-1} T - 2.182878$$

Specific heat (J/Kg-K)

$$c_{\ell} = 3.543145 \times 10^{-4} T^4 - 1.0894305 \times 10^{-1} T^3 + \\ 1.2632769 \times 10^1 T^2 - 6.500754 \times 10^2 T + 1.4495738 \times 10^4$$

Properties of 304 stainless steel

Thermal conductivity (w/m-K)

$$K_p = - 2.25468 \times 10^{-4} T^2 + 9.99792 \times 10^{-2} T + 2.2549$$

Specific heat (J/Kg-K)

$$C_p = - 1.037895 \times 10^{-2} T^2 + 4.982373 T - 1.5772696 \times 10^2$$

Specific heat of Aluminum (J/Kg-K)

$$C_{Al} = - 8.1727423 \times 10^{-5} T^3 - 4.3008433 \times 10^{-3} T^2 + \\ 8.9683338 T - 2.8647838 \times 10^2$$

APPENDIX C

WICK-WALL INTERFACE NODES

Due to the change of variables used (see Appendix A) nodes are spaced exponentially through the wall and wick. It was found that for best results three nodes were needed in the wall and two in the wick with one for the interface. The wick nodes are smaller than the wall nodes and a scale factor SF was calculated so that the same value of DX could be used. Figure 27 shows nodes near the interface in the evaporator.

To place the fourth node on the interface of the wick and wall an artificial radius had to be calculated. This artificial radius was then used for calculating the locations of all nodes in the wall and the scale factor for the nodes in the wick.

The artificial radius is given by:

$$r_{art} = \left[\frac{r_0}{r_B} \right]^{1/(NIE-1)} \frac{(NIE-1)}{(2-NIE)}$$

Wick nodes are smaller than wall nodes by the factor SF given by:

$$SF = \frac{1}{2} (NIE-2) \ln(r_B/r_I) / \ln(r_0/r_{art})$$

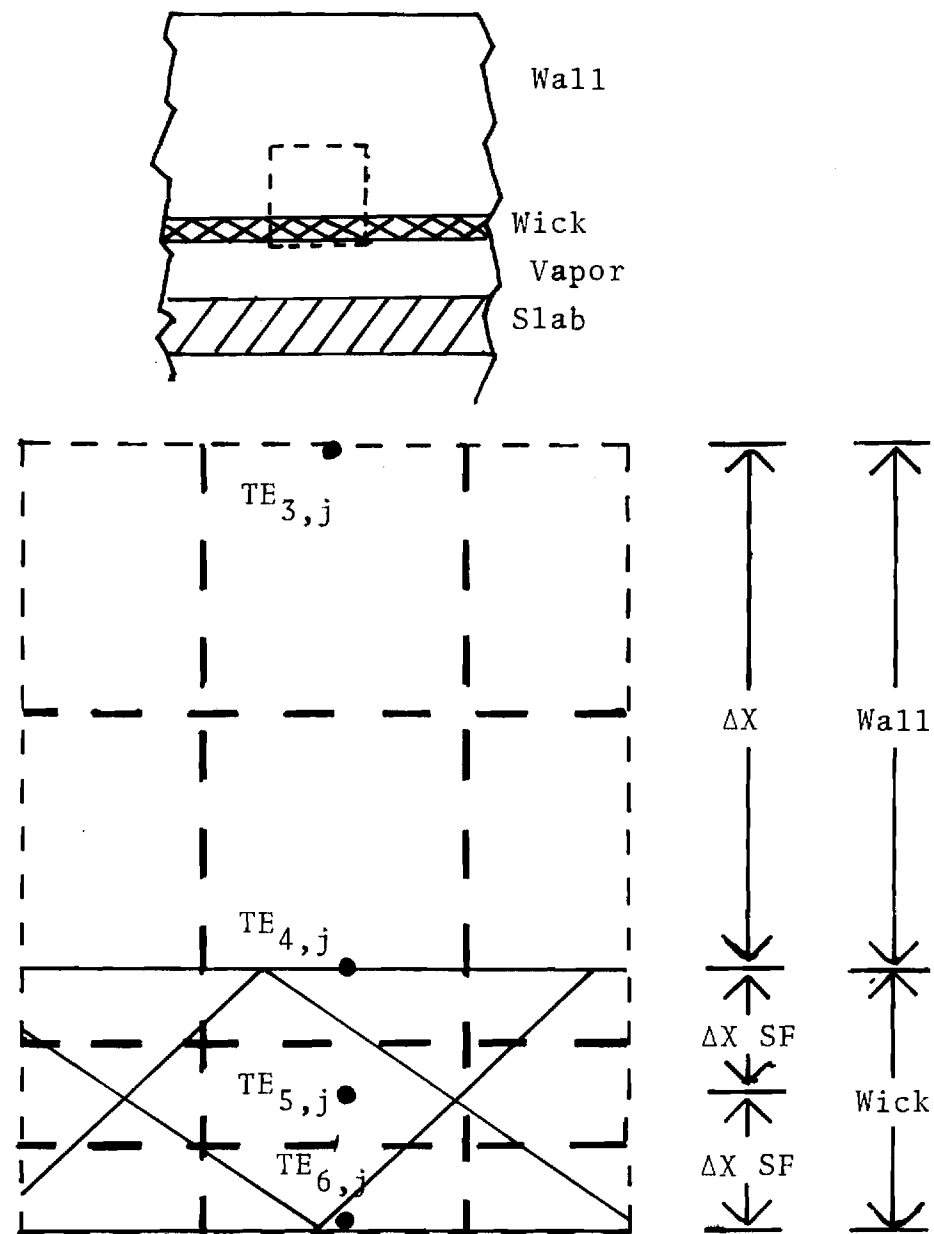


Figure 27. Wick-Wall Interface Nodes

A heat balance on node 4 gives:

$$r_4^2 \rho_4 c_4 \Delta z \Delta y \left(\frac{\Delta x + SF \Delta x}{2} \right) \frac{TE_{4,j}^{n+1/2} - TE_{4,j}^n}{t^{n+1/2} - t^n} = \frac{K_p}{\Delta x} \Delta y \Delta z (TE_{3,j}^{n+1/2} - TE_{4,j}^{n+1/2})$$

$$\begin{aligned} \frac{K_w}{\Delta x} SF \Delta y \Delta z (TE_{5,j}^{n+1/2} - TE_{4,j}^n) + \frac{K_p}{\Delta y} \Delta z \left(\frac{\Delta x + SF \Delta x}{2} \right) (TE_{4,j+1}^n + \\ TE_{4,j-1}^n - 2TE_{4,j}^n) \end{aligned}$$

which can be rearranged for the subroutine to give

$$\begin{aligned} - \left(\frac{K_p \Delta t}{2(\Delta x)^2 (1+SF) \rho_4 c_4 r_4^2} \right) TE_{3,j}^{n+1/2} + \left(1 + \frac{K_p \Delta t}{2(\Delta x)^2 (1+SF) \rho_4 c_4 r_4^2} + \right. \\ \left. \frac{K_w \Delta t}{2(\Delta x)^2 SF (1+SF) \rho_4 c_4 r_4^2} \right) TE_{4,j}^{n+1/2} \\ - \left(\frac{K_w \Delta t}{2(\Delta x)^2 SF (1+SF) \rho_4 c_4 r_4^2} \right) TE_{5,j}^{n+1/2} = \frac{K_p \Delta t}{2(\Delta y)^2 \rho_4 c_4 r_4^2} (TE_{4,j+1}^n + \\ TE_{4,j-1}^n - 2TE_{4,j}^n) + TE_{4,j}^n \end{aligned}$$

APPENDIX D
COMPUTER CODE

```

      PROGRAM MAIN (INPUT,OUTPUT,TAPE5=INPUT,TAPE6=OUTPUT)
      1. DATA,TAPE2=DATA,LIST,TAPE3=LIST)
      DIMENSION TE(6,20),TC(6,30),T(6,30),D(30),E(20),F(30),W(30)
      1,ATE(6),ATC(6),AJ1(6),AYE(6,30),AYC(6,30),AXC(6,30),AYC(6,30)
      1,A(30),CXC(6,30),CYE(6,30),CXC(6,30),CYC(6,30),AXCON(6),RSI2(6)
      1,OCV(15)
      COMMON ET,TS,QIS,TE,TV,TC,TR,QIF,QR,QEV,QCR,QMAX,NIE,NJE,NIC,NJC
      1,LWFE,LWFC,LBO,LNA,CXF,CYE,CXC,CYC,CV,V,TL,EL,ASU,BSU,XL,GC,ICRIT
      1,AXE,AYE,AXC,AYC,AV,RV,AS,RS,AC,BC,CIF,CIC,AIE,AIC
      1,MDOT,RMASS,DT,DT0,IX,KF,F,C,QXC,DYC,CL,NJA,CRESIST
      1,WT,OF,RF,NL,BETA,POFSTY
      REAL NL,KL,MDOT,KF,HFG,KW
      WRITE(6,65)
65  FORMAT("INPUT CASE NUMBER")
      READ(5,*) NO
      WRITE(6,75)
75  FORMAT("INPUT DT,NDT")
      READ(5,*) DT,NDT
      WRITE(6,85)
85  FORMAT("INPUT MDOT,RMASS,QIS,QTP,AR,TI,CRESIST")
      READ(5,*) MDOT,RMASS,QIS,QIR,AR,TI,CRESIST
      WRITE(6,100)
100 FORMAT("TYPE 1 TO INPUT ALL DATA")
      READ(5,*) INPUT
      IF(INPUT.NE.1) GO TO 250
      WRITE(6,200)
200 FORMAT("INPUT NIE,NJE,NIC,NJC,NJA")
      READ(5,*) NIE,NJE,NIC,NJC,NJA
      WRITE(6,300)
300 FORMAT("INPUT TSI,TEI,TVI,TCI,TRI")
      READ(5,*) TSI,TEI,TVI,TCI,TRI
      WRITE(6,400)
400 FORMAT("INPUT LWFE,LBO,LWFC,LNA")
      READ(5,*) LWFE,LBO,LWFC,LNA
      WRITE(6,450)
450 FORMAT("INPUT WT,OF,RF,NL,BETA,POFSTY")
      READ(5,*) WT,OF,RF,NL,BETA,POFSTY
      C INITIALIZE VALUES
      ET=0
      TS=TSI
      DO 2 J=1,NJE
      DO 1 I=1,NIE
1     TE(I,J)=TEI
2     CONTINUE
      TV=TVI
      DO 4 I=1,NIC
      DO 3 J=1,NJC
3     TC(I,J)=TCI
4     CONTINUE
      TR=TRI
      XL=.1524
      GO TO 350
250 CALL DATAIN
350 DT0=DT
      ET=0.
      WRITE(3,500) RMASS,AR,MDOT
500 FORMAT(5X,"MASS OF HEAT SINK",F11.3,1X,"KG AREA",F11.3,1X,
1"***2",3X,"FLOW RATE",3X,1P15.6,3X,"KG/SEC")
      DO 6 I=1,NIE
      ATC(I)=0.
      DO 5 J=1,NJE
5     ATE(I)=TE(I,J)+ATE(I)
6     ATE(I)=ATE(I)/FLOAT(NJE)

```

```

      EM=.72
      ICOUNT=1
      OPTV=TV
      DP=.913E+05
      RF=1.55E-05
      POSTIV=.596
      SMASS=1.E+22
      LWFCQ=LWFC
      WRITE(3,402)NO
402  FORMAT(I3,"CASE NUMBER" ,I3)
      CALL PARAMTR
      QP=5.6637E-8*EM**AP*TP**4+CC*(IR-TI)
      CALL OUTPUT
C  START TIME CYCLES
      DO 1000 N=1,NOI
      ICOUNT=ICOUNT+1
      IF (LWFC.EQ.LWFCQ) GO TO 20
      CALL PARAMTR
      OPTV=TV
      LWFCQ=LWFC
      GO TO 40
20  IF (ABS(TV-OPV).LT..1) GO TO 30
      CALL PARAMTR
      OPTV=TV
      GO TO 40
30  IF (ABS(OT-5).LT..001) GO TO 40
      IF (N-10) 80,80,40
40  IF (ABS(IR-TPQ)-.0013) 50,80,80
50  IF (ABS(TV-TVQ)-.0010) 55,80,80
55  DT=2*DT
      IF (DT-30) 70,70,60
60  DT=30
70  CALL PARAMTR
      OPTV=TV
      ET=ET+DT
80  DO 90 I=1,NIE
90  AXCON(I)=(TC(I,2)-ATE(I))*KF/(OYC**2*NJE*R*C*ATE(I))
      TRO=TR
      TVQ=TV
      CALL VAPOR
      CALL COOLER(AC,BC,CC,II,TC,NJC,NJA,TR,EM,AR,QIR,QR,QCR)
      CALL GRID2D (TF,AXE,AYE,CXE,CYE,NIE,NJE,AXCON,
1AIC,TV,ATC,S.,TS,1.,1.,1.,2,1,2,2,0,CIE,1.,LWFE,LBO)
      DO 11 I=1,NIE
      ATE(I)=0.0
      DO 10 J=1,NJE
10  ATE(I)=TE(I,J)+ATE(I)
11  ATE(I)=ATE(I)/FLOAT(NJE)
      CALL GRID2D (IC,AXC,AYC,CXC,CYC,NIC,NJC,ATC,
1AIC,TV,ATE,C.,TP,1.,1.,1.,3,1,1,2,NJA,CIC,CJC,LWFC,LNA)
      NJAP1=NJA+1
      IF (ICOUNT.EQ.5) GO TO 12
      GO TO 1000
12  CALL OUTPUT
      ICOUNT=1
1000 CONTINUE
      CALL DATAOUT
      STOP
      END

```

```

SUBROUTINE PARAMTR
  DIMENSION TE(6,30),TC(6,30),AXE(6,30),AYE(6,30),AXC(6,30),
  1AYC(6,30),CXE(6,30),CYE(6,30),CXC(6,30),CYC(6,30),AKCON(6)
  1,PSIZ(6)
  COMMON ET,IS,DIS,TE,TV,TC,TR,DIR,OR,DFV,DDR,GMAX,NIF,NJE,NIC,NJC
  1,LWFE,LWFG,LRO,LNA,CXE,CYE,CXC,CYC,CV,V,TL,EL,ASU,BSU,XL,CC,ICRIT
  1,AXE,AYE,AXC,AYC,AV,BV,AS,BS,AC,BC,CIE,CIC,AIE,AIC
  1,MDOJ,PMASS,DI,OTO,IX,KF,P,C,DXC,DYC,CL,NJA,CRESIST
  1,WT,DF,RF,NL,BETA,POFSTY
  REAL NL,KL,MDOJ,KF,HFG,KW,MCPSLAB
  CTV=TV
  IF(CTV.GT.125) CTV=125
C VISCOSITY (N SEC/M**2)
  XMU=-2.25319E-11*CTV**4+6.541176E-9*CTV**3-5.51203E-7*CTV**2
  1 +2.728093E-6*CTV+1.0352966E-3
C SURFACE TENSION (N/M)
  SIGMA=1.026812E-9*CTV**4-.7919365E-6*CTV**3+.5631364E-4*CTV**2
  1 -.3834096E-2*CTV+1.066907E-1
C INVERSE PERMEABILITY OF SLAB (1/M**2)
  FK=6.465E8
C PORE RADIUS (M)
  RPORE=1.905E-5
C DENSITY OF PIPE WALL (KG/M**3)
  P=7917
C SPECIFIC HEAT OF PIPE WALL (WATT SEC/KG K)
  C=-1.37895E-2*CTV**2+4.982373*CTV-1.5772696E2
C SPECIFIC HEAT OF SADDLE (WATT SEC/KG K)
  CS=-8.1727423E-5*CTV**3-4.3008433E-3*CTV**2+8.9683338*CTV
  1 -2.8647838E2
C OUTSIDE RADIUS OF PIPE (M)
  RO=.00635
C EMISSIVITY OF HEAT SINK
  EM=.72
C HEAT PIPE TOTAL LENGTH (M)
  TL=.9144
C EVAPORATOR LENGTH (M)
  FL=.1524
C CONDENSER LENGTH (M)
  CL=.3048
C VAPOR DENSITY (KG/M**3)
  RHOV=9.40
C SPECIFIC HEAT OF VAPOR (WATT SEC/KG K)
  CV=1172.30
  RB=RO-WT
  PI=RB-4.0*RF*NL-BETA*(NL-1.0)
  PSUM=0.0
  NI=INT(PI)
  DO 40 I=1,NI
    FI=FLOAT(I)
    TERM=ALOG((RB-(FI-1.0)*4.0*PF-(FI-1.0)*BETA)/(RB-4.0*FI*RF-(FI-1)
    C*BETA))
    PSUM=TERM+PSUM
40  CONTINUE
    SUMA=PSUM
    PSUM=0.0
    NM1=NI-1
    DO 42 I=1,NM1
      FI=FLOAT(I)
      TERM=ALOG((RB-4.0*FI*RF-(FI-1.0)*BETA)/(RB-4.0*FI*RF-FI*BETA))
      PSUM=TERM+PSUM
42  CONTINUE
    SUM=PSUM
    IF(NM1.EQ.0) SUMR=0.0
C

```

```

C SET DXE,DYE,DXC,DYC, AND DT
  NIEM1=NIEM-1
  NIFM2=NIEM-2
  NIGM2=NIG-2
  NJEM1=NJE-1
  NIGM1=NIG-1
  NJCM1=NJC-1
  ROGUS=(RO**2)/(1.0/FLOAT(NIFM2))/(PR)**
  1 (FLOAT(NIEM2)/(1.0-FLOAT(NIEM2)))

  DXE=(ALOG(PO/ROGUS))/FLOAT(NIEM2)
  DYE=6.243/FLOAT(NJEM1)
  DXC=(ALOG(PO/ROGUS))/FLOAT(NIGM2)
  DYC=(TL-EL)/FLOAT(NJCM1-1)
C THERMAL CONDUCTIVITY OF STAINLESS STEEL (WATT/M K)
  KF=-2.25468E-4*CTV**2.3+9.99792E-2*CTV+2.2549
C THERMAL CONDUCTIVITY OF LIQUID NITROGEN (WATT/M K)
  KL=3.535226E-13*CTV**5.1-1.6795344E-7*CTV**4.0
  C(DF-2.0*RF)+1.0)))*KL/(2.0*RF/(DF-2.0*RF)+1.0)**2.0
  C-2.182979
C THERMAL CONDUCTIVITY OF SCREEN (WATT/M K)
10  KW=KL/((DF/(2.0*RF))*(2.0*(KL/KF)+DF/(2.0*RF)
  C-2.0))+2.0*KL/((DF/(2.0*RF))*((KL/KF)*((2.0*RF)/
  C(DF-2.0*RF)+1.0)))+KL/(2.0*RF/(DF-2.0*RF)+1.0)**2.0
C THERMAL CONDUCTIVITY OF WICK (WATT/M K)
  KW=(K*SUMA+KL*SUMB)/(SUMA+SUMB)
C DENSITY OF LIQUID NITROGEN (KG/M**3)
  RHOL=-5.7784E-13*CTV**7+2.45356E-7*CTV**6-3.49017E-5*CTV**5
  1 +8.3391E-4*CTV**4+2.7794E-1*CTV**3-3.10677E1*CTV**2
  1 +1.31038E3*CTV-1.94571E4
C DENSITY OF WICK (KG/M**3)
  RHOW=(SUMA*(PORSTY*RHOL+(1.-PORSTY)*R)+SUMB*FHOL)/(SUMA+SUMB)
C SPECIFIC HEAT OF LIQUID NITROGEN (WATT SEC/KG K)
  CPL=3.5+3145E-4*CTV**4-1.0894305E-1*CTV**3+1.2632769E1*CTV**2
  1 -6.5017540E2*CTV+1.4495738E4
C HEAT OF VAPORIZATION (WATT SEC/KG)
  HFG=-7.25198085E-6*CTV**6+9.1831855E-4*CTV**5
  1 -3.4322526E-2*CTV**4-1.3994675E+1*CTV**3
  1 +1.9701130E+3*CTV**2-1.005187E+5*CTV
  1 +2.0673544E+6
2000 FORMAT(4E15.6)
C SLAB PROPERTIES
  DELA=7.437E-5
  DELB=6.218E-4
  NLA=4
  NLB=5
  EA=.5961
  EB=.6532
  FPCINWL=(NJC-LWFC)/NJCM1
  MCPSLAB=2.*TL*PI*(DELA*NLA*(EA*PHOL*CPL*FPCINWL+(1.-EA)*R*C)
  1 +DELB*NLB*(EB*PHOL*CPL*FPCINWL+(1.-EB)*R*C))
C SPECIFIC HEAT OF THE WICK (WATT SEC/KG K)
  CW=((1.-PORSTY)**2*C+PORSTY*CPL*PHOL)/((1.-PORSTY)*R+PORSTY*RHOL)
  CW=(CW*SUMA+CPL*SUMB)/(SUMA+SUMB)
  WRITE(3,2000) C,CPL,FPCINWL,RHOL
C DIMENSIONS OF COOLING JACKET (M)
  RCO=.0167
  RCI=.0133
  EW=.00318
  RMASS1=7.1416*((CL*(RCO**2-RCI**2)+2.*EW*(RCC**2-RO**2))*C*R
  1 +CL*(RCI**2-RO**2)*CPL*RHOL)
  IF(MDIT.LT.1.E-9) GO TO 11
  RMASS=RMASS1
  GS=1.

```

```

11      CC=MDOT*CPL

      C1F=KF*DT/(4*G*DXE**2.*R0**2.)
      C1G=DT/CRRESIST/(P*G*DXC**2.*R0)
      AG=6.283*CL*P0/(CRRESIST)
      BC=DT/(PMASS*CS)
      A1F=-DXE*QIS/(KF*6.2832*EL)
      A1G=-KF*CRRESIST/(DXC*R0)
      ASU=2.*SIGMA/(PPORE*PHOL)
      RSU=EK*XMU/PHOL
      QMAX=4*SIGMA*PI*(NLA*DELA+NLR*DELR)*RHOL/
1      (PPORE*EK*XMU*(TL-(EL+CL)/2.))*HFG

      DO 200 I=1,NIEM2
      L=NIEM1-I+1
      RS12(I)=(RBOGUS*(P0/RBOGUS)**(FLOAT(L-1)/NIEM2))**2
      DO 100 J=1,NJE
      AXE(I,J)=KF*DT/(DXE**2*R*C**2.*RS12(I))
      AYE(I,J)=KF*DT/(DYE**2*R*C**2.*RS12(I))
      CXE(I,J)=AXE(I,J)
      CYE(I,J)=AYE(I,J)
100    CONTINUE
200    SF=.5*NIEM2*ALOG(SQRT(RS12(NIEM2))/RI)/ALOG(R0/RBOGUS)
      RI2=RI**2
      RNIM12=(RHOGUS*(R0/RBOGUS)**(7/NIEM2/2))**2
      RINMD2=(RI*(SQRT(RS12(NIEM2))/RI)**.75)**2
      PSI2(NIEM1)=(PI*(SQRT(RS12(NIEM2))/RI)**.5)**2
      XDOSH=((RS12(NIEM2)-RINMD2)*RHOW*CW+(PNIM12-PSI2(NIEM2))*R*C)/
1      (RNIM12-RINMD2)
      AV=TKW*DT*2.*DYE*EL/(DXE*(RHOV*TL*(3.1416*RI2-
12.*RI*SLBTHK)*CV+MCPSLAB+TL*(RINMD2-RI2)*
2      3.1416*CW)*SF)
      BV=TKW*DT*2.*6.283*DYC/(DXC*(PHOV*TL*(3.1416*RI2-
12.*RI*SLBTHK)*CV+MCPSLAB+TL*(RINMD2-RI2)*
2      3.1416*CW)*SF)
      IX=INT(AV*NJE+BV*NJC)+10
      AV=AV/FLOAT(IX)
      BV=BV/FLOAT(IX)
      CV=TKW*DY*EL/(DXE*SF)
      WRITE(3,2000) PMASS,CW,MCPSLAB,CS

10000  FORMAT(2E13.5)

      DO 300 J=1,NJE
      AXE(NIEM2,J)=KF*DT/(DXE**2*XDOSH*(1.+SF)*PSI2(NIEM2))
      CXE(NIEM2,J)=TKW*DT/(DXE**2*XDOSH*(1.+SF)*RS12(NIEM2)*SF)
      AYE(NIEM2,J)=KF*DT/(DXE**2*XDOSH*2.*RS12(NIEM2))
      CYE(NIEM2,J)=AYE(NIEM2,J)
      CXE(NIEM1,J)=TKW*DT/(DXE**2*SF**2*CW*PHOW*2*RS12(NIEM1))
      AXE(NIEM1,J)=CXE(NIEM1,J)
      AYE(NIEM1,J)=TKW*DT/(DYE**2*PHOW*CW*2.*RI2)
      CYE(NIEM1,J)=AYE(NIEM1,J)
      AXE(NIE,J)=PSI2(NIEM1)/RI2*CXE(NIEM1,J)
      CXE(NIE,J)=AXE(NIE,J)
      AYE(NIE,J)=TKW*DT/(DYE**2*PHOW*CW*2.*RI2)
300    CYE(NIE,J)=AYE(NIE,J)

      DO 500 I=1,NIEM2
      DO 400 J=1,NJC
      AXG(I,J)=KF*DT/(DXC**2*R*C**2.*RS12(I))
      AYG(I,J)=KF*DT/(DYC**2*R*C**2.)
      CXG(I,J)=AXG(I,J)
400    CYG(I,J)=AYG(I,J)

```

```

500  CONTINUE
      DO 600 J=1,NJC
        AXG(NIC42,J)=KF*DT/(DXE**2*XDSH*(1.+SF)*PSI2(NICM2))
        AYC(NIC41,J)=TKK*DT/(DYC**2*PHQW*CW*2.)
        AYC(NIC42,J)=KF*DT/(DYC**2*XDSH*2.)
        CYC(NIC42,J)=AYC(NICM2,J)
        CYC(NICM1,J)=AYC(NICM1,J)
        CXG(NIC42,J)=TKW*DT/(DXC**2*YDSH*(1.+SF)*PSI2(NICM2)*SF)
        CXG(NIC41,J)=TKK*DT/(DXC**2*SF**2*CW*PHQW*2*PSI2(NICM1))
        AXG(NIC41,J)=CXG(NICM1,J)
        CYG(NIC,J)=TKW*DT/(DYC**2*PHQW*CW*2.)
        AYC(NIC,J)=CYC(NIC,J)
        AXG(NIC,J)=PSI2(NICM1)/PI2*CXC(NICM1,J)
600  CXC(NIC,J)=AXG(NIC,J)
      RETURN
      END

```



```

SUBROUTINE VAPOR
  DIMENSION IF(6,30),IC(6,30),AXE(6,30),AYE(6,30),AXC(6,30),
  1AYC(6,30),CXE(6,30),CYE(6,30),CXC(6,30),CYC(6,30),AXCON(6)
  1,OCV(15)
  COMMON ET,TS,QIS,TE,TV,TC,TP,QIP,QP,QEV,QCR,QMAX,NIF,NJE,NIC,NJC
  1,LWFE,LWFC,LBO,LNA,CXE,CYE,CXC,CYC,CV,V,TL,FL,ASU,BSU,XL,CC,ICRIT
  1,AXE,AYE,AXC,AYC,AV,BV,AS,BS,AC,BC,CIE,CIC,AIE,AIC
  1,MDO1,PMASS,DT,DT0,IX,KF,P,C,D,KC,DYC,CL,NJA,CRESIST
  1,WT,DE,PE,NL,BETA,PORSTY
  PEAL NL,KL,MDO1,KF,HFG,KW
  GO TO 210
  XLBO=NJE*(1/(1+ABS(QEV)/QMAX))+1
  XLNA=(NIC-NJA)*QEV/QMAX+NJA+1
  LBO=INT(XLBO)+INT(2*(XLBO-INT(XLBO)))
  IF (LBO.GT.(NJE+1)) LBO=NJE+1
  LNA=INT(XLNA)+INT(2*(XLNA-INT(XLNA)))
  IF (LNA.LE.(NJA+1)) GO TO 101
  IF (LNA.GT.(NJC+1)) GO TO 39
  GO TO 210
39  LNA=NJC+1
  GO TO 210
100  LNA=NJA+2
200  NJAP1=NJA+1
  SUMTC=0.0
  DO 28 J=NJAP1,NJC
    SUMTC=SUMTC+IC(NICM1,J)
  SUMTC=SUMTC/FLOAT(NJC-NJA)
  IF (SUMTC.GT.125) GO TO 50
  IF (ICRIT.LT.1) GO TO 55
  DO 29 I=1,1000
    V=DT/1000.*(ASU-BSU*V*XL-V**2)/XL+V
    XL=XL+V*DT/1000.
29  CONTINUE
  IF (XL.GT.(TL-CL/2.)) ICRIT=0
  LOF=INT(FLOAT(NJC-NJA)/2)+INT(XL/DYC)+INT(2*(XL/DYC-INT(XL/DYC)))
  1 +1
  LWFC=NJC-LOF
  IF (LWFC-NJA) 35,30,30
30  LWFC=NJA
  GO TO 45
35  IF (LWFC-1) 40,45,45
40  LWFC=1
  XLBO=(XL-TL+CL/2+EL)/EL*NJE
  LBO=INT(XLBO)+INT(2*(XLBO-INT(XLBO)))+1
  IF (LBO.GT.(NJE+1)) LBO=NJE+1
45  GO TO 55
50  LWFC=NJC
  LBO=1
  ICRIT=1
55  CONTINUE
  IF (LBO.EQ.1) GO TO 1001
  QEV=0.
  OCV(1)=.5*CV
  OCV(NJE)=.5*CV
  NJEM1=NJE-1
  DO 99 J=2,NJEM1
998  OCV(J)=CV
  IRO=0
  DO 1000 J=1,NJE
  IF (IRO.EQ.1) GO TO 1000
  QEV=OCV(J)*(TE(NIE-1,J)-TE(NIE,J))+QEV
  IF (QEV.LT.QMAX) GO TO 1000
  IRO=1

```

```

      ICRIT=1
      LRO=J+1
1000  CONTINUE
1001  CONTINUE
      AVETE=0.0
      AVETEV=0.
      AVETCV=0.
      AVETC=0.0
      LBOM1=LBO-1
      LNAM1=LNA-1
      LWFCP1=LWFC+1
      LWFCP1=LWFCP1+1
      EACTIVE=FLOAT(LBOM1-LWFCP1+1)
      CACTIVE=FLOAT(LNAM1-LWFCP1+1)
      IF (LBO.LE.LWFCP1) GO TO 14
      DO 10 J=LWFCP1,LBOM1
      AVETEV=AVETEV+TE(NIF,J)
10    AVETE=AVETE+TE(NIE-1,J)
      AVETEV=AVETEV/EACTIVE
      AVETE=AVETE/EACTIVE
      IF (NJE-LBOM1) 11,11,12
11    EACTIVE=EACTIVE-.5
12    IF (2-LWFCP1) 16,13,13
13    EACTIVE=EACTIVE-.5
      GO TO 15
14    EACTIVE=0.0
15    IF (LNA.LE.LWFCP1) GO TO 24
16    DO 20 J=LWFCP1, LNAM1
      AVETCV=AVETCV+TC(NIC,J)
20    AVETC=AVETC+TC(NIC-1,J)
      AVETCV=AVETCV/CACTIVE
      AVETC=AVETC/CACTIVE
      IF (NJIC-LNAM1) 21,21,22
21    CACTIVE=CACTIVE-.5
22    IF (2-LWFCP1) 25,23,23
23    CACTIVE=CACTIVE-.5
      GO TO 25
24    CACTIVE=0.0
25    TVO=TV
      DO 26 I=1,IX
26    TV=AV+EACTIVE*(AVETE-AVETEV-TV+TVO)+TV
1    +BV*CACTIVE*(AVETC-TVO-TV+TVO)
      TV=(TV-TVO)*DT/DTO+TVO
      DTO=DT
      WRITE(3,4) LRO,LNA,LWFC,V,XL
49    FORMAT(3I8,2E16.5)
897  FORMAT(+E15.8)
      RETURN
      END

```

```

SUBROUTINE COOLER (A,E,C,II,T,NJC,NJA,TR,E,AF,QIR,QP,QCR)
DIMENSION T(6,70)
SUMT=0.0
QP=5.657E-8*E*AP*TP**4+C*(TP-TI)
NJAP1=NJA+1
DO 10 J=NJAP1,NJC
SUMT=SUMT+T(1,J)-TR
QCR=A*SUMT/FLCAT(NJC-NJA)
TR=3*(QCR+QIR-QR)+TR
RETURN
END
10

```

```

      SUBROUTINE GP1020 (T,AX,AY,CX,CY,NI,NJ,AXIAL,AI1,AIM,AJ1,AJM,
1QI1,QIM,QJ1,QJM,LI1,LIM,LJ1,LJM,NJA,QI1,QJ1,LWF,LRO)
      DIMENSION T(6,30),D(30),W(30),E(30),F(30),AJ1(6),AX(6,30),
1AY(6,30),CX(6,30),CY(6,30),A(30),C(30),AXIAL(6)

      NIM1=NI-1
      NJM1=NJ-1
      C MAKE I SWEEP
      C PICK LEFT BOUNDARY CONDITION
12      IF (LJ1-2) 14,15,100
14      DO 15 I=2,NIM1
15      D(I)=AJ1(I)
      GO TO 110
16      DO 17 I=2,NIM1
17      D(I)=(1.-2.*AY(I,1))*T(I,1)+2.*AY(I,1)*T(I,2)+T(I,1)*AXIAL(I)
      GO TO 110
100     IF(1-NJA)201,200,300
200     LIN=2
      AIN=0.0
      GO TO 400
300     LIN=LI1
      AIN=AI1
400     CONTINUE
      IF(1-LWF)600,600,500
500     IF(1-LRO)700,600,600
600     LIO=2
      AIO=0.0
      GO TO 800
700     LIO=LIM
      AIO=AIM
800     CONTINUE
      DO 1000 I=1,NI
      A(I)=AX(I,1)
1000    C(I)=CX(I,1)
      CALL ROACHE (A,C,D,NI,E,F,W,LIN,LIO,
1AIN,AIO,QI1,QIM)
21      DO 40 J=2,NJM1
      DO 25 I=2,NIM1
25      D(I)=CY(I,J)*T(I,J+1)+AY(I,J)*T(I,J-1)
      1 +(1.-AY(I,J)-CY(I,J))*T(I,J)+T(I,J)*AXIAL(I)
      DO 30 I=1,NI
30      T(I,J-1)=W(I)
101     IF(J-NJA)201,201,301
201     LIN=2
      AIN=0.0
      GO TO 401
301     LIN=LI1
      AIN=AI1
401     CONTINUE
      IF(J-LWF)601,601,501
501     IF(J-LRO)701,601,601
601     LIO=2
      AIO=0.0
      GO TO 801
701     LIO=LIM
      AIO=AIM
801     CONTINUE
      DO 1001 I=1,NI
      A(I)=AX(I,J)
1001    C(I)=CX(I,J)
      CALL ROACHE (A,C,D,NI,E,F,W,LIN,LIO,
1AIN,AIO,QI1,QIM)
40      CONTINUE

```

```

C PICK RIGHT BOUNDARY CONDITION
DO 44 I=2,NIM1
44  D(I)=(1.-2.*AY(I,NJ))*T(I,NJ)+2.*AY(I,NJ)*T(I,NJ-1)
    1 +T(I,NJ)*AXIAL(I)
47  DO 39 I=1,NI
39  T(I,NJ-1)=W(I)
    IF(NJ-LWF)602,602,502
502  IF(NJ-L10)702,602,602
602  LIO=2
    AIO=0.0
    GO TO 402
702  LIO=LIM
    AIO=AIM
802  CONTINUE
    DO 1002 I=1,NI
    A(I)=AX(I,NJ)
1002  C(I)=CX(I,NJ)
    CALL ROACHE (A,C,D,NI,E,F,W,LII,LIO,
    1AII,AIO,OII,OIM)
    DO 48 I=1,NI
48  T(I,NJ)=W(I)
C MAKE J SWEEP
    IF (LII-2) 53,51,53
49  DO 50 J=1,NJ
50  D(J)=AII
    GO TO 55
51  DO 52 J=2,NJM1
52  D(J)=(1.-2.*AX(1,J))*T(1,J)+2.*AX(1,J)*T(2,J)-CII*AI1
    GO TO 55
53  DO 54 J=2,NJM1
102  IF(J-NJA)202,202,302
202  LIN=2
    CIN=0.0
    GO TO 402
302  LIN=LII
    CIN=CII
402  CONTINUE
    D(J)=(1.-2.*AX(1,J)-2.*CIN)*T(1,J)+2.*AX(1,J)*T(2,J)
    1+(2.*CIN)*OII+T(1,J)*AXIAL(1)
54  IF(LIN.EQ.1) D(J)=AII
    DO 1003 J=1,NJ
    A(J)=AY(1,J)
1003  C(J)=CY(1,J)
55  CALL ROACHE (A,C,D,NJ,E,F,W,LJ1,LJM,
    1AJ1(1),AJM,OJ1,OJM)
56  DO 70 I=2,NIM1
    DO 60 J=2,NJM1
60  D(J)=CX(I,J)*T(I+1,J)+AX(I,J)*T(I-1,J)
    1+(1.-AX(I,J)-CX(I,J))*T(I,J)+T(I,J)*AXIAL(I)
    DO 65 J=1,NJ
65  T(I-1,J)=W(J)
    DO 1004 J=1,NJ
    A(J)=AY(I,J)
1004  C(J)=CY(I,J)
    CALL ROACHE (A,C,D,NJ,E,F,W,LJ1,LJM,
    1AJ1(1),AJM,OJ1,OJM)
70  CONTINUE
C PICK BOTTOM BOUNDARY CONDITION
DO 75 J=1,NJ
    IF(J-L4F)73,73,72
72  IF(J-L3D)74,73,73
73  D(J)=(1.-2.*CX(NI,J))*T(NI,J)+2*AX(NI,J)*T(NI-1,J)
    1 +T(NI,J)*AXIAL(NI)
    GO TO 75

```

```
74      D(J)=AI4
75      CONTINUE
      DO 69 J=1,NJ
69      T(NI-1,J)=W(J)
      DO 1005 J=1,NJ
      A(J)=AY(NI,J)
1005    C(J)=CY(NI,J)
      CALL 20ACHE (A,C,D,NJ,E,F,W,LJ1,LJM,
1AJ1(NI),AJM,OJ1,OJM)
      DO 73 J=1,NJ
78      T(NI,J)=W(J)
      RETURN
      END
```

```

SUBROUTINE ROACHE (A,C,D,M,F,F,W,L1,LM,A1,AM,
1 Q1,QM)
DIMENSION A(M),C(M),D(M),E(M),F(M),W(M)
IF (L1-2) 1,2,3
1 E(1)=0
F(1)=A1
GO TO 4
2 E(1)=1.
F(1)=-A1
GO TO 4
3 E(1)=A1/(A1-1.)
F(1)=Q1/(1.-A1)
4 MM=MD-1
DO 5 M=2,MM
DEN=1.+A(M)+C(M)-A(M)*E(M-1)
E(M)=C(M)/DEN
5 F(M)=(D(M)+A(M)*F(M-1))/DEN
IF (LM-2) 6,7,8
6 W(M)=A1
GO TO 9
7 W(M)=(F(M)+AM)/(1.-E(M))
GO TO 9
8 W(M)=(F(M)+QM/AM)/((1.+AM)/AM-E(M))
DO 10 MK=1,MM
M=MD-MK
10 W(M)=E(M)*W(M+1)+F(M)
RETURN
END

```

```

SUBROUTINE OUTPUT
  DIMENSION TE(6,20),TC(6,30),AYE(6,30),AYF(6,30),AXC(6,30)
  1,AYG(6,30),CXF(6,30),CYF(6,30),AXCON(6)
  COMMON ET,TS,WIS,TF,TV,TC,TP,QIR,QP,QEV,QCR,QMAX,NIE,NJE,NIC,NJC
  1,LWFE,LWFC,LBO,LNA,CXE,CYE,CXC,CYC,CV,V,TL,EL,ASU,BSU,XL,CC,ICRIT
  1,AXE,AYE,AXC,AYC,AV,RV,AS,BS,AC,BC,CIE,CTC,AIE,AIC
  1,MDOF,RMASS,DT,DTO,IX,KF,P,C,DXC,DYC,CL,NJA,CRESIST
  1,WT,DF,RF,NL,BETA,POPSY
  REAL NL,KL,MDOF,KF,HFG,KW
  WRITE(3,5)
  WRITE(3,10) ET
  WRITE(3,30)
  DO 1 I=1,NIE
1  WRITE(3,40) (TE(I,J),J=1,NJE)
  WRITE(3,50) TV,QEV,QMAX
  WRITE(3,60)
  DO 2 I=1,NIC
  N=NIC-I+1
2  WRITE(3,70) (TC(N,J),J=1,NJC)
  WRITE(3,80) TP,QCR,QP
5  FORMAT()
10  FORMAT(1X,"ELAPSED TIME",F8.3,1X,"SECONDS")
30  FORMAT(5X,"EVAPORATOR GRID")
40  FORMAT(30F8.3)
50  FORMAT(5X,"VAPOR TEMPERATURE",F8.3,3X,"HEAT IN",F8.3,3X,
1  "QMAX",F8.3,3X,"WATTS")

60  FORMAT(5X,"CONDENSER GRID")
70  FORMAT(10F8.3)
80  FORMAT(5X,"HEAT SINK TEMPERATURE",F8.3,1X,"HEAT IN",F8.3,
11X,"HEAT OUT",F8.3,1X,"WATTS")
  RETURN
  END

```



```

SUBROUTINE DATAIN
  DIMENSION TE(6,30),TC(6,30),T(6,30),D(30),E(30),F(30),W(30)
  1,ATE(6),ATC(6),AJ1(6),AXE(6,30),AYE(6,30),AXC(6,30),AYC(6,30)
  1,A(30),CXF(6,30),CYE(6,30),CXC(6,30),CYC(6,30),AXCON(6),RSI2(6)
  COMMON ET,TS,QIS,TE,TV,TC,TP,QIR,QR,QFV,QCR,GMAX,NIE,NJE,NIC,NJC
  1,LWFE,LWFC,LRO,LNA,CXE,CYE,CXC,CYC,CV,V,TL,EL,ASU,BSU,XL,CG,ICRIT
  1,AXE,AYE,AXC,AYC,AV,RV,AS,BS,AC,BC,CIF,CIC,AIF,AIC
  1,MDOI,RMASS,DT,OTO,IX,KF,R,C,DXC,DYC,CL,NJA,CRESIST
  1,WT,DF,PF,NL,BETA,PORSTY
  REAL NL,KL,MDOI,KF,HFG,KW
  READ(2,50)NIE,NJE,NIC,NJC,NJA
  READ(2,75)LWFE,LRO,LWFC,LNA,ICRIT
  READ(2,80)WT,DF,PF,NL,BETA,PORSTY
  READ(2,100)TS,QSE
  DO 10 I=1,NIE
10  READ(2,200) (TE(I,J),J=1,NJE)
    READ(2,300) TV,V,XL
    DO 20 I=1,NIC
20  READ (2,400) (TC(I,J),J=1,NJC)
    READ(2,500) TP,QCR,QR
50  FORMAT(5I3)
75  FORMAT(5I4)
80  FORMAT(3E10.5,F6.2,2E10.5)
100 FORMAT(2F8.3)
200 FORMAT(15F3.3)
300 FORMAT(F8.3,2F16.5)
400 FORMAT(16F8.3)
500 FORMAT(3F8.3)
  RETURN
  END

```

```

SUBROUTINE DATAOUT
  DIMENSION TE(6,30),TC(6,30),T(6,30),D(30),F(30),F(30),W(30)
  1,ATF(6),ATC(6),AJ1(6),AXF(6,30),AYE(6,30),AXC(6,30),AYC(6,30)
  1,A(30),CXE(6,30),CYE(6,30),CXG(6,30),CYG(6,30),AXCON(6),RSI2(6)
  COMMON ET,TS,DIS,TE,TV,TC,TP,DIR,DR,DFV,OCR,GMAX,NIE,NJE,NIC,NJC
  1,LWFE,LWFC,LPO,LNA,CXF,CYE,CXC,CYC,CV,V,TL,EL,ASU,BSU,XL,CC,ICRIT
  1,AXF,AYE,AXG,AYG,AV,BV,AS,BS,AC,BC,CIE,CIC,AIF,AIC
  1,MDOI,RADS,DI,OTO,IX,KF,R,C,DXC,DYC,CL,NJA,CRESIST
  1,WT,DF,PF,NL,BETA,PORSTY
  REAL IL,KL,MDOI,KF,HFG,KW
  WRITE(2,50)NIE,NJE,NIC,NJC,NJA
  WRITE(2,75)LWFE,LPO,LWFC,LNA,ICRIT
  WRITE(2,80)WT,DF,PF,NL,BETA,PORSTY
  WRITE(2,100)TS,DSE
  DO 10 I=1,NIE
10  WRITE(2,200) (TE(I,J),J=1,NJE)
    WRITE(2,300) TV,V,XL
    DO 20 I=1,NIC
20  WRITE(2,400) (TC(I,J),J=1,NJC)
    WRITE(2,500) TR,OCR,QR
50  FORMAT(5I4)
75  FORMAT(5I8)
80  FORMAT(3E10.5,F6.2,2E10.5)
100 FORMAT(2F8.3)
200 FORMAT(15F8.3)
300 FORMAT(98.3,2E16.5)
400 FORMAT(16F8.3)
500 FORMAT(3F8.3)
  RETURN
  END

```

APPENDIX E

DISCUSSION OF STABILITY AND ACCURACY
OF NUMERICAL TECHNIQUES

The technique used for solution of the vapor temperature is essentially a one dimensional heat balance of the form:

$$T_i^{n+1} = A_i T_{i+1}^n + B_i T_{i-1}^n + (1-A_i+B_i) T_i^n$$

For stability it is necessary that [16,17,18]

$$(A_i + B_i) \leq 1$$

All elements of A and B are fixed except the time step.

Thus the time step must be adjusted to maintain stability.

In solving for the vapor temperature the coefficients A and B are calculated. New values are then defined by

$$A_i' = \frac{A_i}{(A_i+B_i)}$$

$$B_i' = \frac{B_i}{(A_i+B_i)}$$

The solution is then iterated $(A + B)$ times to complete one time step.

The alternating direction implicit method used in this study has an accuracy of $O(\Delta t^2, \Delta x^2, \Delta y^2)$ [16].

According to a von Neumann stability analysis the method is unconditionally stable [16,18]. However in practice this method, although it does permit larger time steps than standard explicit method, will become unstable if time steps used are too large.

APPENDIX F

CALCULATION OF THERMAL CONDUCTIVITY FOR THE WICK

Since the wick is a composite of screen and fluid gaps, a method must be developed for estimating its thermal conductivity.

The thermal conductivity of the fluid gaps is given by the polynomial expression given in Appendix B.

The thermal conductivity of the screen was calculated using the method of Williams [24].

$$\begin{aligned}
 K_s = K_\ell & \frac{1}{\frac{d_f}{2r_f} \left[2 \frac{K_\ell}{K_p} + \frac{d_f}{2r_f} - 2 \right]} \\
 & + \frac{2}{\frac{d_f}{2r_f} \left(\frac{K_\ell}{K_p} \right) \left[\frac{d_f}{2r_f} + 1 \right]} \\
 & + \frac{1}{\left[\frac{d_f}{2r_f} + 1 \right]^2}
 \end{aligned}$$

The overall thermal conductivity is then a weighted average of the values for the screen and fluid. Weighting factors are given by

$$\% \text{ screen} = \sum_{N=1}^{NL} \ln[(r_B - (4r_f + \beta)(N-1)) / (r_B - 4Nr_f - (N-1)\beta)]$$

$$\% \text{ fluid} = \sum_{N=1}^{NL-1} \ln [(r_B - 4Nr_f - (N-1)\beta) / (r_B - (4r_f + \beta)N)]$$

Total thermal conductivity is calculated to be

$$K_w = K_s (\% \text{ screen}) + K_\ell (\% \text{ fluid})$$

APPENDIX G

ANALOG SCALING

Due to the nature of the analog computer equations must be scaled before they can be solved. This scaling is accomplished by making a change of variable. Each variable in the unscaled equation is non-dimensionalized by some maximum value. For example the unscaled form of equation 4.1 is:

$$\frac{dT_1}{dt} = \frac{4\pi\ell_E K_p}{\rho_p c_p v_{pE} \ln(r_O/r_B)} (T_2 - T_1) + \frac{2Q_E}{\rho_p c_p v_{pE}}$$

Make the following changes of variable:

$$T^* = \frac{T - T_{\min}}{T_{\max} - T_{\min}}$$

$$Q_E^* = \frac{Q_E}{Q_{\max}}$$

$$t^* = \frac{t}{t_{\max}}$$

gives

$$\frac{(T_{\max} - T_{\min})}{t_{\max}} \frac{dT_1^*}{dt^*} = \frac{4\pi \ell_E K_p (T_{\max} - T_{\min})}{\rho_p c_p v_{pE} \ln(r_O/r_B)} (T_2^* - T_1^*)$$

$$+ \frac{2Q_E^* Q_{\max}}{\rho_p c_p v_{pE}}$$

which can be simplified to:

$$\frac{dT_1^*}{dt^*} = \frac{4\pi \ell_E K_p t_{\max}}{\rho_p c_p v_{pE} \ln(r_O/r_B)} (T_2^* - T_1^*)$$

$$+ \frac{2 Q_{\max} t_{\max}}{\rho_p c_p v_{pE} (T_{\max} - T_{\min})} Q_E^*$$

Similar scaling for each equation gives a new system of equations that differs from the first in only the time scaling term.

APPENDIX H

DERIVATION OF EXPONENTIAL MODEL

Assume entire system approximated as lumped mass with composite specific heat. Then

$$m_T c_T \frac{dT}{dt} = Q_{IN} + \dot{m}_f c_f (T_I - T)$$

Define $T^* = (T - T_I)$. Equation becomes

$$m_T c_T \frac{dT^*}{dt} = Q_{IN} - \dot{m}_f c_f T^*$$

This first order differential equation can be solved to give

$$T^* = \frac{Q_{IN}}{\dot{m}_f c_f} \left(1 - e^{-\frac{\dot{m}_f c_f}{m_T c_T} t} \right)$$

and

$$Q_{OUT} = \dot{m}_f c_f T^*$$

REFERENCES

1. Cotter, T. P., "Theory of Heat Pipes," Los Alamos Scientific Laboratory, Report LA-3246-MS, 1965.
2. Chisholm, D., The Heat Pipe, Mills and Boon Limited, London, 1971.
3. Cotter, T. P., "Heat Pipe Start-up Dynamics," presented 1967, Thermionic Conversion Specialist Conference, October 30, 1967, Palo Alto, California.
4. Williams, C. L., and G. T. Colwell, "Heat Pipe Model Accounting for Variable Evaporator and Condenser Lengths," AIAA Journal, Vol. 12, no. 9, pp. 1261-1267, September, 1974.
5. Chato, J. C., and J. H. Streckert, "Performance of a Wick-Limited Heat Pipe," ASME Publication 69-HT-20, 1969.
6. Kirkpatrick, J. P., and P. J. Brennan, "The Advanced Thermal Control Flight Experiment," presented at the AIAA 8th Thermophysics Conference, Palm Springs, California, July 16-18, 1973.
7. Sherman, A., and P. Brennan, "Cryogenic and Low Temperature Heat Pipe/Cooler Studies for Spacecraft Application," presented at the AIAA-ASME 1974 Thermophysics and Heat Transfer Conference, Boston, Massachusetts, July 15-17, 1974.
8. Hare, J. D., Performance of a Nitrogen Heat Pipe with Various Capillary Structures, M. S. Thesis, Georgia Institute of Technology, 1975.
9. Colwell, G. T., "Prediction of Cryogenic Heat Pipe Performance," Report no. 2, NASA contract NSG-2054, February, 1976.
10. Groll, M., Bost, H. Kreeb, Schubert, F. Zimmermann, "Heat Transfer Limits, Lifetests, and Dynamic Behavior of Heat Pipes," Institut für Kernenergetik, Universität Stuttgart, Germany.

11. Smirnov, F., V. V. Barsookov, and L. N. Mishchenko, "Engineering Methods of Low-Temperature Heat Pipe Designing Calculations," presented at the 2nd International Heat Pipe Conference, Bologna, Italy, March 21-April 2, 1976.
12. Rice, G., and E. Azad, "Dynamic Characteristics of Heat Pipes," presented at the 2nd International Heat Pipe Conference, Bologna, Italy, March 31-April 2, 1976.
13. Anand, D. K., A. Z. Dybbs, and R. E. Jenkins, "Effect of Condenser Parameters on Heat Pipe Optimization," Journal of Spacecraft, Vol. 4, No. 5, pp. 695-696, May, 1967.
14. Calimbas, and Hulett, "An Avionic Heat Pipe," ASME publication 69-HT-16, 1969.
15. Cosgrove, J. H., A. Ferrel, and A. Carnesale, "Operating Characteristics of Capillary-Limited Heat Pipes," Journal of Nuclear Energy, 1967, Vol. 21, pp. 547-558.
16. Roache, Patrick J., Computational Fluid Dynamics, Hermosa Publishers, Albuquerque, N. M., 1972.
17. Clausing, A. M., "Numerical Methods in Heat Transfer," Advanced Heat Transfer, Ed. by B. T. Chao, University of Illinois Press, Chicago, 1969.
18. Carnahan, B., H. A. Luther, and J. O. Wilkes, Applied Numerical Methods, Wiley, New York, 1957.
19. Eckert, E. R. G., and R. M. Drake, Jr., Analysis of Heat and Mass Transfer, McGraw-Hill, New York, 1972.
20. Kreith, F., Principles of Heat Transfer, Second Edition, International Textbook Co., Scranton, PA, 1966.
21. Larkin, B. K., "Some Stable Explicit Approximations to the Diffusion Equation," Mathematics of Computation, 18, 196-202, 1964.
22. Schwartz, Anthony M., "Capillarity, Theory and Practice," Industrial and Engineering Chemistry, Vol. 61, No. 1, pp. 10-21, January, 1969.
23. Scott, Russel B., Cryogenic Engineering, D. Van Nostrand Co., Inc., Princeton, N.J., 1959.

24. Williams, C. L., Correlation of Heat Pipe Parameters, Ph.D. Dissertation, Georgia Institute of Technology, 1973.
25. National Bureau of Standards, Tech. Note 648, pp. 31-32, December, 1973.
26. Saaski, E. W., "Heat Pipe Temperature Control Utilizing a Soluble Gas Absorption Reservoir," NASA CR-137, 792, February, 1976.
27. Symons, E. P., "Wicking of Liquids in Screens," NASA TN-D 7657, May, 1974.
28. Priester, D. E., "Transient Response of A Cryogenic Heat Pipe", M.S. Thesis, Georgia Institute of Technology, 1976.

PROJECT ADMINISTRATION DATA SHEET



ORIGINAL



REVISION NO. _____

Project No. E-25-650DATE 11/25/81Project Director: Dr. S. V. Shelton *Wright*School/~~EES~~ Mechanical Eng.Sponsor: Gas Research InstituteType Agreement: Contract No. 5081-341-0503Award Period: From 6/1/81 To 9/30/82 (Performance) 12/31/82 (Reports)Sponsor Amount: \$49,283 Contracted through:Cost Sharing: N/A GTRI/~~GPR~~Title: Natural Gas Heat Pump Field Demonstration

ADMINISTRATIVE DATA

OCA Contact Faith G. Costello

1) Sponsor Technical Contact:

Mr. Leslie R. WrightManager, Gas Fired Heat PumpsGas Research Institute8600 West Bryn Mawr Ave.Chicago, IL 60631

2) Sponsor Admin/Contractual Matters:

Mr. F. R. Hayden, DirectorContract AdministrationGas Research Institute860 West Bryn Mawr Ave.Chicago, IL 60631Defense Priority Rating: N/ASecurity Classification: N/A (See below*)

RESTRICTIONS

See Attached Contract Supplemental Information Sheet for Additional Requirements.

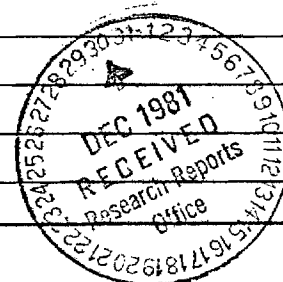
Travel: Foreign travel must have prior approval — Contact OCA in each case. Domestic travel requires sponsor approval where total will exceed greater of \$500 or 125% of approved proposal budget category.

Equipment: Title vests with Sponsor. Includes, without limitation, material, equipment, structures, and test apparatus.

COMMENTS:

*No publicity releases shall be issued without prior written approval from GRI

COPIES TO:

Administrative Coordinator
Research Property Management
Accounting
Procurement/EES Supply ServicesResearch Security Services
~~Reports Coordinator (OGA)~~
Legal Services (OCA)
LibraryEES Public Relations (2)
Computer Input
Project File
Other _____

SPONSORED PROJECT TERMINATION/CLOSEOUT SHEETDate October 31, 1983Project No. E-25-650School/Lab ME
~~XXXX~~Includes Subproject No.(s) N/AProject Director(s) Dr. S. V. Shelton GTRI / ~~XXXX~~Sponsor Gas Research InstituteTitle Natural Gas Heat Pump Field DemonstrationEffective Completion Date: 9/30/82 (Performance) 12/31/82 (Reports)

Grant/Contract Closeout Actions Remaining:

- ☐ None
- ☒ Final Invoice or Final Fiscal Report
- ☒ Closing Documents
- ☒ Final Report of Inventions
- ☒ Govt. Property Inventory & Related Certificate
- ☐ Classified Material Certificate
- ☐ Other _____

Continues Project No. E-25-627

Continued by Project No. _____

COPIES TO:

Project Director
Research Administrative Network
Research Property Management
Accounting
Procurement/EES Supply Services
Research Security Services
Reports Coordinator (OCA)
Legal Services

Library
GTRI
Research Communications (2)
Project File
Other Ina Newton

Georgia Institute of Technology

A UNIT OF THE UNIVERSITY SYSTEM OF GEORGIA

SCHOOL OF MECHANICAL ENGINEERING

ATLANTA, GEORGIA 30332

15 September 1982

Mr. John Shuster
Gas Research Institute
8500 West Bryn Mawr Avenue
Chicago, Illinois 60631

Subject: Monthly Report for May 82
"Natural Gas I.C. Engine Heat Pump Study"
Contract No. 5081-341-0503

Dear John:

During this report period the heating data analysis and correlation was completed. The effect of cycling was studied and is reported as follows.

Heating and cooling systems yield field performance which is lower than steady state performance due to cycle losses. The present water-to-water gas heat pump is turned on/off by space heating/cooling demand and domestic hot water demand. Due to the continuous logging of data during each cycle, the cycle "on" time and prior "off" time is known. Basic thermal analysis indicates that the cycle losses for a given system should be primarily dependent on two variables. One is the length of time the system has been off prior to starting up. If it has been off for several days, the entire system is at ambient temperature and heat will be required to bring the hardware up to operating temperature. This heat will be subtracted from the heat pump output and will not be available for useful heating thereby lowering efficiency. On the other hand, if the system has been off only five minutes, very little cooling of the hardware will have occurred and this hardware heat-up penalty will be small.

The second dominate independent variable is expected to be the time duration for which the heat pump runs; i.e., the cycle on time. If the system runs continuously for three hours, steady state performance will be approached and the hardware heat up time, and associated penalty, will be a small percentage of the total run time. The efficiency and heat output for the total three hour cycle will therefore closely approach the steady state values. On the other hand, if the unit comes on and runs only five minutes, more of the total cycle heat output will be used for hardware heatup and little will be available for useful heating.

Since the data logging system measures, calculates, and records on disc the performance of each individual cycle, a correlation study was made to determine the relationship between a given cycle's performance (heat output, gas consumption, and heating COP) and the two independent variables; 1) the given cycle on time, and 2) the off time prior to that particular cycle. Since the performance is expected to also be dependent on whether the particular cycle was to satisfy space heating or domestic water heating, the operating mode was used as a third independent variable.

Because of the complexity of the data a multiple linear regression (MLR) program was written to correlate the data. The MLR program assumes a linear relationship between independent and dependent variables.

The MLR program used an equation of the form:

$$X = A + B \cdot Y_1 + C \cdot Y_2 + D \cdot Y_3$$

where A, B, C, and D are constants determined by the computer. The variable Y_1 represents the cycle on time in minutes, Y_2 represents the prior time off, and Y_3 is equal to zero for a domestic hot water (DHW) cycle and equal to one for a space heating (SH) cycle. The coefficients B, C, and D show how much the independent variables Y_1 , Y_2 , and Y_3 respectively effect the dependent variable X.

The results of the MLR analysis were as follows:

For the gas heat rate:

$$\begin{aligned} A &= 62960.9 \text{ Btu/hr} \\ B &= -25.5 \text{ Btu/hr.min.} \\ C &= -3.7 \text{ Btu/hr.min.} \\ D &= -3211.5 \text{ Btu/hr} \end{aligned}$$

The coefficient of multiple correlation (CMC) was 0.265.

For the heating COP:

$$\begin{aligned} A &= 1.58 \\ B &= 2.11 \cdot 10^{-3} \text{ 1/min.} \\ C &= -3.65 \cdot 10^{-5} \text{ 1/min.} \\ D &= 0.08 \\ \text{with CMC} &= 0.272 \end{aligned}$$

For the total heating rate:

$$\begin{aligned} A &= 99478 \text{ Btu/hr} \\ B &= 105.4 \text{ Btu/hr min.} \\ C &= -7.5 \text{ Btu/hr min.} \\ D &= -176.0 \\ \text{with CMC} &= 0.249 \end{aligned}$$

Looking at the total heating rate as an example, we see the heat pump has a nominal heating capacity of 75,544.6 Btu/hr with a slightly increasing capacity with longer cycle on time, a very slight decrease in capacity with increasing previous off time, and a slight decrease in capacity if space heating rather than domestic hot water is the heat rejection mode.

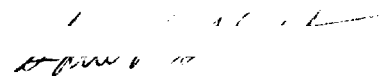
The coefficient of multiple correlation (CMC) is an indication of how well the data fits the linear relationship. Unfortunately the CMC for all cases is far below the maximum possible value of 1.0. The reason for the low coefficient is either the relationship is a function of another parameter or the relationship cannot be accurately modeled as linear. A more complex exponential relationship may correlate the data more closely.

The analysis also showed that the average cycle on time was 16 minutes and the average off time was 34 minutes. The average values were as follows:

	<u>Space Heating</u>	<u>Domestic Water Heating</u>
Gas Heat Rate	59,216 Btu/hr.	62,427 Btu/hr.
Total Heating	100,733 Btu/hr.	100,909 Btu/hr.
Heating COP	1.69	1.61

The results are as expected and all trends follow the theory. Space heating COP exceeds the domestic water heating performance due to the necessary higher condenser pressure required to heat the domestic water to 135°F.

Respectfully,


Sam V. Shelton
Associate Professor and
Principal Investigator

jv

Georgia Institute of Technology

A UNIT OF THE UNIVERSITY SYSTEM OF GEORGIA

SCHOOL OF MECHANICAL ENGINEERING

ATLANTA, GEORGIA 30332

15 September 1982

Mr. John Shuster
Gas Research Institute
8600 West Bryn Mawr Avenue
Chicago, Illinois 60631

Subject: Monthly Report for June 82
"Natural Gas I.C. Engine Heat Pump Study"
Contract No. 5081-341-0503

Dear John:

During the report period the transient and steady state performance of the gas heat pump was determined by use of the data system. Some modifications were required to obtain data with a time resolution of one minute.

The data acquisition system was completely calibrated and modified to increase the number of accumulating counters from one to three. This allows continuous monitoring of the gas flow rate and the two water loop flow rates. The heat pump's transient performance from cold start to steady state was evaluated by monitoring changes in water side temperatures and all flow rates as the heat pump started up from a 'cold' condition operating in the cooling mode. An energy balance was used to check the accuracy of the results.

Figure 1 shows the cooling capacity, (Q_c), the gas consumption, (Q_g), and the total heat rejection, (Q_H), as a function of time from cold start up. The steady state gas consumption is 66,000 Btu/hr. The increased gas consumption on start up is due to an increased oil viscosity at low engine temperature and an increased load on the engine due to higher initial compressor inlet refrigerant gas density. The sum of the steady state energy input to the system (gas plus evaporator input) is 118,000 Btu/hr, while the total heat output is 113,000 Btu/hr. This represents a small net heat loss of 4.2% for a gross 95.8% energy use. The drop in heating output from 15 minutes through 20 minutes can be explained by an intermittent drop in the water mass flow rate through the condenser due to air in the water loop. The transient response time of the system is on the order of 25 minutes.

Figure 2 separates the recovered engine heat from the condenser heating rate. The sum of the two heat rates gives the total heating output shown as Q_h in Figure 1. At steady state, approximately 40% of the total available heat output is recovered engine heat with 60% being condenser heat.

Figure 3 shows the heating and cooling COPs with respect to time. The steady state COP is 1.67 for heating and 0.79 for cooling. This is an increase from previously collected data using the less accurate Btu accumulating meters.

Respectfully,

/ . / . / /

Sam V. Shelton
Associate Professor and
Principal Investigator

jv

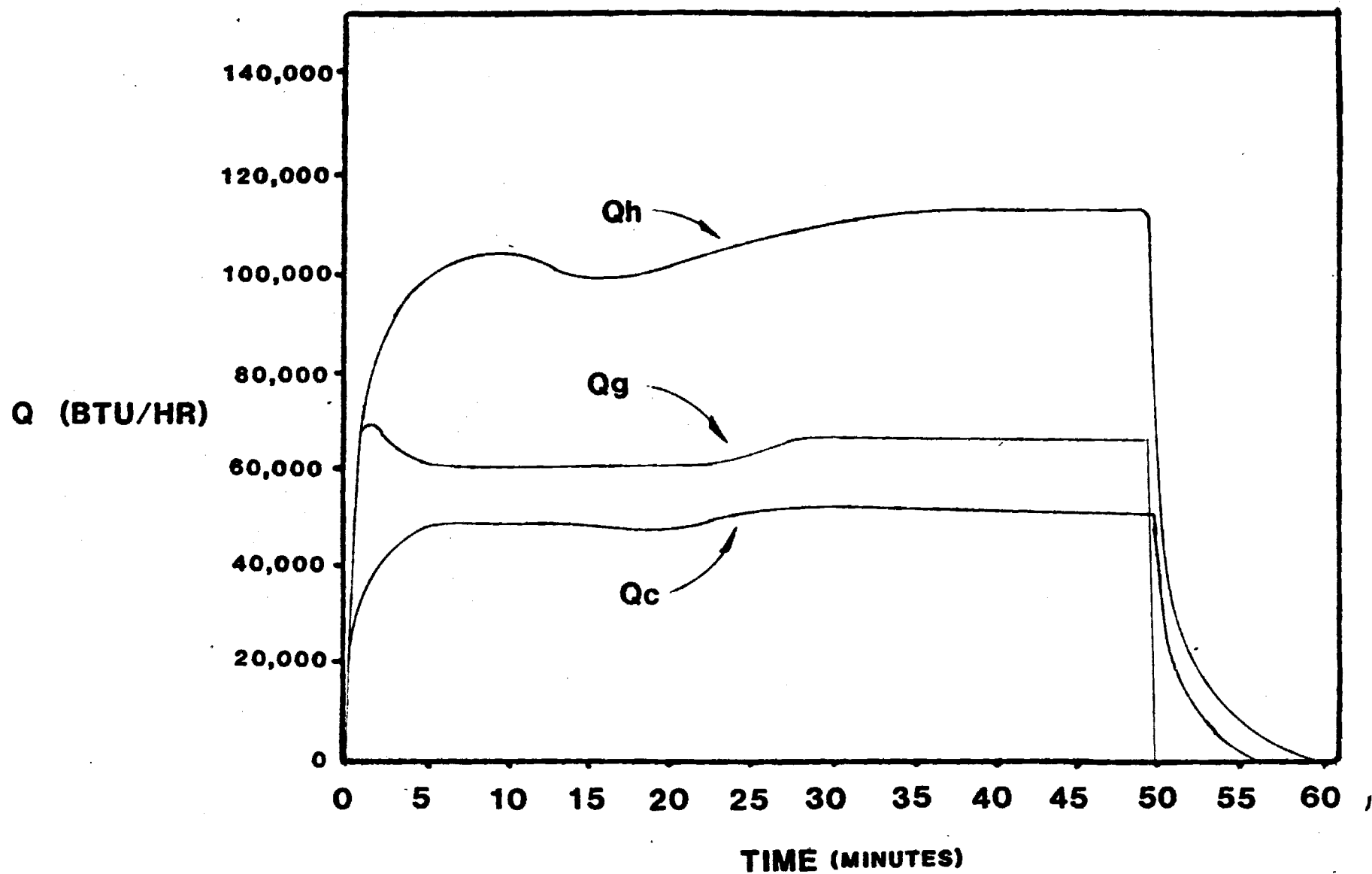


Fig.1 Heat flow vs. time

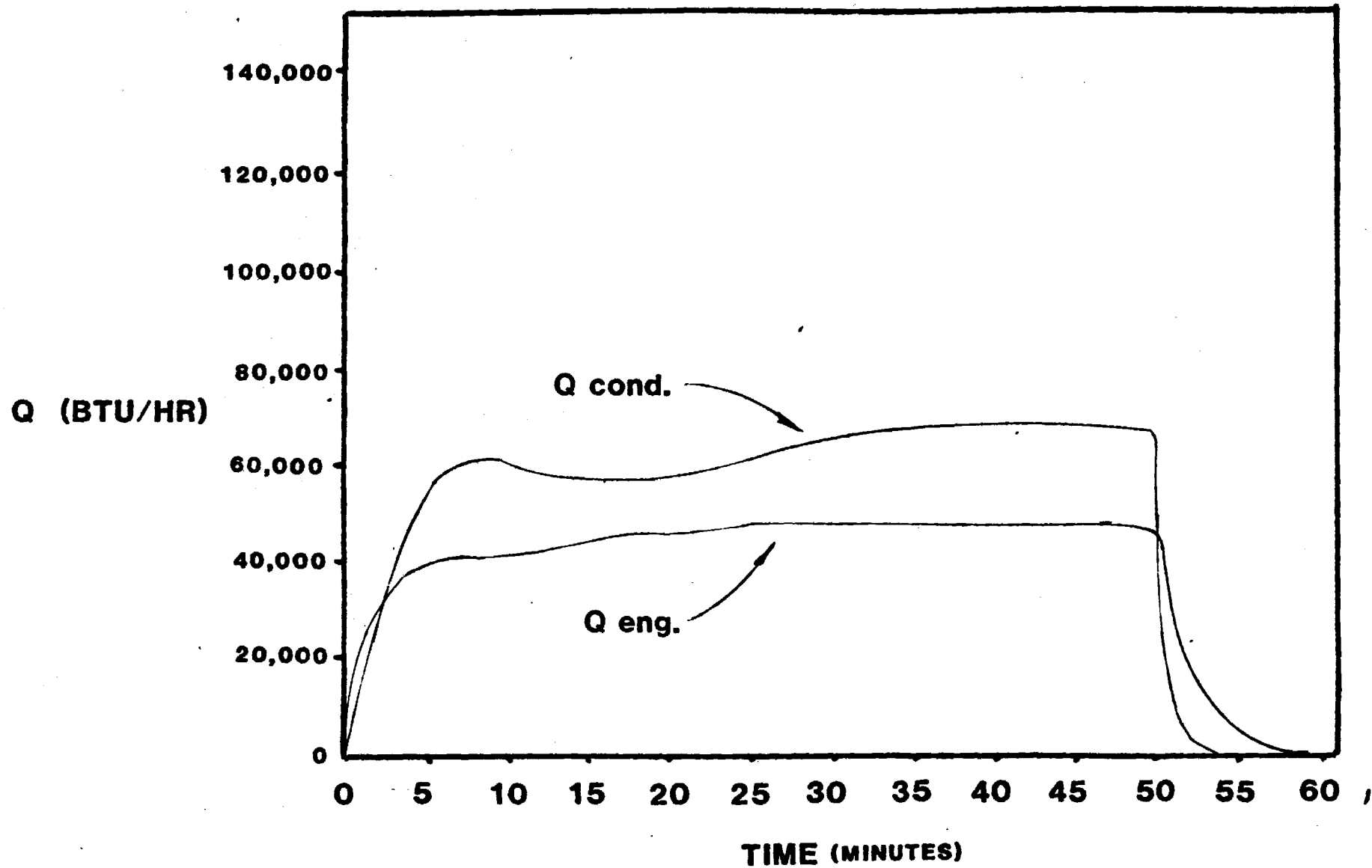


Fig. 2 Q engine and Q condenser vs. time

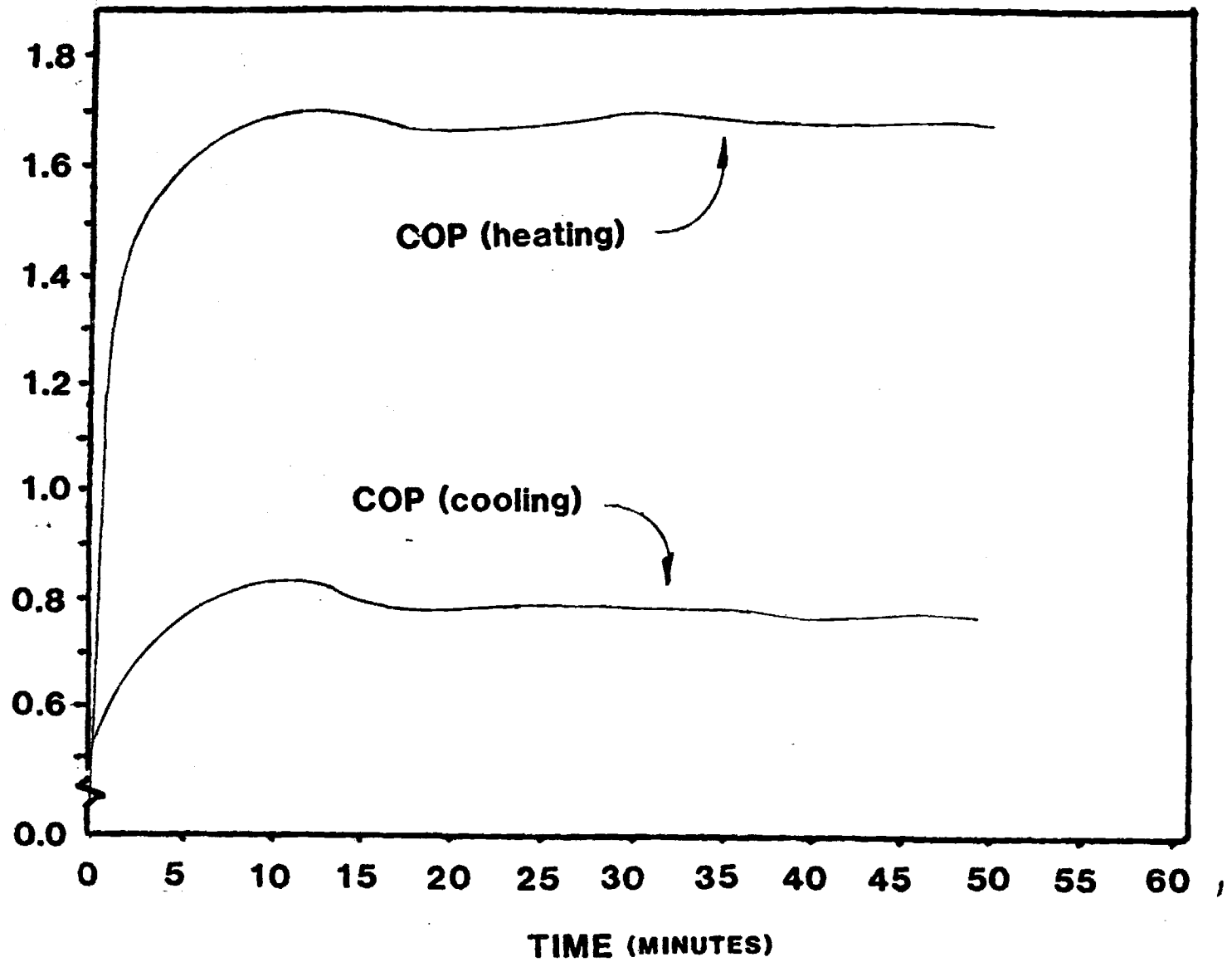


Fig. 3. COP vs. time

Georgia Institute of Technology

A UNIT OF THE UNIVERSITY SYSTEM OF GEORGIA

SCHOOL OF MECHANICAL ENGINEERING

ATLANTA, GEORGIA 30332

15 September 1982

Mr. John Shuster
Gas Research Institute
8600 West Bryn Mawr Avenue
Chicago, Illinois 60631

Subject: Monthly Report for July 82
"Natural Gas I.C. Engine Heat Pump Study"
Contract No. 5081-341-0503

Dear John:

During the month of July 82, no contract funds were expended. Less than \$2500 remain in the budget. However, the heat pump is continuing to be monitored with over 1500 hours having been accumulated. Also, an analytical design study is ongoing to determine the optimum sizing of condenser and evaporator air-to-refrigerant coils which need to be fitted to convert the present water-to-water heat pump to an air-to-air unit.

During July, the brief study was completed to calculate the order of magnitude of present day heat pump running hours. To this end, an air-to-air electric heat pump model coupled to a "typical" house model developed by NBS was used. The computer listing was obtained from the NBS publication NBSIR 80-2145 (DOE).

This NBS program assumes 68°F/78°F indoor Winter/Summer thermostat settings. For Chicago and Atlanta the following results were obtained for actual running hours.

	<u>Chicago</u>	<u>Atlanta</u>
Cooling hours	317 hours	520 hours
<u>Heating hours</u>	<u>2083 hours</u>	<u>778 hours</u>
total hours	2400 hours	1298 hours

These numbers would obviously differ depending on the heat pump capacity vs. house load. These results were obtained using the NBS assumptions without modifications. Their results for Atlanta agree amazingly well with the actual running hours measured in this project.

It is felt that a design goal of 2000 hours per year for ten years is a reasonable gas heat pump design goal. Greater than 2000 annual hours does not appear to be justified in light of present day thermostat settings and actual in-the-field sizing practice. Since house loads may only be estimated with the most elaborate computer programs to 20%, (differences in the large main frame programs are at least this), field estimates by less sophisticated methods are even more uncertain. Therefore, it would not appear that any contractor would risk not oversizing by at least 25%.

Regarding the method of sizing gas heat pumps, the trade off between heat pump capacity and heat pump life in years should be considered. If a gas heat pump has a 20,000 hour life, one may size it to a house load so that it has to run 3000 hours per year to meet the house load yielding a 6.7 year life; or the heat pump size may be doubled so that the running time is 1500 hours per year yielding a 13.3 year life.

Doubling the size of the heat pump will not double the cost, but means a replacement unit will be required only one-half as often. This economic effect will tend to drive gas heat pump sizing to larger units, independent of the corresponding higher efficiency resulting from the lower temperature balance point. The increased cycling losses may or may not be important. As reported last month, the cycling losses on the present unit appears to be very small (less than 3%). This is the result of the absence of flue losses and good insulation.

Work in the heat exchanger sizing will continue next month along with continued heat pump monitoring.

Respectfully,

Sam V. Shelton
Associate Professor and
Principal Investigator

jv

Georgia Institute of Technology

A UNIT OF THE UNIVERSITY SYSTEM OF GEORGIA

SCHOOL OF MECHANICAL ENGINEERING

ATLANTA, GEORGIA 30332

14 September 1982

Mr. John Shuster
Gas Research Institute
8600 West Bryn Mawr Avenue
Chicago, Illinois 60631

Subject: Monthly Report for August 82 "Natural Gas I.C.
Engine Heat Pump Study"
Contract No. 5081-341-0503

Dear John:

The work on modeling the performance of the heat pump after conversion to air-to-air has progressed during August with no dollar expenditures from the contracts. This modeling has been carried out as follows:

- 1) The performance of the present engine/compressor system with varying evaporator and condenser refrigerant temperatures was experimentally determined. This data made possible the determination of equations for the heating rate, cooling rate, gas use rate, and COP's as a function of only the condenser and evaporator refrigerant temperatures.
- 2) Air-to-refrigerant evaporator and condenser heat exchanger models were then developed with the size of each specified by inputting a "UA" value for each. Air flow rates and temperatures were also input.
- 3) By coupling of the engine/compressor performance model and air-to-refrigerant evaporator/condenser model, the complete system performance of the converted air-to-air heat pump package can be calculated.

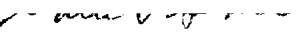
The results of one such calculation with both evaporator and condenser "UA" equal to 4000 BTU/hr°F and air flow rates of 2000 cfm are shown in the attached figure. The assumed indoor return air temperatures are 68°F and 76°F for heating and cooling respectively.

Monthly Report for August 82
Contract No. 5081-341-0503
Page 2 - 14 September 1982

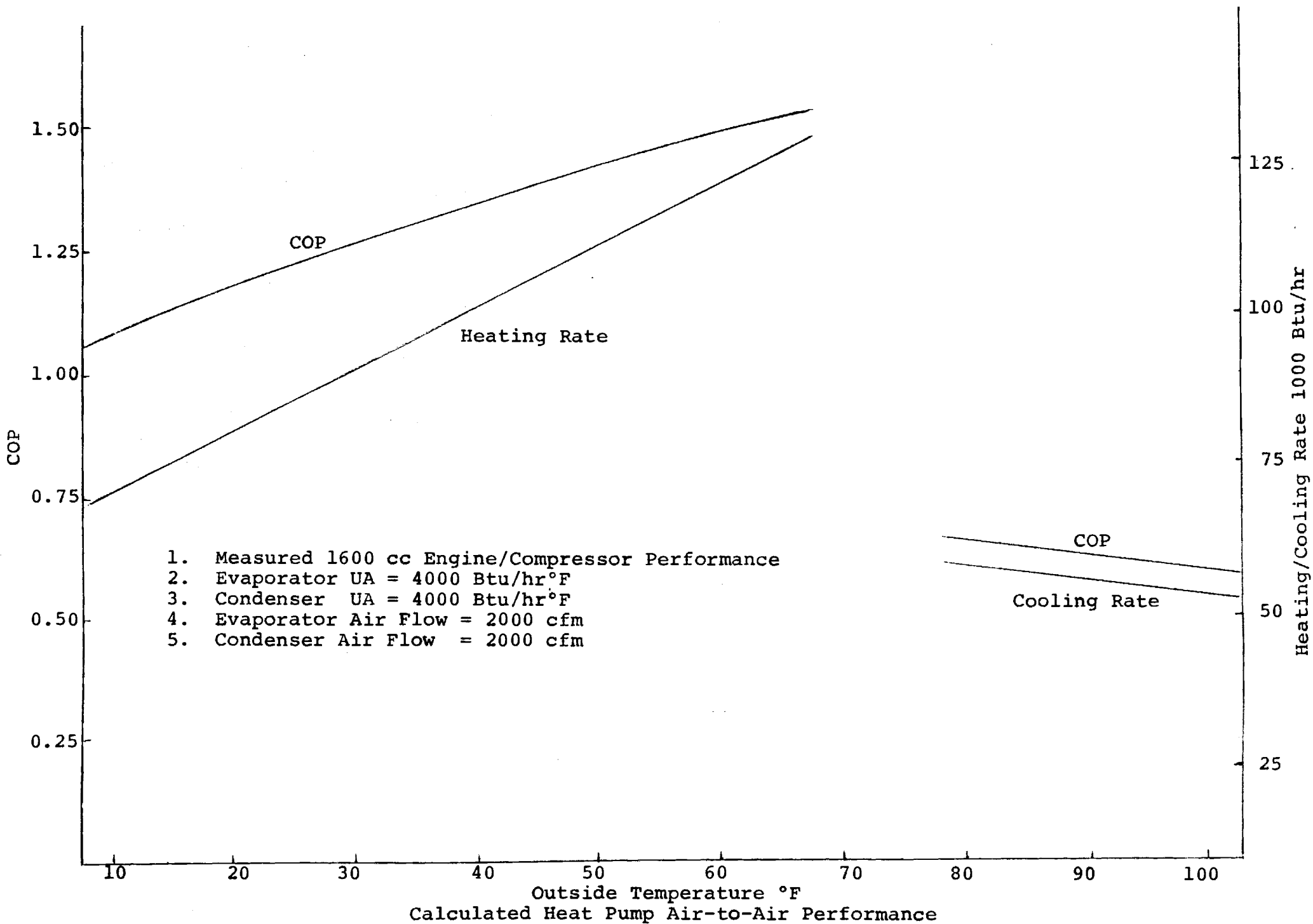
These results will be coupled with a house heating/cooling load model and weather data so that annual COP performance can be calculated. The evaporator and condenser "UA's" will be varied to determine the trade off between air evaporator and condenser heat exchanger sizes and annual gas consumption; i.e., capital investment in heat exchangers vs annual dollar gas savings.

The heat pump has presently accumulated over 1700 hours of operation. It still has received zero maintenance (excepting putting a crankcase cover plate on that was omitted by the manufacturer) with 100% reliability. Cooling SEER is over 0.7 and heating SEER over 1.6.

Respectfully,


Sam V. Shelton
Associate Professor and
Principal Investigator

jv



Calculated Heat Pump Air-to-Air Performance

FINAL REPORT – Draft
GRI Contract No. 5081-341-0503

NATURAL GAS I.C. ENGINE HEAT PUMP STUDY

Principal Investigator

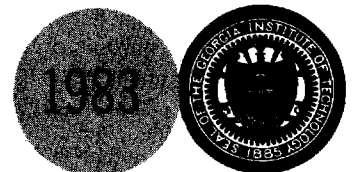
S. V. Shelton, Ph.D.

Prepared for

GAS RESEARCH INSTITUTE
8500 West Bryn Mawr Avenue
Chicago, Illinois 60631

April 1983

GEORGIA INSTITUTE OF TECHNOLOGY
A UNIT OF THE UNIVERSITY SYSTEM OF GEORGIA
SCHOOL OF MECHANICAL ENGINEERING
ATLANTA, GEORGIA 30332



NATURAL GAS I. C. ENGINE HEAT PUMP STUDY

DRAFT COPY
FINAL REPORT
(June 1981 - September 1982)

Prepared by
Sam V. Shelton, Ph.D.

School of Mechanical Engineering
Georgia Institute of Technology
Atlanta, Georgia 30332
Project No. E25-650

for
GAS RESEARCH INSTITUTE
Contract No. 5081-341-0503

GRI Project Manager
Les Wright
Gas Fired Heat Pumps

April 1983

GRI DISCLAIMER

LEGAL NOTICE This report was prepared by the Georgia Institute of Technology as an account of work sponsored by the Gas Research Institute (GRI). Neither GRI, members of GRI, nor any person acting on behalf of either:

- a. Makes any warranty or representation, express or implied, with respect to the accuracy, completeness, or usefulness of the information contained in this report, or that the use of any apparatus, method, or process disclosed in this report may not infringe privately owned rights; or
- b. Assumes any liability with respect to the use of, or for damages resulting from the use of, any information, apparatus, method, or process disclosed in this report.

Title	Natural Gas I.C. Engine Heat Pump Study
Contractor	Georgia Institute of Technology
Principal Investigator	S. V. Shelton, Ph.D.
Report Period	May 81 - October 82 Final Report
Objective	To experimentally assess the technical feasibility of natural gas I.C. engine heat pumps using presently developed technology
Technical Perspective	Space heating and cooling constitutes the major use of natural gas in the U.S. Increasing the efficiency of this process would therefore provide a dramatic impact on the industry. The second law of thermodynamics shows that a natural gas heat pump concept can offer the theoretical potential of improving this present gas heating and cooling technology by as much as a factor of 3. Many efforts to develop a gas heat pump have failed. The I.C. engine heat pump is one gas heat pump technology which uses existing component technology and therefore offers the possibility of early development of a commercially viable gas heat pump. This project carried out field tests on an I.C. engine heat pump providing heating and cooling to a residence over two heating and two cooling seasons to assess the development barriers.
Results	<p>Experimental data from a gas I.C. engine water-to-water heat pump showed steady state and seasonal heating coefficient's of performance (COP) of 1.4 to 1.5 with cooling COP's 0.5 to 0.6. These efficiencies were in spite of the low 16% efficiency of the 1600 cc four cylinder industrial engine due to being loaded only to about 25%.</p> <p>Using experimental engine/compressor data in conjunction with an air-to-air heat pump system configuration model, seasonal heating COP's of 1.33, 1.45, and 1.53 were predicted for Chicago, Atlanta, and Orlando respectively with cooling COP's being 0.73 in all three cities. Higher engine loading would improve all COP's.</p> <p>No maintenance was required over the 2400 hours of operation during two heating and two cooling seasons. Oil analysis showed the oil was fully serviceable. Reliability was 100% except for some failures to start during a fixed five second starter engagement period. Noise in the equipment room was 63 dB with 61 dB measured outside next to the exhaust outlet.</p>

The project has shown that automotive derivative gas industrial engines operating at low speed have the necessary efficiency, noise, maintenance, and short term reliability to serve as the prime mover for an I.C. engine heat pump. It is recommended that available small I.C. engines suitable for I.C. engine heat pumps be surveyed and selected models tested for long life characteristics. Also, it is recommended that an air-to-air system be field tested to verify performance and to study outside coil defrost control strategies.

Technical Approach

A West Germany manufactured water-to-water packaged gas heat pump was installed in an Atlanta residence supplying all space heating and cooling over two heating and two cooling seasons. Well water was used as a heat sink and source after which it was disposed into a creek. An inside water circulating loop carried either hot or chilled water produced by the heat pump through a water coil in the air handler. The hot water loop passed through the condenser, exhaust gas heat exchanger, and engine cooling jacket. The system was fully instrumented for both long term and transient data acquisition. Total accumulated heating and cooling energies were measured along with accumulated gas flow over entire seasons to calculate seasonal performance factors (seasonal COP's). Steady state and transient performance was measured by a microcomputer data acquisition system with a one minute time resolution. Performance of the engine/compressor subcomponent was also measured as a function of condenser and evaporator temperatures. A model was developed to use this engine/compressor data in conjunction with air condenser and evaporator coils. Optimization of the indoor vs. outdoor coil size was established. Also, performance with varying combined total air coil sizes was calculated for Chicago, Atlanta, and Orlando.

TABLE OF CONTENTS

	<u>Page</u>
RESEARCH SUMMARY	iii
LIST OF TABLES	vii
LIST OF FIGURES.	viii
Section	
I. INTRODUCTION	1
Background Fundamental Thermodynamics	
II. I.C. ENGINE HEAT PUMP SYSTEM DESIGN.	17
Description of Experimental System System Controls	
III. INSTRUMENTATION	27
Long Term Monitoring Computer Data Acquisition	
IV. EXPERIMENTAL PERFORMANCE	33
Introduction System Seasonal Performance Engine/Compressor Performance System Steady State Performance Variable Speed Performance Cycling Effects Reliability and Maintenance Noise Levels Electrical Accessory Power Performance Improvements	
V. AIR-TO-AIR I. C. ENGINE HEAT PUMP ANALYSIS	60
Introduction Analysis Input Parameter Consideration Performance Optimization Conclusions	

Section

Page

VI.	CONCLUSIONS AND RECOMMENDATIONS	77
-----	---	----

Introduction

Experimental Performance

Maintenance, Reliability and Noise

Analytical Air-to-Air Performance

Recommendations

LIST OF TABLES

Table		Page
1.	Florian Bauer GWW 35 Heat Pump Specifications . . .	18
2.	Experimental System Valve Positions and Pump Operation	23
3.	Long Term Performance Raw Data	35
4.	Steady-State Operating Conditions	44
5.	Averaged Experimental Data	45
6.	Confidence Intervals for Increase in Condenser Temperature	46
7.	Confidence Intervals for Increase in Evaporator Temperature	47
8.	Results of Multiple Variable, Linear Regression Analysis	48
9.	Steady State Performance	49
10.	Oil Analysis	55
11.	Optimum Coil UA Ratios	73
12.	Annual Heating and Cooling COP's at Optimum Performance	74

LIST OF ILLUSTRATIONS

Figure	Page
1. Energy Flow Diagram of a Heat-driven Heat Pump . .	6
2. Energy Flow Diagram of an Ideal Heat Engine-driven Heat Pump	8
3. Schematic and T-S Diagram of Actual Vapor-Compression Cycle	12
4. I.C. Engine Heat Pump Concept	16
5. Experimental System Schematic	22
6. Heat Pump System Controls	26
7. Computer Data Acquisition Schematic	32
8. Seasonal System Heating Performance	37
9. Seasonal System Cooling Performance	38
10. Heat Pump Energy Rates vs. Speed	51
11. Heat Pump Heating COP vs. Speed	51
12. Engine Efficiency vs. Load	59
13. Air-to-Air Heat Pump Model Diagram	61
14. Annual Gas Consumption versus Coil UA Ratio, Atlanta	68
15. Annual Gas Consumption versus Coil UA Ratio, Chicago	69
16. Annual Gas Consumption versus Coil UA Ratio, Orlando	70
17. Heating and Cooling COP's and Rates at Optimum Performance for Total Coil UA = 10000 Btu/hr-°F	71
18. Annual Gas Consumption at Optimum Performance . .	72

SECTION I

INTRODUCTION

Background

Thermal environmental control presently accounts for the greatest percentage of total energy use in the residential and commercial sectors of the U.S. In 1977, the energy required for heating and cooling of residential and commercial establishments alone represented 21% of the U.S. total energy consumption and two-thirds of the U.S. total natural gas consumption. Increasing the efficiency for space heating and cooling would therefore amount to a significant reduction in the nation's total energy use. From the second law of thermodynamics, the maximum efficiency possible for space heating and cooling is that obtained by the ideal (reversible) heat-driven heat pump which is over 3 times that of ideal natural gas furnaces and boilers. In practice, this ideal efficiency can be approached but never attained.

One of the more promising practical natural gas heat pump systems that has emerged in recent years is the natural gas, internal combustion (IC) engine-driven heat pump. This system offers an attractive efficiency (performance) for space heating, as compared with other heating systems such as the gas furnace, electric heat pump, and electric resistance heating. At the same time, it is capable of a space cooling performance

comparable to that of the electric heat pump (i.e., electric air conditioner).

In the U.S., I.C. engines serving as stationary prime movers were displaced in the 1930's and 1940's by electric drives made possible with the rural electrification program. Therefore, small [less than 2000 cc] I.C. engine technology in this country has moved toward high speed, short term, high specific power output to serve the automobile, portable drive, and emergency drive applications. Therefore, in this country, small I.C. engines are not viewed as being applicable to stationary, high running hours service.

In Europe, however, the use of small I.C. engines in stationary applications, while diminished, is still considered viable and a small market has been maintained. These are low speed, lightly (50%) loaded engines which are designed specifically for the stationary application, or are automobile engines modified for that service.

For this reason, when energy prices escalated in the mid 70's, Europe started looking seriously at the I.C. engine heat pump as a viable energy conservation concept.

In September 1978, a conference on "Drives for Heat Pumps" was held at the University of Essen, West Germany at which the choice of electric motors vs. combustion motors for heat pumps was the primary topic. In the forward of the conference proceedings, it states: "This issue of Drives for

Heat Pumps, as well as the conference in Essen, show that either means of drive has its justification and that there is ample room for both of them on the market." Eleven of the 17 papers presented were on I.C. engine drives for heat pumps. One paper was a survey of 14 I.C. engine heat pump systems installed and operating. Since then, several hundred operating units have been installed in the field and major corporations have started development projects.

In order to experimentally assess the potential problems and opportunity for I.C. engine driven heat pumps, a heating and cooling system for a single family residence was designed, built and tested around the Florian Bauer GWW 35 natural gas driven heat pump package manufactured in West Germany. This heat pump package has evolved over the past four years to a point where many of the packaging, noise, vibration and accessory problems have been resolved. Purchasing this package allowed this project to focus on the system concept rather than its peripheral problems. The objective was to experimentally identify the noise, vibration, reliability and maintenance problems of the I.C. engine gas heat pump concept and to quantify the field efficiency of this particular system. This will allow a more accurate assessment of the potential of the I.C. engine heat pump than has been previously possible.

Fundamental Thermodynamics

The heat pump is a device which operates in a thermodynamic cycle and requires energy input to pump heat from a low temperature reservoir (heat source) to a high temperature reservoir (heat sink). As a heating system, the heat pump extracts heat from the surroundings (such as outdoor air or ground water) and delivers it, along with the heat equivalent of the energy input, to a conditioned space. By extracting heat from the surroundings, the heat pump makes more energy available for heating than is required for input. This gives the heat pump its dramatic advantage over conventional, direct heating systems. As a cooling system, the heat pump removes heat from a conditioned space and rejects it, with the heat equivalent of the energy input, to the surroundings.

The first law efficiency of a thermodynamic system is defined as the ratio of energy sought to energy that costs. For heat pumps, this ratio is expressed as the coefficient of performance. The energy sought is either the heating effect or the cooling effect, and the energy that costs is the energy input. The coefficient of performance based on work energy input is given the notation

COPW, while COPH is used to denote the performance based on heat energy input. Subscripts H and C are used to indicate whether the energy sought is heating or cooling.

When energy is supplied to the heat pump in the form of heat, the result is a heat-driven heat pump. An energy flow diagram for the heat-driven heat pump is presented in Figure 1. As a result of heat input Q_S , at temperature T_S , a quantity of heat Q_C is removed from a reservoir at temperature T_C , and a quantity of heat Q_H is rejected to a reservoir at temperature T_H . From a simple energy balance on the system:

$$Q_S = Q_H - Q_C \quad (1)$$

and the coefficients of performance for heating and cooling are:

$$\text{COPH}_H = \frac{Q_H}{Q_S} = \frac{Q_H}{Q_H - Q_C} \quad (2)$$

$$\text{COPH}_C = \frac{Q_C}{Q_S} = \frac{Q_C}{Q_H - Q_C} = 1 - \text{COPH}_H$$

The maximum performance theoretically possible would be that achieved by a reversible heat-driven heat pump. From the second law of thermodynamics, the Clausius inequality requires that:

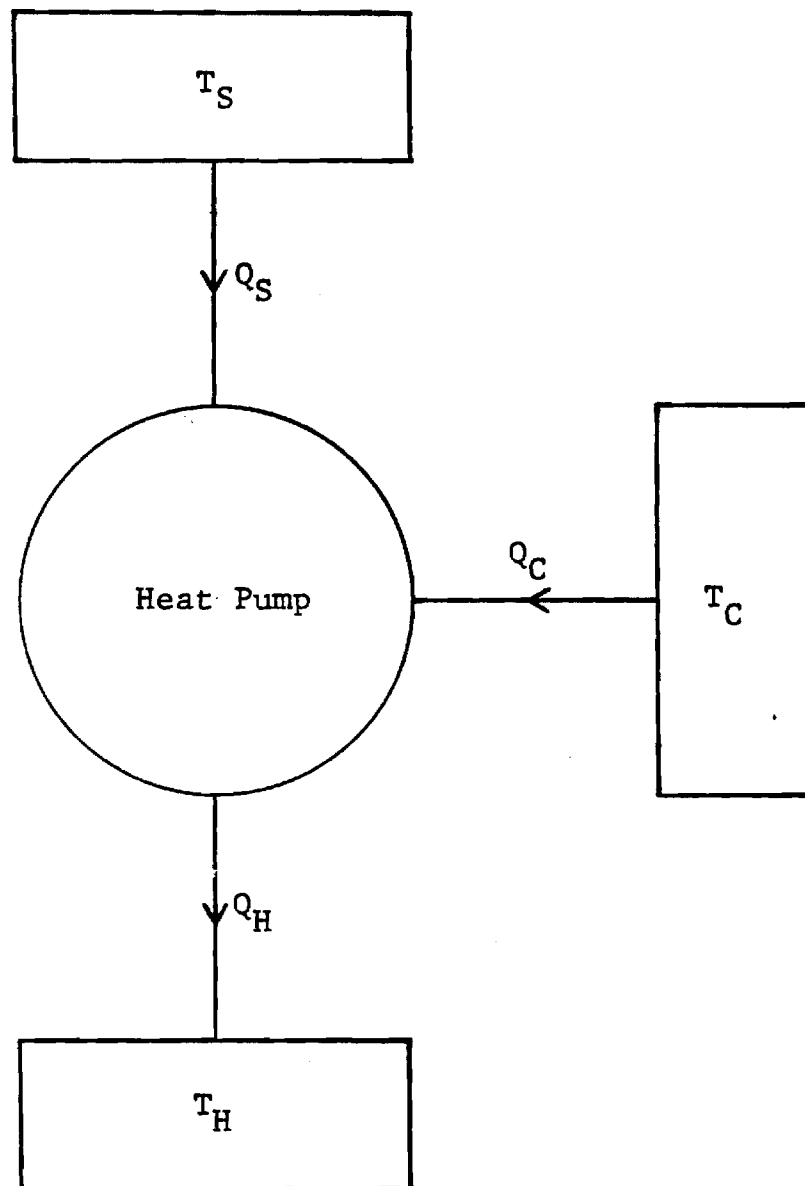


Figure 1. Energy Flow Diagram of a
Heat-Driven Heat Pump

$$\oint \frac{\delta Q}{T} \leq 0 \quad (3)$$

where the equality holds for reversible processes. Then for the reversible heat-driven heat pump:

$$\oint \frac{\delta Q}{T} = \frac{\delta Q_S}{T_S} + \frac{\delta Q_C}{T_C} - \frac{\delta Q_H}{T_H} = 0 \quad (4)$$

or

$$\frac{Q_S}{T_S} + \frac{Q_C}{T_C} = \frac{Q_H}{T_H} \quad (5)$$

Combining equations (2) and (5), and simplifying, yields:

$$(\text{COP}_{H_H})_{\text{rev.}} = \left(\frac{1 - T_C/T_S}{1 - T_C/T_H} \right) \quad (6)$$

$$\begin{aligned} (\text{COP}_{H_C})_{\text{rev.}} &= \left(\frac{T_C}{T_H} \right) \left(\frac{1 - T_C/T_S}{1 - T_C/T_H} \right) \\ &= 1 - (\text{COP}_{H_H})_{\text{rev.}} \end{aligned}$$

A system utilizing a Carnot cycle heat engine to drive a Carnot cycle heat pump would represent a reversible heat-driven heat pump. Such a system is shown in Figure 2. The heat engine operates between temperatures T_S and T_C to produce shaft work W_S . From an energy balance on the heat engine:

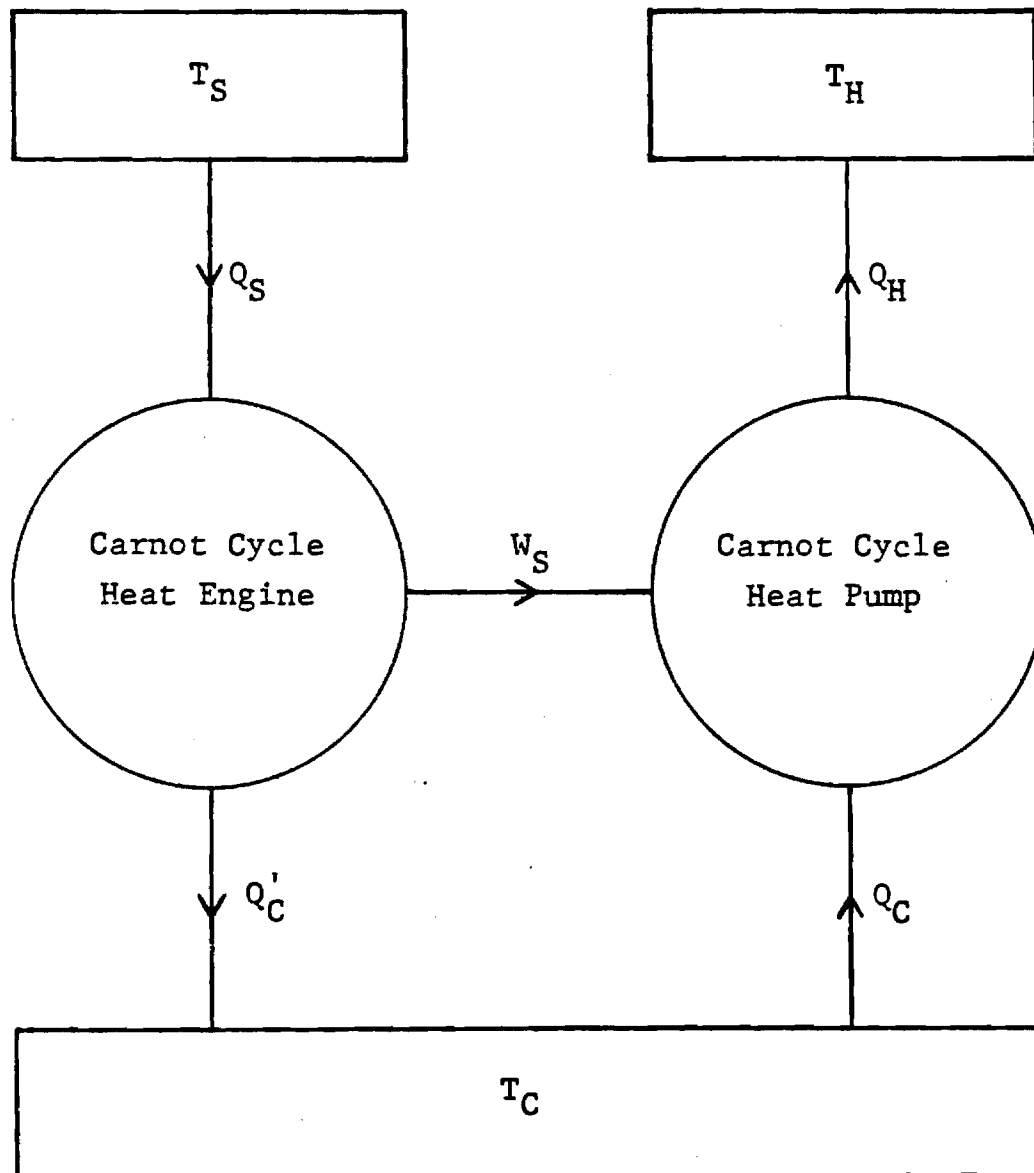


Figure 2. Energy Flow Diagram of an
Ideal Heat Engine-Driven Heat Pump

$$W_S = Q_S - Q_C' \quad (7)$$

and the engine efficiency is:

$$\eta = \frac{W_S}{Q_S} = \frac{Q_S - Q_C'}{Q_S} \quad (8)$$

Since all processes of the Carnot cycle heat engine are reversible, equation (3) yields:

$$\frac{Q_S}{T_S} = \frac{Q_C'}{T_C} \quad (9)$$

Equation (8) then simplifies to:

$$\eta_{\text{Carnot}} = 1 - \frac{T_C}{T_S} \quad (10)$$

The heat pump receives work input, W_S , from the heat engine to remove heat, Q_C , from the reservoir at T_C and reject heat, Q_H , to the reservoir at T_H . From an energy balance on the heat pump:

$$W_S + Q_C = Q_H \quad (11)$$

and the coefficients of performance are:

$$\text{COP}_{W_H} = \frac{Q_H}{W_S} = \frac{Q_H}{Q_H - Q_C} \quad (12)$$

$$\text{COPW}_C = \frac{Q_C}{W_S} = \frac{Q_C}{Q_H - Q_C}$$

Since the Carnot cycle heat pump can be represented thermodynamically as a Carnot cycle heat engine operating in reverse, and all processes of the Carnot cycle heat engine are reversible, all processes of the Carnot cycle heat pump must also be reversible. Then equation (3) yields:

$$\frac{Q_H}{T_H} = \frac{Q_C}{T_C} \quad (13)$$

and equations (12) simplify to:

$$(\text{COPW}_H)_{\text{Carnot}} = \frac{1}{1 - T_C/T_H} \quad (14)$$

$$(\text{COPW}_C)_{\text{Carnot}} = \frac{T_C/T_H}{1 - T_C/T_H}$$

$$= 1 - (\text{COPW}_H)_{\text{Carnot}}$$

The products of equations (10) and (14) yield the coefficients of performance for the combined system (i.e., the ideal heat engine-driven heat pump):

$$(\text{COPH}_H)_{\text{Ideal}} = (\eta)_{\text{Carnot}} (\text{COPW}_H)_{\text{Carnot}} \quad (15)$$

$$= \left(\frac{1 - T_C/T_S}{1 - T_C/T_H} \right)$$

$$\begin{aligned}
 (\text{COPH}_C)_{\text{Ideal}} &= (\eta)_{\text{Carnot}} (\text{COPW}_C)_{\text{Carnot}} \\
 &= \left(\frac{T_C}{T_H} \right) \left(\frac{1 - T_C/T_S}{1 - T_C/T_H} \right) = 1 - (\text{COPH}_H)_{\text{Ideal}}
 \end{aligned}$$

which are the same results obtained in equations (6).

Using typical temperatures for natural gas space heating/cooling, the ideal efficiencies for gas heat pumps may be calculated and compared with the ideal efficiencies of one for furnances and boilers. For heating, typical values of T_C , T_S , and T_H are 20°F, 1000°F, and 140°F resulting in a COPH_H of 3.7. For typical space cooling values of 50°F, 1000°F, and 120°F for T_C , T_S , and T_H respectively, COPH_C is 5.4. This demonstrates the potential of the concept.

In practice, the Carnot cycle heat engine and Carnot cycle heat pump cannot be achieved because they require that all processes be reversible. Actual processes involve irreversibilities, such as frictional losses and heat transfer through finite temperature differences. An actual cycle can, at best, only approach the Carnot cycle efficiency or performance for a given application.

For heat pumps, the Carnot cycle performance is best approached by the actual vapor-compression cycle, which is shown schematically and on a temperature-entropy (T-S) diagram in Figure 3.

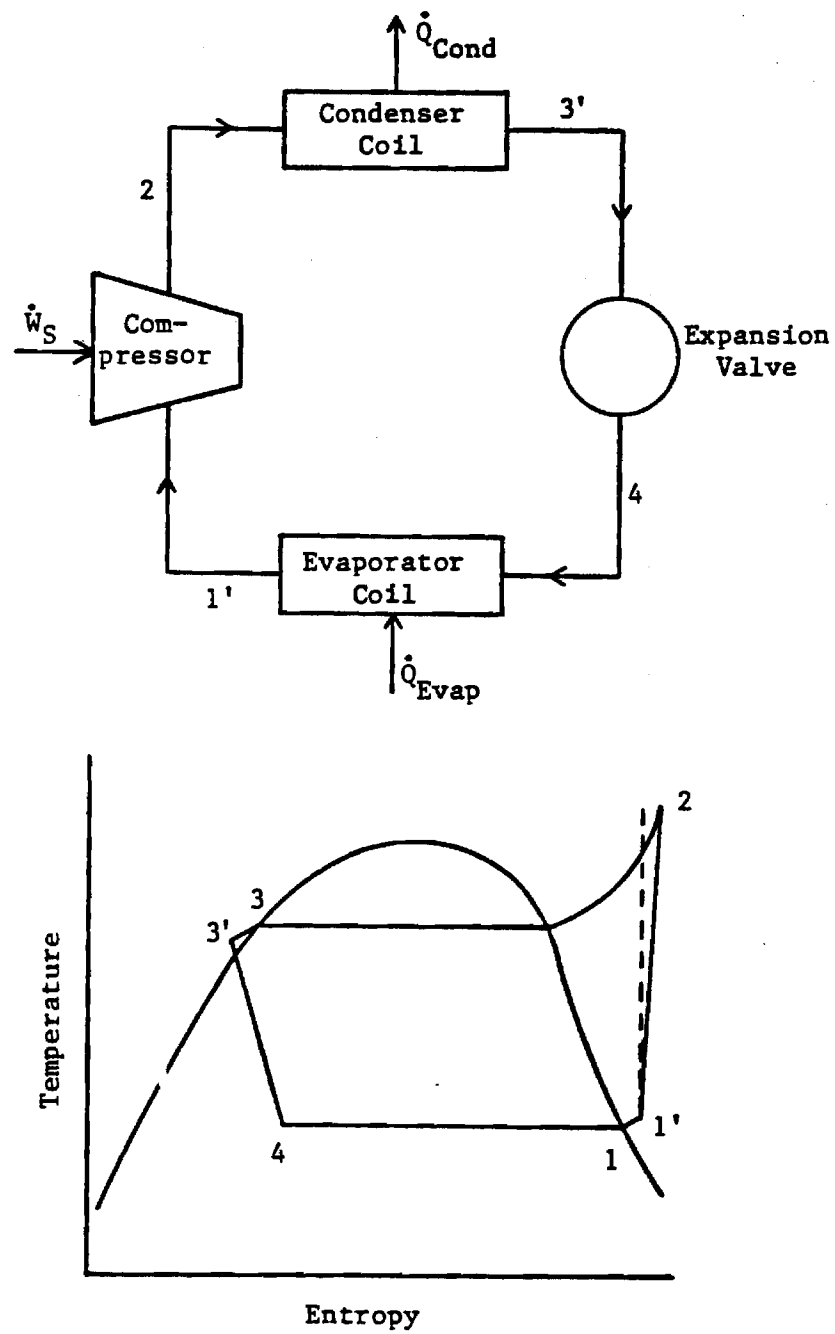


Figure 3. Schematic and T-S Diagram
of Actual Vapor-Compression Cycle

For the vapor-compression cycle heat pump, work is input to the compressor at a rate \dot{W}_S , heat is removed from a low temperature reservoir by the evaporator coil at a rate \dot{Q}_{Evap} , and heat is rejected to a high temperature reservoir from the condenser at a rate \dot{Q}_{Cond} . The heating and cooling coefficients of performance are then:

$$\text{COPW}_H = \frac{\dot{Q}_{\text{Cond}}}{\dot{W}_S} \quad (16)$$

$$\text{COPW}_C = \frac{\dot{Q}_{\text{Evap}}}{\dot{W}_S}$$

The natural gas-fired IC engine provides one means for approaching the efficiency of the Carnot cycle heat engine. In an IC engine, the working fluid operates on an open cycle. Fuel is mixed with air, and the resulting gas mixture is ignited in one of the combustion chambers of a spark ignition engine. The product gas (or exhaust gas) is then released from the chamber and rejected to the surroundings. In the combustion process, the chemical energy of the fuel is converted to thermal energy. Some of the thermal energy is then converted to mechanical

energy (shaft work) through the use of reciprocating pistons. The thermal energy that is not converted to shaft work is the engine rejected heat. A fraction of the engine rejected heat is dissipated through the engine block, while the remainder is carried away by the exhaust gas.

For the IC engine, the energy rate sought is the shaft work rate \dot{W}_S , and the energy rate that costs is the gas input rate \dot{Q}_{Gas} . The gas input rate is a product of the heating value of the fuel and the rate of fuel consumption. The heating value (frequently termed "energy of combustion" or "heat of reaction") is a measure of heat transfer from a constant volume chamber during combustion at constant temperature. The first law efficiency of the IC engine is then:

$$\eta_{Eng} = \frac{\dot{W}_S}{\dot{Q}_{Gas}} \quad (17)$$

It follows that the engine rejected heat rate is:

$$\dot{Q}_{Eng} = (1 - \eta_{Eng})\dot{Q}_{Gas} \quad (18)$$

When the IC engine is utilized strictly for performing work, the engine rejected heat is not useful and is commonly released to the surroundings. On the other hand, when the IC engine is used to drive a heat pump

for which heating is the energy sought, the engine rejected heat is useful if it can be recovered. Therefore, a major advantage of the IC engine-driven heat pump is its potential for utilizing heat that is normally wasted.

An actual heat-driven heat pump results from the use of a natural gas-fired IC engine to drive the compressor of a vapor-compression cycle heat pump. If a fraction, ϵ , of the engine rejected heat is recovered through some type of heat exchange process, then an additional rate of heat, \dot{Q}_{Rec} , is available for space heating. From equation (18):

$$\dot{Q}_{\text{Rec}} = \epsilon \dot{Q}_{\text{Eng}} = \epsilon(1 - \eta_{\text{Eng}}) \dot{Q}_{\text{Gas}} \quad (19)$$

Then for the actual heat-driven heat pump, the coefficients of performance obtained from equations (16), (17), and (19) are:

$$\text{COP}_{\text{H}} = \frac{\dot{Q}_{\text{Cond}}}{\dot{Q}_{\text{Gas}}} + \frac{\dot{Q}_{\text{Rec}}}{\dot{Q}_{\text{Gas}}} = \eta_{\text{Eng}} \text{COP}_{\text{W}_\text{H}} + \epsilon(1 - \eta_{\text{Eng}}) \quad (20)$$

$$\text{COP}_{\text{C}} = \eta_{\text{Eng}} \text{COP}_{\text{W}_\text{C}} = \frac{\dot{Q}_{\text{Evap}}}{\dot{Q}_{\text{Gas}}}$$

These are the coefficients of performance referred to throughout the remainder of this text.

Using off-the-shelf advanced technology, reasonable hardware values for an I.C. engine heat pump is:

$$\eta_{\text{Eng}} = 0.25$$

$$\epsilon = 0.8$$

$$\text{COP}_{W_H} = 4$$

$$\text{COP}_{W_C} = 4$$

This shows the present available component hardware potential is 1.6 for COP_{H_H} and 1.0 for COP_{H_C} . A diagram of the I.C. engine heat pump concept using this available component technology is shown in Figure 4.

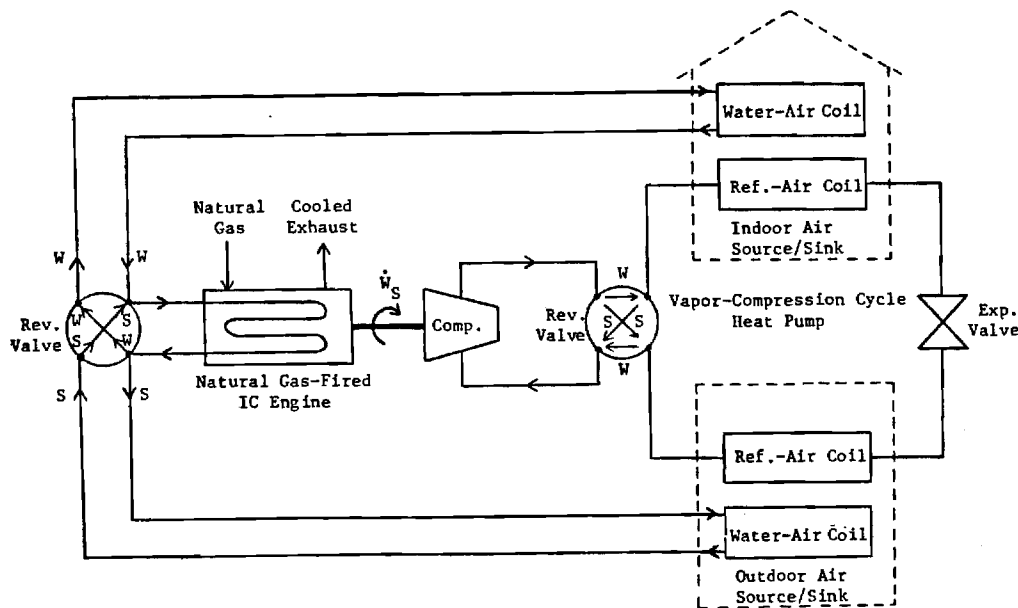


Figure 4. I.C. Engine Heat Pump Concept

SECTION II

I. C. ENGINE HEAT PUMP SYSTEM DESIGN

Description of Experimental System

The experimental system consists of a Florian Bauer GWW 35 natural gas driven heat pump package with an accessory exhaust gas/water heat exchanger for recovery of engine rejected heat, an integrated air/water heat exchanger with a central air handling system, and instrumentation.

The Florian Bauer GWW 35 heat pump package utilizes a 1600 cc four cylinder spark ignition engine built by the Ford Motor Company of Europe to drive a vapor compression cycle heat pump. This package, manufactured and marketed in West Germany, was designed to provide hot water for space heating via a radiator system, as is common practice in Europe. The manufacturer's specifications for this heat pump package appear in Table 1. It was also designed to use underground water rather than outdoor air as the external heat source/sink.

This water source type system is not the development goal for gas heat pumps due to the limited applications having underground water available along with a water disposal sink (injection or stream). However, the prime subcomponent under question in I. C. engine heat pumps is the engine/compressor. This system allows testing of this major subcomponent without the added development effort to design and construct the out-

Table 1. Florian Bauer GWW 35 Heat Pump Specifications

Maximum Heating Output @ 1800 rpm:	129,700 Btu/hr
Fuel Consumption Rate:	84.9 ft ³ /hr
COP _H at Maximum Output:	1.49
Required Water Flowrate @ 50°F Water Temperature:	15.4 gallons per minute
Weight:	1,430 lb.
Length:	53 inches
Width:	34 inches
Height:	52 inches

door coil, refrigeration reversing valve, and defrost controls. It was felt these outdoor air coil problems should be decoupled from the engine/compressor testing and focused on after the engine/compressor was proven quiet and reliable with satisfactory maintenance.

This water-to-water heat pump was integrated with an air duct system for producing heated and cooled air for space heating and cooling. A water-to-water heat pump has both an advantage and disadvantage with respect to an air-to-air system. In heating, the well water evaporator is advantageous over an outside air evaporator but the hot water producing condenser will be at a disadvantage compared to an air condenser placed directly in the air handler. In the cooling mode, the well water cooled condenser will be advantageous over an outside air condenser, but the chilled water evaporator will be at a disadvantage compared to an air evaporator placed directly in the air handler. In short, a water-to-water system has the advantage of a well water "outside" coil but the disadvantage of having two inside heat exchangers in series, i.e. refrigerate-to-water and water-to-air rather than a single refrigerate-to-air.

An air-water heat exchanger and central air handling system was integrated with the Florian Bauer heat pump to provide heated and cooled air for space conditioning. Heat is exchanged between a circulating water loop and house air in an air handler with an ARKLA 5-ton vertical chill water

coil, model number 60-136. The coil has a UA value of approximately 4500 Btu/hr-°F. Indoor air is circulated through the coil by a blower in the air handler with 1/2 hp at flow rated at 2000 cfm. Hot or cold water is circulated through the coil at a rated 10 gpm by one of two March Model 830, 1/5 HP pumps. An underground well behind the residence supplies water at approximately 60°F year-round as the external heat source/sink for this system. The well water is pumped at a rated 6 gpm through one of the heat pump heat exchanger coils by a self-priming Teel 1-1/2 inch, 1/2 HP pump.

The well was drilled with a small portable drilling rig to a total depth of twenty-nine feet. A well screen and two inch PVC casing were inserted and cemented in place. A series of pumping tests were conducted concluding that the well could supply ground water at a rate approximating ten gallons per minute for a sustained period of time. After the water has been utilized as a heat sink/source, it is disposed of in Burnt Creek, which flows behind the residence. This plan of disposal has been approved by the Georgia Department of Natural Resources. An alternate plan of disposal that implemented a recharge well was discarded due to the convenience the creek offered and its close proximity to the installation.

The Florian Bauer GWW 35 heat pump package was designed to provide heat recovery from the engine jacket and the exhaust manifold. As an accessory to this package, an external

exhaust gas/water heat exchanger is utilized to recover additional engine exhaust rejected heat.

The experimental system was designed to provide space heating and cooling and domestic hot water. In winter, the system can provide space heating ("Mode 1") or it can heat water for domestic use ("Mode 2"). In the summer, the experimental system can provide simultaneous space cooling and domestic water heating ("Mode 3") or it can provide only space cooling when the domestic hot water storage tank is fully heated ("Mode 4").

A configuration of the experimental system is shown in Figure 5. The system employs seven manually operated valves, two automatic valves, two circulation pumps, and a well pump. The manual valves are opened or closed only when it is desired to change between the winter and summer modes. Essentially, the manual valves perform the same function as a heat pump refrigerant reversing valve. The automatic valves and pumps are thermostatically controlled in order to change operating modes in a given season of the year (i.e., between Modes 1 and 2, or between Modes 3 and 4). Table 2 provides a summary of valve positions and pump operation for each of the four modes of operation.

System Control

The system is controlled in an on/off manner. The four modes (2 winter and 2 summer) were chosen by a Smart-Stat solid state house thermostat and the domestic hot water

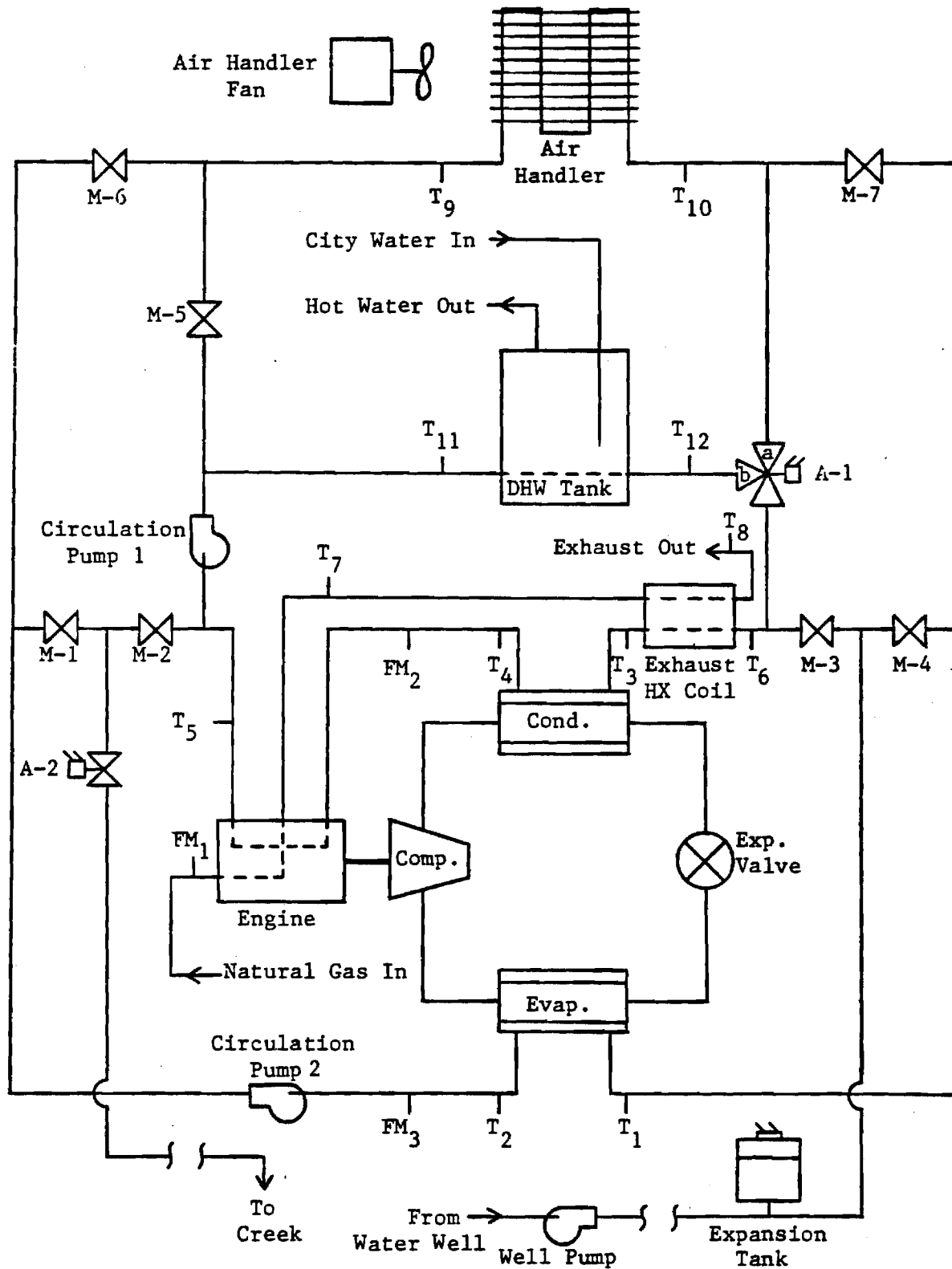


Figure 5. Experimental System Schematic

Table 2. Experimental System Valve Positions
and Pump Operation

<p>Winter (Space Heating)</p> <p>Mode 1</p> <p>Valve A-1 in position "a" Valve A-2 OPEN Pump P-1 ON Pump P-2 OFF Well Pump ON</p>	<p>MANUAL VALVES</p> <p>Valve M-1 OPEN Valve M-2 CLOSED Valve M-3 CLOSED Valve M-4 OPEN Valve M-5 OPEN Valve M-6 CLOSED Valve M-7 CLOSED</p>
<p>Mode 2</p> <p>Valve A-1 in position "b" Valve A-2 OPEN Pump P-1 ON Pump P-2 OFF Well Pump ON</p>	
<p>Summer (Space Cooling)</p> <p>Mode 3</p> <p>Valve A-1 in position "b" Valve A-2 CLOSED Pump P-1 ON Pump P-2 ON Well Pump OFF</p>	<p>MANUAL VALVES</p> <p>Valve M-1 CLOSED Valve M-2 OPEN Valve M-3 OPEN Valve M-4 CLOSED Valve M-5 CLOSED Valve M-6 OPEN Valve M-7 OPEN</p>
<p>Mode 4</p> <p>Valve A-1 in position "a" Valve A-2 OPEN Pump P-1 OFF Pump P-2 ON Well Pump ON</p>	

thermostat. The winter space temperature control points are 69°F-on/72°F-off, with summer conditions set at 77°F-on/74°F-off. The thermostat time clock provided winter set back to 55°F from 11:00 PM to about 6:00 AM. The actual morning reset time was determined by the Smart-Stat's optimal warmup strategy which reset the thermostat as necessary to reach 72°F by 6:30 AM. The domestic hot water temperature setting varied but was typically 110°F-on/130°F-off.

The thermostats provided 24 volt control signals to a group of relays which controlled the circulating pumps, air handler fan, and engine/heat pump. Also, 3 two position (winter/summer) toggle switches were incorporated with the relays to choose the space heating modes vs the space cooling modes.

The priority of the two possible modes in each season was set as follows:

- (1) Winter: Space heating was taken as priority over domestic water heating (DWH). If the heat pump was in the DWH mode when space heating was called for, the relays would immediately switch the system to the space heating mode.
- (2) Summer: Two modes were possible, i.e., space cooling with simultaneous DWH, and space cooling with rejected heat to the outside. DWH without simultaneous space cooling was not possible. When space cooling was called for, the system

simultaneously heated water if the tank temperature was below 130°F. If the tank was above 130°F, the system would reject its heat outside. The domestic hot water thermostat would bring on DWH when the tank dropped below 110°F. In this case, it would always simultaneously cool the house regardless of the room thermostat condition.

The summer condition of providing space cooling when DWH was required regardless of the space temperature did not overcool the house except during some cool summer mornings when 4 showers would be taken during a 30 minute period. This however, provided stored cooling so that thermostat demand for space cooling was delayed until later in the day.

The relay controls are shown in Figure 6. This is the detailed relay circuit controlling the circulating pumps, air handler, and engine/heat pump. The engine/heat pump was activated by closure of CR-1, 2, or 3. At this point, starting of the engine/heat pump was carried out by separate controls in the engine/heat pump package. The starter engaged for a period of 5 seconds and the compressor bypass solenoid valve (to prevent starting against a compressor load) was opened for a period of 10 seconds. If the engine failed to sense oil pressure within 10 seconds, the engine/heat pump shut down on default requiring a manual reset to reinitiate the starting cycle. These engine/heat pump starting controls were provided as part of the package by Florian Bauer.

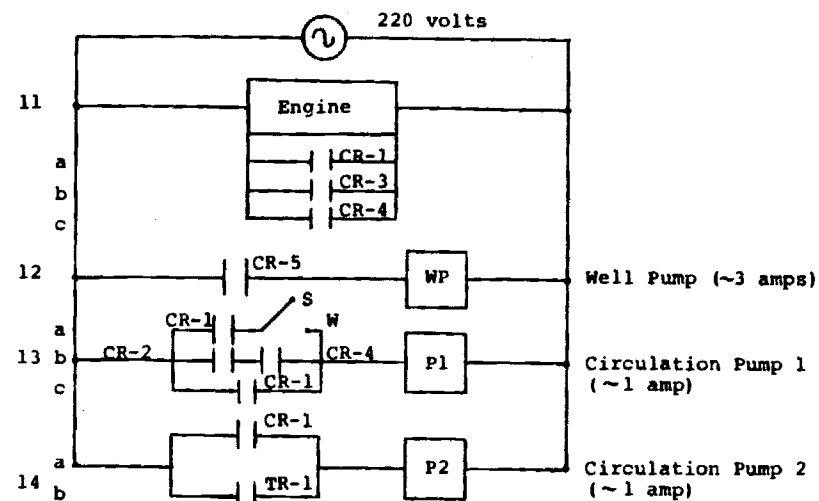
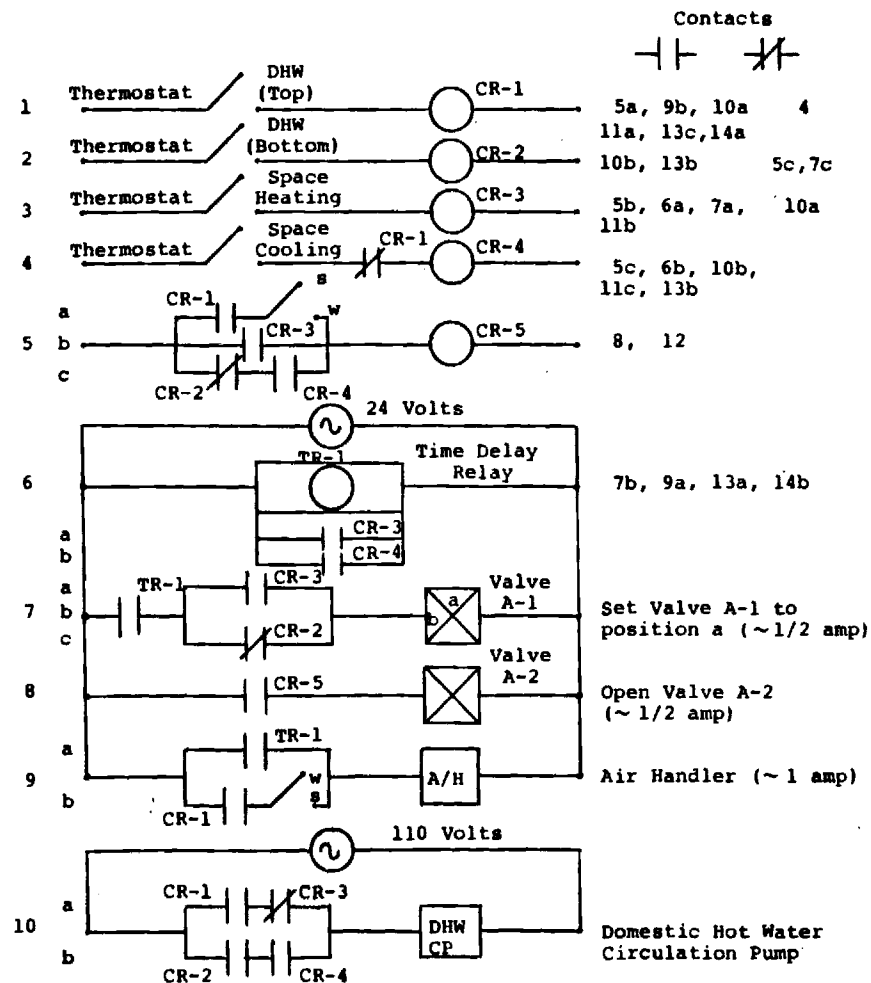


Figure 6: Heat Pump System Controls

SECTION III

INSTRUMENTATION

Long Term Monitoring

The monitoring of the heat pump over long time periods required an accumulating instrumentation system to accumulate 1) gas usage, 2) heat output, 3) cooling output, and 4) run hours.

The natural gas input was measured by installing a meter on the gas line leading to the engine. This meter is of the same type used by a gas utility company to measure domestic consumption for billing purposes. An hour meter was installed on the heat pump to measure the cumulative run time. The accumulated gas consumption could then be read from the meter and the average rate of gas consumption could be calculated by dividing the net gas consumption by the measured run time.

Energy supplied by the hot and chilled water loops were measured through the use of a pair of RHO-SIGMA model RS-805 Btu meters employing a flowmeter and a pair of temperature sensors placed in the supply and return of the respective hot and chilled water circuits. The Btu meters display the cumulative number of gallons of water that have flowed and the cumulative number of Btu's of heat transferred in the heated and chilled water circuits. The heating and cooling rates can be calculated by dividing the net number of Btu's of heat transferred by the run time.

The BTU meter thermisters have manufacturer's stated precision of $\pm 0.4^{\circ}\text{F}$ with a nonlinearity which "does not have a measurable affect on the Btu-meter." The signals from the thermisters enter the RS-805 two bridge resistors which are matched to an accuracy of $\pm 0.04\%$.

The arithmetic circuitry directly measures the temperature difference between the two sensors rather than the absolute temperature of the sensors. This minimizes signal processing which can introduce error. The temperature difference is converted to a digital signal through use of a digitally generated voltage staircase specifically shaped to eliminate the remaining non-linear influences of the thermisters. The 255 steps in the staircase determine the 1°F resolution of the temperature differential measurement. One step is generated for each 1°F .

The flow meters are Kent model number C-700-FE (plastic) on the cold water circuit producing 4 pulses per gallons, and a RS-807B (brass) on the hot water circuit producing 200 pulses per gallon. The maximum stated error of the flow meters above 0.5 gpm is $\pm 1\%$. The pulses from the flowmeters trigger the voltage staircase which in turn triggers an oscillator in phase with the staircase. A positive temperature differential opens a gate which feeds the oscillator pulses into a counter. The number of pulses sent to the counter is directly proportional to Btus. When the counter accumulates the equivalent of 1,000

Btus, it increments a 6-digit counter and resets the circuitry. The overall stated accuracy for the Btu meters with a 10°F water ΔT , which was typical, is $\pm 5\%$.

Computer Data Acquisition

In order to obtain more detailed data on the heat pump system's performance, a data acquisition system was designed and implemented to allow measurement of 12 temperatures, 2 water flow rates, natural gas flow rate, and all energy flow rates with a time resolution of 1 minute. The data system used an Apple II microcomputer with an ISAAC A/D interface made by Cyborg Corp.

Twelve thermocouple millivolt outputs were conditioned by 12 Analog Devices 252A amplifiers with internal reference. These 0 to 5 volt signals were feed into the ISAAC where they were digitized on a 0 to 4096 count scale and read by the computer on command. The location of the 12 thermocouples are shown in Figure 5.

Two counter channels in the ISAAC accumulate 0 to 5 volt pulses from the same two Kent water flow meters used by the Rho Sigma Btu meters previously described. These hot and cold loop water meters produce 200 pulses per gallon and 4 pulses per gallon, respectfully. A third counter channel accumulates pulses from a DARCOM encoder fitted to the 1/4 cubic foot per resolution dial of the gas meter. This magnetic activated pulser produced five 0 to 5 volt pulses per revolution and was input to the ISAAC. These three counter channels were read each minute by the computer, which automatically

zeroed the counters, giving flow rate per minute.

Additionally, two binary input ISAAC channels read the on/off status of control relays which determined when the system was on and which of the four operating modes the system was in.

The 12 bit digital thermocouple readings and 16 bit flow rate readings were read by the computer each minute after startup. The ISAAC's internal calender/clock supplied the day of week, date, hour, minute and second for these readings. A complete system calibration was carried out on the thermocouple channels by placing all thermocouples, along with a mercury thermometer certified to a $\pm 0.1^\circ\text{C}$ accuracy, in an ice bath, 50°C bath, and boiling water bath. A second order calibration curve was derived for each thermocouple channel to convert the counts to degrees C.

A basic language program was written for the Apple II which upon heat pump startup would log the time and date, and read all data channels each minute. The energy flows were calculated as follows:

$$\dot{Q}_{\text{Gas}} = \dot{V}_{\text{Gas}} (1028 \text{ Btu/ft}^3)$$

$$\dot{Q}_{\text{Cond}} = (\dot{m}C_p)_{\text{Cond}} (T_4 - T_3)$$

$$\dot{Q}_{\text{Evap}} = (\dot{m}C_p)_{\text{Evap}} (T_1 - T_2)$$

The total rate of engine rejected heat that is recovered was determined by:

$$\dot{Q}_{\text{Rec}} = (\dot{m}C_p)_{\text{Cond}}(T_4 - T_5) + (\dot{m}C_p)_{\text{Cond}}(T_6 - T_3)$$

$$\left[\begin{array}{l} \text{Engine Jacket} \\ \text{+Exhaust Manifold} \end{array} \right] \quad \left[\begin{array}{l} \text{Exhaust Heat} \\ \text{Exchanger} \end{array} \right]$$

Minute by minute COP's were calculated by the program with:

$$\text{COP}_C = \dot{Q}_{\text{Evap}} / \dot{Q}_{\text{Gas}}$$

$$\text{COP}_H = (\dot{Q}_{\text{Cond}} + \dot{Q}_{\text{Rec}}) / \dot{Q}_{\text{Gas}}$$

A complete schematic of the data acquisition system is shown in Figure 7. All data was converted to engineering units.

This temperature and flow rate data, with calculated energy flow rates and efficiencies, were then printed on the screen, paper printer, or floppy disk as appropriate. An accumulating subroutine was used to yield accumulative run times, energy flows and efficiencies in longer term tests.

INSTRUMENTATION SCHEMATIC

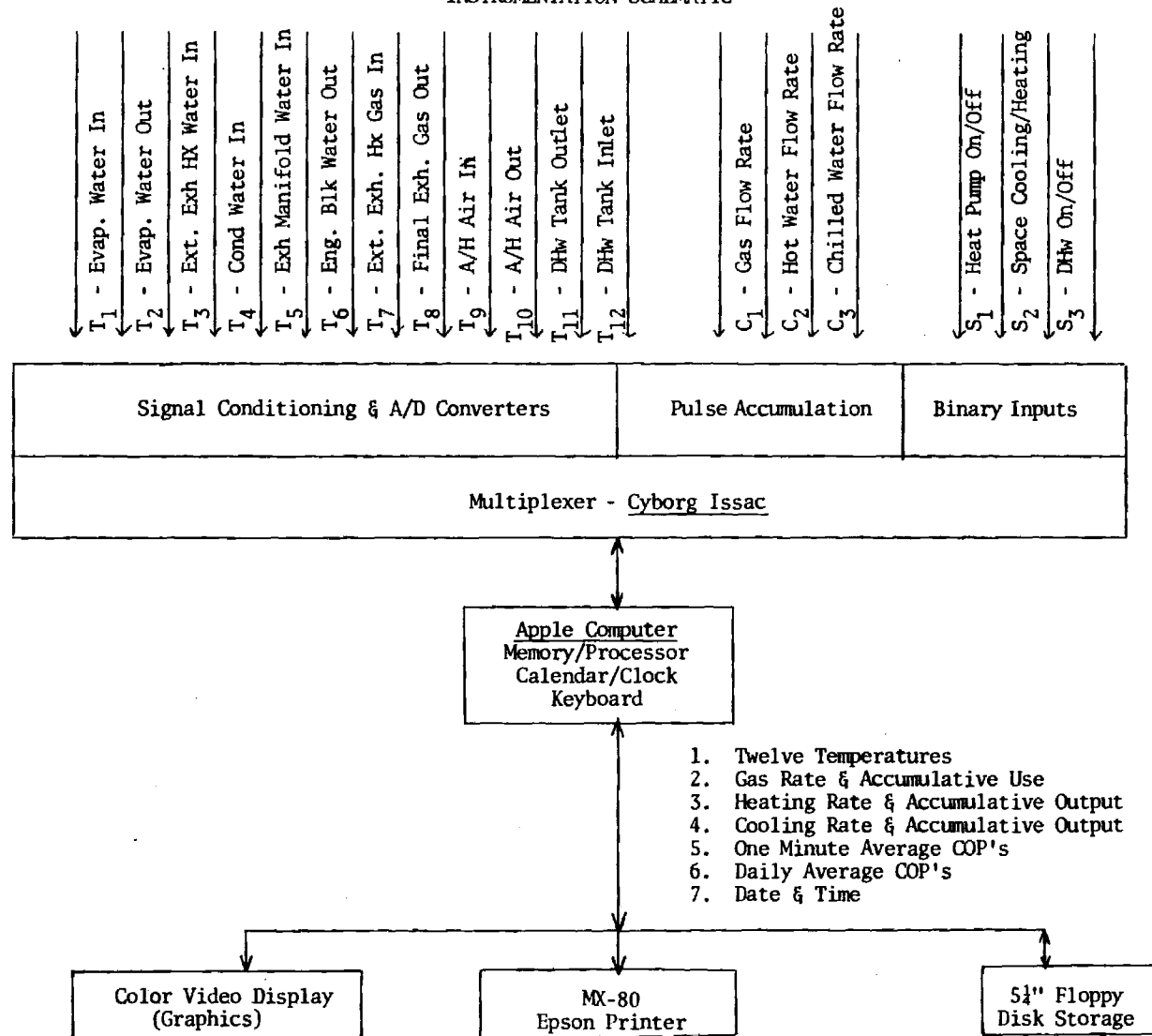


Figure 7: Computer Data Acquisition Schematic

SECTION IV

EXPERIMENTAL PERFORMANCE

Introduction

The Florian Bauer heat pump package was received from West Germany in December 1980. It was integrated into a residential heating/cooling system during early 1981 and since June 1981, has provided the space heating/cooling for the residence.

The residence is a 3200 square foot three story brick structure with 50% of the southeastern wall glass. This glazing has a ten foot overhang for summer shading. The structure was built in 1965. A 200,000 Btu/hr furnace was installed in 1976, with a five ton electric air conditioner installed in 1965 providing space cooling. Hot water was supplied by a 40 gallon gas water heater installed in 1976. The house thermal "UA" value is about 680 Btu/hr-°F.

Analysis of data from 1978 to 1980 showed that natural gas consumption for space heating averaged 1000 therms annually with the furnace operating about 500 hours per year. An hour meter was installed on the electric air conditioner from 1979 to 1980 showing an average of 525 hours per year with 4200 kwhr electrical consumption annually.

Seasonal data was accumulated by the Btu and gas meters during the summer of 1981 and winter of 1981-82. In early 1982 the computer data acquisition system was installed allowing more accurate data acquisition with one minute

time resolution. During the summer of 1982, the Btu meters were checked against the computer data acquisition system. Both steady state and transient data was then taken determining detailed performance data.

Seasonal Performance

The system became operational on June 13, 1981. The Btu meters became fully operational July 24, 1981 and the system closely monitored as it provided space cooling until October 13, 1981 when the heat pump cooling run time was 547 hrs. On almost a daily basis, the gas meter, hot and chilled water Btu meters, and heat pump hour meter were read and recorded. An abbreviated tabulation of this data is shown in Table 3. The engine speed was fixed at 1200 rpm.

In January 1982, new thermisters were installed on both Btu meters. This was done since questions has arisen regarding the Btu meter accuracy. There was a slight (5%) reduction in the hot water Btu output after the new calibrated thermisters were installed. At the end of February 1983, a fan and inside circulating pump delay was added which left them on for 6 minutes after the engine turned off. This "spindown" recovered additional heat from the engine. The system ran in the space heating mode until 5/24/82 when it was switched to cooling. On 10/18/82, it was again switched to heating.

All readings have been plotted vs run hours and a least squares straight line fitted to each season's segment. The results agree with merely taking the seasonal incremental

TABLE 3

Long Term Performance Raw Data

<u>Date</u>	<u>Run</u> (Hrs)	<u>V_{Gas}</u> (100 ft ³)	<u>Q_{Heat}</u> (1000 Btus)	<u>Q_{Evap}</u> (1000 Btus)
7/27/81	401	2,317	18,441	13,143
9/10/81	534	2,403	20,434	18,130
10/13/81	547	2,411	32,192	18,710
10/13/81	----- Switched to Heating-----			
10/13/81	547	2,411	32,192	18,710
12/08/81	682	2,505	44,877	22,801
01/02/82	827	2,600	59,014	27,720
01/30/82	1,048	2,747	81,361	34,903
01/30/82	-----New Thermisters Installed-----			
02/28/82	1,188	2,836	93,721	39,524
02/28/82	-----Added A/H Fan and Pump Delay----			
03/31/82	1,288	2,897	102,600	42,792
05/02/82	1,306	2,909	104,180	43,364
05/29/82	1,339	2,929	107,274	44,388
05/29/82	-----Switched to Cooling-----			
05/29/82	1,339	2,929	107,274	44,388
06/26/82	1,413	2,978	114,826	47,016
07/31/82	1,539	3,063	128,302	52,419
08/18/82	1,631	3,124	137,975	55,569
09/09/82	1,731	3,178	146,981	59,164
10/18/82	-----Switched to Heating-----			
10/18/82	1,731	3,206	151,926	Broken
04/19/83	2,402	3,646	218,705	-----

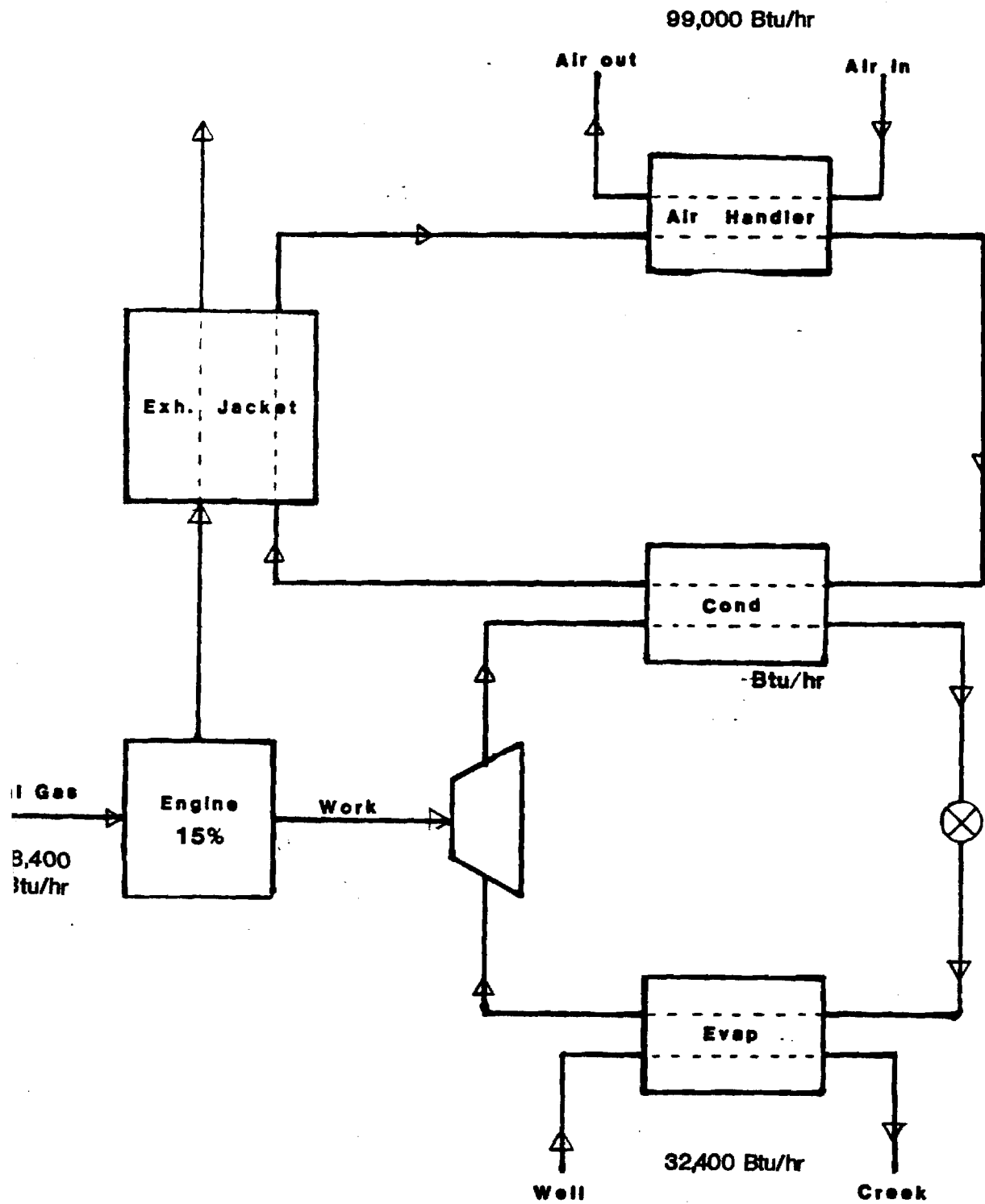
accumulative numbers and dividing by the incremental seasonal run time. Doing this, the following results.

<u>Season</u>	<u>Run</u>	<u>\dot{Q}_{Gas}</u>	<u>\dot{Q}_{Heat}</u>	<u>COPH_H</u>	<u>\dot{Q}_{Evap}</u>	<u>COPH_C</u>
	(Hrs)	(Btu/hr)	(Btu/hr)		(Btu/hr)	
Summer 81*	146	66,000	94,000		38,100	0.58
Winter 81-2	792	67,100	94,800	1.41	32,400	
Summer 82	415	68,500	107,600		39,500	0.58
Winter 82-3	648	69,700	103,100	1.48		

*Partial Summer starting 7/24/81. Full summer hours = 547.

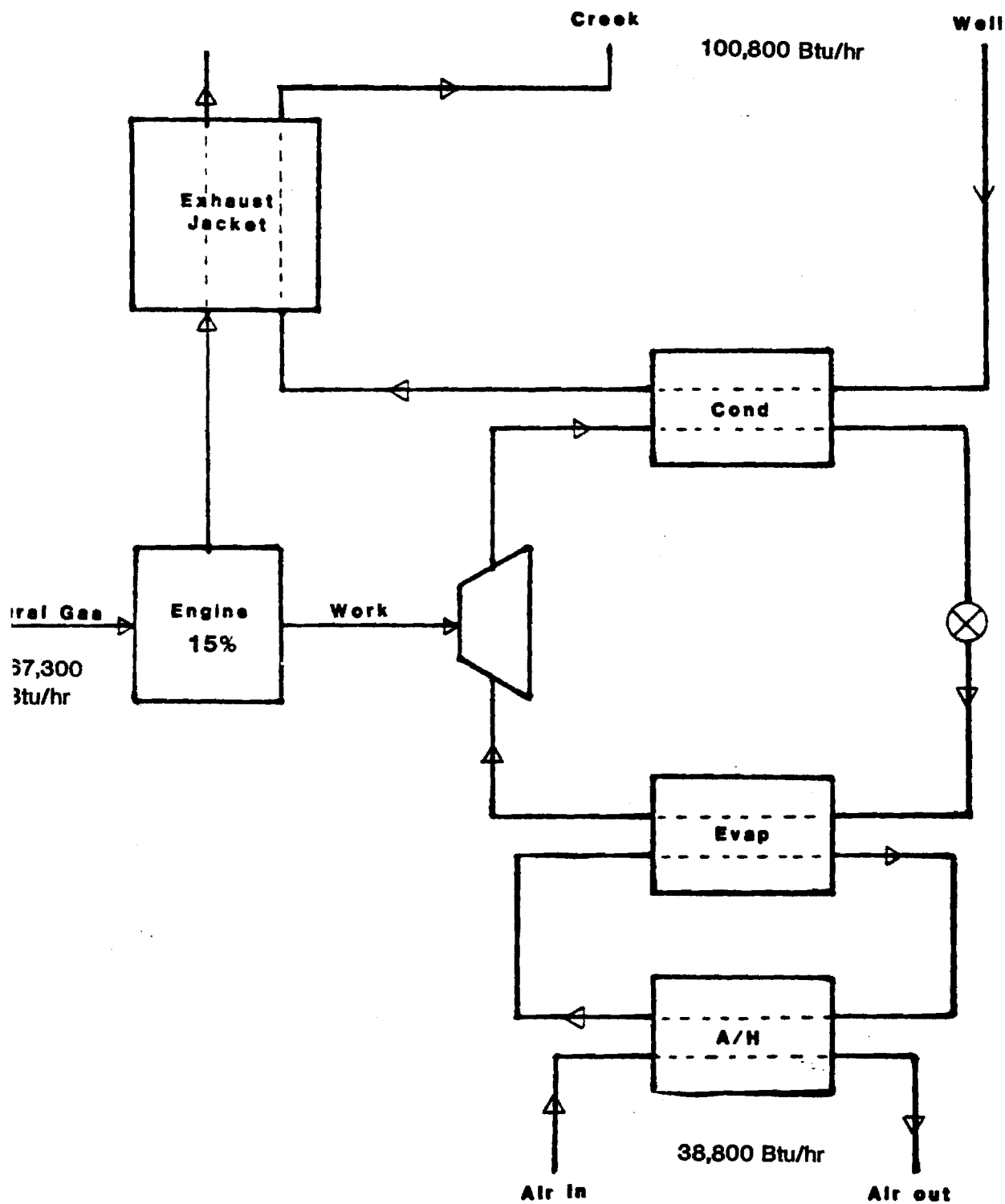
These results are summarized graphically on the heat pump system schematic in Figure 8 for heating and Figure 9 for cooling. In these figures, the values for the two heating seasons are averaged and the two cooling seasons were averaged to get overall heating and cooling performance. They represent Seasonal Performance Factor values.

FIGURE 8: SEASONAL SYSTEM HEATING PERFORMANCE 37



HEATING C.O.P. : 1.45

FIGURE 9: SEASONAL SYSTEM COOLING PERFORMANCE



COOLING C.O.P. : 0.58

Engine/Compressor Performance

Data was taken from the experimental heat pump system for the purpose of determining engine/compressor performance (gas input rate, condenser and evaporator heat rates, and the heat recovery rate) as functions of the condenser and evaporator refrigerant temperatures. With the engine speed held constant, the gas input rate and condenser and evaporator heat rates are uniquely determined by the two refrigerant temperatures. The heat recovery rate is additionally dependent upon the water temperature and flow rate at the inlet to the exhaust heat exchanger, which vary from one operating mode to another.

Four operating conditions, each specified by a condenser refrigerant temperature and an evaporator refrigerant temperature, were used to obtain the experimental data. The operating conditions, listed in Table 4, were chosen near lower and upper temperature extremes in order to obtain a good representation over the range of experimental operating conditions. In order to achieve steady-state for each of the specified operating conditions, three different operating modes were required as indicated in Table 4.

The water temperature at the inlet to the exhaust heat exchanger (and, therefore, the heat recovery rate) varies with the operating mode. During normal heating operation, this temperature would be constant, yielding a constant exhaust temperature of approximately 130°F at the heat exchanger outlet. Therefore, the measured heat recovery rate was corrected by calculating the change

in exhaust heat recovery due to fixing the final exhaust temperature at 130°F.

A total of forty tests (ten for each of the four operating conditions) were conducted at a constant engine speed of 1200 rpm. After establishing steady-state (as determined by continuous monitoring of water temperatures in the condenser and evaporator loops), the gas input rate, condenser and evaporator heat rates, and heat recovery rate were computed for one-minute tests and logged by the APPLE/ISAAC instrumentation system. For each set of operating conditions, the data was averaged over ten tests, and the results are given in Table 5. Included are the mean values and estimated true population standard deviations for the measured gas input rate, the measured condenser and evaporator heat rates, the measured heat recovery rate, and the corrected heat recovery rate.

The data presented in Table 5 provides an indication of the dependence of engine/compressor performance and the heat recovery rate on the condenser and evaporator refrigerant temperatures. For a change in one of the refrigerant temperatures with the other held constant, a change is estimated for the gas input rate, condenser and evaporator heat rates, and the heat recovery rate. The question was raised as to whether these changes are actual, or due to random error in the experimental data. A statistical analysis was performed to determine confidence intervals for changes in the data (dependent variables) resulting

from changes in the refrigerant temperatures (independent variables).

$$\text{Confidence Interval} = \bar{X}_2 - \bar{X}_1 \pm t_p \left[\frac{(n+m)(n\sigma_1^2 + m\sigma_2^2)}{nm(n+m-2)} \right]$$

where \bar{X}_1 and \bar{X}_2 are the averaged dependent variables involved in the change of one of the independent variables, σ_1 and σ_2 are the estimated true population standard deviations for the dependent variables, and n and m are the numbers of dependent variable data points. The variable t_p is tabulated⁶ as a function of the degrees of freedom $(n+m-2)$ and the confidence coefficient. For this data, the degrees of freedom are 18, and for a confidence of 90%, $t_p = 1.734$; 95%, $t_p = 2.101$; and 99%, $t_p = 2.878$. Confidence intervals for the changes in data resulting from the increase in condenser refrigerant temperature are listed in Table 6. The negative signs on some of the interval bounds indicate that those rates decreased when the condenser temperature was increased. Confidence intervals for the changes in data resulting from the increase in evaporator refrigerant temperature are given in Table 7.

A good degree of confidence is indicated when the intervals are small relative to the magnitudes of their bounds. A review of Tables 5 and 6 indicates a good degree of confidence in the change in condenser and evaporator heat rates for a change in either of the refrigerant temperatures. This implies that the rate changes

are more likely due to changes in operating conditions than random error in the data. On the other hand, little confidence can be placed in the change in heat recovery rate accompanying changes in either of the refrigerant temperatures. For instance, it is not known with a 99% certainty whether the heat recovery rate increases or decreases when the condenser temperature is increased.

A multiple variable, linear regression analysis program, available through an APPLE computer software package, was used to determine a linear relationship between the heat pump performance and the condenser and evaporator refrigerant temperatures. Data from all forty tests was used for the analysis. The results are included in Table 8 along with statistical analysis of the curve fits. These results are useful in design optimization of I. C. Engine heat pumps.

System Steady State Performance

Data was obtained using the computer data acquisition system from startup to establishment of steady state conditions for both the heating and cooling modes. Steady state was established in 20 to 30 minutes in the cooling mode and 30 to 40 minutes in the heating mode. The warmup period was longer for the heating cycle due to the higher equilibrium temperatures in the hot water loop (about 140°F vs 70°F). The speed was held constant at 1200 rpm.

Table 9 shows the steady state values for the temperatures, energy flow rates, and COPH's. The temperature #'s are labeled on the system schematic in Figure 5. In the heating mode, 57% of the heat was produced by the condenser, 41% from the engine cooling jacket and integral

exhaust manifold/HX, and 2% from the external exhaust heat exchanger. The evaporator and condenser temperatures were about 31°F and 132°F respectively. Only $1\frac{1}{2}\%$ of the gas input plus evaporator input energy is unaccounted for. The only significant loss would be in the exhaust gases which are at 117°F . The accuracy of this "lost" heat number is very low due to accumulative errors of the numbers totaled to derive it.

In the cooling mode, 59% of the rejected heat comes from the condenser, 39% from the engine cooling jacket and exhaust manifold, with 2% coming from the external exhaust heat exchanger. The evaporator and condenser temperatures were approximately 33°F and 88°F respectively. Only 3% of the total gas and evaporator energy input is unaccounted for. Again, the accuracy of this number is low, but with a 75°F final exhaust temperature and insulated heat pump package, the unmeasured energy flow should be small.

The larger fraction of heat coming from the condenser in the cooling mode is due to the lower condenser temperature and pressure giving a higher refrigerant mass flow and a lower engine loading.

Table 4. Steady-State Operating Conditions

Operating Condition	T _{Evap} (°F)	T _{Cond} (°F)	Operating Mode
1	27.5	86.9	3*
2	27.5	145.4	4
3	14.0	95.0	1
4	39.2	95.0	3*

*Mode 3 was modified by opening valve M-5 and placing valve A-1 in position "a".

Table 5. Averaged Experimental Data

Operating Condition	$T_{\text{Evap}} (^{\circ}\text{F})$	$T_{\text{Cond}} (^{\circ}\text{F})$	$\bar{Q}_{\text{Gas}} \left(\frac{\text{Btu}}{\text{hr}} \right)$ [$\sigma \left(\frac{\text{Btu}}{\text{hr}} \right)$]	$\bar{Q}_{\text{Cond}} \left(\frac{\text{Btu}}{\text{hr}} \right)$ [$\sigma \left(\frac{\text{Btu}}{\text{hr}} \right)$]	$\bar{Q}_{\text{Evap}} \left(\frac{\text{Btu}}{\text{hr}} \right)$ [$\sigma \left(\frac{\text{Btu}}{\text{hr}} \right)$]	$\bar{Q}_{\text{Rec}} \left(\frac{\text{Btu}}{\text{hr}} \right)$ [$\sigma \left(\frac{\text{Btu}}{\text{hr}} \right)$]	$\bar{Q}_{\text{Corr}} \left(\frac{\text{Btu}}{\text{hr}} \right)$ [$\sigma \left(\frac{\text{Btu}}{\text{hr}} \right)$]
1	27.5	86.9	76950 [0]	67384 [1871]	49804 [957]	55374 [3041]	49813 [3041]
2	27.5	145.4	84645 [1539]	49639 [863]	29781 [363]	47261 [1127]	47261 [1127]
3	14.0	95.0	70178 [1231]	43492 [2424]	32438 [439]	51791 [3396]	47176 [3396]
4	39.2	95.0	79412 [1231]	82614 [1821]	61362 [1520]	57706 [1488]	51968 [1488]

Table 6. Confidence Intervals for Increase
in Condenser Temperature

	Confidence Coefficient		
	90%	95%	99%
$\Delta \bar{Q}_{\text{Gas}} (\frac{\text{Btu}}{\text{hr}})$	[6805; 8585]	[6617; 8773]	[6219; 9171]
$\Delta \bar{Q}_{\text{Cond}} (\frac{\text{Btu}}{\text{hr}})$	[-18936; -16554]	[-19188; -16302]	[-19722; -15768]
$\Delta \bar{Q}_{\text{Evap}} (\frac{\text{Btu}}{\text{hr}})$	[-20615; -19431]	[-20740; -19306]	[-21005; -19041]
$\Delta \bar{Q}_{\text{Rec}} (\frac{\text{Btu}}{\text{hr}})$	[-4426; -677]	[-4823; -281]	[-5663; 559]

Table 7. Confidence Intervals for Increase
in Evaporator Temperature

	Confidence Coefficient		
	90%	95%	99%
$\Delta \bar{Q}_{\text{Gas}} (\frac{\text{Btu}}{\text{hr}})$	[8228;10740]	[8015;10453]	[7564;10904]
$\Delta \bar{Q}_{\text{Cond}} (\frac{\text{Btu}}{\text{hr}})$	[37370;40874]	[36999;41245]	[36213;42031]
$\Delta \bar{Q}_{\text{Evap}} (\frac{\text{Btu}}{\text{hr}})$	[28010;29838]	[27816;30032]	[27406;30442]
$\Delta \bar{Q}_{\text{Rec}} (\frac{\text{Btu}}{\text{hr}})$	[2649;6935]	[2195;7389]	[1235;8349]

Table 8. Results of Multiple Variable,
Linear Regression Analysis

$\dot{Q}_{\text{gas}} \left(\frac{\text{Btu}}{\text{hr}} \right) = 372.91T_{\text{Evap}} + 159.80T_{\text{Cond}} + 50838 *$ <p>Coefficient of Determination (R^2) = .89434</p> <p>Coefficient of Multiple Correlation = .94570</p> <p>Standard Error of Estimate ($\frac{\text{Btu}}{\text{hr}}$) = 1801.6</p>
$\dot{Q}_{\text{Cond}} \left(\frac{\text{Btu}}{\text{hr}} \right) = 1553.5T_{\text{Evap}} - 298.68T_{\text{Cond}} + 50292 *$ <p>Coefficient of Determination (R^2) = .98577</p> <p>Coefficient of Multiple Correlation = .99286</p> <p>Standard Error of Estimate ($\frac{\text{Btu}}{\text{hr}}$) = 1918.3</p>
$\dot{Q}_{\text{Evap}} \left(\frac{\text{Btu}}{\text{hr}} \right) = 1145.8T_{\text{Evap}} - 351.09T_{\text{Cond}} + 49420 *$ <p>Coefficient of Determination (R^2) = .99377</p> <p>Coefficient of Multiple Correlation = .99688</p> <p>Standard Error of Estimate ($\frac{\text{Btu}}{\text{hr}}$) = 1064.6</p>
$\dot{Q}_{\text{Rec}} \left(\frac{\text{Btu}}{\text{hr}} \right) = 189.52T_{\text{Evap}} - 46.400T_{\text{Cond}} + 48827 *$ <p>Coefficient of Determination (R^2) = .39396</p> <p>Coefficient of Multiple Correlation = .62766</p> <p>Standard Error of Estimate ($\frac{\text{Btu}}{\text{hr}}$) = 2558.6</p>

* T_{Evap} and T_{Cond} in °F

TABLE 9
Steady State Performance

<u>Temperatures ($^{\circ}\text{F}$)</u>	<u>Heating Mode</u>	<u>Cooling Mode</u>
T ₁ - Evaporator water inlet	57.5	52.2
T ₂ - Evaporator water outlet	43.3	42.3
T ₆ - External exhaust HX water inlet	113.2	60.7
T ₃ - Condenser water inlet	113.7	61.2
T ₄ - Engine water inlet	129.4	77.6
T ₅ - Engine water outlet	140.7	88.3
T ₈ - Exhaust gas outlet	117.8	74.7
T ₉ - A/H air inlet	70.9	77.5
T ₁₀ - A/H air outlet	108.9	59.0
 <u>Energy Flows (Btu/hr)</u>		
Gas consumption	68,700	67,700
Engine & exhaust manifold recovery	40,100	40,600
External exhaust HX recovery	1,800	1,900
Condensor heating	55,700	62,300
Total heating	97,600	104,800
Evaporator Cooling	30,400	40,700
 <u>COPH's</u>		
Heating	1.42	
Cooling		0.60

Variable Speed Performance

The heat pump engine speed was controlled by an electronic governor. The speed could be infinitely varied from 1200 rpm to 1600 rpm. The three stage room thermostat was set up with the capability to change engine speed from 1200 rpm to 1600 rpm in two 200 rpm steps. However, the heat pump's output at the 1200 rpm setting closely matched the peak heat/cooling demand at the extreme 100°F and 10°F temperatures experienced, and the variable speed controls were therefore never implemented.

For future design information, the effect of speed on the heat pump's heating performance was determined by running steady state tests from 1200 rpm to 1600 rpm. Figure 10 shows the gas consumption rate, condenser heat rate and engine recovery heat rate as the speed varies from 1200 rpm to 1600 rpm. All parameters are nondimensionalized by their respective values at 1200 rpm.

The gas rate is seen to vary linearly with speed indicating a near constant torque compressor load. The condenser heating rate increases only slightly, by about 10% while the engine heat recovery increases by about 33%. The condenser temperature increased by about 20°F to 152°F while the evaporator temperature decreased only slightly by about 2°F. This higher compressor discharge pressure causes the compressor to decrease its volumetric efficiency due to the clearance volume effect. The condenser temperature is changes faster than the:

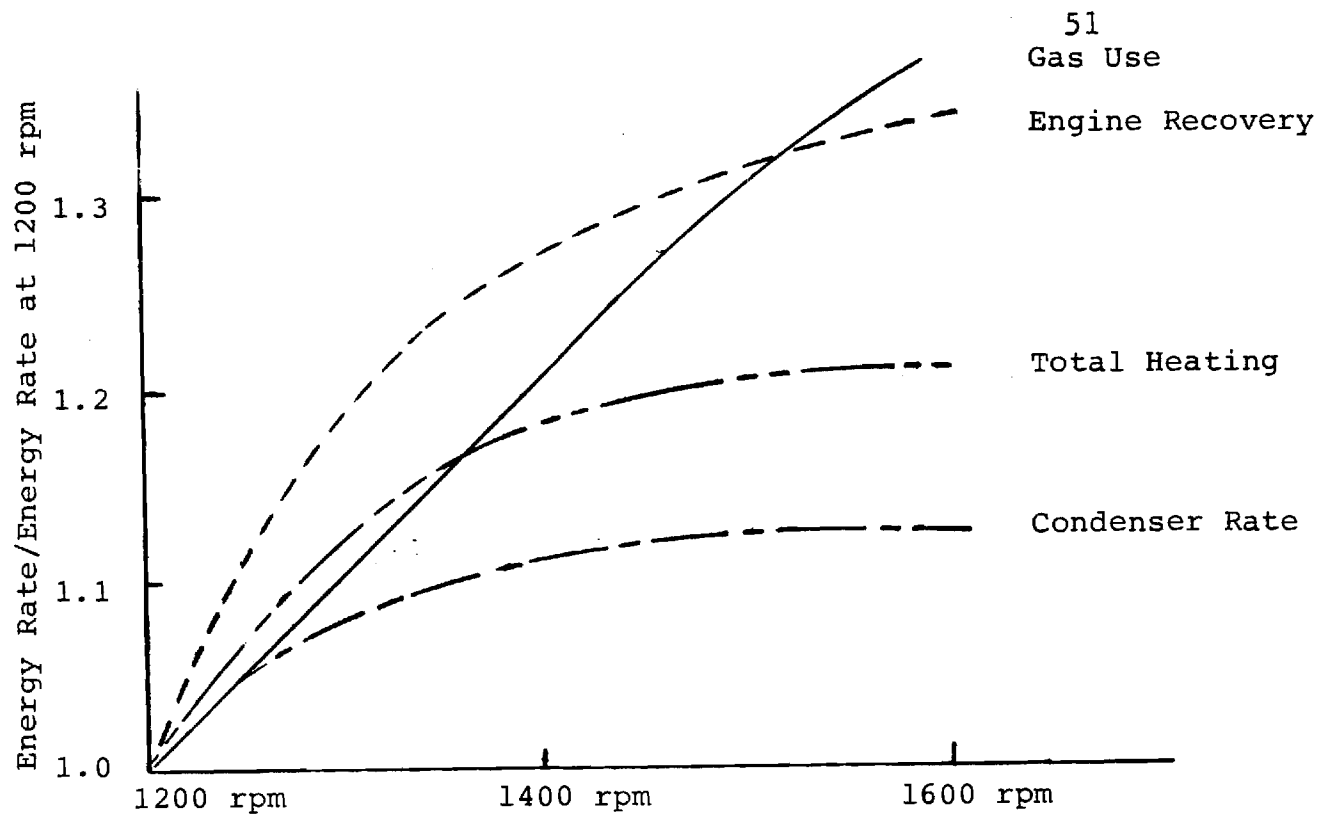


Figure 10. Heat Pump Energy Rates vs. Speed

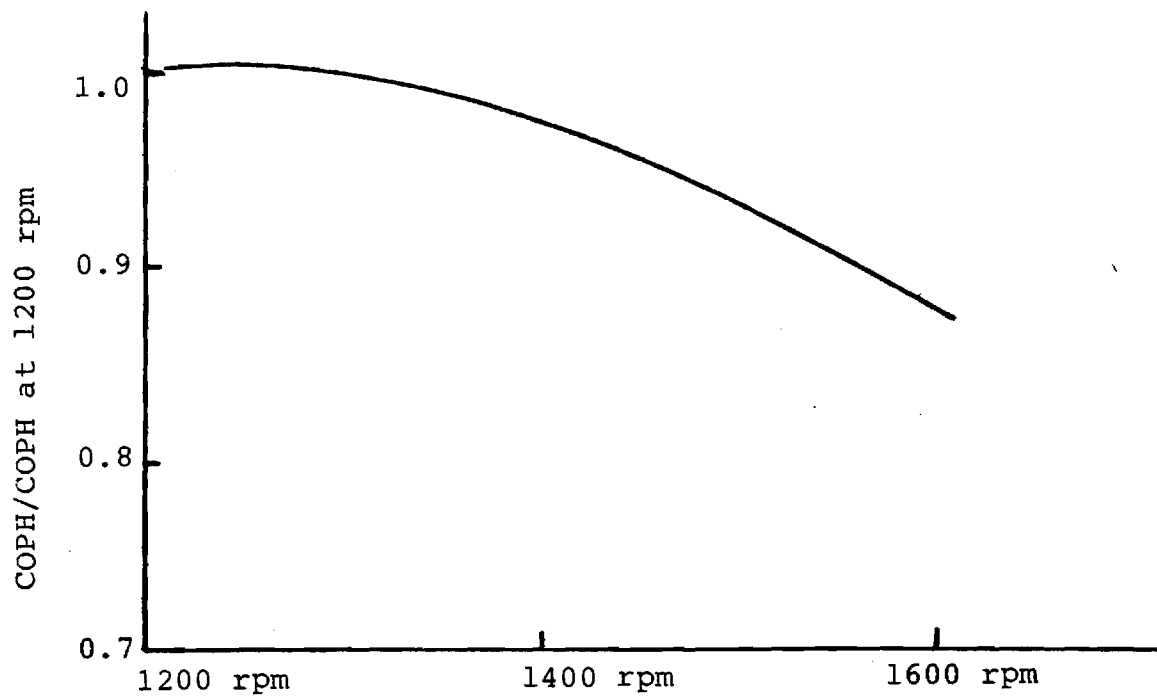


Figure 11. Heat Pump Heating COP vs. Speed

evaporator because the return water temperature from the air handler was driven up as a higher heat rate was put through the air-water coil. The well water temperature supplying the evaporator is of course constant with varying speed. These speed effects would not be as large with an air-to-air system without the additional water heat exchange process.

Figure 11 shows the resulting COPH for the varying speed. The efficiency is seen to decrease by about 15%, while the total heating rate increases by just over 20%, for a 25% speed increase. Again, it should be noted that the water-to-water heat pump will show larger efficiency penalties with increasing speed than an air-to-air system.

Cycling Effects

The effect of on/off cycling of the heat pump in its performance was studied in two ways. First, run-by-run data was accumulated by the computer data acquisition system. It printed out the average energy flow rates and COP's for each on-cycle, along with that cycle's on-time and prior off-time. Statistical analysis was carried out on this data to determine the correlation of the average cycle performance as a function of the cycle's on-time and the prior off-time. No significant dependence of any of the variables were found on these cycle times.

Due to this unexpected result, a cycling test was run which was patterned after U.S. Department of Energy's test

procedure for measuring electric air conditioner and electric heat pump cycling effects published January 1, 1982, Chapter 2, Title 10, Subpart B, Appendix M. In this test a 30 minute run is made to establish steady state conditions followed by a 30 minutes period during which the steady state performance is measured. During the next 30 minutes period, the heat pump is off 24 minutes and then turned on for 6 minutes. This 24 minutes off, 6 minutes on cycle is repeated twice more with the last 6 minute cycle being used to measure the performance during cycling relative to the initial steady state values.

A DOE cycling degradation coefficient, C_D , is defined as:

$$C_D = 1 - \frac{COP_{cyc}}{COP_{ss}} = 1 - \frac{Q_{cyc}}{Q_{ss}}$$

where $()_{cyc}$ indicates the values for the last 6 minute on cycle and $()_{ss}$ is the 30 minute steady state measured values. In this tests the C_D repeatedly came out negative, indicating an improvement in efficiency during cycling.

This unusual result is shown to be due to the "spin down" cycle which extracts the engine/condenser heat for 6 minutes following an on-cycle. This reduces the hot water temperature from about 140°F to less than 110°F. Since the condenser is in the same hot water loop with the engine and exhaust, this significantly reduces the average condenser temperature during cycling compared with steady state, while still extracting all the engine heat. Accessory energy is also increased.

This cycling effect may not be the same with an air-to-air system since the I. C. engine heat pump condenser temperature would not be tied to the engine temperature. However, since approximately half of the total heat comes from the engine, cycling effects of an I. C. engine heat pump would be expected to be substantially less than an electric heat pump, particularly if a spin down cycle is used.

Reliability and Maintenance

One of the goals for the I.C. engine heat pump is to have a maintenance interval greater than once annually. This goal was exceeded by this experimental system in that no scheduled or unscheduled maintenance was carried out during the over 2400 running hours, except for the installation of an oil sealing gasket on a cover plate on the side of the engine. No oil changes, spark plug replacement, timing adjustment, or any other maintenance has been required or done. Spark plug gap is still under 0.040 inch due to special tip materials.

Oil analysis has been carried out showing at the 1750 hour point, the oil was still completely serviceable. The analysis at 1750 hours is shown in Table 10. The 15 quart capacity is continually recirculated.

Reliability has been 100% except for several occasions, increasing in frequency, when the engine failed to start during the first 5 second fixed starting period. It occurs generally after the heat pump has not

TABLE 10: Oil Analysis

WEAR CHECK

ENGINE AND OIL
CONDITION
ANALYSIS
REPORT

Spectro/Metrics, Inc.
35 Executive Park Drive, N.E.
Atlanta, Georgia 30329
(404) 321-7909

FORD

MODEL: 2270

FLEET/UNIT #: 1

NATURAL GAS

SAMPLE DATA	WEAR METALS						SILI- CON	ADDITIVES				CONTAMINANTS				VISC	TBN
	ALUM- INUM	CHRO- MIUM	COPPER	IRON	LEAD	TIN		MAGNE- SIUM	MOLY	BORON	SODIUM	WATER (%)	GLY- COL	DIEL- ECTRIC	FUEL (%)		
	PISTON BEARINGS	RINGS	BEARINGS	CYLINDER RINGS CRANK SH- CAM SH	GASOLINE ADDITIVE - DIESEL BEARING	BEARINGS		ADDITIVE (HOUSING)	ADDITIVE (RINGS)	ADDITIVE (COOLANT)	ADDITIVE (COOLANT)	CONDEN- SATION (COOLANT)	ANT- FREEZE	SOLIDS CARBON			
10-2-82	4.6	5.1	22	72	6.2	9.2	13	805	2.7	13	18	-.05	NEG	4	0	31	
14026	N	N	N	N	N	N	N	N	N	N	N	N	N	N	N		
214058	ENGINE WEAR RATES AND CONTAMINANT LEVELS SATISFACTORY. OIL STILL																
Hrs 1750	SERVICEABLE. RESAMPLE NEXT SERVICE INTERVAL TO MONITOR AND																
Since 1750	ESTABLISH WEAR TREND. (NO PREVIOUS RECORD WITH THIS UNIT I.D.																
Since 1750	PLEASE PROVIDE LAST LAB NUMBER.) -ANALYST RT																
Range 1750																	

ID: Normal, Abnormal, Severe.

" + " means greater than, " - " means less than.

DR. SAM. V. SHELTON
SCHOOL OF MECHANICAL ENG.
GEORGIA TECH
ATLANTA, GA 30332

LAST OVERHAUL:
SYSTEM CAPACITY: 15 QTS.
OIL MAKE & TYPE: ?
HISTORY & REMARKS:

SHEATL 1

DiesGasNat 75

A MEMBER OF THE SPECTROMETRIC OIL ANALYSIS LABORATORY ASSOCIATION

run for a long period of time. After five seconds, the starter is deactivated and if oil pressure is not sensed 10 seconds after starter initiation, the controls shut the unit down on default. In most every case, a manual reset to allow a second try was successful. A third and four try was required in isolated instances. This could be overcome by controls to automatically reinitiate the start cycle.

Noise Levels

Sound levels of the unit have been measured using a an A weighting scale. Inside the furnace room the levels were as follows for individual components running and with the total system running.

Background	-	57dBA
Air Handler only	-	61 dBA
Water Pump Only	-	57 dBA
Heat Pump Only	-	62 dBA
Total System	-	63 dBA

Sound levels were also measured outside at a 6 foot distance from the exhaust outlet. The outlet is 8 inches above a concrete slab and 6 inches from a 8 foot high concrete block wall. The sound level at a distance 6 feet from this wall is 60 dBA.

Electrical Accessary Power

The electrical accessories with this gas heat pump are:

1) 1/2 hp A/H fan drive; 2) two 1/5 hp closed loop water circulating pump drives (only one is on in any mode); 3) 1/2 hp well water pump drive, and 4) lead acid battery charger. The battery charger draws about 10 watts and is not significant.

The kilowatt draw of the other accessories are:

Fan	-	-	0.73 kw
Well Pump	-	-	0.61
Circulating Pump (1)	-		<u>0.24</u>
Total	-		1.58 kw

The 1.6 kw power is drawn during the heat pump operating hours. In addition, for 6 minutes after the heat pump is shut down, the fan and one circulating pump operates, drawing a total of 1.0 kw.

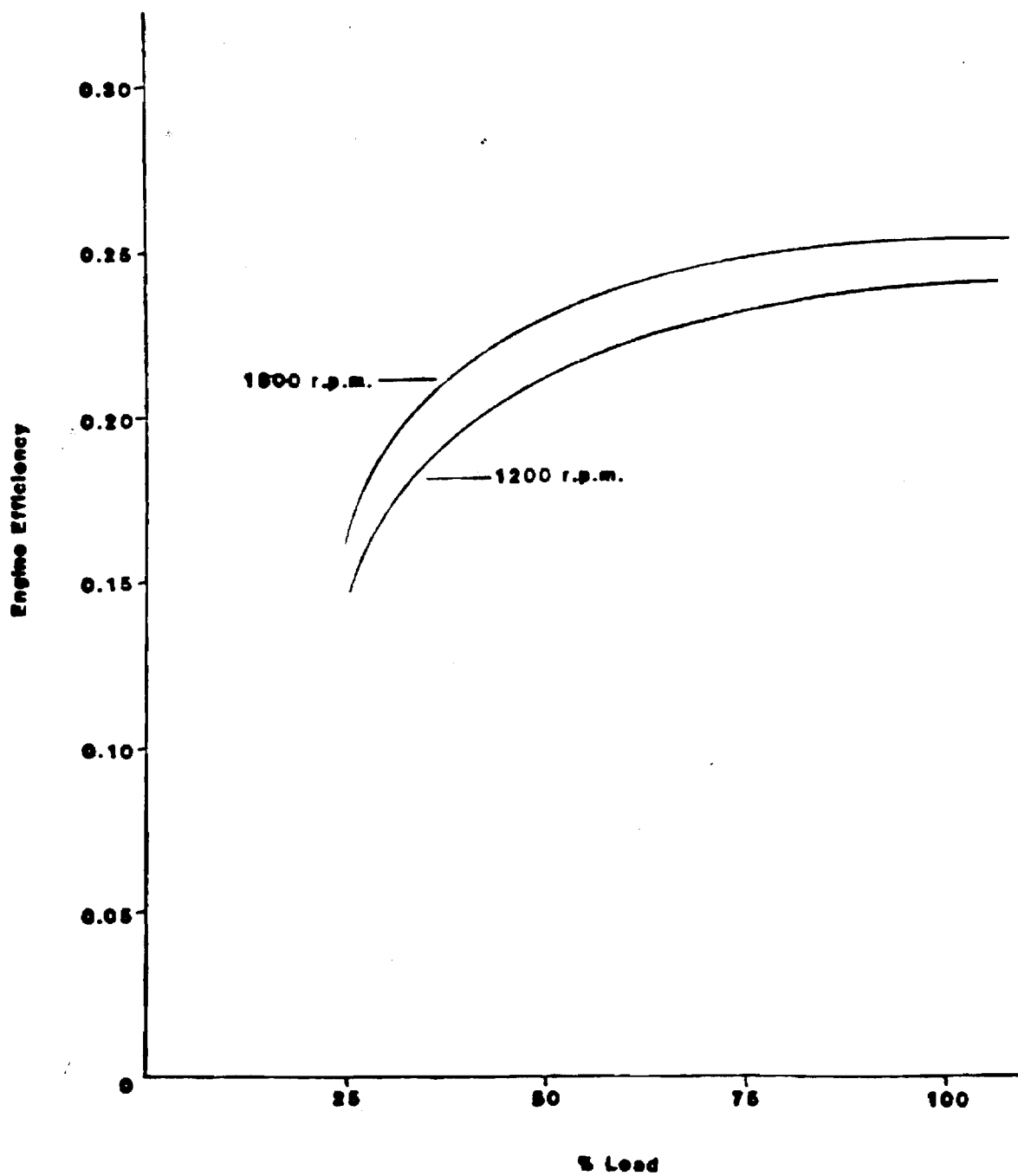
A separate kilowatt hour meter accumulated the electrical consumption of these accessories. The average kwhr consumption was 1.91 kwhr per hour of heat pump running time. This compares with the gas consumption of 0.67 therms per hour. At a 3.5 ratio for electrical energy cost to gas energy cost (6.5 ¢/kwhr and 55 ¢/therm), the electrical accessories energy cost is 25% of the total heat pump system operating cost.

Performance Improvements

Changes for improved efficiency performance would be to retrofit the heat pump with a smaller displacement engine. The present Ford 2274E 1600 cc engine is

operating at 25% of its rated full load. Figure 12 is a plot of engine efficiency vs. % load with engine speed as a parameter. From this figure it can be seen that at 25% loading and 1200 rpm, the engine's thermal efficiency is about 16%. If this engine were replaced by a Ford 2271E 1100 cc engine, the loading would increase to approximately 36%. From Figure 12, this increased load at 1200 rpm would result in a thermal efficiency of about 19%. This change alone would yield a 25% improvement in cooling COP and a about a 10% improvement in heating COP.

Figure 12: Engine Efficiency vs Load



SECTION V

AIR-TO-AIR I.C. ENGINE HEAT PUMP ANALYSIS

Introduction

While the water-to-water heat pump tested gave information on the critical engine/compressor subcomponent regarding the physical characteristics, maintenance, noise, and reliability of I.C. engine heat pumps, the efficiency information is not directly applicable to air-to-air heat pumps. However, the experimental data taken on just the engine/compressor yielding energy rates and efficiencies for varying condenser and evaporator pressures, makes it possible to accurately calculate the performance of the same engine/compressor operating with a given size of air condenser and evaporator coils.

The proposed system model diagram is given in Figure 13. Indoor and outdoor air are used as the heat source/sink for the vapor-compression cycle heat pump. Heat is removed from the source and rejected to the sink via two refrigerant-air heat exchanger coils. These coils are fixed in position, but the reversing valve makes possible a change in the direction of refrigerant flow to and from the compressor. The direction of refrigerant flow defines which coil is the condenser and which is the evaporator, and thereby defines the direction of heat flow.

Water is used as a transfer medium to remove combustion waste heat from the natural gas-fired IC engine. Heat removed from the engine block and exhaust gas is rejected

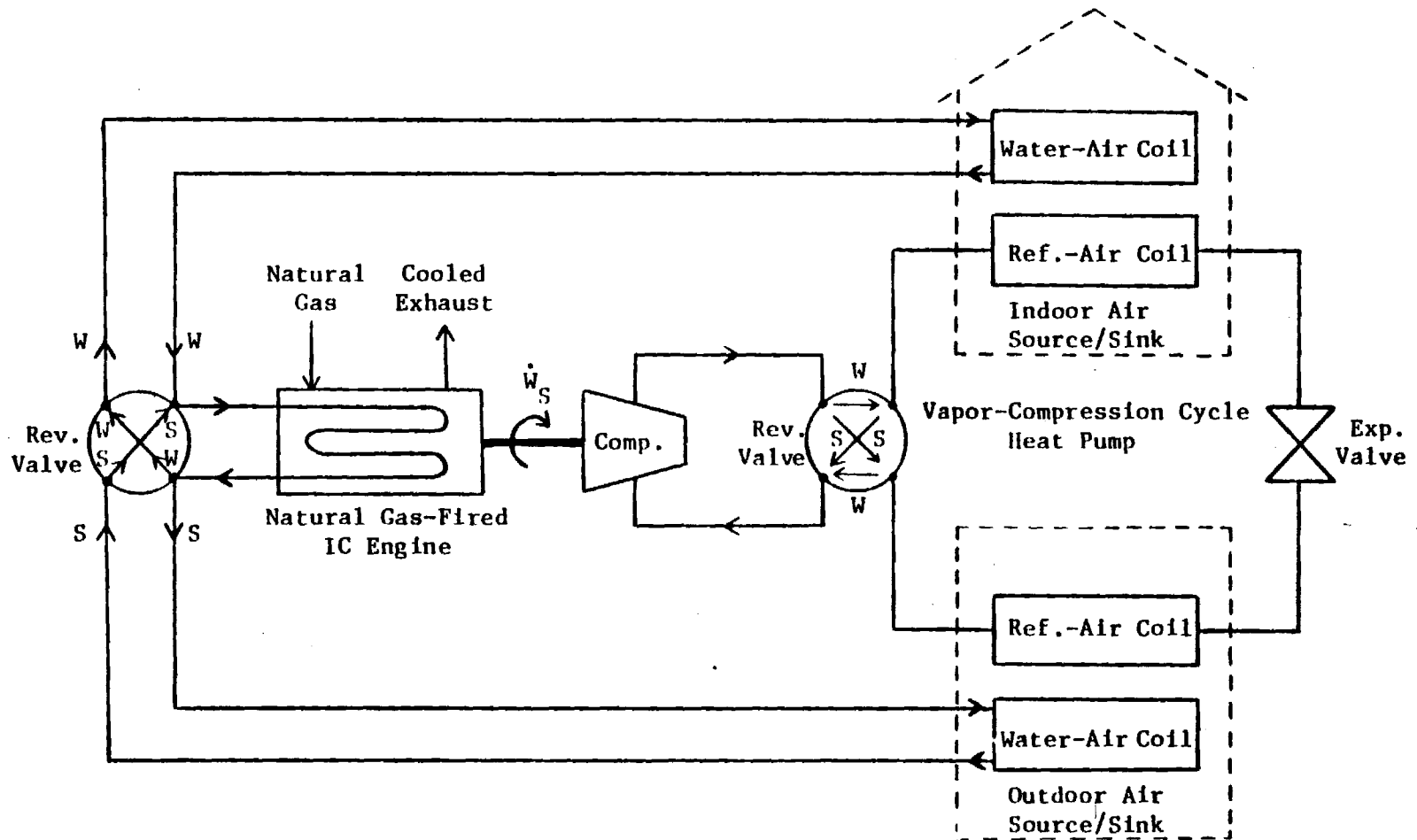


Figure 13: Air-to-Air Heat Pump Model Diagram

to the heat sink via one of two water-air heat exchanger coils. A reversing valve is used to circulate water from the engine to the indoor coil (for simultaneous engine cooling and space heating) or to the outdoor coil (for engine cooling during space cooling).

An analytical model is used to optimize the air coils for the engine/compressor tested. The engine/compressor performance and heat recovery data are taken as input from the experimental data shown in Section IV. The operating performance for space heating and cooling is determined as a function of the refrigerant-air coil air flow rates and heat exchanger UA's (overall heat transfer coefficient times total wall surface area) for a range of outdoor air temperatures. The annual gas consumption required for space heating and cooling is then calculated for fixed residential thermal characteristics ($UA = 680 \text{ Btu/hr-}^{\circ}\text{F}$) and weather data using the "bin" method of analysis. From this data, the indoor vs outdoor refrigerant coil UA is optimized. The annual performance for varying total indoor plus outdoor coil UA is then calculated so that the performance of this engine/compressor subcomponent operating in an air-to-air system may be determined for a given total air coil size and cost.

Analysis

The fundamental equations resulting from energy balances on the air flowing through the condenser and evaporator coils are:

$$\dot{Q}_{\text{Cond}} = (\dot{m}C_p)_{\text{Cond}}(T_o - T_i)_{\text{Cond}}$$

$$\dot{Q}_{\text{Evap}} = (\dot{m}C_p)_{\text{Evap}}(T_i - T_o)_{\text{Evap}}$$

where the C_p 's have been assumed constant and the temperature subscripts, i and o, refer to the air inlet and outlet of the coils. Another set of fundamental equations is obtained from counter-flow heat exchanger analysis.

These are:

$$\dot{Q}_{\text{Cond}} = [UA(\text{LMTD})]_{\text{Cond}} = UA \frac{T_o - T_i}{\ln \frac{T_{\text{Cond}} - T_i}{T_{\text{Cond}} - T_o}} \quad \text{Cond}$$

$$\dot{Q}_{\text{Evap}} = [UA(\text{LMTD})]_{\text{Evap}} = UA \frac{T_i - T_o}{\ln \frac{T_i - T_{\text{Evap}}}{T_o - T_{\text{Evap}}}} \quad \text{Evap}$$

where LMTD is the logarithmic mean temperature difference between the refrigerant and the air.

The heating and cooling requirements of the residential structure define the house load, from which the annual gas consumption can be determined. When the outdoor air temperature (or ambient air temperature) is below the desired indoor air temperature, the required heating rate is:

$$\dot{Q}_{\text{HL}} = (UA)_{\text{House}}(T_i - T_{\text{amb}})_{\text{Heating}}$$

heat losses. Similarly, when the ambient air temperature is above the desired indoor air temperature, the required cooling rate is:

$$\dot{Q}_{CL} = (UA)_{House} (T_{amb} - T_i)_{Cooling}$$

These equations assume that the house model UA is independent of the ambient air temperature. In a study by the National Bureau of Standards, the historical energy consumption for heating and cooling was correlated with weather data and good agreement was obtained using a constant house model UA. The bin method is used to estimate the annual heating and cooling loads from the last two equations.

The above equations represent the analytical heat pump model. Together, they comprise nine equations with unknowns. The unknowns are T_{Cond} , T_{Evap} , T_{oCond} , T_{oEvap} , \dot{Q}_{Cond} , \dot{Q}_{Evap} , \dot{Q}_{Rec} , \dot{Q}_{Gas} , and Q_{Gas}^{Annual} . The remaining variables are input parameters. These include the house model UA and the condenser and evaporator coil inlet air temperatures, air flow rates, and UA's. For heating, T_{iCond} is the desired indoor air temperature and T_{iEvap} is the outdoor air temperature. For cooling, the coils are reversed so that T_{iCond} is the outdoor air temperature and T_{iEvap} is the desired indoor air temperature. In matrix form, these equations are easily solved (for a given set of input conditions) by Gauss elimination. If these calculations are performed at the median outdoor air temperature of each bin, the results can be used to determine the total annual gas consumption for heating and cooling of the residential structure.

A computer program was set up on an APPLE II computer to run through all of these calculations.

Input Parameter Considerations

The desired indoor air temperatures are chosen to be 68°F for heating, and 76°F for cooling. These are normal conditions for residential and small commercial establishments. The house model UA is taken from a heating and cooling load study on the Atlanta residence accommodating the experimental heat pump system. In that study, the UA was estimated at 680 Btu/hr-°F for both heating and cooling. The analytical heat pump design is optimized for this house load. The results are applicable to varying house loads if all system components are scaled proportionally.

In cooling, approximately 75% of the heat removed from the indoor air was assumed to be in the form of sensible heat. The remaining 25% was assumed to be latent heat due to dehumidification. To account for this dehumidification, the specific heat of the air flowing through the evaporator in the cooling mode is increased by a factor of 33% (25%/75%).

The indoor air flow rate is taken to be constant at 2500 cfm. This is necessary to ensure a high enough condenser air outlet temperature (105-115°F) in the heating mode to prevent draft chill, and a low enough evaporator air outlet temperature (50-55°F) in the cooling mode for sufficient dehumidification. The outdoor air flow rate is varied proportionally with the outdoor coil UA, such that

the ratio of coil UA to volumetric flow rate for the outdoor coil is fixed at a typical value of $2.0 \frac{\text{Btu/hr-}^{\circ}\text{F}}{\text{cfm}}$.

Three locations, Atlanta, Chicago, and Orlando, are chosen as having representative average, cold, and warm climates. The weather data (hours per year at each temperature bin) for these cities is found in U.S. Air Force Manual 88-29. In climates much colder than Chicago's, the heat pump may become less cost effective than direct heating systems because of the lower outdoor air (source) temperatures. In climates much warmer than Orlando's, the natural gas heat pump begins to lose its advantage over the electric heat pump because of the reduced heating hours.

Performance Optimization

The optimum heat pump performance for each city is determined by varying the ratio of indoor coil UA to outdoor coil UA. The optimum UA ratio, for a fixed total coil UA (indoor coil UA plus outdoor coil UA), or a fixed total coil cost, is defined as that yielding the lowest annual gas consumption. The annual gas consumption is calculated for total coil UA's of 2500, 5000, 10000, and 15000 Btu/hr- $^{\circ}\text{F}$ at various UA ratios. The results of these calculations are graphed in Figures 14-16.

A curve is drawn through the optimum performance points in each of the graphs, and it is expected that the optimum performance for other values of total coil UA lies along these curves. The shape of these optimum performance curves is explained by considering that the total annual gas consumption is the sum of the annual gas consumption

for both heating and cooling. The optimum UA ratio for heating decreases with increasing total coil UA, while that for cooling increases with increasing total coil UA. The degree of interaction between the two separate performance curves is dependent upon the heating and cooling load requirements. Listed in Table 11 are the heating and cooling load for each city, along with the optimum heating, cooling, and overall UA ratios. In Chicago, where the heating load requirement is predominant, the optimum overall performance is essentially determined by the optimum heating performance. On the other hand, in Orlando, where the cooling load requirement is on the same order as the heating load requirement, the optimum overall performance is essentially determined by the optimum cooling performance (more gas is required per Btu of cooling than per Btu of heating).

The heat pump design for optimum performance can be determined from Figures 14-16 for any total coil UA. For a total coil UA of 10000 Btu/hr- $^{\circ}$ F, the optimum UA ratio is found to be 0.6 for Atlanta, Chicago, and Orlando. Then for optimum performance, the heat pump design would include an indoor coil with a UA of 3750 Btu/hr- $^{\circ}$ F and an outdoor coil with a UA of 6250 Btu/hr- $^{\circ}$ F. The heating and cooling COP's and rates at optimum performance for this design are plotted in Figure 17 as functions of the outdoor air temperature. Since the optimum UA ratio for a total coil UA of 10000 Btu/hr- $^{\circ}$ F was found to be the same for Atlanta, Chicago, and Orlando, the curves in Figure 17

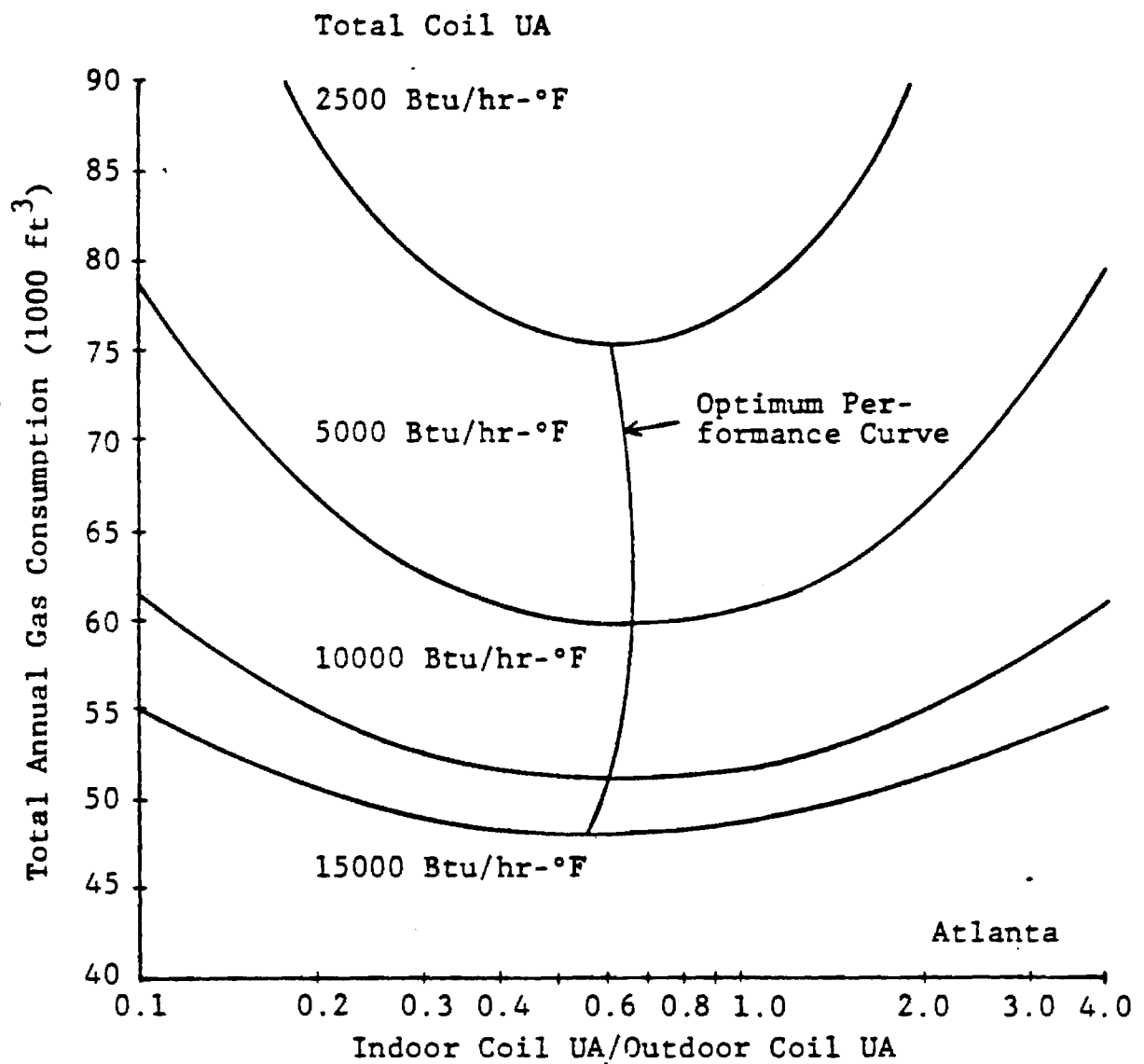


Figure 14: Annual Gas Consumption
versus Coil UA Ratio, Atlanta

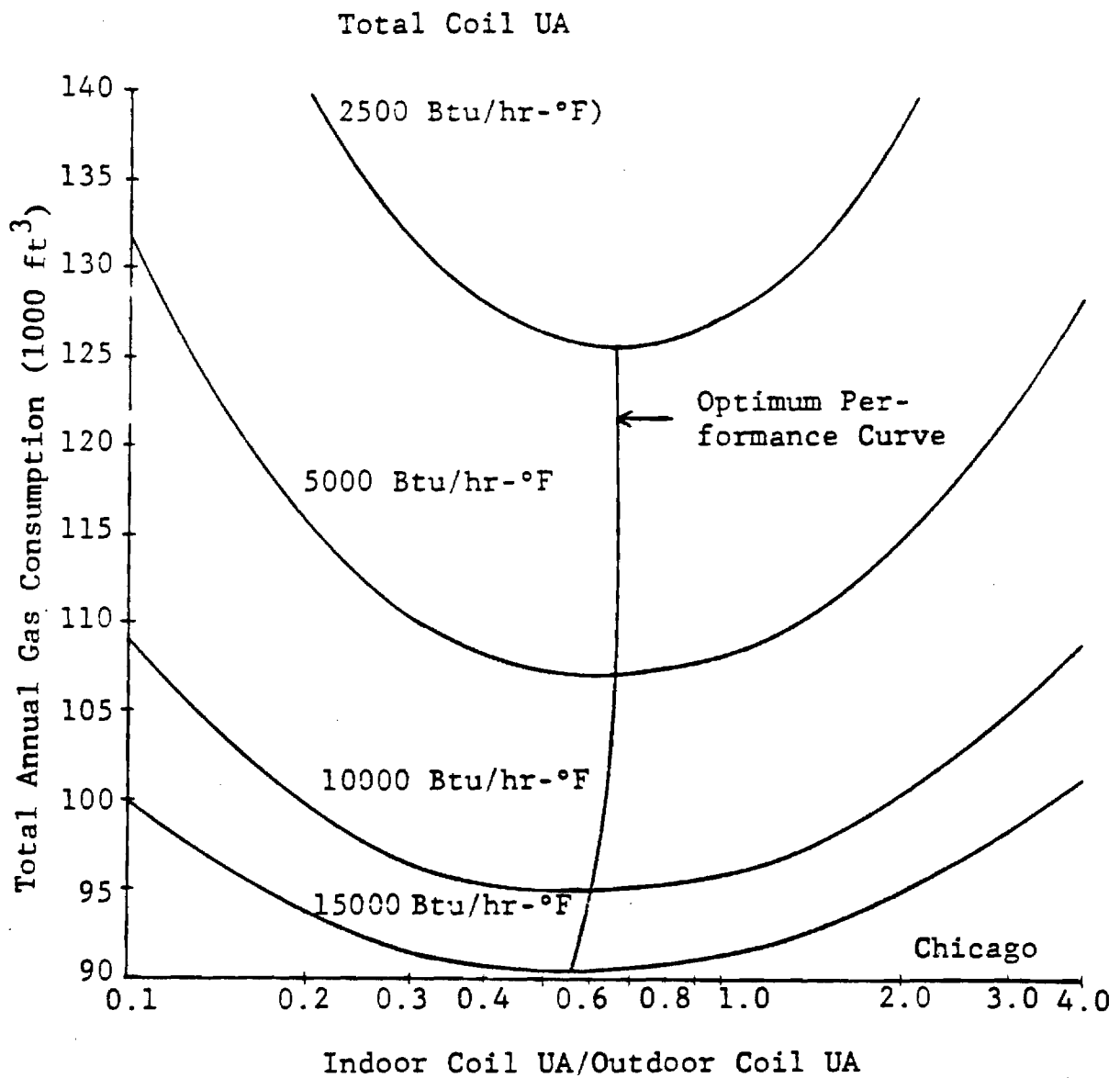


Figure 15: Annual Gas Consumption
versus Coil UA Ratio, Chicago

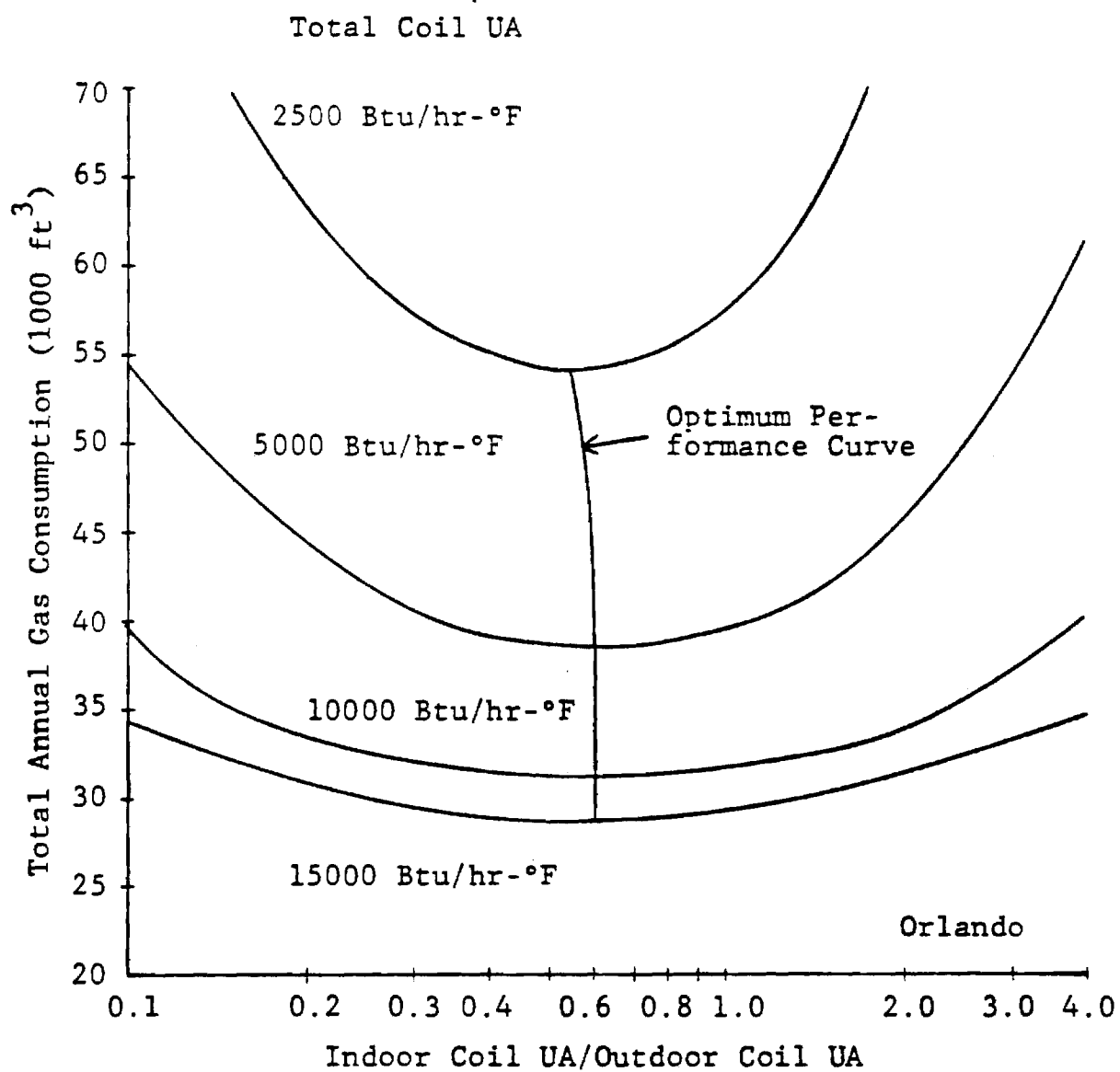


Figure 16: Annual Gas Consumption
versus Coil UA Ratio, Orlando

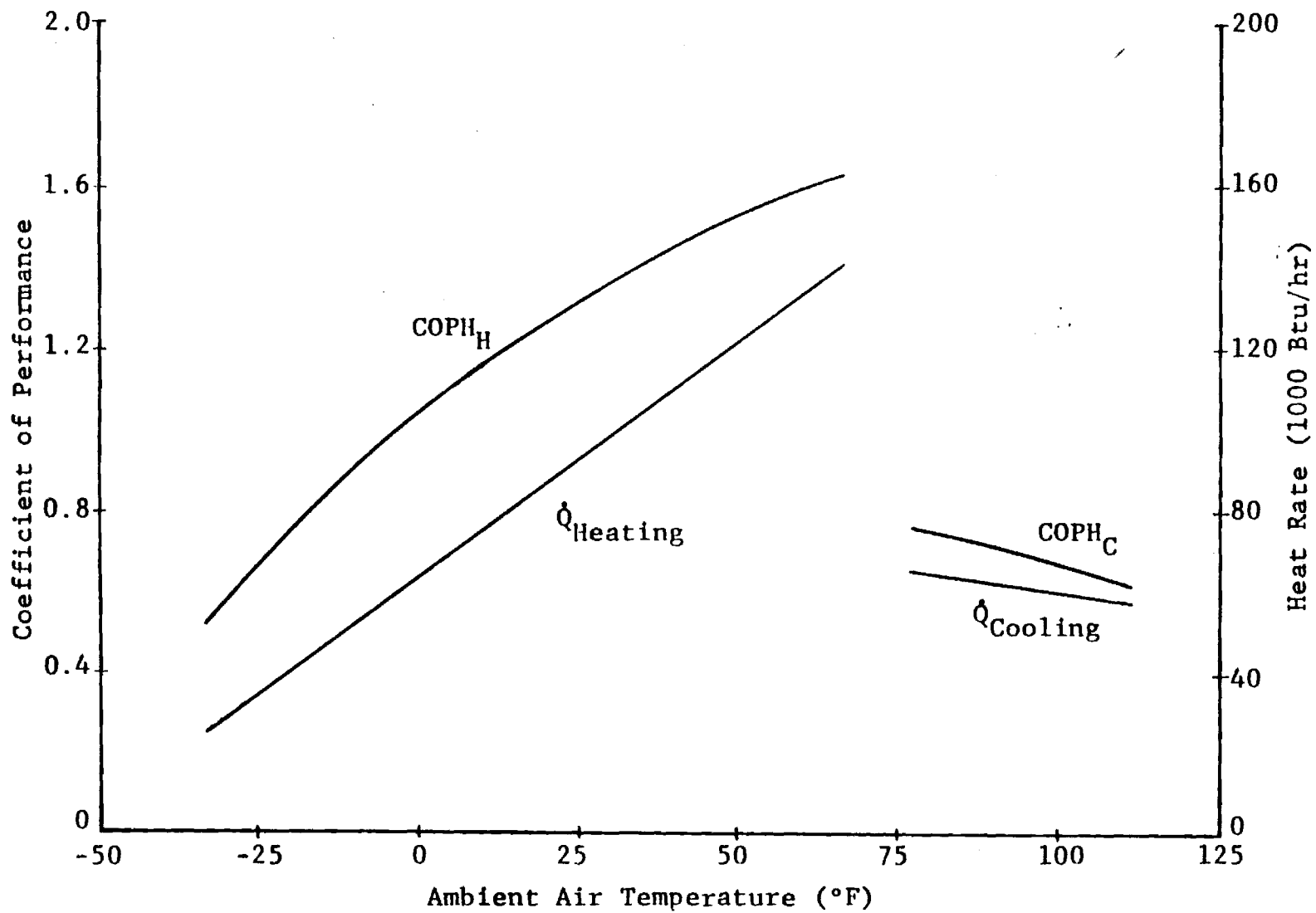


Figure 17: Heating and Cooling COP's and Rates at Optimum Performance
for Total Coil UA = 10000 Btu/hr-°F

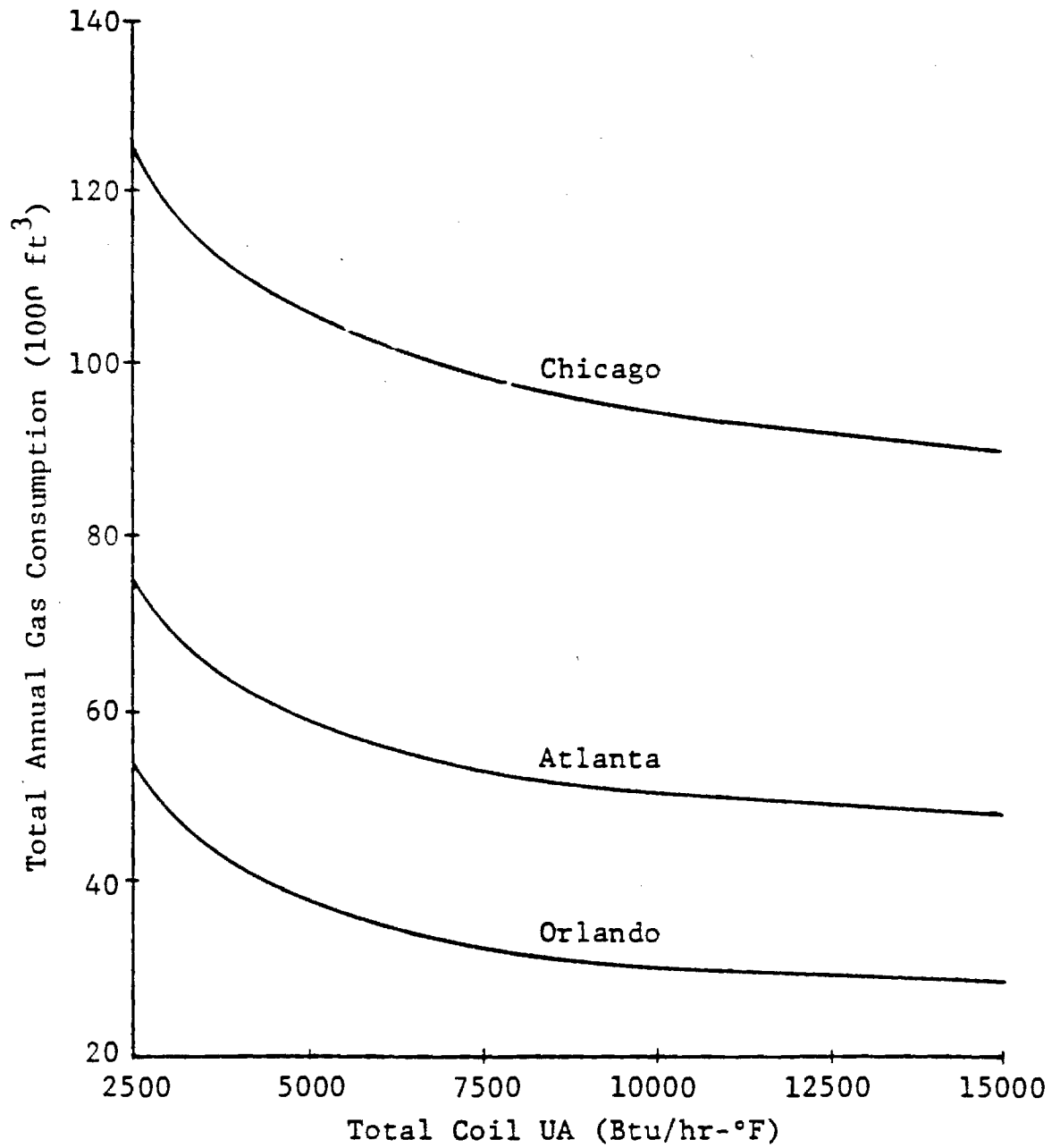


Figure 18: Annual Gas Consumption
at Optimum Performance

Table 11: Optimum Coil UA Ratios

City 1 - Annual Heating Load Requirement (Btu) 2 - Annual Cooling Load Requirement (Btu)	Total Coil UA (Btu/hr-°F)	Optimum UA Ratio ($\frac{\text{Indoor Coil UA}}{\text{Outdoor Coil UA}}$)		
		Heating	Cooling	Overall
Atlanta 1 - 59,866,860 2 - 8,255,880	5,000 10,000 15,000	0.65 0.60 0.55	0.60 0.60 0.60	0.65 0.60 0.55
Chicago 1 - 122,283,380 2 - 3,957,600	5,000 10,000 15,000	0.65 0.60 0.55	0.55 0.60 0.60	0.65 0.60 0.55
Orlando 1 - 20,342,880 2 - 13,623,460	5,000 10,000 15,000	0.70 0.60 0.60	0.60 0.60 0.60	0.60 0.60 0.60

Table 12: Annual Heating and Cooling COP's
at Optimum Performance

City	Total Coil UA (Btu/hr-°F)	COP _H	COP _C
Atlanta	5000	1.28	0.56
	10000	1.45	0.73
	15000	1.52	0.80
Chicago	5000	1.19	0.56
	10000	1.33	0.73
	15000	1.39	0.80
Orlando	5000	1.35	0.56
	10000	1.53	0.73
	15000	1.61	0.80

apply to all three cities. The annual heating and cooling COP's at optimum performance are presented in Table 12.

The annual gas consumption at optimum performance (from Figures 14-16) is given in Figure 18 as a function of total coil UA. This figure provides an indication of the savings in annual gas consumption that would be gained through the use of coils with a higher total UA. As one might expect, the annual gas savings diminishes with increasing increments of total coil UA.

Conclusions

This air-to-air I.C. engine heat pump analysis using actual engine/compressor data, shows that the indoor coil UA should be about 0.6 of the outdoor coil UA and that for a total UA above 10000 Btu/hr-°F, gas savings diminish rapidly. The heat pump size and coil UA should be proportional to the house thermal load, so that for a house half the size of that used, (UA = 680 Btu/hr-°F), the total air coil UA should be scaled down to one-half as well as all other components.

The resulting heating and cooling COP's for this particular package with a typical total inside plus outside coil UA of 10000 Btu/hr-°F, would then be;

	<u>COP_H</u>	<u>COP_C</u>
Atlanta	1.45	0.73
Chicago	1.33	0.73
Orlando	1.53	0.73

Since the engine used to obtain data for this analysis was only 25% loaded, a more closely matched engine/compressor, (smaller engine), would improve these air-to-air heat pump COP's.

information also was obtained. The next potential problem areas which need study are long term engine durability, manufacturing and installation costs, air-to-air system performance, and defrost control.

The automotive derivative natural gas industrial engine tested has shown this class of engine has merit. Continued study of available engines is needed to determine their suitability regarding size, cost, and long term life. Many are available.

Specifically, engine tests need to be started on engines that are found to be suitably sized and available for this application. After making necessary modifications for gasification, such as cam shaft and compression ratio changes, two or three engines of each type should be run continuously at constant speed and two or three should be run on a thirty minute start/stop basis. Long term engine life information can then be gained within about two years.

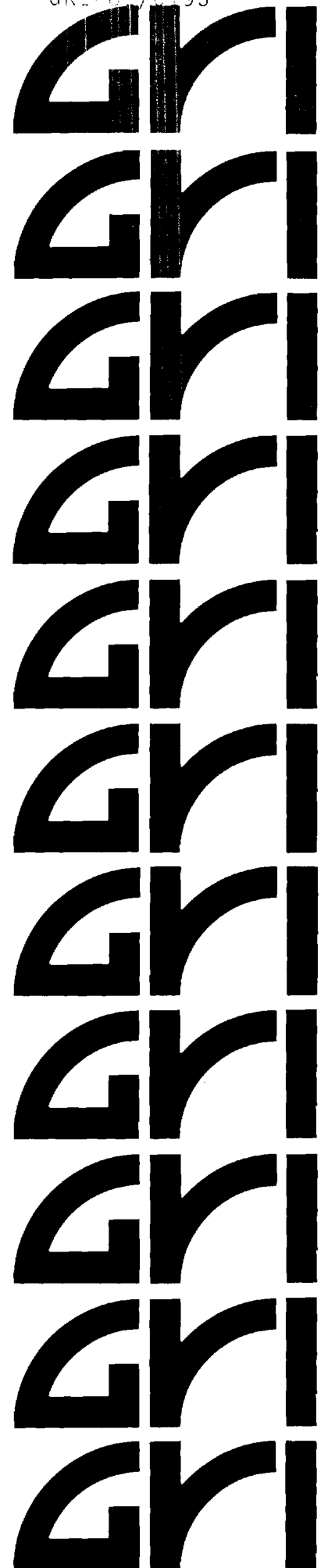
Simultaneously, an air-to-air heat pump with a matched engine/compressor should be field tested studying efficiencies and optimizing defrost strategy.

NATURAL GAS I.C. ENGINE HEAT PUMP STUDY

FINAL REPORT

April 1983

**Gas Research Institute
8600 West Bryn Mawr Avenue
Chicago, Illinois 60631**



NATURAL GAS I. C. ENGINE HEAT PUMP STUDY

FINAL REPORT
(June 1981 - September 1982)

Prepared by
Sam V. Shelton, Ph.D.

School of Mechanical Engineering
Georgia Institute of Technology
Atlanta, Georgia 30332
Project No. E25-650

for
GAS RESEARCH INSTITUTE
Contract No. 5081-341-0503

GRI Project Manager
Les Wright
Gas Fired Heat Pumps

April 1983

GRI DISCLAIMER

LEGAL NOTICE This report was prepared by the Georgia Institute of Technology as an account of work sponsored by the Gas Research Institute (GRI). Neither GRI, members of GRI, nor any person acting on behalf of either.

- a. Makes any warranty or representation, express or implied, with respect to the accuracy, completeness, or usefulness of the information contained in this report, or that the use of any apparatus, method, or process disclosed in this report may not infringe privately owned rights; or
- b. Assumes any liability with respect to the use of, or for damages resulting from the use of, any information, apparatus, method, or process disclosed in this report.

REPORT DOCUMENTATION PAGE	1. REPORT NO. GRI-81/0193 Final Report	2.	3. Recipient's Accession No.
4. Title and Subtitle Natural Gas I.C. Engine Heat Pump Study		5. Report Date April 1983	
6. Author(s) Sam V. Shelton		7. Performing Organization Rept. No. E25-650	
8. Performing Organization Name and Address Georgia Institute of Technology School of Mechanical Engineering Atlanta, Georgia 30332		9. Project/Task/Work Unit No. GRI-81/0193 10. Contract(C) or Grant(G) No. (C) 5081-341-0503 (G)	
11. Sponsoring Organization Name and Address gri - Gas Research Institute 8600 West Bryn Mawr Avenue Chicago, Illinois 60631		12. Type of Report & Period Covered Final Report 6/81-9/82 13.	
14. Supplementary Notes To experimentally assess the technical performance of a natural gas I.C. engine heat pump using commercially available technology.			
15. Abstract (Limit: 200 words) The I.C. engine heat pump is one gas heat pump technology which uses existing component technology; it therefore offers the possibility of early development of a commercially viable gas heat pump. In order to assess the development barriers, this project carried out field tests on an I.C. engine heat pump providing heating and cooling to a residence over two heating and two cooling seasons. Experimental results showed steady state and seasonal heating coefficients of performance (COP) of 1.4 to 1.5 with cooling COP's 0.5 to 0.6. These efficiencies were in spite of the low 16% efficiency of the 1600 cc four cylinder industrial engine due to being loaded only to about 25%. Using experimental engine/compressor data in conjunction with an air-to-air heat pump system configuration model, seasonal heating COP's of 1.33, 1.45, and 1.53 were predicted for Chicago, Atlanta, and Orlando respectively. Cooling COP's were 0.73 in all three cities. Higher engine loading would improve all COP's. No maintenance was required for the 2400 hours of operation during two heating and two cooling seasons. Noise in the equipment room was 63 dB with 61 dB measured outside next to the exhaust outlet.			
16. Document Analysis a. Descriptors			
17. Identifiers/Open-Ended Terms			
18. COSATI Field/Group Availability Statement: 19. Security Class (This Report) 20. Security Class (This Page) 21. No. of Pages 22. Price			

Title	Natural Gas I.C. Engine Heat Pump Study
Contractor	Georgia Institute of Technology
Principal Investigator	S. V. Shelton, Ph.D.
Report Period	May 31 - October 1982 Final Report
Objective	To experimentally assess the technical performance of a natural gas I.C. engine heat pump using commercially available technology.
Technical Perspective	Space heating and cooling constitutes the major use of natural gas in the U.S. Increasing the efficiency of this process would, therefore, provide a dramatic impact on the industry. The I.C. engine heat pump is one gas heat pump technology which uses existing component technology; it therefore offers the possibility of early development of a commercially viable gas heat pump. In order to assess the development barriers, this project carried out field tests on an I.C. engine heat pump providing heating and cooling to a residence over two heating and two cooling seasons performance of the system.
Results	<p>Experimental data from a gas I.C. engine water-to-water heat pump showed steady state and seasonal heating coefficients of performance (COP) of 1.4 to 1.5 with cooling COP's 0.5 to 0.6. These efficiencies were in spite of the low 16% efficiency of the 1600 cc four cylinder industrial engine which was due to being loaded only to about 25% of full load.</p> <p>Using experimental engine/compressor data in conjunction with an air-to-air heat pump system configuration model, seasonal heating COP's of 1.33, 1.45 and 1.53 were predicted for Chicago, Atlanta and Orlando respectively. Cooling COP's were 0.73 in all three cities. Higher engine loading would improve all COP's.</p> <p>No maintenance was required for the 2400 hours of operation during two heating and two cooling</p>

seasons. Oil analysis showed the oil was fully servicable. The only reliability problems encountered were a few failures to start during a fixed five second starter engagement period. Noise in the equipment room was 63 dB with 61 dB measured outside next to the exhaust outlet.

The project has shown that automotive derivative gas industrial engines operating at low speed have the necessary efficiency, noise, maintenance, and short term reliability to serve as the prime mover for an I.C. engine heat pump. It is recommended that available small I.C. engines suitable for I.C. engine heat pumps be surveyed and that selected models be tested for long life characteristics. Also, it is recommended that an air-to-air system be field tested to verify performance and to study outside coil defrost control strategies.

Technical Approach

A West German manufactured water-to-water packaged gas heat pump was installed in an Atlanta residence and supplied all space heating and cooling over two heating and two cooling seasons. Well water was used as a heat sink and source and was disposed afterward into a creek. An inside water circulating loop carried either hot or chilled water produced by the heat pump through a water coil in the air handler. The hot water loop passed through the condenser, exhaust gas heat exchanger, and engine cooling jacket. The system was fully instrumented for both long term and transient data acquisition. Total accumulated heating and cooling energies were measured along with accumulated gas flow over entire seasons to calculate seasonal performance factors (seasonal COP's). Steady state and transient performance was measured by a microcomputer data acquisition system with a one minute time resolution. Performance of the engine/compressor subcomponent was also measured as a function of condenser and evaporator temperature. A model was developed to use this engine/compressor data in conjunction with air condenser and evaporator coils. Optimization of the indoor vs. outdoor coil size was established. Also, performance with varying combined total air coil sizes was calculated for Chicago, Atlanta, and Orlando.

Project Implications

GRI plans to initiate another program on internal combustion engine driven heat pumps with appropriate manufacturers. The intent is to develop a heat pump

that will have a low unit cost and near term market entry. During the first half of 1983, discussions have taken place between GRI and candidate engine manufacturers to determine their interest in teaming with a qualified space conditioning manufacturer to develop a gas engine heat pump. Proposals are being evaluated, and a program will be initiated by the end of 1983.

TABLE OF CONTENTS

	<u>Page</u>
RESEARCH SUMMARY	iii
LIST OF TABLES	vii
LIST OF FIGURES.	viii
Section	
I. INTRODUCTION	1
Background Fundamental Thermodynamics	
II. I.C. ENGINE HEAT PUMP SYSTEM DESIGN.	17
Description of Experimental System System Controls	
III. INSTRUMENTATION	27
Long Term Monitoring Computer Data Acquisition	
IV. EXPERIMENTAL PERFORMANCE	33
Introduction System Seasonal Performance Engine/Compressor Performance System Steady State Performance Variable Speed Performance Cycling Effects Reliability and Maintenance Noise Levels Electrical Accessory Power Performance Improvements	
V. AIR-TO-AIR I. C. ENGINE HEAT PUMP ANALYSIS	60
Introduction Analysis Input Parameter Consideration Performance Optimization Conclusions	

Section	Page
VI. CONCLUSIONS AND RECOMMENDATIONS	77
Introduction	
Experimental Performance	
Maintenance, Reliability, and Noise	
Analytical Air-to-Air Performance	
Recommendations	

LIST OF TABLES

Table	Page
1. Florian Bauer GWW 35 Heat Pump Specifications	18
2. Experimental System Valve Positions and Pump Operation	23
3. Long Term Performance Raw Data	35
4. Steady-State Operating Conditions	44
5. Averaged Experimental Data	45
6. Confidence Intervals for Increase in Condenser Temperature	46
7. Confidence Intervals for Increase in Evaporator Temperature	47
8. Results of Multiple Variable, Linear Regression Analysis	48
9. Steady State Performance	49
10. Oil Analysis	55
11. Optimum Coil UA Ratios	73
12. Annual Heating and Cooling COP's at Optimum Performance	74

LIST OF ILLUSTRATIONS

Figure	Page
1. Energy Flow Diagram of a Heat-driven Heat Pump . .	6
2. Energy Flow Diagram of an Ideal Heat Engine-driven Heat Pump	8
3. Schematic and T-S Diagram of Actual Vapor-Compression Cycle	12
4. I.C. Engine Heat Pump Concept	16
5. Experimental System Schematic	22
6. Heat Pump System Controls	26
7. Computer Data Acquisition Schematic	32
8. Seasonal System Heating Performance	37
9. Seasonal System Cooling Performance	38
10. Heat Pump Energy Rates vs. Speed	51
11. Heat Pump Heating COP vs. Speed	51
12. Engine Efficiency vs. Load	59
13. Air-to-Air Heat Pump Model Diagram	61
14. Annual Gas Consumption versus Coil UA Ratio, Atlanta	68
15. Annual Gas Consumption versus Coil UA Ratio, Chicago	69
16. Annual Gas Consumption versus Coil UA Ratio, Orlando	70
17. Heating and Cooling COP's and Rates at Optimum Performance for Total Coil UA = 10000 Btu/hr-°F	71
18. Annual Gas Consumption at Optimum Performance . .	72

SECTION I

INTRODUCTION

Background

Thermal environmental control presently accounts for the greatest percentage of total energy use in the residential and commercial sectors of the U.S. In 1977, the energy required for the heating and cooling of residential and commercial establishments alone represented 21% of the U.S. total energy consumption and two-thirds of the U.S. total natural gas consumption. Increasing the efficiency for space heating and cooling would therefore amount to a significant reduction in the nation's total energy use. From the second law of thermodynamics, the maximum efficiency possible for space heating and cooling is that obtained by the ideal (reversible) heat-driven heat pump, an efficiency over 3 times that of ideal natural gas furnaces and boilers. In practice, this ideal efficiency can be approached but never attained.

One of the more promising practical natural gas heat pump systems that has emerged in recent years is the natural gas, internal combustion (IC) engine-driven heat pump. This system offers an attractive efficiency (performance) for space heating, as compared with other heating system such as the gas furnace, electric heat pump, and electric resistance heating. At the same time, it is capable of a space cooling performance

comparable to that of the electric heat pump (i.e., electric air conditioner).

In the U.S., I.C. engines serving as stationary prime movers were displaced in the 1930's and 1940's by electric drives accompanying the rural electrification program. Therefore, small [less than 2000 cc] I.C. engine technology in this country has moved toward high speed, short term, high specific power output to serve automobile, portable drive, and emergency drive applications. Therefore, in this country, small I.C. engines are not viewed as being applicable to stationary, high running hours service.

In Europe, however, the use of small I.C. engines in stationary applications is still considered viable and a small market has been maintained. These are low speed, lightly (50%) loaded engines which are designed specifically for the stationary application, or are automobile engines modified for that service.

For this reason, when energy prices escalated in the mid-70's, Europe started looking seriously at the I.C. engine heat pump as a viable energy conservation concept.

In September 1978, a conference on "Drive for Heat Pumps" was held at the University of Essen, West Germany at which the investigation of electric motors vs. combustion motors for heat pumps was the primary topic. The forward of the conference proceedings states: "This issue of Drives for

Heat Pumps, as well as the conference in Essen, show that either means of drive has its justification and that there is ample room for both of them on the market." Eleven of the 17 papers presented were on I.C. engine drives for heat pumps. One paper was a survey of 14 I.C. engine heat pump systems installed and operating. Since then, several hundred operating units have been installed in the field and major corporations have started development projects.

In order to assess experimentally the potential problems and opportunities for I.C. engine driven heat pumps, a heating and cooling system for a single family residence was designed, built, and tested around the Florian Bauer GWW 35 natural gas driven heat pump package manufactured in West Germany. This heat pump package has evolved over the past four years so that many of the packaging, noise, vibration, and accessory problems have now been resolved. Purchasing this package allowed this project to focus on the system concept rather than its peripheral problems. The objective was to identify experimentally the noise, vibration, reliability, and maintenance problems of the I.C. engine gas heat pump concept and to quantify the field efficiency of this particular system. The project results will allow a more accurate assessment of the potential of the I.C. engine heat pump than has been previously possible.

Fundamental Thermodynamics

The heat pump is a device which operates in a thermodynamic cycle and requires energy input to pump heat from a low temperature reservoir (heat source) to a high temperature reservoir (heat sink). As a heating system, the heat pump extracts heat from the surroundings (such as outdoor air or ground water) and delivers it, along with the heat equivalent of the energy input, to a conditioned space. By extracting heat from the surroundings, the heat pump makes more energy available for heating than is required for input. This gives the heat pump its dramatic advantage over conventional, direct heating systems. As a cooling system, the heat pump removes heat from a conditioned space and rejects it, with the heat equivalent of the energy input, to the surroundings.

The first law efficiency of a thermodynamic system is defined as the ratio of energy sought to energy that costs. For heat pumps, this ratio is expressed as the coefficient of performance. The energy sought is either the heating effect or the cooling effect, and the energy that costs is the energy input. The coefficient of performance based on work energy input is given the notation COPW, while COPH is used to denote the performance based on heat energy input. Subscripts H and C are used to indicate whether the energy sought is heating or cooling.

When energy is supplied to the heat pump in the form of heat, the result is a heat-driven heat pump. An energy flow diagram for the heat-driven heat pump is presented in Figure 1. As a result of heat input Q_S , at temperature T_S , a quantity of heat Q_C is removed from a reservoir at temperature T_C , and a quantity of heat Q_H is rejected to a reservoir at temperature T_H . From a simple energy balance on this system:

$$Q_S = Q_H - Q_C \quad (1)$$

and the coefficients of performance for heating and cooling are:

$$\text{COPH}_H = \frac{Q_H}{Q_S} = \frac{Q_H}{Q_H - Q_C} \quad (2)$$

$$\text{COPH}_C = \frac{Q_C}{Q_S} = \frac{Q_C}{Q_H - Q_C} = 1 - \text{COPH}_H$$

The maximum performance theoretically possible would be that achieved by a reversible heat-driven heat pump. From the second law of thermodynamics, the Clausius inequality requires that:

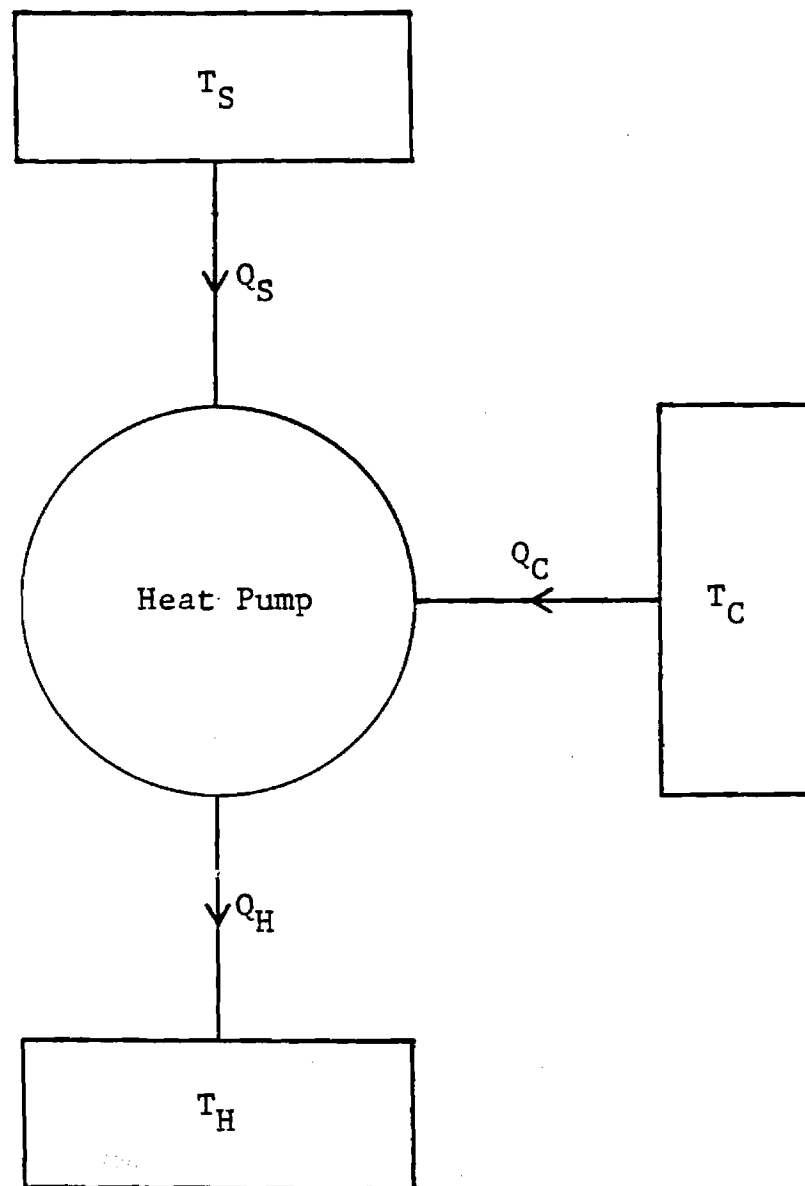


Figure 1. Energy Flow Diagram of a
Heat-Driven Heat Pump

$$\oint \frac{\delta Q}{T} \leq 0 \quad (3)$$

where the equality holds for reversible processes. Then for the reversible heat-driven heat pump:

$$\oint \frac{\delta Q}{T} = \frac{\delta Q_S}{T_S} + \frac{\delta Q_C}{T_C} - \frac{\delta Q_H}{T_H} = 0 \quad (4)$$

or

$$\frac{Q_S}{T_S} + \frac{Q_C}{T_C} = \frac{Q_H}{T_H} \quad (5)$$

Combining equations (2) and (5), and simplifying, yields:

$$(\text{COPH}_H)_{\text{rev.}} = \left(\frac{1 - T_C/T_S}{1 - T_C/T_H} \right) \quad (6)$$

$$\begin{aligned} (\text{COPH}_C)_{\text{rev.}} &= \left(\frac{T_C}{T_H} \right) \left(\frac{1 - T_C/T_S}{1 - T_C/T_H} \right) \\ &= 1 - (\text{COPH}_H)_{\text{rev.}} \end{aligned}$$

A system utilizing a Carnot cycle heat engine to drive a Carnot cycle heat pump would represent a reversible heat-driven heat pump. Such a system is shown in Figure 2. The heat engine operates between temperatures T_S and T_C to produce shaft work W_S . From an energy balance on the heat engine:

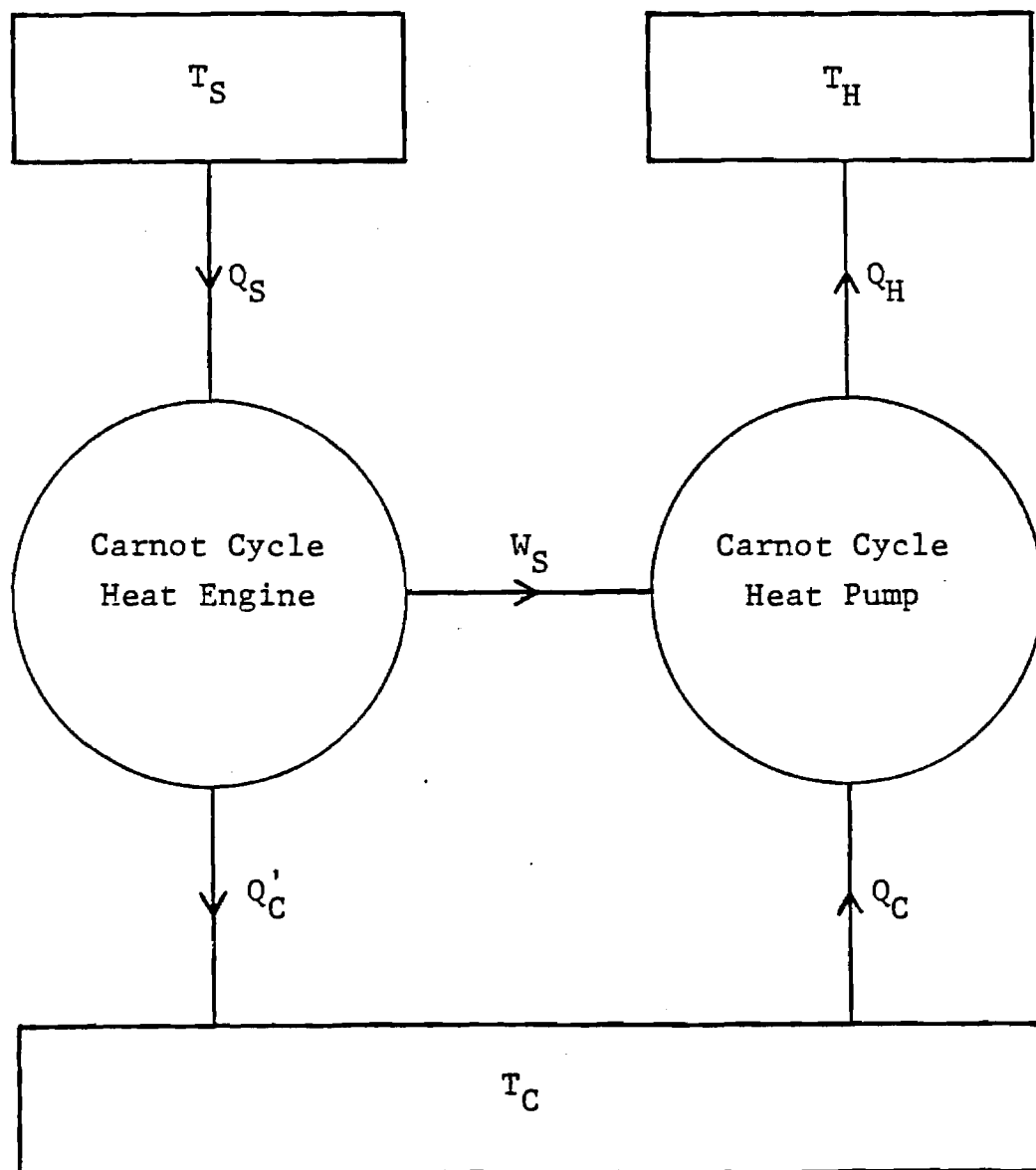


Figure 2. Energy Flow Diagram of an
Ideal Heat Engine-Driven Heat Pump

$$W_S = Q_S - Q_C' \quad (7)$$

and the engine efficiency is:

$$\eta = \frac{W_S}{Q_S} = \frac{Q_S - Q_C'}{Q_S} \quad (8)$$

Since all processes of the Carnot cycle heat engine are reversible, equation (3) yields:

$$\frac{Q_S}{T_S} = \frac{Q_C'}{T_C} \quad (9)$$

Equation (8) then simplifies to:

$$\eta_{\text{Carnot}} = 1 - \frac{T_C}{T_S} \quad (10)$$

The heat pump receives work input, W_S , from the heat engine to remove heat, Q_C , from the reservoir at T_C and reject heat, Q_H , to the reservoir at T_H . From an energy balance on the heat pump:

$$W_S + Q_C = Q_H \quad (11)$$

and the coefficients of performance are:

$$\text{COP}_{W_H} = \frac{Q_H}{W_S} = \frac{Q_H}{Q_H - Q_C} \quad (12)$$

$$\text{COPW}_C = \frac{Q_C}{W_S} = \frac{Q_C}{Q_H - Q_C}$$

Since the Carnot cycle heat pump can be represented thermodynamically as a Carnot cycle heat engine operating in reverse, and all processes of the Carnot cycle heat engine are reversible, all processes of the Carnot cycle heat pump must also be reversible. Then equation (3) yields:

$$\frac{Q_H}{T_H} = \frac{Q_C}{T_C} \quad (13)$$

and equations (12) simplify to:

$$(\text{COPW}_H)_{\text{Carnot}} = \frac{1}{1 - T_C/T_H} \quad (14)$$

$$(\text{COPW}_C)_{\text{Carnot}} = \frac{T_C/T_H}{1 - T_C/T_H}$$

$$= 1 - (\text{COPW}_H)_{\text{Carnot}}$$

The products of equations (10) and (14) yield the coefficients of performance for the combined system (i.e., the ideal heat engine-driven heat pump):

$$(\text{COPH}_H)_{\text{Ideal}} = (\eta)_{\text{Carnot}} (\text{COPW}_H)_{\text{Carnot}} \quad (15)$$

$$= \left(\frac{1 - T_C/T_S}{1 - T_C/T_H} \right)$$

$$(\text{COPH}_C)_{\text{Ideal}} = (\eta)_{\text{Carnot}} (\text{COPW}_C)_{\text{Carnot}}$$

$$= \left(\frac{T_C}{T_H} \right) \left(\frac{1 - T_C/T_S}{1 - T_C/T_H} \right) = 1 - (\text{COPH}_H)_{\text{Ideal}}$$

which are the same results obtained in equations (6).

Using typical temperatures for natural gas space heating/cooling, the ideal efficiencies for gas heat pumps may be calculated and compared with the ideal efficiencies of one for furnaces and boilers. For heating, typical values of T_C , T_S , and T_H are 20°F, 1000°F, and 140°F resulting in a COPH_H of 3.7. For typical space cooling values of 50°F, 1000°F, and 120°F for T_C , T_S , and T_H respectively, COPH_C is 5.4. This demonstrates the potential of the concept.

In practice, the Carnot cycle heat engine and Carnot cycle heat pump cannot be achieved because they require that all processes be reversible. Actual processes involve irreversibilities, such as frictional losses and heat transfer through finite temperature differences. An actual cycle can, at best, only approach the Carnot cycle efficiency or performance for a given application.

For heat pumps, the Carnot cycle performance is best approached by the actual vapor-compression cycle, which is shown schematically and on a temperature-entropy (T-S) diagram in Figure 3.

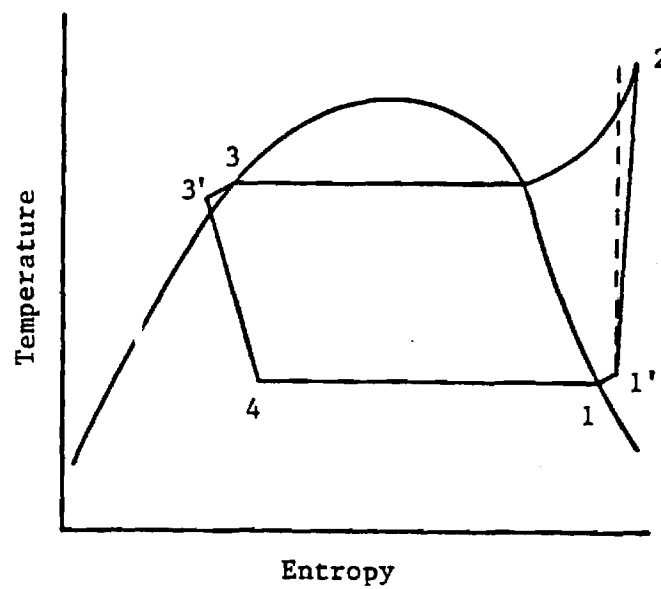
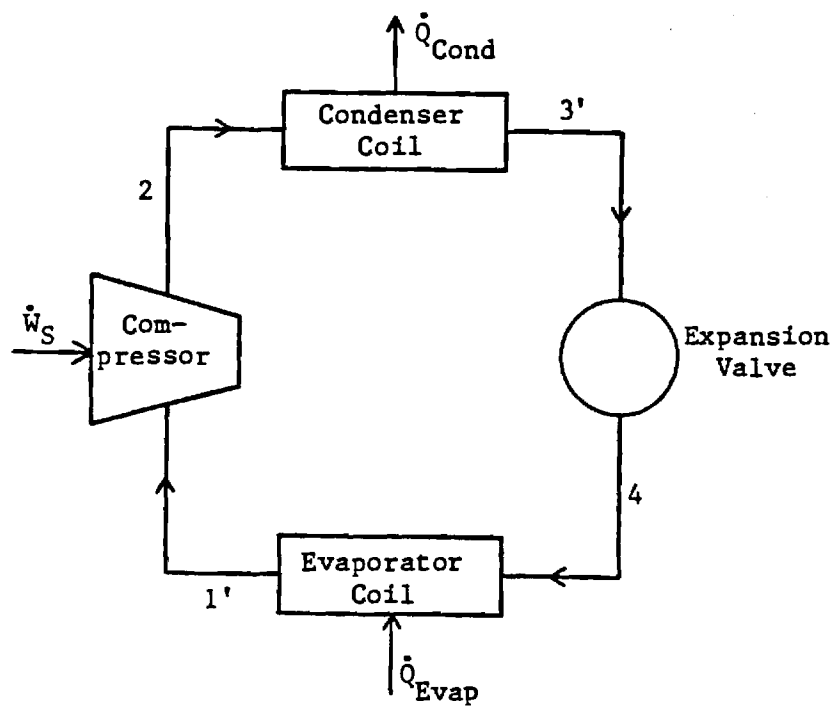


Figure 3. Schematic and T-S Diagram
of Actual Vapor-Compression Cycle

For the vapor-compression cycle heat pump, work is input to the compressor at a rate \dot{W}_S , heat is removed from a low temperature reservoir by the evaporator coil at a rate \dot{Q}_{Evap} , and heat is rejected to a high temperature reservoir from the condenser at a rate \dot{Q}_{Cond} . The heating and cooling coefficients of performance are then:

$$\text{COPW}_H = \frac{\dot{Q}_{\text{Cond}}}{\dot{W}_S} \quad (16)$$

$$\text{COPW}_C = \frac{\dot{Q}_{\text{Evap}}}{\dot{W}_S}$$

The natural gas-fired IC engine provides one means for approaching the efficiency of the Carnot cycle heat engine. In an IC engine, the working fluid operates on an open cycle. Fuel is mixed with air, and the resulting gas mixture is ignited in one of the combustion chambers of a spark ignition engine. The product gas (or exhaust gas) is then released from the chamber and rejected to the surroundings. In the combustion process, the chemical energy of the fuel is converted to thermal energy. Some of the thermal energy is then converted to mechanical

energy (shaft work) through the use of reciprocating pistons. The thermal energy that is not converted to shaft work is the engine rejected heat, a fraction of which is dissipated through the engine block. The remainder is carried away by the exhaust gas.

For the I.C. engine, the energy rate sought is the shaft work rate \dot{W}_S , and the energy rate that costs is the gas input rate \dot{Q}_{Gas} . The gas input rate is a product of the heating value of the fuel and the rate of fuel consumption. The heating value (Frequently termed "energy of combustion" or "heat of reaction") is a measure of heat transfer from a constant volume chamber during combustion at constant temperature. The first law efficiency of the I.C. engine is then:

$$\eta_{Eng} = \frac{\dot{W}_S}{\dot{Q}_{Gas}} \quad (17)$$

It follows that the engine rejected heat rate is:

$$\dot{Q}_{Eng} = (1 - \eta_{Eng})\dot{Q}_{Gas} \quad (18)$$

When the I.C. engine is utilized strictly for performing work, the engine rejected heat is not useful and is commonly released to the surroundings. On the other hand, when the I.C. engine is used to drive a heat pump

for which heating is the energy sought, the engine rejected heat is useful if it can be recovered. Therefore, a major advantage of the I.C. engine-driven heat pump is its potential for utilizing heat that is normally wasted.

The work of an actual heat-driven heat pump results from the use of a natural gas-fired I.C. engine to drive the compressor of a vapor-compression cycle heat pump. If a fraction, ϵ , of the engine rejected heat is recovered through some type of heat exchange process, then an additional rate of heat, \dot{Q}_{Rec} , is available for space heating. From equation (18):

$$\dot{Q}_{\text{Rec}} = \epsilon \dot{Q}_{\text{Eng}} = \epsilon (1 - \eta_{\text{Eng}}) \dot{Q}_{\text{Gas}} \quad (19)$$

Then for the actual heat-driven heat pump, the coefficients of performance obtained from equations (16), (17), and (19) are:

$$\text{COP}_{\text{H}} = \frac{\dot{Q}_{\text{Cond}}}{\dot{Q}_{\text{Gas}}} + \frac{\dot{Q}_{\text{Rec}}}{\dot{Q}_{\text{Gas}}} = \eta_{\text{Eng}} \text{COP}_{\text{W}_\text{H}} + \epsilon (1 - \eta_{\text{Eng}}) \quad (20)$$

$$\text{COP}_{\text{C}} = \eta_{\text{Eng}} \text{COP}_{\text{W}_\text{C}} = \frac{\dot{Q}_{\text{Evap}}}{\dot{Q}_{\text{Gas}}}$$

These are the coefficients of performance referred to throughout the remainder of this text.

Using off-the-shelf advanced technology, reasonable hardware values for an I.C. engine heat pump are:

$$\eta_{\text{Eng}} = 0.25$$

$$\epsilon = 0.8$$

$$\text{COPW}_H = 4$$

$$\text{COPW}_C = 4.$$

These values show that the present available component hardware potential is 1.6 for COPH_H and 1.0 for COPH_C . A diagram of the I.C. engine heat pump concept using this available component technology is shown in Figure 4.

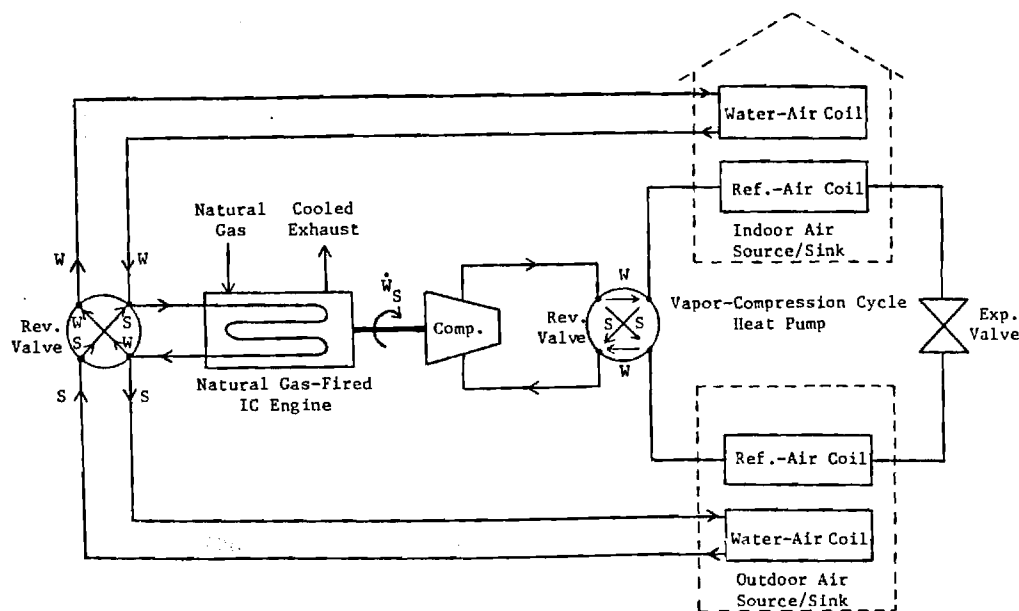


Figure 4. I.C. Engine Heat Pump Concept

SECTION II

I. C. ENGINE HEAT PUMP SYSTEM DESIGN

Description of Experimental System

The experimental system consists of a Florian Bauer GWW 35 natural gas driven heat pump package with an accessory exhaust gas/water heat exchanger for recovery of engine rejected heat, an integrated air/water heat exchanger with a central air handling system, and instrumentation.

The Florian Bauer GWW 35 heat pump package utilizes a 1600 cc four cylinder spark ignition engine built by the Ford Motor Company of Europe to drive a vapor compression cycle heat pump. This package, manufactured and marketed in West Germany, was designed to provide hot water for space heating via a radiator system, as is common practice in Europe. The manufacturer's specifications for this heat pump package appear in Table 1. It was also designed to use underground water rather than outdoor air as the external heat source/sink.

This water source system is not the development goal for gas heat pumps, because applications using underground water along with a water disposal sink (injection or stream) are limited. However, the prime subcomponent under question in I.C. engine heat pumps is the engine/compressor. This system allows testing of this major subcomponent without the added development effort to design and construct the outdoor coil,

Table 1. Florian Bauer GWW 35 Heat Pump Specifications

Maximum Heating Output @ 1800 rpm:	129,700 Btu/hr
Fuel Consumption Rate:	84.9 ft ³ /hr
COP _H at Maximum Output:	1.49
Required Water Flowrate @ 50°F Water Temperature:	15.4 gallons per minute
Weight:	1,430 lb.
Length:	53 inches
Width:	34 inches
Height:	52 inches

refrigeration reversing valve, and defrost controls. It was believed that these outdoor air coil problems should be decoupled from the engine/compressor testing and focused on after the engine/compressor was proven quiet and reliable with satisfactory maintenance.

This water-to-water heat pump was integrated with an air duct system for producing heated and cooled air for space conditioning. A water-to-water heat pump has both an advantage and disadvantage with respect to an air-to-air system. In heating, the well water evaporator is advantageous over an outside air evaporator, but the hot water producing condenser will be at a disadvantage compared to an air condenser placed directly in the air handler. In the cooling mode, the well water cooled condenser will be advantageous over an outside air condenser, but the chilled water evaporator will be at a disadvantage compared to an air evaporator placed directly in the air handler. In short, a water-to-water system has the advantage of a well water "outside" coil but the disadvantage of having two inside heat exchangers in series, i.e. refrigerate-to-water and water-to-air rather than a single refrigerate-to-air.

An air-water heat exchanger and central air handling system was integrated with the Florian Bauer heat pump to provide heated and cooled air for space conditioning. Heat is exchanged between a circulating water loop and house air in an air handler with an ARKLA 5-ton vertical chill water

coil, model number 60-136. The coil has a UA value of approximately 4500 Btu/hr-°F. Indoor air is circulated through the coil by a blower in the air handler with 1/2 hp at a flow rated at 2000 cfm. Hot or cold water is circulated through the coil at a rated 10 gpm by one of two March Model 830, 1/5 HP pumps. An underground well behind the residence supplies water at approximately 60°F year-round as the external heat source/sink for this system. The well water is pumped at a rated 6 gpm through one of the heat pump heat exchanger coils by a self-priming Teel 1-1/2 inch, 1/2 HP pump.

The well was drilled with a small portable drilling rig to a total depth of twenty-nine feet. A well screen and two-inch PVC casing were inserted and cemented in place. A series of pumping tests were conducted, demonstrating that the well could supply ground water at a rate approximating ten gallons per minute for a sustained period of time. After the water has been utilized as a heat sink/source, it is disposed of in Burnt Creek, which flows behind the residence. This plan of disposal has been approved by the Georgia Department of Natural Resources. An alternate plan of disposal that implemented a recharge well was discarded due to the convenience the creek offered and to its close proximity to the installation.

The Florian Bauer GWW 35 heat pump package was designed to provide heat recovery from the engine jacket and the exhaust manifold. As an accessory to this package, an external

exhaust gas/water heat exchanger is utilized to recover additional engine exhaust rejected heat.

The experimental system was designed to provide space heating and cooling and domestic hot water. In winter, the system can provide space heating ("Mode 1") or it can heat water for domestic use ("Mode 2"). In the summer, the experimental system can provide simultaneous space cooling and domestic water heating ("Mode 3") or it can provide only space cooling when the domestic hot water storage tank is fully heated ("Mode 4").

A configuration of the experimental system is shown in Figure 5. The system employs seven manually operated valves, two automatic valves, two circulation pumps, and a well pump. The manual valves are opened or closed only when it is desired to change between the winter and summer modes. Essentially, the manual valves perform the same function as a heat pump refrigerant reversing valve. The automatic valves and pumps are thermostatically controlled in order to change operating modes in a given season of the year (i.e., between Modes 1 and 2, or between Modes 3 and 4). Table 2 provides a summary of valve positions and pump operation for each of the four modes of operation.

System Control

The system is controlled in an on/off manner. The four modes (2 winter and 2 summer) were chosen by a Smart-Stat solid state house thermostat and the domestic hot water

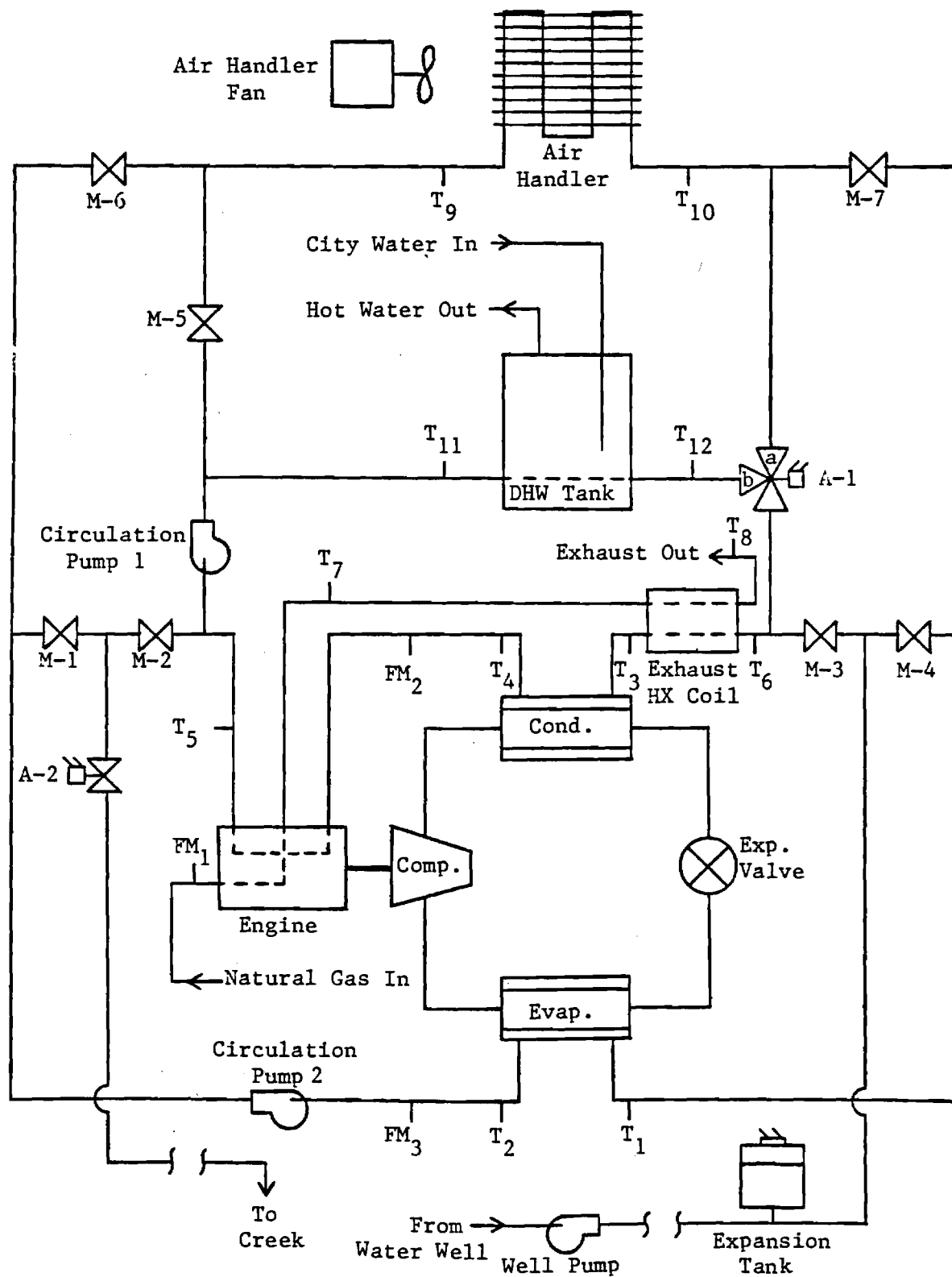


Figure 5. Experimental System Schematic

Table 2. Experimental System Valve Positions
and Pump Operation

<p>Winter (Space Heating)</p> <p>Mode 1</p> <p>Valve A-1 in position "a" Valve A-2 OPEN Pump P-1 ON Pump P-2 OFF Well Pump ON</p>	<p>MANUAL VALVES</p> <p>Valve M-1 OPEN Valve M-2 CLOSED Valve M-3 CLOSED Valve M-4 OPEN Valve M-5 OPEN Valve M-6 CLOSED Valve M-7 CLOSED</p>
<p>Mode 2</p> <p>Valve A-1 in position "b" Valve A-2 OPEN Pump P-1 ON Pump P-2 OFF Well Pump ON</p>	
<p>Summer (Space Cooling)</p> <p>Mode 3</p> <p>Valve A-1 in position "b" Valve A-2 CLOSED Pump P-1 ON Pump P-2 ON Well Pump OFF</p>	<p>MANUAL VALVES</p> <p>Valve M-1 CLOSED Valve M-2 OPEN Valve M-3 OPEN Valve M-4 CLOSED Valve M-5 CLOSED Valve M-6 OPEN Valve M-7 OPEN</p>
<p>Mode 4</p> <p>Valve A-1 in position "a" Valve A-2 OPEN Pump P-1 OFF Pump P-2 ON Well Pump ON</p>	

thermostat. The winter space temperature control points are 69°F-on/72°F-off, with summer conditions set at 77°F-on/74°F-off. The thermostat time clock provided winter set back to 55°F from 11:00 PM to about 6:00 AM. The actual morning reset time was determined by the Smart-Stat's optimal warmup strategy which reset the thermostat as necessary to reach 72°F by 6:30 AM. The domestic hot water temperature setting varied but was typically 110°F-on/130°F-off.

The thermostats provided 24 volt control signals to a group of relays which controlled the circulating pumps, air handler fan, and engine/heat pump. Also, 3 two position (winter/summer) toggle switches were incorporated with the relays to choose the space heating modes vs. the space cooling modes.

The priority of the two possible modes in each season was set as follows:

- (1) Winter: Space heating was taken as priority over domestic water heating (DWH). If the heat pump was in the DWH mode when space heating was called for, the relays would immediately switch the system to the space heating mode.
- (2) Summer: Two modes were possible: space cooling with simultaneous DWH, and space cooling with rejected heat to the outside. DWH without simultaneous space cooling was not possible. When space cooling was called for, the system

simultaneously heated water if the tank temperature was below 130°F. If the tank was above 130°F, the system would reject its heat outside. The domestic hot water thermostat would bring on DWH when the tank dropped below 110°F. In this case, it would always simultaneously cool the house regardless of the room thermostat condition.

Providing space cooling in the summer when DWH was required, regardless of the space temperature, did not overcool the house except during some cool summer mornings when 4 showers would be taken during a 30 minute period. This condition however, provided stored cooling so that thermostat demand for space cooling was delayed until later in the day.

The relay controls are shown in Figure 6. This is the detailed relay circuit controlling the circulating pumps, air handler, and engine/heat pump. The engine/heat pump was activated by closure of CR-1, 2, or 3. At this point, starting of the engine/heat pump was carried out by separate controls in the engine/heat pump package. The starter was engaged for a period of 5 seconds, and the compressor bypass solenoid valve (to prevent starting against a compressor load) was opened for a period of 10 seconds. If the engine failed to sense oil pressure within 10 seconds, the engine/heat pump shut down on default, requiring a manual reset to reinitiate the starting cycle. These engine/heat pump starting controls were provided as part of the package by Florian Bauer.

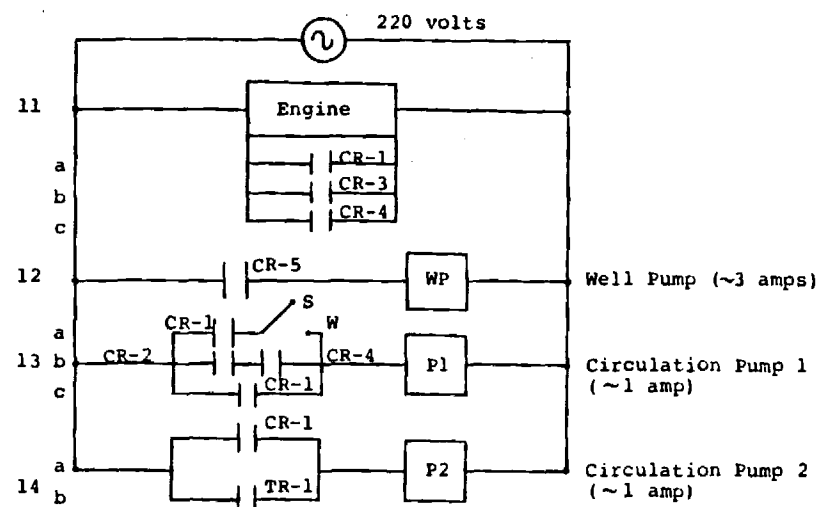
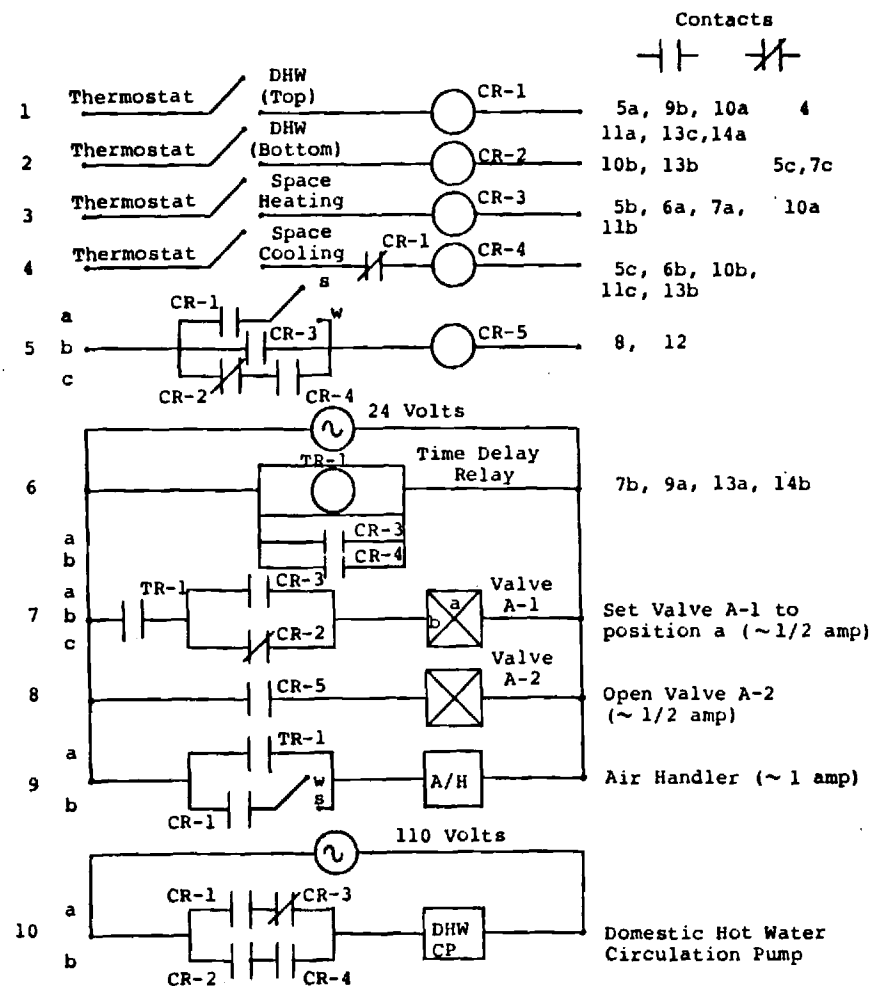


Figure 6: Heat Pump System Controls

SECTION III

INSTRUMENTATION

Long Term Monitoring

The monitoring of the heat pump over long time periods required an accumulating instrumentation system to accumulate 1) gas usage, 2) heat output, 3) cooling output, and 4) run hours.

The natural gas input was measured by installing a meter on the gas line leading to the engine. This meter is of the same type used by a gas utility company to measure domestic consumption for billing purposes. An hour meter was installed on the heat pump to measure the cumulative run time. The accumulated gas consumption could then be read from the meter and the average rate of gas consumption could be calculated by dividing the net gas consumption by the measured run time.

Energy supplied by the hot and chilled water loops was measured through the use of a pair of RHO-SIGMA model RS-805 Btu meters; they employ a flowmeter and a pair of temperature sensors placed in the supply and return of the respective hot and chilled water circuits. The Btu meters display the cumulative number of gallons of water that have flowed and the cumulative number of Btu's of heat transferred in the heated and chilled water circuits. The heating and cooling rates can be calculated by dividing the net number of Btu's of heat transferred by the run time.

The BTU meter thermistors have a manufacturer's stated precision of $\pm 0.4^{\circ}\text{F}$ with a nonlinearity which "does not have a measurable effect on the Btu-meter." The signals from the thermistors enter the RS-805 two bridge resistors which are matched to an accuracy of $\pm 0.04\%$.

The arithmetic circuitry directly measures the temperature difference between the two sensors rather than the absolute temperature of the sensors. This direct measurement minimizes signal processing which can introduce error. The temperature difference is converted to a digital signal through use of a digitally generated voltage staircase specifically shaped to eliminate the remaining non-linear influences of the thermistors. The 255 steps in the staircase determine the 1°F resolution of the temperature differential measurement. One step is generated for each 1°F .

The flow meters are a Kent model number C-700-FE (plastic) on the cold water circuit producing 4 pulses per gallons, and a RS-807B (brass) on the hot water circuit producing 200 pulses per gallon. The maximum stated error of the flow meters above 0.5 gpm is $\pm 1\%$. The pulses from the flowmeters trigger the voltage staircase which in turn triggers an oscillator in phase with the staircase. A positive temperature differential opens a gate which feeds the oscillator pulses into a counter. The number of pulses sent to the counter is directly proportional to Btus. When the counter accumulates the equivalent of 1,000

Btus, it increments a 6-digit counter and resets the circuitry. The overall stated accuracy for the Btu meters with a 10°F water ΔT , which was typical, is $\pm 5\%$.

Computer Data Acquisition

In order to obtain more detailed data on the heat pump system's performance, a data acquisition system was designed and implemented to allow measurement of 12 temperatures, 2 water flow rates, natural gas flow rate, and all energy flow rates with a time resolution of 1 minute. The data system used an Apple II microcomputer with an ISAAC A/D interface made by Cyborg Corp.

Twelve thermocouple millivolt outputs were conditioned by 12 Analog Devices 252A amplifiers with internal reference. These 0 to 5 volt signals were fed into the ISAAC where they were digitized on a 0 to 4096 count scale and read by the computer on command. The location of the 12 thermocouples is shown in Figure 5.

Two counter channels in the ISAAC accumulate 0 to 5 volt pulses from the same two Kent water flow meters used by the Rho Sigma Btu meters previously described. These hot and cold loop water meters produce 200 pulses per gallon and 4 pulses per gallon, respectively. A third counter channel accumulates pulses from a DARCOM encoder fitted to the 1/4 cubic foot per resolution dial of the gas meter. This magnetic activated pulser produced five 0 to 5 volt pulses per revolution and

was input to the ISAAC. These three counter channels were read each minute by the computer, which automatically zeroed the counters, giving flow rate per minute.

Additionally, two binary input ISAAC channels read the on/off status of control relays which determined when the system was on and which of the four operating modes the system was in.

The 12 bit digital thermocouple readings and 16 bit flow rate readings were read by the computer each minute after startup. The ISAAC's internal calender/clock supplied the day of week, date, hour, minute, and second for these readings. A complete system calibration was carried out on the thermocouple channels by placing all thermocouples, along with a mercury thermometer certified to a $\pm 0.1^{\circ}\text{C}$ accuracy, in a 50°C ice bath and boiling water bath. A second order calibration curve was derived for each thermocouple channel to convert the counts to degrees C.

A basic language program was written for the Apple II which, upon heat pump startup, would log the time and date and read all data channels each minute. The energy flows were calculated as follows:

$$\dot{Q}_{\text{Gas}} = \dot{V}_{\text{Gas}} (1028 \text{ Btu/ft}^3)$$

$$\dot{Q}_{\text{Cond}} = (\dot{m}C_p)_{\text{Cond}}(T_4 - T_3)$$

$$\dot{Q}_{\text{Evap}} = (\dot{m}C_p)_{\text{Evap}}(T_1 - T_2)$$

The total rate of engine rejected heat recovered was determined by:

$$\dot{Q}_{\text{Rec}} = (\dot{m}C_p)_{\text{Cond}}(T_4 - T_5) + (\dot{m}C_p)_{\text{Cond}}(T_6 - T_3)$$

$$\left[\begin{array}{l} \text{Engine Jacket} \\ +\text{Exhaust Manifold} \end{array} \right] \quad \left[\begin{array}{l} \text{Exhaust Heat} \\ \text{Exchanger} \end{array} \right]$$

Minute by minute COP's were calculated by the program with:

$$\text{COPH}_C = \dot{Q}_{\text{Evap}} / \dot{Q}_{\text{Gas}}$$

$$\text{COPH}_H = (\dot{Q}_{\text{Cond}} + \dot{Q}_{\text{Rec}}) / \dot{Q}_{\text{Gas}}$$

A complete schematic of the data acquisition system is shown in Figure 7. All data was converted to engineering units.

This temperature and flow rate data, with calculated energy flow rates and efficiencies, was then printed on the screen, paper printer, or floppy disk, as appropriate. An accumulating subroutine was used to yield accumulative run times, energy flow, and efficiencies in longer term tests.

INSTRUMENTATION SCHEMATIC

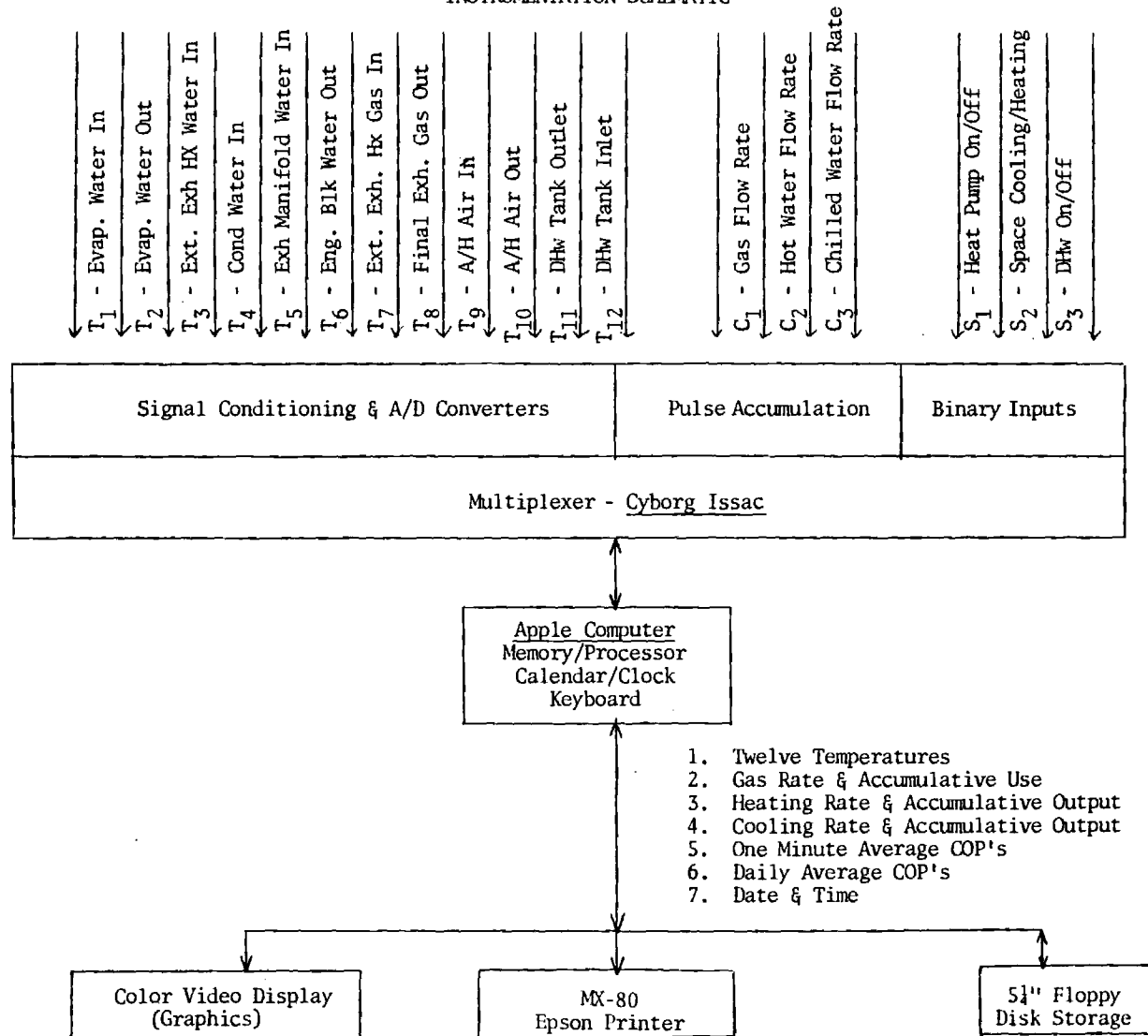


Figure 7: Computer Data Acquisition Schematic

SECTION IV

EXPERIMENTAL PERFORMANCE

Introduction

The Florian Bauer heat pump package was received from West Germany in December 1980. It was integrated into a residential heating/cooling system during early 1981, and since June 1981, has provided the space heating/cooling for the residence.

The residence is a 3200 square foot three story brick structure with glass composing 50% of the southeastern wall. This glazing has a ten foot overhang for summer shading. The structure was built in 1965. A five ton electric air conditioner was installed in 1965, with a 200,000 Btu/hr furnace installed in 1976. Hot water was supplied by a 40 gallon gas water heater installed in 1976. The house thermal "UA" value is about 680 Btu/hr-oF.

Analysis of data from 1978 to 1980 showed that natural gas consumption for space heating averaged 1000 therms annually with the furnace operating about 500 hours per year. An hour meter was installed on the electric air conditioner from 1979 to 1980 showing an average of 525 hours per year with 4200 kwhr electrical consumption annually.

Seasonal data was accumulated by the Btu and gas meters during the summer of 1981 and winter of 1981-82. In early

1982 the computer data acquisition system was installed, allowing more accurate data acquisition with one minute time resolution. During the summer of 1982, the Btu meters were checked against the computer data acquisition system. Both steady state and transient data were then taken to determine performance in detail.

Seasonal Performance

The system became operational on June 13, 1981 and the Btu meters became fully operational July 24, 1981. The system was closely monitored as it provided space cooling until October 13, 1981 when the heat pump cooling run time was 547 hrs. On almost a daily basis, the gas meter, hot and chilled water Btu meters, and heat pump hour meter were read and recorded. An abbreviated tabulation of this data is shown in Table 3. The engine speed was fixed at 1200 rpm.

In January 1982, new thermisters were installed on both Btu meters, since questions had arisen regarding the Btu meter accuracy. There was a slight (5%) reduction in the hot water Btu output after the new calibrated thermisters were installed. At the end of February 1982, a time delay relay was added to keep the air handler fan and air coil water circulating pump on for 6 minutes after the engine turned off. This "spindown" recovered additional heat from the engine. The system ran in the space heating mode until May 24, 1982, when it was then switched to cooling. On October 18, 1982, it was again switched to heating.

TABLE 3

Long Term Performance Raw Data

<u>Date</u>	<u>Run</u> (Hrs)	<u>V_{Gas}</u> (100 ft ³)	<u>Q_{Heat}</u> (1000 Btus)	<u>Q_{Evap}</u> (1000 Btus)
7/27/81	401	2,317	18,441	13,143
9/10/81	534	2,403	20,434	18,130
10/13/81	547	2,411	32,192	18,710
10/13/81	----- Switched to Heating-----			
10/13/81	547	2,411	32,192	18,710
12/08/81	682	2,505	44,877	22,801
01/02/82	827	2,600	59,014	27,720
01/30/82	1,048	2,747	81,361	34,903
01/30/82	-----New Thermisters Installed-----			
02/28/82	1,188	2,836	93,721	39,524
02/28/82	-----Added A/H Fan and Pump Delay----			
03/31/82	1,288	2,897	102,600	42,792
05/02/82	1,306	2,909	104,180	43,364
05/29/82	1,339	2,929	107,274	44,388
05/29/82	-----Switched to Cooling-----			
05/29/82	1,339	2,929	107,274	44,388
06/26/82	1,413	2,978	114,826	47,016
07/31/82	1,539	3,063	128,302	52,419
08/18/82	1,631	3,124	137,975	55,569
09/09/82	1,731	3,178	146,981	59,164
10/18/82	-----Switched to Heating-----			
10/18/82	1,731	3,206	151,926	Broken
04/19/83	2,402	3,646	218,705	-----

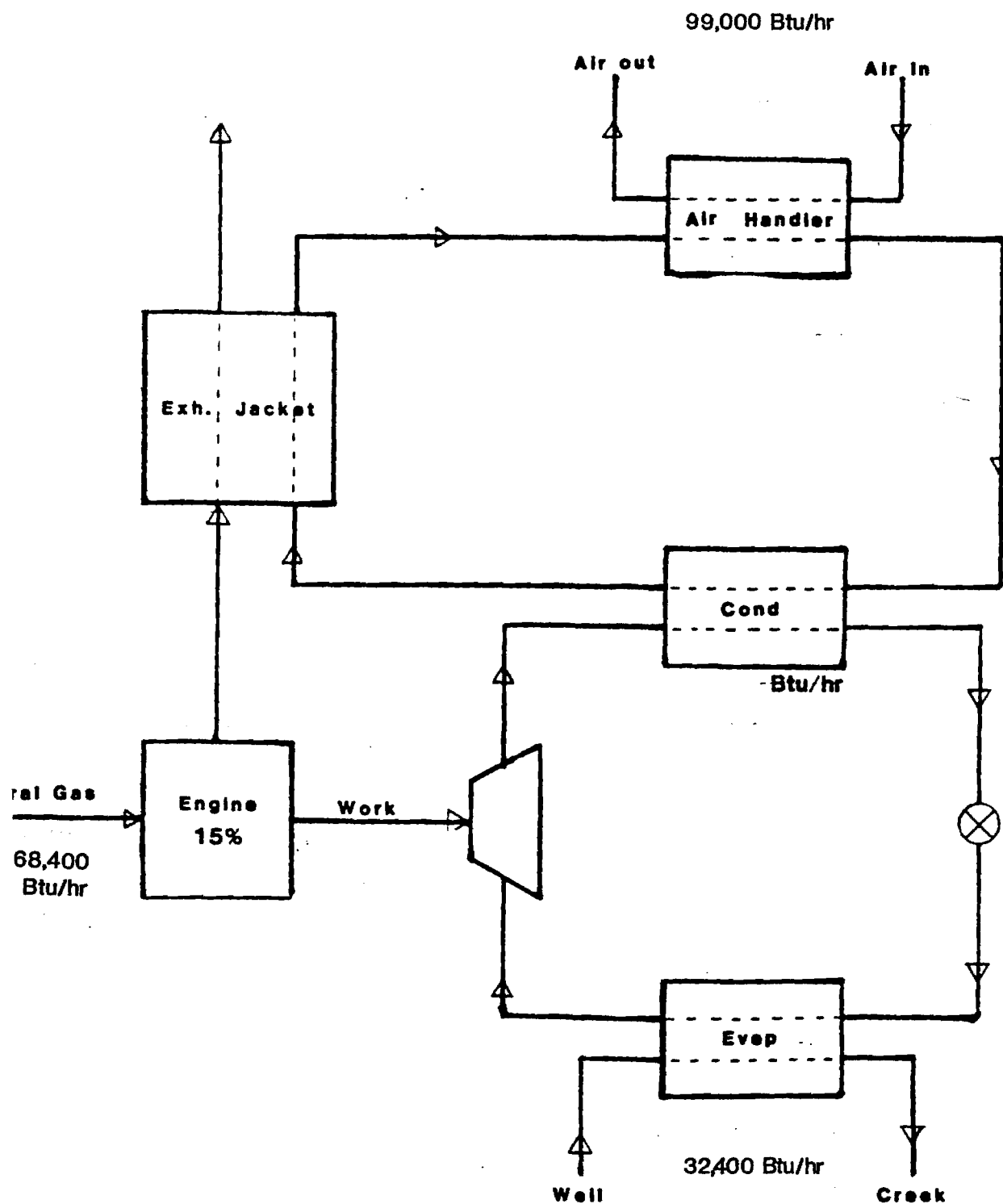
All readings have been plotted against run hours and a least squares straight line was fitted to each season's segment. The results agree with merely taking the seasonal incremental accumulative numbers and dividing by the incremental seasonal run time. The following resulted:

<u>Season</u>	<u>Run</u> (Hrs)	\dot{Q}_{Gas} (Btu/hr)	\dot{Q}_{Heat} (Btu/hr)	COP_{H}	\dot{Q}_{Evap} (Btu/hr)	COP_{C}
Summer 81*	146	66,000	94,000		38,100	0.58
Winter 81-2	792	67,100	94,800	1.41	32,400	
Summer 82	415	68,500	107,600		39,500	0.58
Winter 82-3	648	69,700	103,100	1.48		

*Partial Summer starting 7/24/81. Full summer hours - 547.

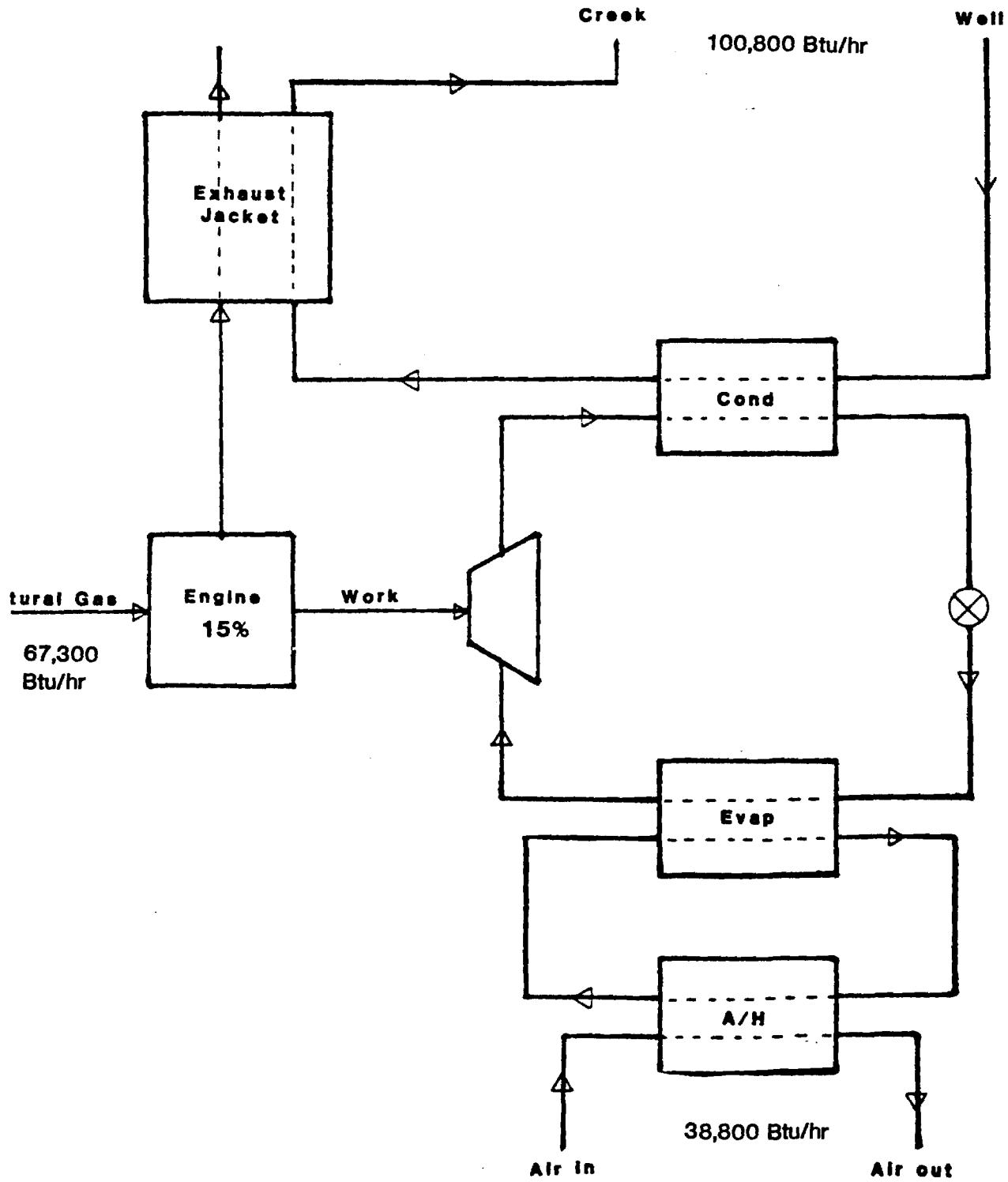
These results are summarized graphically on the heat pump system schematic in Figure 8 for heating and Figure 9 for cooling. In these figures, the values for the two heating seasons are averaged and the two cooling seasons were averaged to get overall heating and cooling performance. They represent Seasonal Performance Factor values.

FIGURE 8: SEASONAL SYSTEM HEATING PERFORMANCE 37



HEATING C.O.P. : 1.45

FIGURE 9: SEASONAL SYSTEM COOLING PERFORMANCE



COOLING C.O.P. : 0.58

Engine/Compressor Performance

Data was taken from the experimental heat pump system for the purpose of determining engine/compressor performance (gas input rate, condenser and evaporator heat rates, and the heat recovery rate) as functions of the condenser and evaporator refrigerant temperatures. With the engine speed held constant, the gas input rate and condenser and evaporator heat rates are uniquely determined by the two refrigerant temperatures. The heat recovery rate is additionally dependent upon the variable water temperature and flow rate at the inlet to the exhaust heat exchanger.

Four operating conditions, each specified by a condenser refrigerant temperature and an evaporator refrigerant temperature, were used to obtain the experimental data. The operating conditions, listed in Table 4, were chosen near lower and upper temperature extremes in order to obtain a good representation over the range of experimental operating conditions. In order to achieve steady-state for each of the specified operating conditions, three different operating modes were required as indicated in Table 4.

The water temperature at the inlet to the exhaust heat exchanger (and, therefore, the heat recovery rate) varies with the operating mode. During normal heating operation, this temperature would be constant, yielding a constant exhaust temperature of approximately 130°F at the heat exchanger outlet.

Therefore, the measured heat recovery rate was corrected by calculating the change in exhaust heat recovery due to fixing the final exhaust temperature at 130°F.

A total of forty tests (ten for each of the four operating conditions) were conducted at a constant engine speed of 1200 rpm. After establishing steady-state (as determined by continuous monitoring of water temperatures in the condenser and evaporator loops), the gas input rate, condenser and evaporator heat rates, and heat recovery rate were computed for one-minute tests and logged by the APPLE/ISAAC instrumentation system. For each set of operating conditions, the data was averaged over ten tests, and the results are given in Table 5. Included are the mean values and estimated true population standard deviations for the measured gas input rate, the measured condenser and evaporator heat rates, the measured heat recovery rate, and the corrected heat recovery rate.

The data presented in Table 5 provides an indication of the dependence of engine/compressor performance and the heat recovery rate on the condenser and evaporator refrigerant temperatures. For a change in one of the refrigerant temperatures with the other held constant, a change is estimated for the gas input rate, condenser and evaporator heat rates, and the heat recovery rate. The question was raised as to whether these changes are actual, or due to random error in the experimental data. A statistical analysis was performed to determine

confidence intervals for changes in the data (dependent variables) resulting from changes in the refrigerant temperatures (independent variables).

$$\text{Confidence Interval} = \bar{X}_2 - \bar{X}_1 \pm t_p \left[\frac{(n+m)(n\sigma_1^2 + m\sigma_2^2)}{nm(n+m-2)} \right]$$

where \bar{X}_1 and \bar{X}_2 are the averaged dependent variables involved in the change of one of the independent variables, σ_1 and σ_2 are the estimated true population standard deviations for the dependent variables, and n and m are the numbers of dependent variable data points. The variable t_p is tabulated⁶ as a function of the degrees of freedom ($n+m-2$) and the confidence coefficient. For this data, the degrees of freedom are 18, and for a confidence of 90%, $t_p = 1.734$; 95%, $t_p = 2.101$; and 99%, $t_p = 2.878$. Confidence intervals for the changes in data, resulting from the increase in condenser refrigerant temperature are listed in Table 6. The negative signs on some of the interval bounds indicate that those rates decreased when the condenser temperature was increased. Confidence intervals for the changes in data resulting from the increase in evaporator refrigerant temperature are given in Table 7.

A good degree of confidence is indicated when the intervals are small relative to the magnitudes of their bounds. A review of Table 5 and 6 indicates a good degree of confidence in the change in condenser and evaporator heat rates for a change in

either of the refrigerant temperatures. This implies that the rate changes are more likely due to changes in operating conditions than to random error in the data. On the other hand, little confidence can be placed in the change in heat recovery rate accompanying changes in either of the refrigerant temperatures. For instance, it is not known with a 99% certainty whether the heat recovery rate increases or decreases when the condenser temperature is increased.

A multiple variable, linear regression analysis program, available through an APPLE computer software package, was used to determine a linear relationship between the heat pump performance and the condenser and evaporator refrigerant temperatures. Data from all forty tests was used for the analysis. The results are included in Table 8 along with statistical analysis of the curve fits. These results are useful in design optimization of I.C. engine heat pumps.

System Steady State Performance

The computer data acquisition system supplied data from startup to establishment of steady state conditions for both the heating and cooling modes. Steady state was established in 20 to 30 minutes in the cooling mode and 30 to 40 minutes in the heating mode. The warmup period was longer for the heating cycle due to the higher equilibrium temperature in the hot water loop (about 140°F vs. 70°F). The speed was held constant at 1200 rpm.

Table 9 shows the steady state values for the temperatures, energy flow rates, and COPH's. The temperature numbers are labeled on the system schematic in Figure 5. In the heating mode, 57% of the heat was produced by the condenser, 41% from the engine cooling jacket and integral exhaust manifold/HX, and 2% from the external exhaust heat exchanger. The evaporator and condenser temperatures were about 31°F and 132°F, respectively. Only 1 1/2% of the gas input plus evaporator input energy is unaccounted for. The only significant loss would be in the exhaust gases which are at 117°F. The accuracy of this "lost" heat number is very low due to accumulative errors of the numbers totaled to derive it.

In the cooling mode, 59% of the rejected heat comes from the condenser, 39% from the engine cooling jacket and exhaust manifold, with 2% coming from the external exhaust heat exchanger. The evaporator and condenser temperatures were approximately 33°F and 88°F, respectively. Only 3% of the total gas and evaporator energy input is unaccounted for. Again, the accuracy of this number is low, but with a 75°F final exhaust temperature and insulated heat pump package, the unmeasured energy flow should be small.

The larger fraction of heat coming from the condenser in the cooling mode is due to the lower condenser temperature and pressure, yielding both a higher refrigerant mass flow and a lower engine loading.

Table 4. Steady-State Operating Conditions

Operating Condition	T _{Evap} (°F)	T _{Cond} (°F)	Operating Mode
1	27.5	86.9	3*
2	27.5	145.4	4
3	14.0	95.0	1
4	39.2	95.0	3*

*Mode 3 was modified by opening valve M-5 and placing valve A-1 in position "a".

Table 5. Averaged Experimental Data

Operating Condition	$T_{\text{Evap}} (^{\circ}\text{F})$	$T_{\text{Cond}} (^{\circ}\text{F})$	$\bar{Q}_{\text{Gas}} \left(\frac{\text{Btu}}{\text{hr}} \right)$ [$\sigma \left(\frac{\text{Btu}}{\text{hr}} \right)$]	$\bar{Q}_{\text{Cond}} \left(\frac{\text{Btu}}{\text{hr}} \right)$ [$\sigma \left(\frac{\text{Btu}}{\text{hr}} \right)$]	$\bar{Q}_{\text{Evap}} \left(\frac{\text{Btu}}{\text{hr}} \right)$ [$\sigma \left(\frac{\text{Btu}}{\text{hr}} \right)$]	$\bar{Q}_{\text{Rec}} \left(\frac{\text{Btu}}{\text{hr}} \right)$ [$\sigma \left(\frac{\text{Btu}}{\text{hr}} \right)$]	$\bar{Q}_{\text{Rec}}^{\text{Corr}} \left(\frac{\text{Btu}}{\text{hr}} \right)$ [$\sigma \left(\frac{\text{Btu}}{\text{hr}} \right)$]
1	27.5	86.9	76950 [0]	67384 [1871]	49804 [957]	55374 [3041]	49813 [3041]
2	27.5	145.4	84645 [1539]	49639 [863]	29781 [363]	47261 [1127]	47261 [1127]
3	14.0	95.0	70178 [1231]	43492 [2424]	32438 [439]	51791 [3396]	47176 [3396]
4	39.2	95.0	79412 [1231]	82614 [1821]	61362 [1520]	57706 [1488]	51968 [1488]

Table 6. Confidence Intervals for Increase
in Condenser Temperature

	Confidence Coefficient		
	90%	95%	99%
$\Delta \bar{Q}_{\text{Gas}} (\frac{\text{Btu}}{\text{hr}})$	[6805; 8585]	[6617; 8773]	[6219; 9171]
$\Delta \bar{Q}_{\text{Cond}} (\frac{\text{Btu}}{\text{hr}})$	[-18936; -16554]	[-19188; -16302]	[-19722; -15768]
$\Delta \bar{Q}_{\text{Evap}} (\frac{\text{Btu}}{\text{hr}})$	[-20615; -19431]	[-20740; -19306]	[-21005; -19041]
$\Delta \bar{Q}_{\text{Rec}} (\frac{\text{Btu}}{\text{hr}})$	[-4426; -677]	[-4823; -281]	[-5663; 559]

Table 7. Confidence Intervals for Increase
in Evaporator Temperature

	Confidence Coefficient		
	90%	95%	99%
$\Delta \bar{Q}_{\text{Gas}} (\frac{\text{Btu}}{\text{hr}})$	[8228;10740]	[8015;10453]	[7564;10904]
$\Delta \bar{Q}_{\text{Cond}} (\frac{\text{Btu}}{\text{hr}})$	[37370;40874]	[36999;41245]	[36213;42031]
$\Delta \bar{Q}_{\text{Evap}} (\frac{\text{Btu}}{\text{hr}})$	[28010;29838]	[27816;30032]	[27406;30442]
$\Delta \bar{Q}_{\text{Rec}} (\frac{\text{Btu}}{\text{hr}})$	[2649;6935]	[2195;7389]	[1235;8349]

Table 8. Results of Multiple Variable,
Linear Regression Analysis

$\dot{Q}_{\text{gas}} \left(\frac{\text{Btu}}{\text{hr}} \right) = 372.91T_{\text{Evap}} + 159.80T_{\text{Cond}} + 50838 *$ <p>Coefficient of Determination (R^2) = .89434</p> <p>Coefficient of Multiple Correlation = .94570</p> <p>Standard Error of Estimate ($\frac{\text{Btu}}{\text{hr}}$) = 1801.6</p>
$\dot{Q}_{\text{Cond}} \left(\frac{\text{Btu}}{\text{hr}} \right) = 1553.5T_{\text{Evap}} - 298.68T_{\text{Cond}} + 50292 *$ <p>Coefficient of Determination (R^2) = .98577</p> <p>Coefficient of Multiple Correlation = .99286</p> <p>Standard Error of Estimate ($\frac{\text{Btu}}{\text{hr}}$) = 1918.3</p>
$\dot{Q}_{\text{Evap}} \left(\frac{\text{Btu}}{\text{hr}} \right) = 1145.8T_{\text{Evap}} - 351.09T_{\text{Cond}} + 49420 *$ <p>Coefficient of Determination (R^2) = .99377</p> <p>Coefficient of Multiple Correlation = .99688</p> <p>Standard Error of Estimate ($\frac{\text{Btu}}{\text{hr}}$) = 1064.6</p>
$\dot{Q}_{\text{Rec}} \left(\frac{\text{Btu}}{\text{hr}} \right) = 189.52T_{\text{Evap}} - 46.400T_{\text{Cond}} + 48827 *$ <p>Coefficient of Determination (R^2) = .39396</p> <p>Coefficient of Multiple Correlation = .62766</p> <p>Standard Error of Estimate ($\frac{\text{Btu}}{\text{hr}}$) = 2558.6</p>

* T_{Evap} and T_{Cond} in °F

TABLE 9
Steady State Performance

<u>Temperatures ($^{\circ}\text{F}$)</u>	<u>Heating Mode</u>	<u>Cooling Mode</u>
T ₁ - Evaporator water inlet	57.5	52.2
T ₂ - Evaporator water outlet	43.3	42.3
T ₆ - External exhaust HX water inlet	113.2	60.7
T ₃ - Condenser water inlet	113.7	61.2
T ₄ - Engine water inlet	129.4	77.6
T ₅ - Engine water outlet	140.7	88.3
T ₈ - Exhaust gas outlet	117.8	74.7
T ₉ - A/H air inlet	70.9	77.5
T ₁₀ - A/H air outlet	108.9	59.0
<u>Energy Flows (Btu/hr)</u>		
Gas consumption	68,700	67,700
Engine & exhaust manifold recovery	40,100	40,600
External exhaust HX recovery	1,800	1,900
Condensor heating	55,700	62,300
Total heating	97,600	104,800
Evaporator Cooling	30,400	40,700
<u>COPH's</u>		
Heating	1.42	
Cooling		0.60

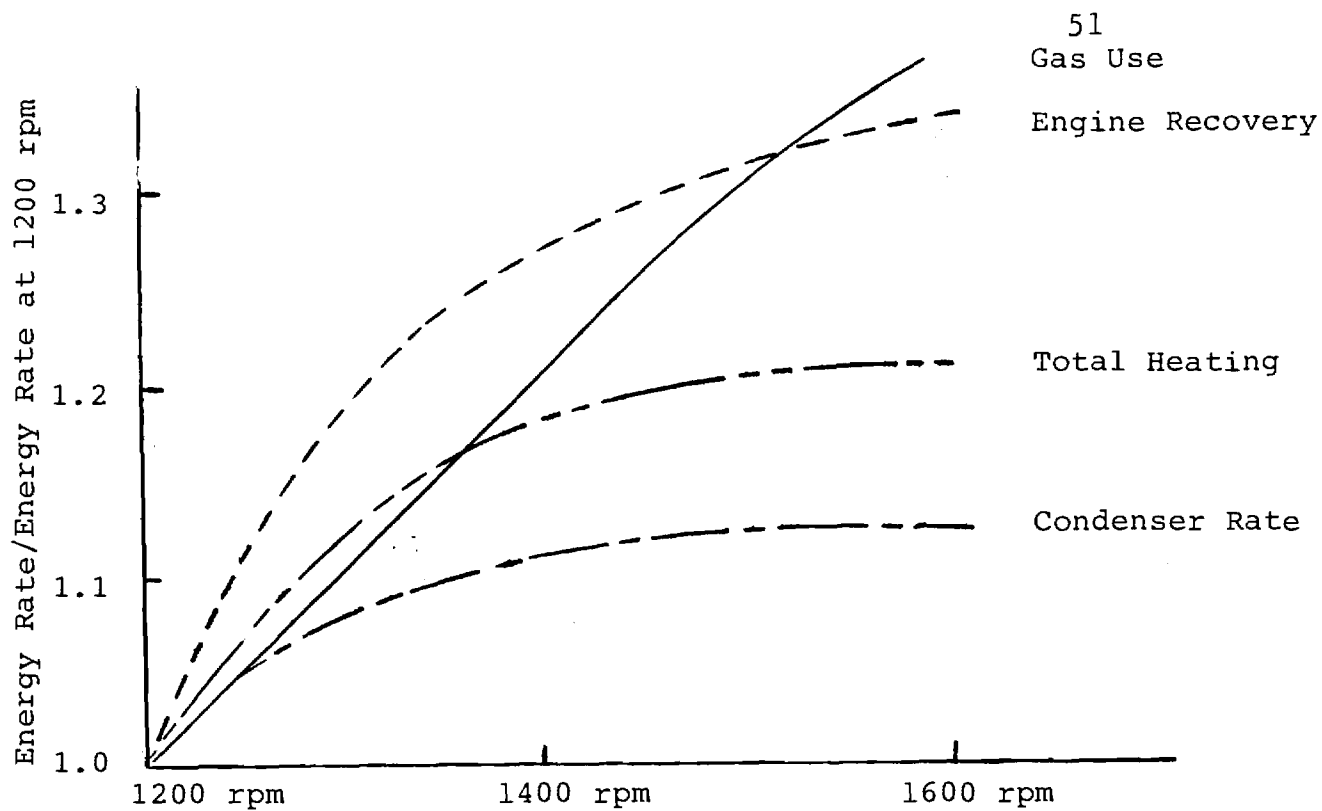


Figure 10. Heat Pump Energy Rates vs. Speed

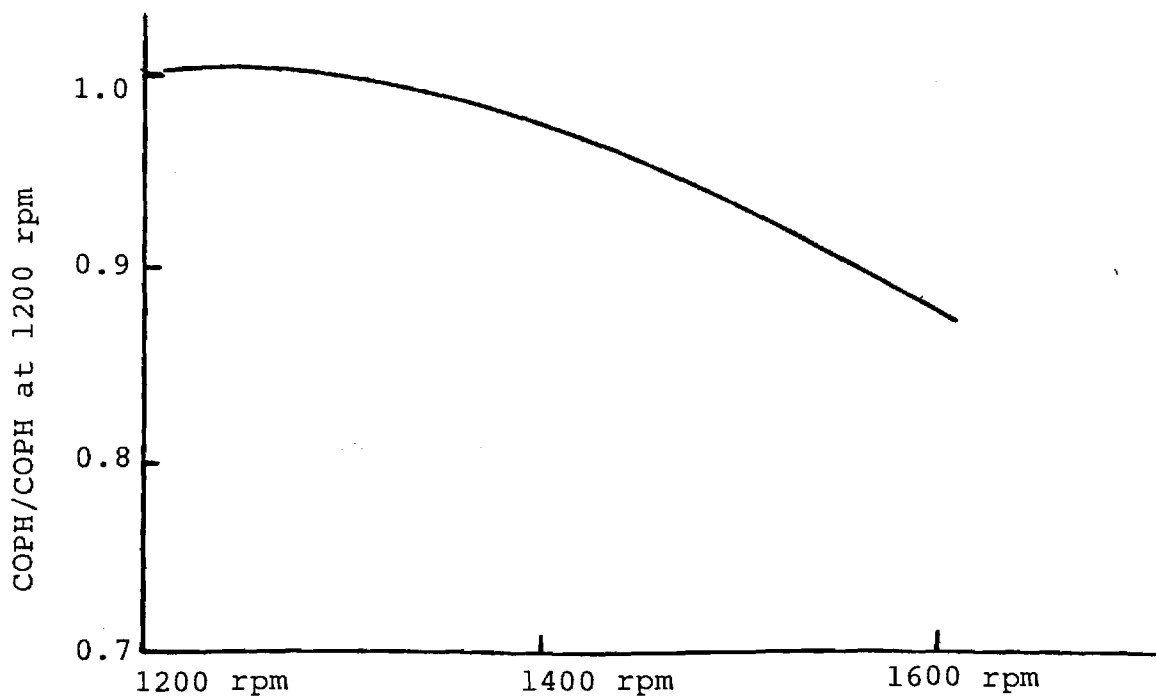


Figure 11. Heat Pump Heating COP vs. Speed

because the return water temperature from the air handler was driven up as a higher rate was put through the air-water coil. The well water temperature supplying the evaporator is of course constant with varying speed. These speed effects would not be as large with an air-to-air system without the additional water heat exchange process.

Figure 11 shows the resulting COPH for the varying speed. The efficiency is seen to decrease by about 15%, while the total heating rate increases by just over 20%, for a 25% speed increase. Again, it should be noted that the water-to-water heat pump will show larger efficiency penalties with increasing speed than does an air-to-air system.

Cycling Effects

The effect of on/off cycling of the heat pump in its performance was studied two ways. First, run-by-run data was accumulated by the computer data acquisition system. It printed out the average energy flow rates and COP's for each on-cycle, along with that cycle's on-time and prior off-time. Statistical analysis was carried out on this data to determine the correlation of the average cycle performance as a function of the cycle's on-time and the prior off-time. No significant dependence of any of the variables was found on these cycle times.

Due to this unexpected result, a cycling test was run which was patterned after the U.S. Department of Energy's test

procedure for measuring electric air conditioner and electric heat pump cycling effects, published January 1, 1982, (Chapter 2, Title 10, Subpart B, Appendix M). In this test a 30 minute run is made to establish steady-state conditions, followed by a 30 minute period during which the steady-state performance is measured. During the next 30 minute period, the heat pump is off 24 minutes and then turned on for 6 minutes. This 24 minutes off, 6 minutes on cycle is repeated twice with the last 6 minute cycle being used to measure the performance during cycling relative to the initial steady-state values.

A DOE cycling degradation coefficient, C_D , is defined as:

$$C_D = 1 - \frac{COP_{cyc}}{COP_{ss}} = 1 - \frac{Q_{cyc}}{Q_{ss}}$$

where $()_{cyc}$ indicates the values for the last 6 minute on cycle and $()_{ss}$ is the 30 minute steady-state measured values. In these tests the C_D repeatedly came out negative, indicating and improvement in efficiency during cycling.

This unusual result is shown to be due to the "spin down" cycle which extracts the engine/condenser heat for 6 minutes following an on-cycle. This spin down reduces the hot water temperature from about 140°F to less than 110°F. Since the condenser is in the same hot water loop with the engine and exhaust, this significantly reduces the average condenser temperature during cycling compared with steady-state, while still extracting all the engine heat. Accessory energy is also increased.

This cycling effect may not be the same with an air-to-air system, since the I.C. engine heat pump condenser temperature would not be tied to the engine temperature. However, since approximately half of the total heat comes from the engine, cycling effects of an I.C. engine heat pump would be expected to be substantially less than an electric heat pump, particularly if a spin down cycle is used.

Reliability and Maintenance

One of the goals for the I.C. engine heat pump is to have a maintenance interval greater than once annually. This goal was exceeded by this experimental system in that no scheduled or unscheduled maintenance was carried out during the over 200 running hours, except for the installation of an oil sealing gasket on a cover plate on the side of the engine. No oil changes, spark plug replacement, timing adjustment, or any other maintenance has been required or performed. Spark plug gap is still under 0.040 inch due to special tip materials.

Oil analysis has been carried out, showing at the 1750 hour point, that the oil was still completely serviceable. The analysis at 1750 hours is shown in Table 10. The 15 quart capacity is continually recirculated.

Reliability has been nearly 100%, except for several increasingly frequent occasions when the engine failed to start during the first 5 second fixed starting period. This failure occurs generally after the heat pump has not run for a long period of time. After five seconds, the starter is

TABLE 10: Oil Analysis

WEAR CHECK

ENGINE AND OIL
CONDITION
ANALYSIS
REPORT

Spectro/Metrics, Inc.
35 Executive Park Drive, N.E.
Atlanta, Georgia 30329
(404) 321-7909

FORD

MODEL: 2270

FLEET/UNIT #: 1

NATURAL GAS

SAMPLE DATA	WEAR METALS						SILI- CON	ADDITIVES				CONTAMINANTS				VISC.	TBN
	ALUM- INUM	CHRO- MIUM	COPPER	IRON	LEAD	TIN		MAGNE- SIUM	MOLY	BORON	SODIUM	WATER (%)	GLY- COL	DIEL- ECTRIC	FUEL (%)		
	PISTONS BEARINGS	RINGS	BEARINGS	CYLINDER RINGS CRANK SH CAM SH	GASOLINE ADDITIVE - DIESEL BEARINGS	BEARINGS		ADDITIVE (HOUSING)	ADDITIVE (RINGS)	ADDITIVE (COOLANT)	ADDITIVE (COOLANT)	CONDEN- SATION (COOLANT)	ANTI- FREEZE	SOLIDS CARBON		SAE	ALKALINE RESERVE
Re-pled 10-2-82	4.6	5.1	22	72	6.2	9.2	13	805	2.7	13	18	-.05	NEG	4	0	31	
let.# 14026	N	N	N	N	N	N	N	N	N	N	N	N	N	N	N		
2# 214058	ENGINE WEAR RATES AND CONTAMINANT LEVELS SATISFACTORY. OIL STILL																
iles Hrs 1750	SERVICEABLE. RESAMPLE NEXT SERVICE INTERVAL TO MONITOR AND																
rs Since change 1750	ESTABLISH WEAR TREND. (NO PREVIOUS RECORD WITH THIS UNIT I.D.																
rs since change 1750	PLEASE PROVIDE LAST LAB NUMBER.) -ANALYST RT																

END: Normal, Abnormal, Severe.

" + " means greater than, " - " means less than.

DR. SAM. V. SHELTON
SCHOOL OF MECHANICAL ENG.
GEORGIA TECH
ATLANTA, GA 30332

LAST OVERHAUL:
SYSTEM CAPACITY: 15 QTS.
OIL MAKE & TYPE: ?
HISTORY & REMARKS:

SHEATL 1

DiesGasNat 75.

A MEMBER OF THE SPECTROMETRIC OIL ANALYSIS LABORATORY ASSOCIATION

deactivated; if oil pressure is not sensed 10 seconds after starter initiation, the controls shut the unit down on default. In almost every start failure, a manual reset to allow a second try was successful. A third and four try was required in isolated instances. This problem could be overcome by using controls to reinitiate the start cycle automatically.

Noise Levels

Sound levels of the unit have been measured using a an A weighting scale. Inside the furnace room the levels were as follows for individual components running and with the total system running:

Background	-	57 dBA
Air Handler Only	-	61 dBA
Water Pump Only	-	57 dBA
Heat Pump Only	-	62 dBA
Total System	-	63 dBA

Sound levels were also measured outside at a 6 foot distance from the exhaust outlet. The outlet is 8 inches above a concrete slab and 6 inches from a 8 foot high concrete block wall. The second level at a distance 6 feet from this wall is 60 dBA.

Electrical Accessory Power

The electrical accessories with this gas heat pump are 1) a 1/2 hp A/H fan drive; 2) two 1/5 hp closed loop water circulating pump drives (only one is on in any mole); 3) a 1/2 hp well water pump drive, and 4) a lead acid battery charger. The battery charger draws about 10 watts and is not significant. The kilowatt draw of the other accessories are:

Fan	-	0.73 kw
Well Pump	-	0.61
Circulating Pump (1)	-	<u>0.24</u>
Total	-	1.58 kw

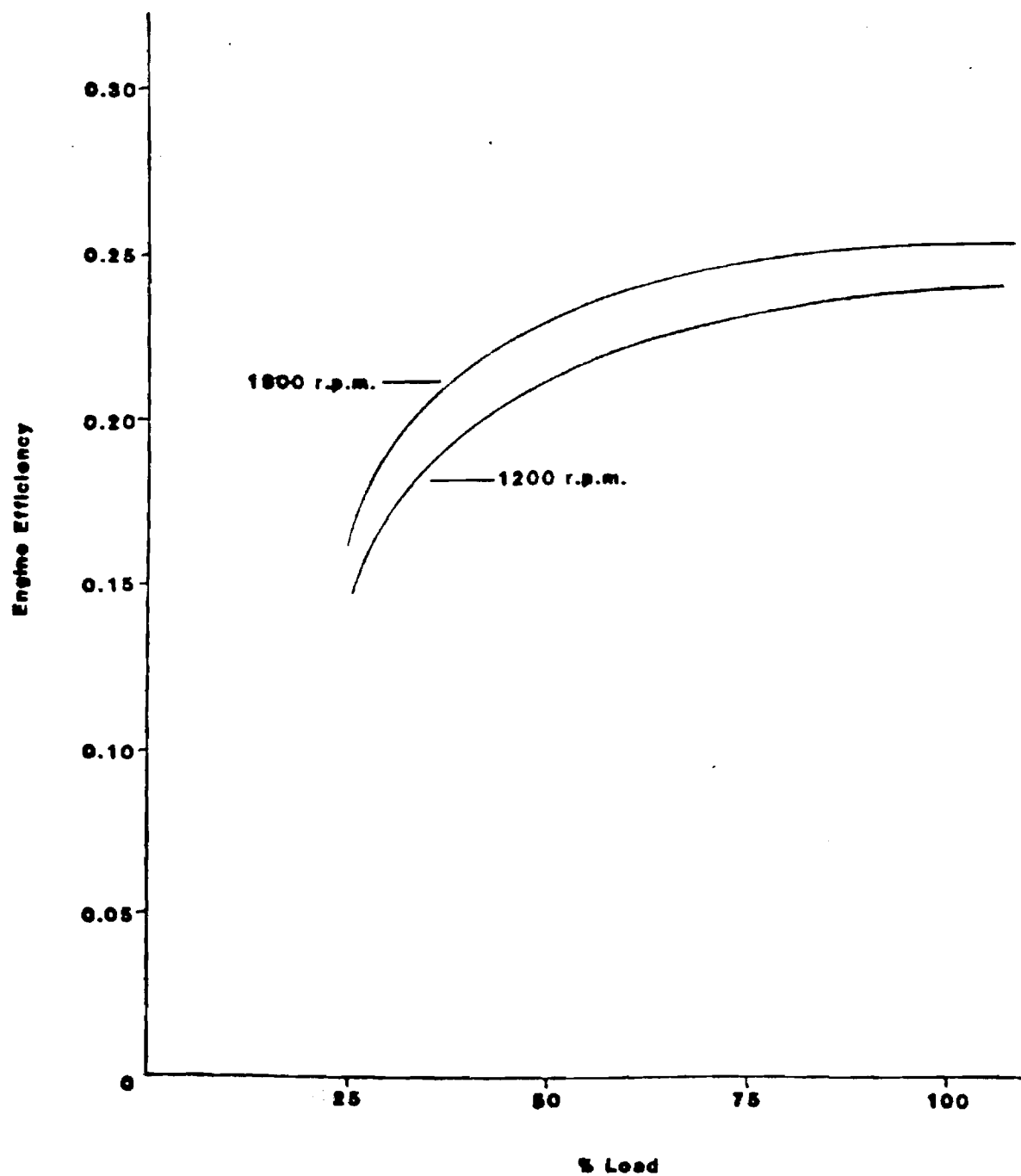
The 1.6 kw power is drawn during the heat pump operating hours. In addition, for 6 minutes after the heat pump is shut down, the fan and one circulating pump operate, drawing a total of 1.0 kw.

A separate kilowatt hour meter accumulated the electrical consumption of these accessories. The average kwhr consumption was 1.91 kwhr per hour of heat pump running time. This average compares with the gas consumption of 0.67 therms per hour. At a 3.5 ratio for electrical energy cost to gas energy cost (6.5 ¢/kwhr and 55 ¢/therm), the electrical accessories energy cost is 25% of the total heat pump system operating cost.

Performance Improvements

Changes for improved efficiency performance would be to retrofit the heat pump with a smaller displacement engine. The present Ford 227E 1600 cc engine is operating at 25% of its rated full load. Figure 12 is a plot of engine efficiency vs. % load with engine speed as a parameter. From this figure it can be seen that at 25% loading and 1200 rpm, the engine's thermal efficiency is about 16%. If this engine were replaced by a Ford 2271E 1100 cc engine, the loading would increase to approximately 36%. From Figure 12, this increased load at 1200 rpm would result in a thermal efficiency of about 19%. This change alone would yield a 25% improvement in cooling COP and about a 10% improvement in heating COP.

Figure 12: Engine Efficiency vs Load



SECTION V

AIR-TO-AIR I.C. ENGINE HEAT PUMP ANALYSIS

Introduction

The water-to-water heat pump tested gave information on the critical engine/compressor subcomponent in terms of the physical characteristics, maintenance, noise, and reliability of I.C. engine heat pumps. However, the efficiency information is not directly applicable to air-to-air heat pumps. Even so, the experimental data taken on just the engine/compressor yielding energy rates and efficiencies for varying condenser and evaporator pressures makes it possible to calculate accurately the performance of the same engine/compressor operating with a given size of air condenser and evaporator coils.

The proposed system model diagram is given in Figure 13. Indoor and outdoor air are used as the heat source/sink for the vapor-compression cycle heat pump. Heat is removed from the source and rejected to the sink via two refrigerant-air heat exchanger coils. These coils are fixed in position, but the reversing valve makes possible a change in the direction of refrigerant flow to and from the compressor. The direction of refrigerant flow defines which coil is the condenser and which is the evaporator, and thereby defines the direction of heat flow.

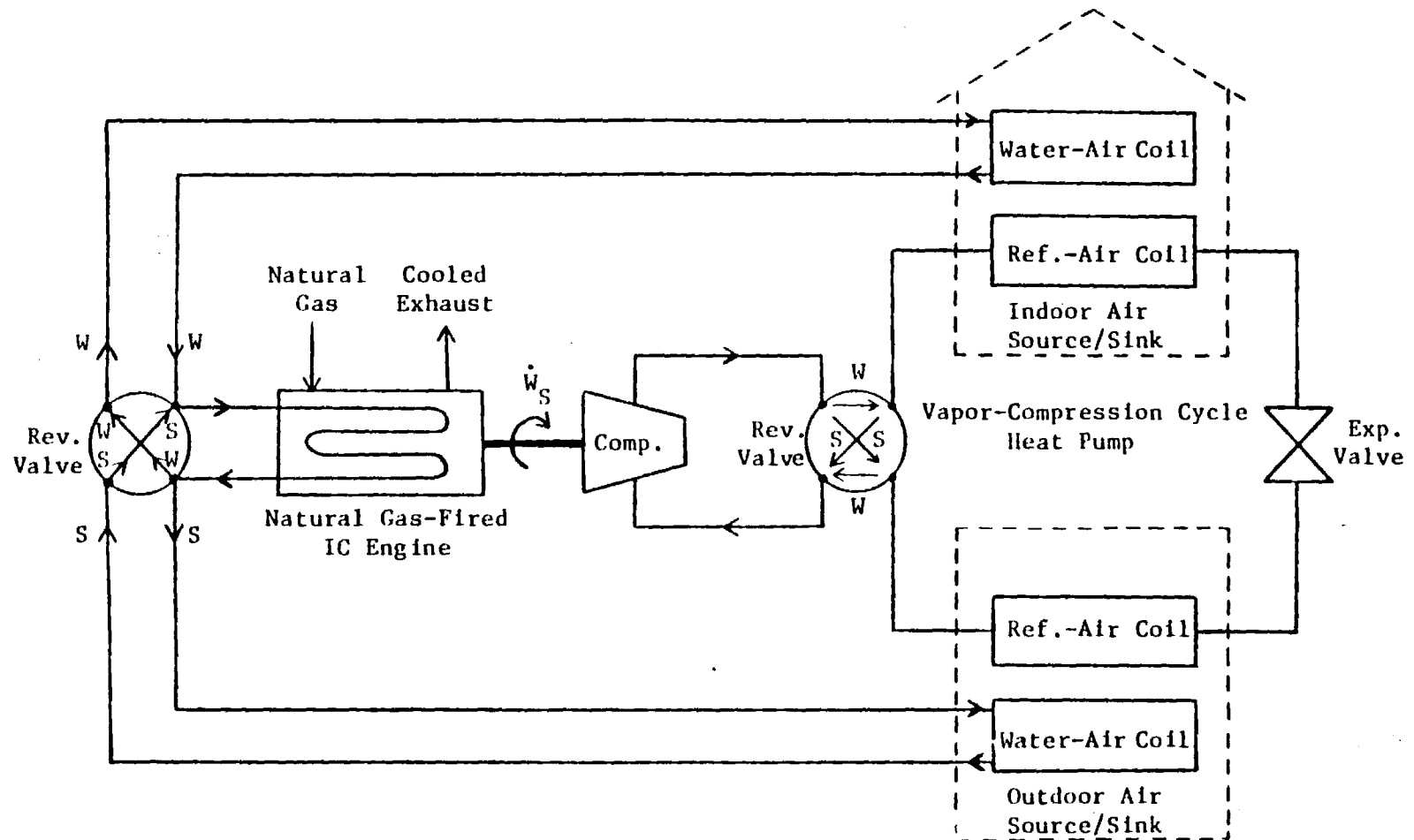


Figure 13: Air-to-Air Heat Pump Model Diagram

Water is used as a transger medium to remove combustion waste heat from the natural gas-fired I.C. engine. Heat removed from the engine block and exhaust gas is rejected to the heat sink via one of two water-air heat exchanger coils. A reversing valve is used to circulate water from the engine to the indoor coil (for simultaneous engine cooling and space heating) or to the outdoor coil (for engine cooling during space cooling).

An analytical model optimizes the air coils for the engine/compressor tested. The engine/compressor performance and heat recovery data are taken as input from the experimental data shown in Section IV. The operating performance for space heating and cooling is determined as a function of the refrigerant-air coil air flow rates and heat exchanger UA's (overall heat transfer coefficient times total wall surface area) for a range of outdoor air temperatures. The annual gas consumption required for space heating and cooling is then calculated for fixed residential thermal characteristics ($UA = 680 \text{ Btu/hr-}^{\circ}\text{F}$) and weather data using the "bin" method of analysis. From this data, the indoor vs. outdoor refrigerant coil UA is optimized. The annual performance for varying total indoor plus outdoor coil UA is then calculated so that the performance of this engine/compressor subcomponent, operating in an air-to-air system, may be determined for a given total air coil size and cost.

Analysis

Energy balances on the air flowing through the condenser and evaporator coils produce these fundamental equations:

$$\dot{Q}_{\text{Cond}} = (\dot{m}C_p)_{\text{Cond}}(T_o - T_i)_{\text{Cond}}$$

$$\dot{Q}_{\text{Evap}} = (\dot{m}C_p)_{\text{Evap}}(T_i - T_o)_{\text{Evap}}$$

where the C_p 's have been assumed constant and the temperature subscripts, i and o , refer to the air inlet and outlet of the coils. Another set of fundamental equations is obtained from counter-flow heat exchanger analysis:

$$\dot{Q}_{\text{Cond}} = [UA(\text{LMTD})]_{\text{Cond}} = UA \frac{T_o - T_i}{\ln \frac{T_{\text{Cond}} - T_i}{T_{\text{Cond}} - T_o}} \quad \text{Cond}$$

$$\dot{Q}_{\text{Evap}} = [UA(\text{LMTD})]_{\text{Evap}} = UA \frac{T_i - T_o}{\ln \frac{T_i - T_{\text{Evap}}}{T_o - T_{\text{Evap}}}} \quad \text{Evap}$$

where LMTD is the logarithmic mean temperature difference between the refrigerant and the air.

The heating and cooling requirements of the residential structure define the house load, from which the annual gas consumption can be determined. When the outdoor air temperature (or ambient air temperature) is below the desired indoor air temperature, the required heating rate is:

$$\dot{Q}_{HL} = (UA)_{House} (T_i - T_{amb})_{Heating}$$

Similarly, when the ambient air temperature is above the desired indoor air temperature, the required cooling rate is:

$$\dot{Q}_{CL} = (UA)_{House} (T_{amb} - T_i)_{Cooling}$$

These equations assume that the house model UA is independent of the ambient air temperature. In a study by the National Bureau of Standards, the historical energy consumption for heating and cooling was correlated with weather data, and good agreement was obtained using a constant house model UA. The bin method is used to estimate the annual heating and cooling loads from the last two equations.

The above equations represent the analytical heat pump model. Together, they comprise nine equations with unknowns. The unknowns are T_{Cond} , T_{Evap} , T_{oCond} , T_{oEvap} , \dot{Q}_{Cond} , \dot{Q}_{Evap} , \dot{Q}_{Rec} , \dot{Q}_{Gas} , and \dot{Q}_{Gas}^{Annual} . The remaining variables are input parameters. These include the house model UA and the condenser and evaporator coil inlet air temperatures, air flow rates, and UA's. For heating, T_{iCond} is the desired indoor air temperature and T_{iEvap} is the outdoor air temperature. For cooling, the coils are reversed so that T_{iCond} is the outdoor air temperature and T_{iEvap} is the desired indoor air temperature. In matrix form, these equations are easily solved (for a given

set of input conditions) by Gauss elimination. If these calculations are performed at the median outdoor air temperature of each bin, the results can be used to determine the total annual gas consumption for heating and cooling of the residential structure.

A computer program was set up on an APPLE II computer to run through all of these calculations.

Input Parameter Considerations

The desired indoor air temperatures are chosen to be 68°F for heating, and 76°F for cooling, normal conditions for residential and small commercial establishments. The house model UA is taken from a heating and cooling load study on the Atlanta residence accommodating the experimental heat pump system. In that study, the UA was estimated at 680 Btu/hr-°F for both heating and cooling. The analytical heat pump design is optimized for this house load. The results are applicable to varying house loads if all system components are scaled proportionally.

In cooling, approximately 75% of the heat removed from the indoor air was assumed to be in the form of sensible heat. The remaining 25% was assumed to be latent heat due to dehumidification. To account for this dehumidification, the specific heat of the air flowing through the evaporator in the cooling mode is increased by a factor of 33% (25%/75%).

The indoor air flow rate is taken to be constant at 2500 cfm. This constant is necessary to ensure a high enough condenser air outlet temperature (105-115°F) in the heating mode to prevent draft chill, and a low enough evaporator air outlet temperature (50-55°F) in the cooling mode for sufficient dehumidification. The outdoor air flow rate is varied proportionally with the outdoor coil UA, such that the ratio of coil UA to volumetric flow rate for the outdoor coil is fixed. The outdoor coil UA to volumetric flow rate ratio is fixed at a typical value of $2.0 \frac{\text{Btu/hr-}^\circ\text{F}}{\text{cfm}}$.

Three locations, Atlanta, Chicago, and Orlando, are chosen as having representative average, cold, and warm climates. The weather data (hours per year at each temperature bin) for these cities is found in U.S. Air Force Manual 88-29. In climates much colder than Chicago's, the heat pump may become less cost effective than direct heating systems because of the lower outdoor air (source) temperatures. In climates much warmer than Orlando's, the natural gas heat pump begins to lose its advantage over the electric heat pump because of the reduced heating hours.

Performance Optimization

The optimum heat pump performance for each city is determined by varying the ratio of indoor coil UA to outdoor coil UA. The optimum UA ratio, for a fixed total coil UA (indoor coil UA plus outdoor coil UA), or a fixed total coil

cost, is defined as that yielding the lowest annual gas consumption. The annual gas consumption is calculated for total coil UA's of 2500, 5000, 10000, and 15000 Btu/hr-°F at various UA ratios. The results of these calculations are graphed in Figures 14-16.

A curve is drawn through the optimum performance points in each of the graphs, and it is expected that the optimum performance for other values of total coil UA lies along these curves. The shape of these optimum performance curves is explained by considering that the total annual gas consumption is the sum of the annual gas consumption for both heating and cooling. The optimum UA ratio for heating decreases with increasing total coil UA, while that for cooling increases with increasing total coil UA. The degree of interaction between the two separate performance curves is dependent upon the heating and cooling load requirements. Listed in Table 11 are the heating and cooling loads for each city, along with the optimum heating, cooling, and overall UA ratios. In Chicago, where the heating load requirement is predominant, the optimum overall performance is essentially determined by the optimum heating performance. On the other hand, in Orlando, where the cooling load requirement is predominant, the optimum overall performance is essentially determined by the optimum cooling performance (more gas is required per Btu of cooling than per Btu of heating).

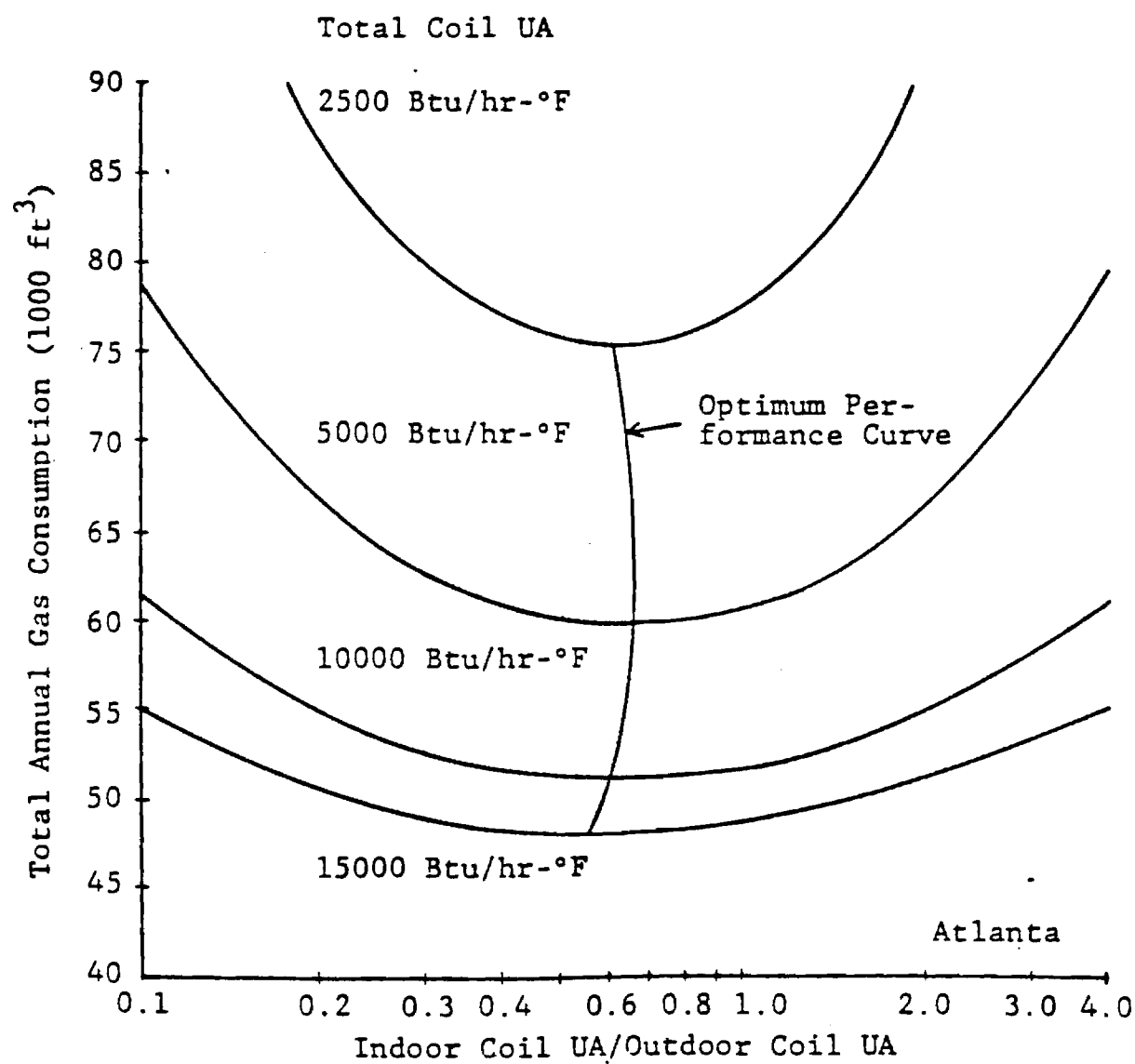


Figure 14: Annual Gas Consumption
versus Coil UA Ratio, Atlanta

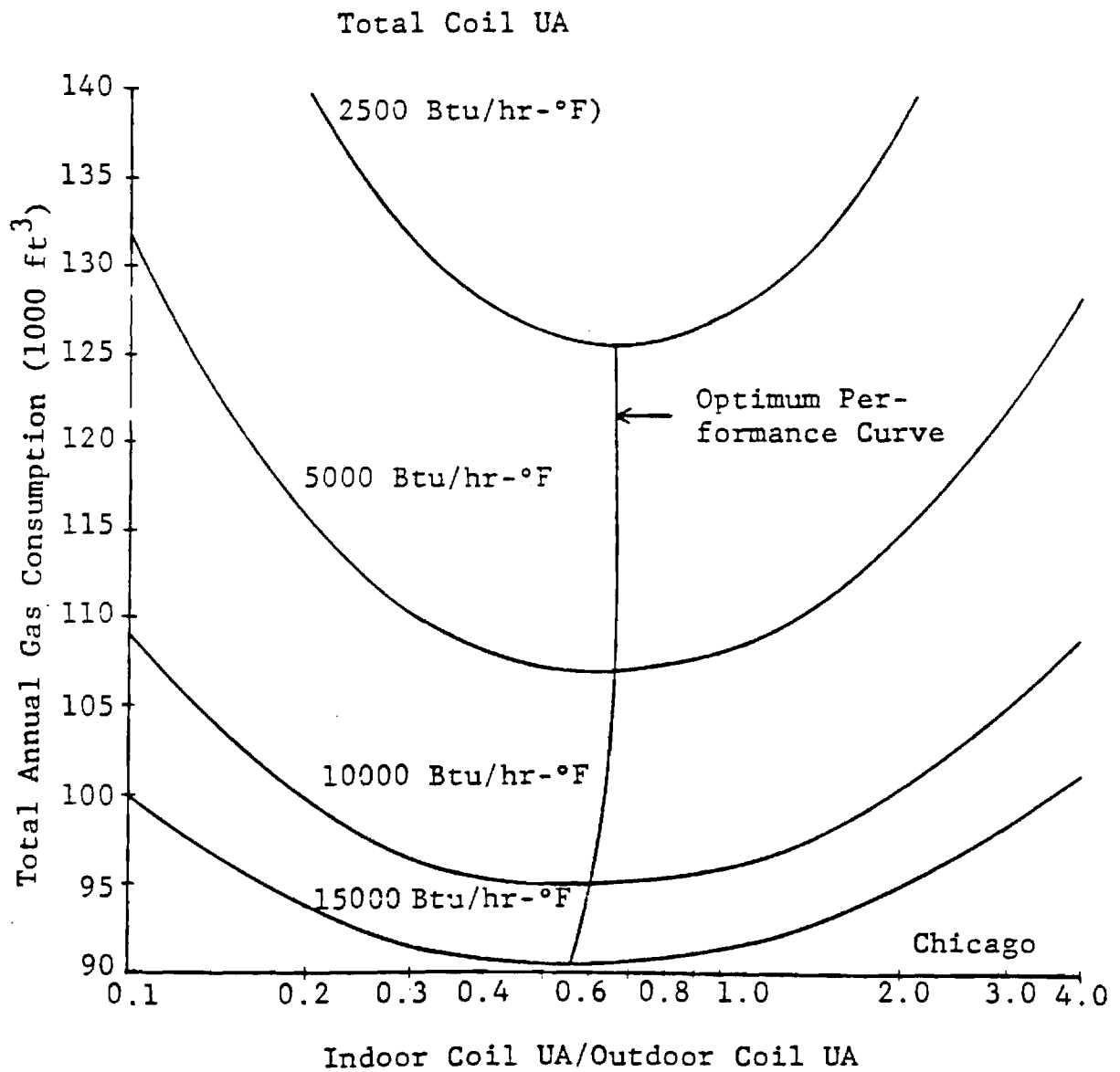


Figure 15: Annual Gas Consumption
versus Coil UA Ratio, Chicago

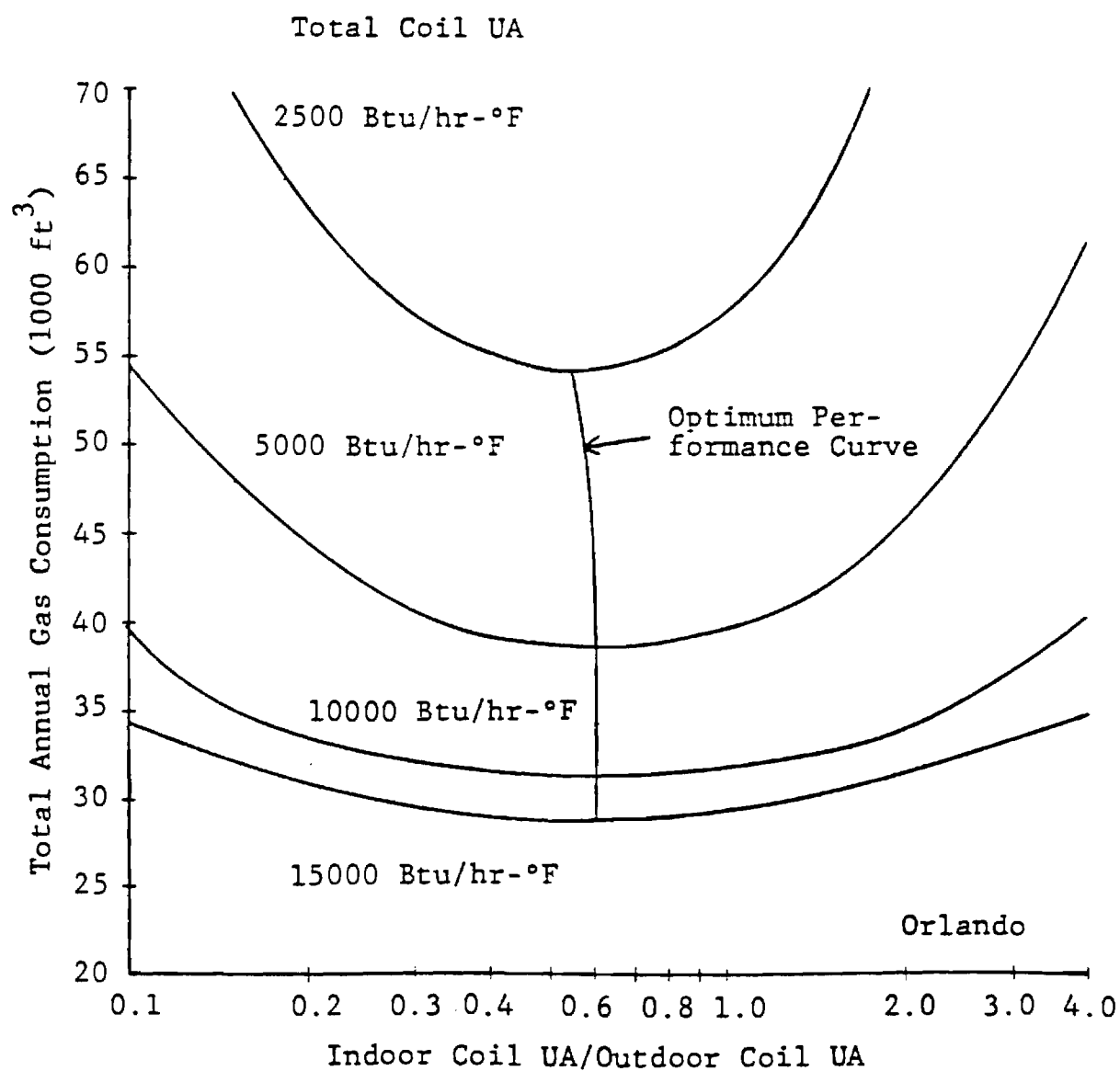


Figure 16: Annual Gas Consumption
versus Coil UA Ratio, Orlando

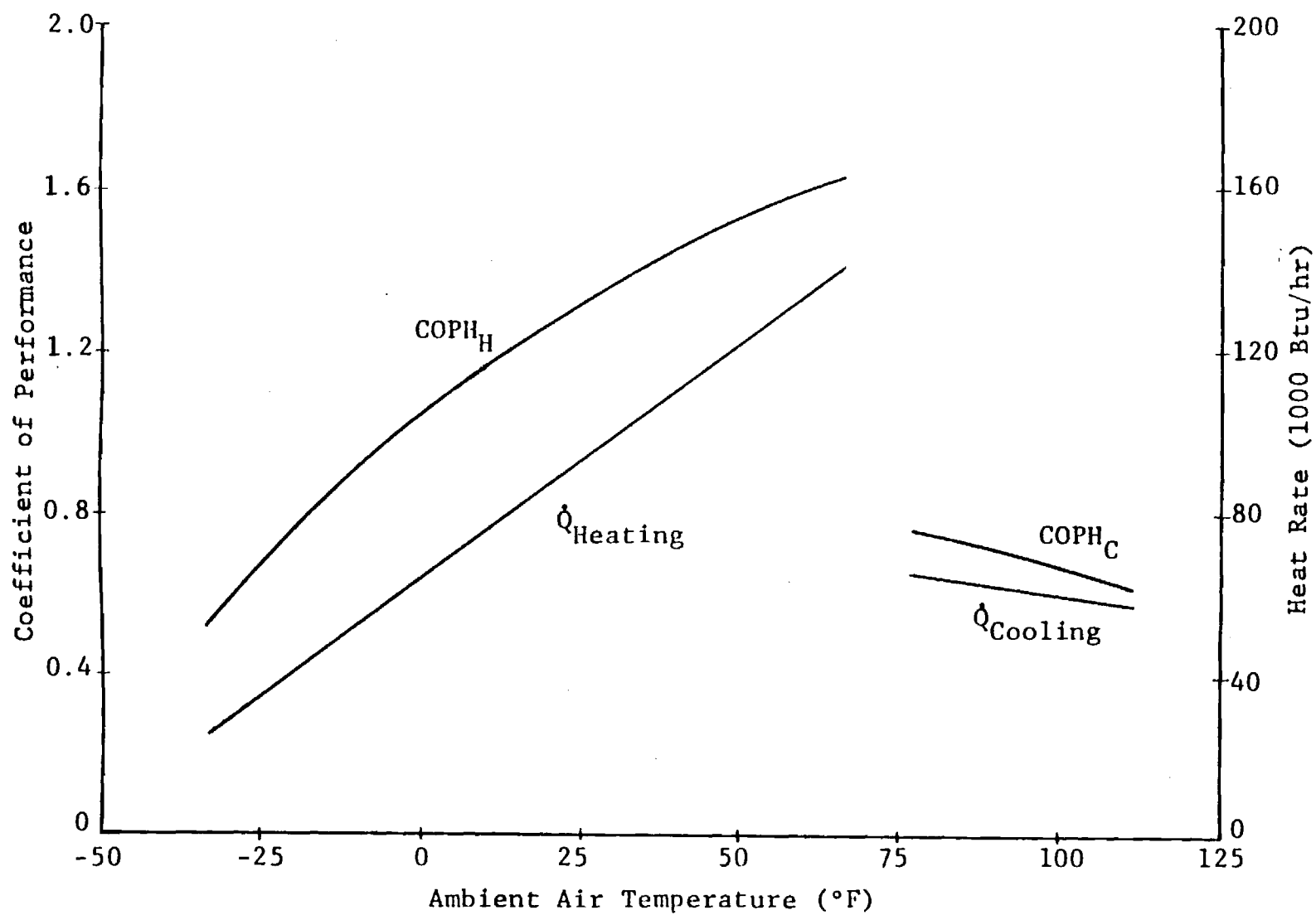


Figure 17: Heating and Cooling COP's and Rates at Optimum Performance
for Total Coil $UA = 10000 \text{ Btu/hr-}^\circ\text{F}$

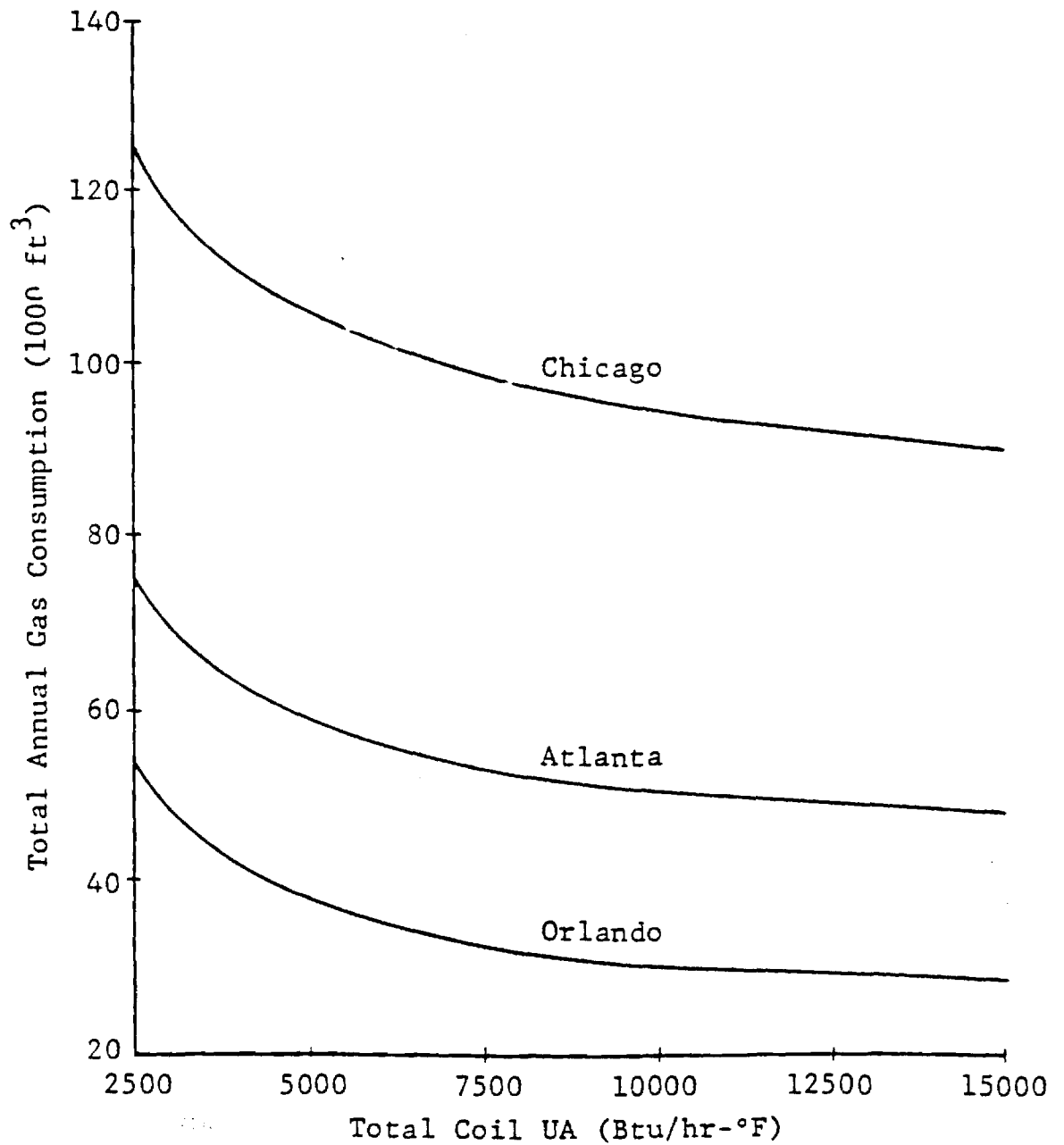


Figure 18: Annual Gas Consumption
at Optimum Performance

Table 11: Optimum Coil UA Ratios

City 1 - Annual Heating Load Requirement (Btu) 2 - Annual Cooling Load Requirement (Btu)	Total Coil UA (Btu/hr-°F)	Optimum UA Ratio ($\frac{\text{Indoor Coil UA}}{\text{Outdoor Coil UA}}$)		
		Heating	Cooling	Overall
Atlanta 1 - 59,866,860 2 - 8,255,880	5,000 10,000 15,000	0.65 0.60 0.55	0.60 0.60 0.60	0.65 0.60 0.55
Chicago 1 - 122,283,380 2 - 3,957,600	5,000 10,000 15,000	0.65 0.60 0.55	0.55 0.60 0.60	0.65 0.60 0.55
Orlando 1 - 20,342,880 2 - 13,623,460	5,000 10,000 15,000	0.70 0.60 0.60	0.60 0.60 0.60	0.60 0.60 0.60

Table 12: Annual Heating and Cooling COP's
at Optimum Performance

City	Total Coil UA (Btu/hr-°F)	COP _H	COP _C
Atlanta	5000	1.28	0.56
	10000	1.45	0.73
	15000	1.52	0.80
Chicago	5000	1.19	0.56
	10000	1.33	0.73
	15000	1.39	0.80
Orlando	5000	1.35	0.56
	10000	1.53	0.73
	15000	1.61	0.80

The heat pump design for optimum performance can be determined from Figures 14-16 for any total coil UA. For a total coil UA of 10000 Btu/hr-°F, the optimum UA ratio is found to be 0.6 for Atlanta, Chicago, and Orlando. Then for optimum performance, the heat pump design would include an indoor coil with a UA of 3750 Btu/hr-°F and an outdoor coil with a UA of 6250 Btu/hr-°F. The heating and cooling COP's and rates at optimum performance for this design are plotted in Figure 17 as functions of the outdoor air temperature. Since the optimum UA ratio for a total coil UA of 10000 Btu/hr-°F was found to be the same for Atlanta, Chicago, and Orlando, the curves in Figure 17 apply to all three cities. The annual heating and cooling COP's at optimum performance are presented in Table 12.

The annual gas consumption at optimum performance (from Figures 14-16) is given in Figure 18 as a function of total coil UA. This figure provides an indication of the savings in annual gas consumption that would be gained through the use of coils with a higher total UA. As one might expect, annual gas savings diminish with increasing increments of total coil UA.

Conclusions

This air-to-air I.C. engine heat pump analysis, using actual engine/compressor data, shows that the indoor coil UA should be about 0.6 of the outdoor coil UA and that for

a total UA above 10000 Btu/hr- $^{\circ}$ F, gas savings diminish rapidly. The heat pump size and coil UA should be proportional to the house thermal load, so that for a house half the size of that used, (UA - 680 Btu/hr- $^{\circ}$ F), the total air coil UA should be scaled down to one-half as should all other components.

The resulting heating and cooling COP's for this particular package with a typical total inside plus outside coil UA of 10000 Btu/hr- $^{\circ}$ F would then be:

	<u>COP_H</u>	<u>COP_C</u>
Atlanta	1.45	0.73
Chicago	1.33	0.73
Orlando	1.53	0.73

Since the engine used to obtain data for this analysis was only 25% loaded, a more closely matched engine/compressor (smaller engine) would improve these air-to-air heat pump COP's.

SECTION VI

CONCLUSIONS AND RECOMMENDATIONS

Introduction

The field testing and analysis of a natural gas I.C. engine heat pump has provided important information regarding the state of technology, potential performance, problem areas, and optimization of I.C. engine heat pumps. The most important of these conclusions is that several formerly perceived problem areas have been shown to be either non-existent or unimportant. Other conclusions are related to the performance of the tested unit, including seasonal performance, steady state performance, cycling effects, and speed variation effects. Design criteria for air-to-air I.C. engine heat pumps have also been developed. These specific conclusions and recommendations for further development of this concept are as follows.

Experimental Performance

The I.C. engine heat pump, with its Ford of Europe 1600 cc natural gas industrial engine, operated as a water-to-water heat pump to provide all space conditioning for an Atlanta residence over two heating and two cooling seasons. Measurement of its performance provided the following data. Speed was constant at 1200 rpm. The measured average winter seasonal energy rates were 68,400 Btu/hr for the gas use rate and 99,000 Btu/hr for the total heating rate, yielding a 1.47 seasonal heating COP. During the 561 hours of monitored

summer cooling operation, the gas use rate was 67,300 Btu/hr with a cooling rate of 38,800 Btu/hr for a seasonal cooling COP of 0.57. The electrical accessory power for the water circulating pumps and air handler fan was 1.91 kw.

Monitored steady state performance at 1200 rpm showed a heating COP of 1.42 with a cooling COP of 0.60. Cycling effects during heating were shown to have a positive effect on heating efficiency because (1) a six minute spin down cycle was used after engine shut down and (2) the water-cooled condenser was in the same water loop with the engine jacket and exhaust heat exchanger. Cycling then led to a lower average condenser temperature and pressure while still recovering the engine heat through spin down.

The engine was found to be oversized for the compressor, resulting in only a 25% loading of the engine and a low engine efficiency of about 16%. Variable engine speed tests from 1200 rpm to 1600 rpm showed a heating output increase of 20% with a drop in heating COP of 11%. The sensitivity of the heating efficiency to speed for this condenser-to-water-to-air system is expected to be greater than a direct condenser-to-air system.

The performance of the engine/compressor itself was measured for varying evaporator and condenser temperatures. These tests showed that for a 1°F increase in condenser temperature, gas consumption increased 0.21%, condenser

output decreased 0.49%, recovered engine/exhaust heat remained about constant, and the evaporator cooling rate decreased 0.81% with a 0.70% decrease in heating COP and 0.92% decrease in cooling COP. For a 1°F increase in evaporator temperature, the gas consumption increased 0.48%, condenser output increased 2.56%, engine/exhaust heat recovery increased 0.39%, and the evaporator cooling rate increased 2.6% with the heating COP increasing 1.1% and the cooling COP increasing 2.1%.

Maintenance, Reliability and Noise

A major conclusion of this study concerns maintenance, reliability, and noise. During the 2400 operating hours over a 20 month period, no maintenance was performed. Oil analyses have been carried out and found to be completely within serviceable specifications. The specially tipped spark plugs have been checked and found to be within reasonable gap tolerance at 0.042 inch. Reliability has been 100% except for starting failures. Failure to start within the fixed five second starter engagement period would usually occur after a long period of not running. Manually resetting the controls was, the only action required to resume normal operation.

Noise levels in the equipment room were 63 dB with a 60 dB measured six feet from the outside exhaust.

In summary, the generally perceived problems of reliability, maintenance, and noise produced by an I.C. engine operating in the home have been shown not to be significant problems.

Analytical Air-to-Air Performance

A model was developed for calculating the performance of the same gas heat pump engine/compressor, but with air evaporator and air condenser coils in place of the water coils. Actual experimental data from the engine/compressor was used in the model. This data was then coupled with weather data in Chicago, Orlando, and Atlanta to yield annual performance efficiencies. The relative sizes of the indoor versus outdoor coils were optimized and performance was calculated for varying total coil size. For a fixed total investment in air coils, it was found that the indoor coil size should be about 60% of the outdoor coil size. Also, increasing the combined coil UA up to about 10,000 Btu/hr-°F was found to be beneficial. Beyond this value minimal gas was conserved. For size scaling, this would mean a ratio of combined heat pump air coil UA per house UA of about 15, assuming the engine/compressor size was also scaled. This figure is not out of line with coil sizes used in present day electric heat pumps. At this value the seasonal heating COP's were 1.33, 1.45, and 1.53 for Chicago, Atlanta, and Orlando, respectively. All three cities showed a 0.73 seasonal cooling COP.

Recommendations

The water-to-water I.C. engine heat pump tested has shown reasonable efficiency and excellent short term (one to two years) maintenance and reliability. Advanced information also was obtained. The next potential problem areas for study should include long term engine durability, manufacturing and installation costs, air-to-air system performance, and defrost control.

The automotive derivative natural gas industrial engine tested has shown that this class of engine has merit. Continued study of the many available engines is needed to determine their suitability in terms of size, cost, and longevity.

Specifically, engines that are found to be suitably sized and available for this test application should undergo necessary modifications for gasification, such as cam shaft and compression ratio changes. Then two or three engines of each type should be run continuously at constant speed, and two or three should be run on a thirty minute start/stop basis. Long term engine life information can then be gained within about two years.

Simultaneously, an air-to-air heat pump with a matched engine/compressor should be field tested to study efficiencies and to optimize defrost strategy.